

# Wave Slam Response of Large High-Speed Catamarans

by

Giles Thomas

*Giles Anthony*

B.Eng.(Hons), University of Newcastle upon Tyne (1988)

M.Phil., University of Newcastle upon Tyne (1992)

Submitted in fulfilment of the requirements for the degree of

Doctor of Philosophy

*Engineering  
(Civil & Mech.)*

at the

UNIVERSITY OF TASMANIA

October 2003

# Declaration of Originality

This thesis contains no material that has been accepted for a degree or diploma by the University of Tasmania or any other institution, and to the best of my knowledge and belief no material previously published or written by another person except where due acknowledgement is made in the text of the thesis.

A handwritten signature in black ink, appearing to read 'Giles Thomas', written in a cursive style.

Giles Thomas October 2003

## Statement of Authority of Access

This thesis is not to be made available for loan or copying for two years following the date this statement was signed. Following that time the thesis may be made available for loan and limited photocopying in accordance with the *Copyright Act 1968*.

A handwritten signature in black ink, appearing to read 'Giles Thomas', written in a cursive style.

Giles Thomas October 2003

# Abstract

The rapid evolution of high-speed sea transportation has led to the development of large, fast, lightweight vessels. The structural design optimisation of such vessels requires knowledge of the effect of sea loads on their structure. Of particular importance for high-speed catamarans are severe wet-deck slam events, which can impart a large global load onto a vessel's structure and as a consequence cause significant structural damage. The dynamic whipping response of the structure may also be important by making a significant contribution to fatigue damage.

Extensive full-scale hull stress, motion and wave measurements were conducted on two Incat high-speed catamaran ferries. A definition of a slam event, for these vessels, was proposed and used to identify slam events from the data records. The character and effects of these slamming events are investigated with respect to a number of factors. Slam events were found to produce bending moments up to 700% of the largest underlying global wave loads.

The data from the full-scale slam events, including an extreme slam event that caused extensive structural damage, was used in conjunction with finite element modelling to develop a realistic quasi-static slam loading scenario for structural design purposes. This slam load case gives a maximum bending moment approximately 16% greater than that stipulated by classification society Det Norske Veritas, with a greater bias towards the bow of the vessel. A method for scaling the design load case for use with new designs is also proposed.

A technique for predicting the mode shape and frequency of the whipping behaviour utilising finite element analysis including the fluid-structure interaction is presented. The hydrodynamic added mass of the surrounding fluid was calculated using a two-dimensional panel method for a range of speeds. The calculated whipping modes are then compared favourably with those found through the full-scale measurements and exciter experiments. The exciter experiments were conducted on two vessels with the anchors being dropped and instantaneously arrested to excite the vessels' first longitudinal mode of vibration. The level of damping of the whipping behaviour is investigated through the full-scale results and exciter experiments. Methods for evaluating the various hydrodynamic components which constitute the damping are also presented including wavemaking damping, viscous damping and acoustic damping. It is concluded that structural damping is the dominant damping component.

Fatigue life estimates, utilising full-scale slam data and derived whipping behaviour information, were conducted which found that slamming and whipping behaviour have a large influence on fatigue life.

Finally, knowledge of the dynamic slamming response was utilised to develop a dynamic extreme slam design load case. This dynamic load case more realistically simulates the dynamic structural response of the vessel to a slam. It is the core component of a new practical methodology for the structural design of large high-speed catamarans for slamming.

# Acknowledgements

I would like to thank my friends and colleagues at the University of Tasmania, Incat Tasmania and Revolution Design for the help and encouragement they have provided during the course of this project. I am particularly grateful to:

- Professor Mike Davis from the University of Tasmania for his guidance and support throughout the project.
- Tim Roberts from Incat Tasmania/Revolution Design for his enthusiasm, practical knowledge and advice.
- Dr. Damien Holloway from the University of Tasmania for his technical input and encouragement.

My partner Judy, and daughters Isobel and Sassafras have been a source of great strength and inspiration. I give them extra special thanks.

This was a collaborative project between the University of Tasmania and Incat Tasmania. The project was supported by the Federal Government through the Australian Research Council's SPIRT Scheme.

# Contents

<b>1</b>	<b>Introduction</b>	<b>1</b>
1.1	Background . . . . .	1
1.1.1	Design Aspects of Incat High-Speed Catamarans . . . . .	3
1.2	Problem Definition . . . . .	4
1.3	Scope of Work . . . . .	10
<b>2</b>	<b>Full-Scale Trials Measurements</b>	<b>12</b>
2.1	Introduction . . . . .	12
2.2	Vessel Details, Measurement Systems and Location of Trials . . . . .	16
2.2.1	Vessel Details . . . . .	16
2.2.2	Monitoring System Instrumentation and Data Acquisition . . . . .	16
2.2.3	Location of Trials . . . . .	24
2.3	Data Analysis . . . . .	26
2.3.1	Slam Definition . . . . .	26
2.3.2	Slam Identification and Analysis . . . . .	30
2.4	Results and Discussion . . . . .	36
2.4.1	Slam Occurrences . . . . .	36
2.4.2	Extreme Slam Event . . . . .	55
2.4.3	Dynamic Features of Slamming Response . . . . .	58
2.4.4	Additional Slam Analysis Results . . . . .	62
2.5	Conclusions . . . . .	67
2.6	Summary: Full-Scale Trials . . . . .	70
<b>3</b>	<b>Quasi-Static Slam Loads</b>	<b>72</b>
3.1	Introduction . . . . .	72
3.1.1	Load Types . . . . .	72
3.1.2	Load Calculation Techniques . . . . .	73
3.1.3	Finite Element Methods . . . . .	76
3.1.4	Summary . . . . .	77
3.2	Det Norske Veritas Classification Rules . . . . .	78

3.3	Extreme Slam Events Details . . . . .	79
3.4	Additional Slam Event Details . . . . .	80
3.5	Finite Element Model . . . . .	80
3.6	Wave-Induced Load Model . . . . .	82
3.7	Hull 050 Slam Load Case . . . . .	86
	3.7.1 Global Loads Correlation . . . . .	86
	3.7.2 Slam Correlation . . . . .	88
	3.7.3 Comparison of Extreme Slam Load Case with DNV Classification Rules . . . . .	96
3.8	Slam Load Case Application . . . . .	99
	3.8.1 Proposed Slam Load Scaling Method . . . . .	99
	3.8.2 Slam Load Scaling Example . . . . .	103
3.9	Summary . . . . .	104
<b>4</b>	<b>Dynamic Slamming Response</b>	<b>105</b>
4.1	Introduction . . . . .	105
	4.1.1 Whipping Behaviour . . . . .	105
	4.1.2 Whipping Mode Prediction . . . . .	108
	4.1.3 Damping . . . . .	110
	4.1.4 Summary . . . . .	110
4.2	Exciter Tests . . . . .	112
	4.2.1 Experimental Details . . . . .	112
	4.2.2 Data Analysis . . . . .	113
	4.2.3 Results and Discussion . . . . .	113
	4.2.4 Conclusions . . . . .	117
4.3	Whipping Mode Prediction . . . . .	119
	4.3.1 Normal Mode Theory . . . . .	119
	4.3.2 Fluid Structure Interaction - Hydrodynamic Model . . . . .	121
	4.3.3 Normal Mode Analysis . . . . .	127
	4.3.4 Results - Dry Modes . . . . .	130
	4.3.5 Results - Added Mass . . . . .	130
	4.3.6 Results - Wet Modes . . . . .	140
	4.3.7 Conclusions . . . . .	142
4.4	Damping . . . . .	147
	4.4.1 Energy Dissipation in the System . . . . .	147
	4.4.2 Hydrodynamic Damping - Theory . . . . .	149
	4.4.3 Hydrodynamic Damping - Calculation . . . . .	155
	4.4.4 Structural Damping . . . . .	159
	4.4.5 Comparison of Predicted and Measured Damping . . . . .	164

4.4.6	Conclusions . . . . .	165
4.5	Summary . . . . .	166
<b>5</b>	<b>Influence of Slamming and Whipping on Fatigue Life</b>	<b>167</b>
5.1	Introduction . . . . .	167
5.2	Estimation of Fatigue Life . . . . .	169
5.3	Fatigue Analysis: Influence of Slamming . . . . .	169
5.3.1	Analysis Procedure . . . . .	171
5.3.2	Results and Discussion . . . . .	172
5.4	Fatigue Analysis: Influence of Whipping . . . . .	176
5.4.1	Analysis Procedure . . . . .	176
5.4.2	Results and Discussion . . . . .	176
5.5	Implications of Fatigue Analysis on Slam Definition . . . . .	177
5.6	Conclusions . . . . .	177
<b>6</b>	<b>Dynamic Slam Loads</b>	<b>181</b>
6.1	Introduction . . . . .	181
6.2	Dynamic Finite Element Analysis . . . . .	182
6.2.1	Finite Element Dynamic Analysis Theory . . . . .	182
6.2.2	Finite Element Model . . . . .	185
6.3	Extreme Slam Correlation - Dynamic Analysis . . . . .	185
6.4	Practical Methodology for Structural Design of Large High-Speed Catamarans for Slamming . . . . .	192
6.5	Conclusions . . . . .	193
<b>7</b>	<b>Conclusions</b>	<b>195</b>
7.1	Summary . . . . .	195
7.1.1	Slam Occurrence and Characteristics . . . . .	195
7.1.2	Extreme Slam Event and Quasi-Static Slam Loads . . . . .	196
7.1.3	Dynamic Slamming Response . . . . .	197
7.1.4	Influence of Slamming and Whipping on Fatigue Life . . . . .	198
7.1.5	Dynamic Slam Loads . . . . .	198
7.2	Implications of Research . . . . .	198
7.3	Recommendations for Further Work . . . . .	201

<b>A Strain Gauge Locations: Detailed Drawings</b>	<b>215</b>
<b>I Hull 042</b>	<b>216</b>
<b>II Hull 050</b>	<b>226</b>

# List of Figures

1-1	Incat 98m Catamaran . . . . .	2
1-2	Austral 101m Catamaran . . . . .	2
1-3	Stena 125m Catamaran . . . . .	2
1-4	High-Speed Craft - Maximum Ship Length for Build Year . . . . .	3
1-5	Cross Section of Incat Hull Girder showing Dual Box-Like Structure . . . . .	5
1-6	Cut Away Section of Incat Hull Girder (Starboard Side) showing Horizontal and Vertical Cross Bracing . . . . .	5
1-7	Bow Slamming Damage on Stena HSS “Discovery” . . . . .	6
1-8	Port Side Portal Buckling due to Slamming . . . . .	7
1-9	Tripped C- Bracket due to Slamming . . . . .	7
1-10	Cracking Possibly due to Fatigue . . . . .	7
2-1	Incat Hull 042, 86m Catamaran . . . . .	17
2-2	Incat Hull 050, 96m Catamaran . . . . .	17
2-3	Hull 042 - Strain Gauge Locations . . . . .	20
2-4	Hull 050 - Strain Gauge Locations . . . . .	23
2-5	Map of Hull 042 Delivery Route between Sydney and Fremantle . . . . .	25
2-6	Map of Hull 050 Service Route between Wellington and Picton . . . . .	25
2-7	Hull 042 - Typical Raw Strain Gauge Data Traces . . . . .	27
2-8	Hull 050 - Typical Raw Strain Gauge Data Traces . . . . .	28
2-9	Hull 050 - Typical Raw Strain Gauge Data Traces . . . . .	28
2-10	Effect of Filtering Raw Strain Gauge Data . . . . .	31
2-11	Hull 050 - Raw Strain Gauge Data Trace showing Two Identified Slam Events .	31
2-12	Normalised Number of Slam Events versus Rate Constant . . . . .	32
2-13	Definition of Decay Coefficient . . . . .	35
2-14	Hull 042 - Distribution of Slam Peak Stress for Slam Events . . . . .	36
2-15	Hull 050 - Distribution of Slam Peak Stress for Slam Events . . . . .	37
2-16	Hull 042 - Distribution of Slam Peak Stress for Slam Events for varying Signif- icant Wave Height . . . . .	37

2-17 Hull 050 - Distribution of Slam Peak Stress for Slam Events for varying Significant Wave Height . . . . .	38
2-18 Hull 042 - Number of Slams per Hour vs. Significant Wave Height in Head Seas (Vessel Speed = 10 -15 knots) . . . . .	38
2-19 Hull 042 - Normalised Slam Peak Stress for varying Significant Wave Height and Wave Length . . . . .	40
2-20 Hull 050 - Normalised Slam Peak Stress for varying Significant Wave Height and Wave Length . . . . .	40
2-21 Hull 042 - Percentage of Slam Occurrence for varying Non-Dimensional Encounter Frequency . . . . .	41
2-22 Hull 050 - Percentage of Slam Occurrence for varying Non-Dimensional Encounter Frequency . . . . .	42
2-23 Definition of Tunnel Height . . . . .	42
2-24 Hull 042 Body Plan showing Centrebow Configuration . . . . .	43
2-25 Hull 050 Body Plan showing Centrebow Configuration . . . . .	43
2-26 Hull 042 - Number of Slam Events for varying Heading Angle . . . . .	45
2-27 Hull 050 - Number of Slam Events for varying Heading Angle . . . . .	45
2-28 Hull 042 - Normalised Slam Max Stress for varying Heading Angle . . . . .	45
2-29 Hull 050 - Normalised Slam Max Stress for varying Heading Angle . . . . .	46
2-30 Hull 042 - Slam Peak Stress as a function of Froude Number . . . . .	47
2-31 Hull 050 - Slam Peak Stress as a function of Froude Number . . . . .	47
2-32 Hull 042 - Froude Number for Operating Significant Wave Height . . . . .	47
2-33 Hull 050 - Froude Number for Operating Significant Wave Height . . . . .	48
2-34 Hull 042 - Slam Peak Stress for varying $F_{n_{rel\ vel}}$ . . . . .	48
2-35 Hull 050 - Slam Peak Stress for varying $F_{n_{rel\ vel}}$ . . . . .	48
2-36 Hull 042 - $F_{n_{rel\ vel}}$ for varying Froude Number . . . . .	49
2-37 Hull 050 - $F_{n_{rel\ vel}}$ for varying Froude Number . . . . .	49
2-38 Hull 042 - $F_{n_{rel\ vel}}$ for varying Significant Wave Height . . . . .	49
2-39 Hull 050 - $F_{n_{rel\ vel}}$ for varying Significant Wave Height . . . . .	50
2-40 Hull 042 - Normalised Strain Gauges . . . . .	52
2-41 Hull 050 - System 1 Normalised Strain Gauges . . . . .	53
2-42 Hull 050 - System 2 Normalised Strain Gauges . . . . .	54
2-43 Hull 050 Extreme Slam Damage - Buckling of External Plating . . . . .	56
2-44 Hull 050 Extreme Slam Damage - Internal Structure at Frame 60 showing Bending of Longitudinals and Plate Buckling . . . . .	56
2-45 Hull 050 Extreme Slam Damage - External Plating at Frame 60. View to Waterline down Outer Surface of Hull showing Buckled External Plating and Sponson . . . . .	57

2-46	Hull 050 - Extreme Slam Event Raw Data . . . . .	57
2-47	Hull 042 - Time from Slam Event registering at Frame 54 and registering at other Strain Gauges, plotted against varying Strain Gauge Longitudinal Location	59
2-48	Hull 050 - Time from Slam Event registering at Frame 67 and registering at other Strain Gauges, plotted against varying Strain Gauge Longitudinal Location	60
2-49	Hull 042 - Strain Gauge and Wave Spectra . . . . .	61
2-50	Hull 042 - Principal Frequencies for Strain Gauges . . . . .	62
2-51	Hull 050 - Strain Gauge and Wave Spectra . . . . .	63
2-52	Hull 050 - Principal Frequencies for Strain Gauges . . . . .	64
2-53	Hull 042 - Average Decay Coefficient for varying Cycle Number for Strain Gauges	65
2-54	Hull 050 - Average Decay Coefficient vs. Cycle Number for Strain Gauges . . .	66
2-55	Hull 042 - Number of Slam Occurrences as a function of Number of Waves Encountered between Slams . . . . .	67
2-56	Hull 042 - Ratio of Slam Peak Stress for Consecutive Slam Events . . . . .	68
2-57	Hull 042 - Number of Boat Lengths Travelled between Record of Extreme Bow Down Position & Slam Peak for varying Slam Peak Stress . . . . .	68
2-58	Hull 042 - Normalised Slam Peak Stress for varying Estimated Distance of Water Surface above Calm Waterline at Frame 55 at Time of Slam Impact . . . . .	68
3-1	Definition of Principal Catamaran Global Loads . . . . .	73
3-2	Hull 050 - Refined FE Mesh on Frames 65, 66, 67 and 69 . . . . .	82
3-3	Hull 050 - Original FE Mesh on Keel at Frame 24.5 . . . . .	83
3-4	Hull 050 - Refined FE Mesh on Keel at Frame 24.5 . . . . .	83
3-5	Hull 050 - Full FE Model . . . . .	84
3-6	Hull 050 - Vehicle Layout on Tier 1 . . . . .	84
3-7	Hull 050 - Global Longitudinal Bending Full-Scale Results, Scenario 1 . . . . .	87
3-8	Comparison of FEA and Full-Scale Data for Longitudinal Bending Scenario 1 .	89
3-9	Comparison of FEA and Full-Scale Data for Longitudinal Bending Scenario 2 .	89
3-10	Increase in FEA Stress due to Increase in Fuel Loading . . . . .	90
3-11	Distribution of Slam Impact Load for Extreme Slam Event . . . . .	91
3-12	Longitudinal Distribution of Applied Force for Extreme Slam Event . . . . .	91
3-13	Exaggerated Deflection Plot (units in mm) for Extreme Slam Load Case . . .	92
3-14	Stress Plot (units in MPa) for Extreme Slam Load Case. The zone identified by the circle highlights the area of external damage as indicted in Chapter 2. .	92
3-15	Hull 050 - Comparison of FEA and Full-Scale Data for Extreme Slam Impact .	93
3-16	Hull 050 - Comparison of FEA and Full-Scale Data for Extreme Slam Impact (Symmetric Analysis) . . . . .	95
3-17	Hull 050 - Comparison of FEA and Full-Scale Data for Slam Number 2 . . . .	96

3-18	Hull 050 - Comparison of FEA and Full-Scale Data for Slam Number 3 . . . . .	97
3-19	Hull 050 - Comparison of FEA and Full-Scale Data for Slam Number 4 . . . . .	97
3-20	Hull 050 - Comparison of FEA and Full-Scale Data for Slam Number 5 . . . . .	98
3-21	Hull 050 - Slam Impact Load for varying Relative Vertical Velocity for Slam Load Cases . . . . .	98
3-22	Hull 050 - Comparison of Slam Load Case FEA (Fully Loaded Design Condition) and DNV Longitudinal Sagging Moment . . . . .	100
3-23	Hull 050 - Comparison of Bending Moment Curves for Slam Load Case FEA (Fully Loaded Design Condition) and DNV Longitudinal Sagging Moment . . . . .	100
3-24	Hull 050 - Comparison of Shear Force Curves for Slam Load Case FEA (Fully Loaded Design Condition) and DNV Longitudinal Sagging Moment . . . . .	101
3-25	Comparison of Bending Moment Curves for Extreme Slam FE Load Case and DNV Sag Rule Moment for 112m Design . . . . .	103
4-1	Hull 045 - Exciter Test Accelerometer Locations . . . . .	114
4-2	Hull 050 - Exciter Test Accelerometer Locations . . . . .	114
4-3	Hull 050 - Exciter Test Raw Data, In-Water . . . . .	115
4-4	Hull 050 - Exciter Test Response Spectrum, In-Water . . . . .	115
4-5	Hull 050 - Exciter Test Response Spectrum, Out-of-Water . . . . .	116
4-6	Hull 050 - Exciter Test Decay Coefficients, In-Water . . . . .	118
4-7	Hull 050 - Exciter Mode Shape on Centreline . . . . .	118
4-8	Decay Coefficient: Comparison of Exciter Test Results with Betts et al. (1977) Data . . . . .	118
4-9	Coordinate System 1 in Cross Sectional Plane of the Hull (Equations 4.8 - 4.25)	121
4-10	Coordinate System 2 (Equations 4.26 - 4.39) . . . . .	125
4-11	Hull 042 Finite Element Model . . . . .	128
4-12	Hull 050 - Lateral Torsion Dry Mode (2.48 Hz), units in mm . . . . .	131
4-13	Hull 050 - 1st longitudinal Dry Mode (3.97 Hz), units in mm . . . . .	131
4-14	Hull 042 Offsets with Design Waterline (DWL) shown . . . . .	133
4-15	Hull 050 Offsets with Design Waterline (DWL) shown . . . . .	133
4-16	Hull 042 - Sectional Added Mass, Trials Condition 1, Draft = 3.45m . . . . .	134
4-17	Hull 042 - Sectional Added Mass, Trials Condition 2, Draft = 3.12m . . . . .	134
4-18	Hull 042 - Sectional Added Mass, Exciter Test Condition, Draft = 2.88m . . . . .	135
4-19	Hull 050 - Sectional Added Mass, Trials/Exciter Test Condition, Draft = 3.10m	135
4-20	Hull 050 - Added Mass Coefficient for varying Frame Number, Frequency = 3.0 Hz . . . . .	136
4-21	Hull 050 - Influence of Panel Density on Sectional Added Mass, Frame 40 . . . . .	136
4-22	Hull 050 - Effect of Froude Number on Total Added Mass . . . . .	137

4-23	Added Mass Distribution according to Horizontal Projected Area around a Hull Section ( $\cos\alpha$ Distribution) . . . . .	138
4-24	Added Mass Distributions . . . . .	138
4-25	Hull 050 - Effect of Added Mass Inclusion Techniques on Natural Frequency . .	139
4-26	Hull 042 - Natural Frequencies, Trials Condition 1 . . . . .	143
4-27	Hull 042 - Natural Frequencies, Trials Condition 2 . . . . .	143
4-28	Hull 042/045 - Natural Frequencies, Exciter Condition . . . . .	144
4-29	Hull 050 - Natural Frequencies, Exciter Test/Trials Condition 1 . . . . .	144
4-30	Hull 042/045 - First Longitudinal Mode Shape Comparison on Centreline . . .	145
4-31	Hull 042/045 - First Longitudinal Mode Shape Comparison off Centreline . . .	145
4-32	Hull 050 - First Longitudinal Mode Shape Comparison on Centreline . . . . .	145
4-33	Hull 050 - Wavemaking Sectional Damping in Trials/Exciter Test Condition, Draft = 3.10m . . . . .	156
4-34	Influence of Panel Density on Sectional Damping, Frequency = 18 rad/sec . . .	156
4-35	Hull 050 - Total Vessel Damping for varying Frequency, in Full-Scale Trials Condition, Draft = 3.10m . . . . .	157
4-36	Material Damping Experiment - I-Beam Section . . . . .	162
4-37	Material Damping Experiment - Square Beam Section . . . . .	162
4-38	Example of Aluminium Material Damping Testing Raw Data . . . . .	163
4-39	Damping for 86m Austal Catamaran . . . . .	164
4-40	Hull 050 - Comparison of Measured, Calculated and Estimated Damping . . . .	165
5-1	BS8118 Weld Details at End Connections of Member . . . . .	170
5-2	BS8118 Weld Details on Surface of Member . . . . .	170
5-3	Summary of Hull 042 Delivery Voyage showing Fatigue Data Zone. Time period is from 00.00 hours on 19th December to 00.00 hours on 23rd December. . . . .	171
5-4	S-N Curve for Bat Wing on Cross Brace at Frame 17 . . . . .	173
5-5	S-N Curve for Keel at Frame 35.5 . . . . .	173
5-6	Change in Fatigue Life due to Slamming - Hull 042 . . . . .	173
5-7	Reduction in Fatigue Life due to Slamming - Hull 042 . . . . .	174
5-8	Fatigue Life for varying Significant Wave Height - Hull 042 . . . . .	174
5-9	Cycle Count to Failure for Significant Waveheight 3m to 3.5m - Hull 042 . . . .	175
5-10	Damage Contribution for Significant Waveheight 3m to 3.5m - Hull 042 . . . .	175
5-11	Estimated Fatigue Life for varying Frequency of Slam Occurrence and Slam Peak Stress - Hull 042 . . . . .	179
5-12	Example Simulated Slam Events . . . . .	179
5-13	Fatigue Life for varying Slams per Hour Rate and Decay Coefficient . . . . .	180
5-14	Fatigue Life for varying Slams per Hour Rate and Slam Peak Stress . . . . .	180

6-1	Global Wave Load Time History for Extreme Slam Event . . . . .	186
6-2	Slam Load Time History for Extreme Slam Event . . . . .	186
6-3	Distribution of Slam Impact Load for Extreme Slam Event - Dynamic Analysis	187
6-4	Longitudinal Distribution of Applied Force for Extreme Slam Event - Dynamic Analysis at Time of Maximum Slam Load . . . . .	188
6-5	Exaggerated Deflection and Von Mises Stress Plot (units in MPa) for Dynamic Extreme Slam Load Case at Time of Maximum Slam Load . . . . .	189
6-6	Von Mises Stress Plot (units in MPa) for Dynamic Extreme Slam Load Case - Starboard Side, Frames 55 to 60 at Time of Maximum Slam Load . . . . .	189
6-7	Time History of Steel Post Stress Results for Extreme Slam Event . . . . .	190
6-8	Time History of Steel Vehicle Deck Stress Results for Extreme Slam Event . . .	190
6-9	Time History of Keel Stress Results for Extreme Slam Event . . . . .	191
6-10	Comparison of Maximum FE Analysis and Full-Scale Data for Dynamic Ex- treme Slam Impact . . . . .	191
A-1	Hull 042 - Profile View Guide to Detailed Drawings of Strain Gauge Locations	218
A-2	Hull 042 - Plan View Guide to Detailed Drawings of Strain Gauge Locations .	219
A-3	Hull 042 - Frame 1 Portal View (Looking Aft) showing Strain Gauges 1 & 2 on Steel Chevron Brace . . . . .	220
A-4	Hull 042 - Longitudinal Girder 4600mm off Centreline (Looking Outboard to Port) showing Strain Gauges 3 & 4 on Transverse Box Girder . . . . .	220
A-5	Hull 042 - Plan View of Cross Bracing showing Strain Gauges 3 & 4 on Trans- verse Box Girder, Strain Gauge 5 on Cross Bracing and Strain Gauge 6 on Bat Wing on Cross Bracing . . . . .	221
A-6	Hull 042 - Longitudinal Girder 4600mm off Centreline (Looking Outboard to Port) showing Strain Gauges 7 & 9 on Longitudinal Girder and Strain Gauge 10 on Transverse Girder . . . . .	221
A-7	Hull 042 - Plan View of Cross Bracing showing Strain Gauges 7 & 9 on Longi- tudinal Girder and Strain Gauge 10 on Transverse Girder . . . . .	222
A-8	Hull 042 - Frame 24 Portal Top (Port Side Looking Forward) showing Strain Gauge 8 on Port Portal Top . . . . .	222
A-9	Hull 042 - Hull Inboard Profile showing Strain Gauge 11 on Keel at Frame 24.5	223
A-10	Hull 042 - Hull Inboard Profile showing Strain Gauges 12 & 13 on Keel at Frame 35.5 and 41.5 . . . . .	223
A-11	Hull 042 - Hull Frame 41 (Stb. Looking Aft) showing Detail of Strain Gauge 13 on Keel at Frame 41.5 . . . . .	224
A-12	Hull 042 - Fwd. Longitudinal Girder 4600/3840mm Off Centreline (Stb. Side Looking Inboard) showing Strain Gauge 15 on Lower Steel Post . . . . .	224

A-13 Hull 042 - Hull Section 24 showing Strain Gauge 16 on Cross Bridge Web . . .	225
A-14 Hull 050 - Profile View Guide to Detailed Drawings of Strain Gauge Locations	228
A-15 Hull 050 - Plan View Guide to Detailed Drawings of Strain Gauge Locations .	229
A-16 Hull 050 - Centrebow Hull Frame 69 (Looking Aft) showing Strain Gauge 1 on Top Rider at Frame 69 . . . . .	230
A-17 Hull 050 - Centrebow Hull Frame 67 (Looking Aft) showing Strain Gauge 2 on Top Rider at Frame 67 . . . . .	230
A-18 Hull 050 - Centrebow Hull Frame 66 (Looking Aft) showing Strain Gauge 3 on Top Rider at Frame 66 . . . . .	231
A-19 Hull 050 - Centrebow Hull Frame 65 (Looking Aft) showing Strain Gauge 4 on Top Rider at Frame 65 . . . . .	231
A-20 Hull 050 - Fwd. Longitudinal Girder 4500mm Off Centreline (Stb. Side Looking Inboard) showing Strain Gauges 5 & 6 on Fwd. and Aft Steel Diagonals and Strain Gauge 10 on Steel Posts . . . . .	232
A-21 Hull 050 - Plan View of Cross Bracing showing Strain Gauges 11 & 12 on Portal Top Crossing Bracing at Frames 23 and 41 . . . . .	232
A-22 Hull 050 - Section at 3450mm Off Centreline (Stb. Side Looking Inboard) showing Strain Gauge 13 on Steel Diagonal on Vehicle Deck . . . . .	233
A-23 Hull 050 - Hull Inboard Profile showing Strain Gauge 14 on Keel at Frame 49.5	233
A-24 Hull 050 - Hull Inboard Profile showing Strain Gauge 15 on Keel at Frame 40.5	234
A-25 Hull 050 - Hull Inboard Profile showing Strain Gauge 16 on Keel at Frame 24.5	234
A-26 Hull 050 - Hull Frame 49 (Looking Aft) showing Detail of Strain Gauge 14 on Keel at Frame 49.5 . . . . .	235

# List of Tables

2.1	Hulls 042 and 050 - Principal Parameters . . . . .	16
2.2	Hull 042 Instrumentation . . . . .	19
2.3	Hull 050 - System 1 Instrumentation . . . . .	22
2.4	Hull 050 - System 2 Instrumentation . . . . .	24
2.5	Slam Frequency of Occurrence Data for Head Seas, 10 - 15 knots . . . . .	39
2.6	Tunnel Heights - Hull 042 and Hull 050 . . . . .	44
3.1	Hull 050 Extreme Slam Event On Board Observations . . . . .	80
3.2	Hull 050 Loading at Extreme Slam Event . . . . .	80
3.3	Hull 050 Slam Event Details . . . . .	81
3.4	Hull 050 Longitudinal Bending Details . . . . .	87
3.5	Comparison of FE Analysis and Full-Scale Data for Extreme Slam Impact . . .	90
3.6	Proposed Extreme Slam Load Case for Hull 050 . . . . .	94
3.7	Hull 050 Slam Event Impact Loads . . . . .	96
4.1	Exciter Test Vessel Loading Conditions . . . . .	112
4.2	Hull 045 - Exciter Test Accelerometer Locations . . . . .	114
4.3	Hull 050 - Exciter Test Accelerometer Locations . . . . .	114
4.4	Exciter Test Average First Longitudinal Natural Frequencies . . . . .	116
4.5	Hulls 042/045 and 050 Loading Conditions . . . . .	129
4.6	Hull 042 and 050 Dry Natural Frequencies . . . . .	130
4.7	Hulls 042/045 and 050 Displacement and Added Mass . . . . .	132
4.8	Hull 050 - Effect of Added Mass Inclusion Techniques on Normal Mode Analysis Natural Frequencies . . . . .	139
4.9	Hull 050 - Effect of Added Mass Frequency on Natural Frequency . . . . .	140
4.10	Hull 050 - Effect of Including Added Mass Speed Influence on Natural Frequency	140
4.11	Hulls 042 and 050 - Wet Natural Frequencies . . . . .	141
4.12	Definitions of Damping Measures . . . . .	149
4.13	Hydrodynamic Damping Decay Factor Values . . . . .	159
4.14	Beam Section Decay Coefficient Values . . . . .	161

6.1 Comparison of Maximum FE Analysis and Full-Scale Data for Dynamic Extreme Slam Impact . . . . .	192
A.1 Hull 042- Strain Gauge Guide . . . . .	217
A.2 Hull 050- Strain Gauge Guide . . . . .	227

## Publications Relevant to the Thesis

A list of publications which are relevant to the thesis is given below:

- Thomas, G., Davis, M., Whelan, J. and Roberts, T. “Slamming Response of Large High Speed Catamarans.” In *FAST '01*, Vol. 3, Pages 97-107. September 2001.
- Thomas, G., Davis, M., Holloway, D. and Roberts, T. “Extreme Asymmetric Slam Loads on Large High Speed Catamarans.” In *6th Symposium of High Speed Marine Vehicles*, Pages I.15-I.23. September 2002.
- Thomas, G., Davis, M., Holloway, D., Watson, N. and Roberts, T. “Slamming Response of a Large High-Speed Wave-Piercer Catamaran.” *SNAME Marine Technology Journal*. Vol. 40, Number 2, Pages 126-140. April 2003.
- Holloway, D., Thomas, G. and Davis, M. “Boundary Element Methods in the Prediction of the Acoustic Damping of Ship Whipping Vibrations.” *International Congress on Industrial and Applied Mathematics*, July 2003.
- Holloway, D., Thomas, G. and Davis, M. “Added Mass of Whipping Modes for Ships at High Froude Number by a Free Surface Boundary Element Method Coupled with Strip Theory.” *International Congress on Industrial and Applied Mathematics*, July 2003.
- Thomas, G., Davis, M., Holloway, D. and Roberts, T. “Transient Slam Response of Large High Speed Catamarans.” In *FAST '03*, Vol. 2, Pages B1.1-B1.8. October 2003.
- Thomas, G., Davis, M., Holloway, D. and Roberts, T. “The Whipping Vibration of Large High Speed Catamarans.” Accepted for publication in *International Journal of Maritime Engineering* (RINA Transactions Part A), 2003.

# Chapter 1

## Introduction

### 1.1 Background

The requirement for fast and efficient sea transportation has led to the rapid evolution of large high-speed marine vehicles. Applications have primarily focussed on commercial ferry routes, providing transport options for passengers, cars, coaches and trucks. In addition, military needs based on the fast deployment of men and equipment have recently begun to be met by large high-speed vessels. Catamaran configurations have proved particularly popular for both commercial and military uses due to their ability to provide lightweight high-speed vessels with relatively large deadweights and deck areas.

In the 1970s and 1980s the original development of commercial high-speed catamarans was carried out by Incat Tasmania. The success of smaller passenger vessels, between 30m and 40m in length, led to the development of a 74m wave piercing catamaran in 1990 which was the first high-speed catamaran designed to include a car capacity. The desire of vessel operators to carry more passengers and cargo at higher speeds has seen the size of high-speed catamarans increase rapidly. Incat Tasmania has built vessels up to 98m in length (Fig. 1-1), whilst Austal Ships of Western Australia has developed a 101m vehicle-passenger catamaran (Fig. 1-2). To date the largest catamaran launched was the 125m long Stena HSS 1500 (Fig. 1-3) which commenced commercial operations in 1996. The increase in size of high-speed craft over recent years is illustrated in Fig. 1-4, where a high-speed vessel is defined as a commercially operating craft capable of carrying at least 50 passengers with a minimum service speed of 25 knots. This plot, which shows the maximum length of high-speed craft (monohull and catamaran) built in each calendar year, uses data collated from the worldwide industry magazine *Fast Ferry International* (1990 - 2000) [1].

The increase in size of vessels being built in recent years has given rise to new technical challenges. In particular, structural design optimisation has grown in importance with a strong focus on maintaining lightweight structures in order to carry adequate payloads and achieve



Figure 1-1: Incat 98m Catamaran



Figure 1-2: Austal 101m Catamaran



Figure 1-3: Stena 125m Catamaran

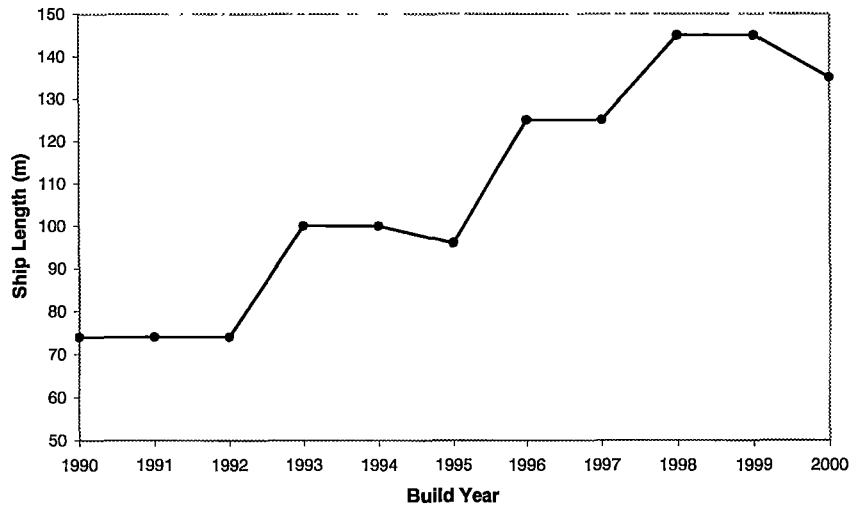


Figure 1-4: High-Speed Craft - Maximum Ship Length for Build Year

high operational speeds economically whilst preserving sufficient strength, often in more severe seas. Global loads have become increasingly more significant compared to local loads and knowledge of their effect on the structure of such vessels is required to carry out structural design. Classification societies have traditionally used an empirical approach to developing their design rules, based on years of operational experience. However the rapid development of these novel craft has meant that the rules have begun to lag behind the vessels' technological development. The use of direct calculations to estimate the expected operational loads by classification societies has increased as the vessels develop further away from the database of experiential knowledge.

The desire to structurally optimise the vessels has also seen a strong focus on the efficient utilisation of lightweight materials such as aluminium alloys for the construction of large fast vessels. The resulting hull structures tend to be more flexible making dynamic behaviour more pronounced. In turn this has increased the importance of estimating fatigue life of such vessels [2].

### 1.1.1 Design Aspects of Incat High-Speed Catamarans

In order to acquaint the reader with this novel type of craft a significant number of design aspects of Incat vessels are now introduced. These vessels have grown out of the desire to transport passengers and freight at high-speed, and to date their advantages over traditional monohull vessels have seen them used for both commercial and military applications. The major aim during the design process is to optimise the ratio of deadweight to lightship whilst maintaining structural integrity and achieving high vessel speed.

Much effort is therefore centred on the structural optimisation of the hull girder. In cross

section the vessel is essentially a dual box-like structure: the outer box incorporates the demi-hulls through to portals and horizontal cross bracing whilst the inner box consists of the deck, vertical cross bracing and longitudinal inboard structure, as shown in Fig. 1-5.

The majority of the longitudinal strength is gained from the aluminium longitudinal girders and vertical steel cross bracing. Steel is used for the vertical cross bracing to keep structural member dimensions to a minimum thus maximising the available vehicle deck space. The horizontal cross bracing, for which aluminium extrusions are used, takes the majority of the torsional and transverse loads, as shown in Fig. 1-6. Since the back of the vehicle deck is open for loading and unloading of vehicles, an opportunity is lost for additional strength in torsion. Therefore the aft bulkhead uses thick plate ( $\sim 40\text{mm}$ ) in order to absorb the load. The vessel's superstructure, which accommodates all the passenger lounges and operating bridge, is resiliently mounted onto the main hull girder using rubber mounts with the aim of reducing noise and vibration within the superstructure.

Incat catamarans have a distinct centrebow between the two demi-hulls at the front of the vessel. This is designed to counter deck diving in following seas and reduce vessel motions by providing a buoyancy force as the bow pitches into a wave. As a consequence, the vessels do not have a traditional flat wet-deck in the fore part of the vessel, rather a centrebow with an archway wet-deck on either side. The centrebow is usually between  $\frac{1}{3}$  to  $\frac{1}{4}$  of the length of the vessel, with the wet-deck aft of the centrebow being flat.

Propulsion is provided by two waterjets in each hull. Waterjets provide efficient propulsive coefficients at high-speed and also give the vessels good manoeuvrability without the need for rudders. A ride control system is usually fitted to the catamarans in order to reduce motions in rough seas. A computer system, which receives signals from motion sensors, directs hydraulic servo-mechanisms to continually adjust flaps and T-foils, producing forces that oppose the vessel motions. Reductions in motions of up to 50% are achievable.

## 1.2 Problem Definition

When a ship is operating in rough seas it may experience large relative motions between its hull and the water surface. An impact, known as a slam, may occur as the hull strikes the water surface upon re-entry of the keel after emergence. The shudder or vibration felt throughout the hull after a slam is known as whipping. As a consequence of slamming, local structural damage may occur in the area of impact. Extreme slams may impart sufficient global loads on the hull to cause major global structural damage. Such damage will have repercussions for the vessel builder and operator, with direct repair costs being incurred as well as a loss of earnings due to lost service time.

High-speed vessels tend to experience increased encounter frequencies and greater motions in head or bow quartering seas than slow-speed craft and are therefore more susceptible to

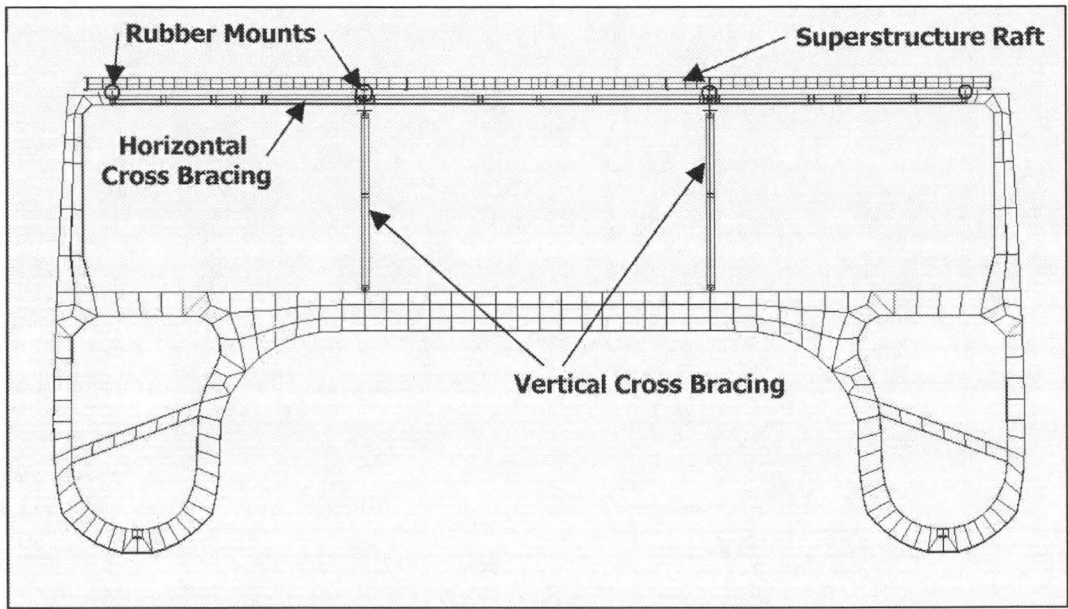


Figure 1-5: Cross Section of Incat Hull Girder showing Dual Box-Like Structure

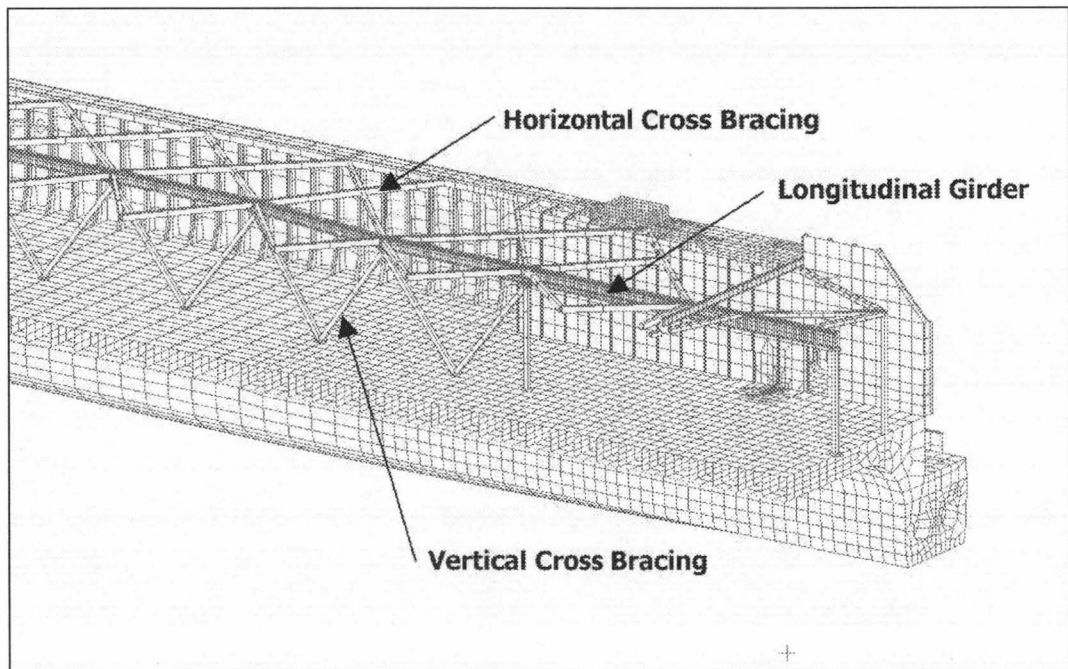


Figure 1-6: Cut Away Section of Incat Hull Girder (Starboard Side) showing Horizontal and Vertical Cross Bracing

slamming. Catamarans may be subject to an additional form of slamming known as wet-deck slamming. This occurs when the water surface impacts with the underside of the bridge structure between the two hulls and has the potential to cause both local and global damage.

There is an obligation on the designers of large high-speed catamarans to ensure that structural design is optimised so that the vessels remain light enough to travel at high-speed and carry large payloads, yet are strong enough to withstand severe ocean conditions. At times this conflict of requirements has led to problems and several large high-speed catamarans are known to have suffered damage due to slamming. Details on such incidents are usually difficult to obtain due to the desire of shipbuilders and operators to minimise publicity of such events. However, in January 1998 the Stena HSS “Discovery” experienced a slam during service operations across the North Sea which caused severe bow damage, as shown in Fig. 1-7. Rothe et al. [3] reported on wet-deck damage to an 86m Austal catamaran which included deformation of the longitudinal stiffeners.

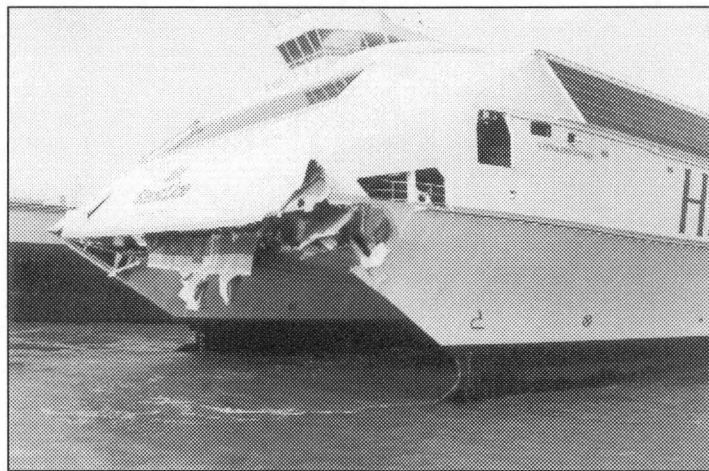


Figure 1-7: Bow Slamming Damage on Stena HSS “Discovery”

Slamming damage has been noted on several Incat vessels, particularly when operating in areas prone to rough seas. For example during delivery voyages from Australia to Europe and on service routes across Cook Strait in New Zealand and Bass Strait in Australia. Slam damage reported on Incat vessels has included the following:

- Localised dishing of plate in centrebow region between longitudinals and frames.
- Flattening and extensive distortion of longitudinal T-bars in centrebow.
- Side shell buckling at one third length aft of bow.
- Distortion of internal frames aft of centrebow.

Examples of slamming damage on Incat vessels are shown in Figs. 1-8 and 1-9.



Figure 1-8: Port Side Portal Buckling due to Slamming

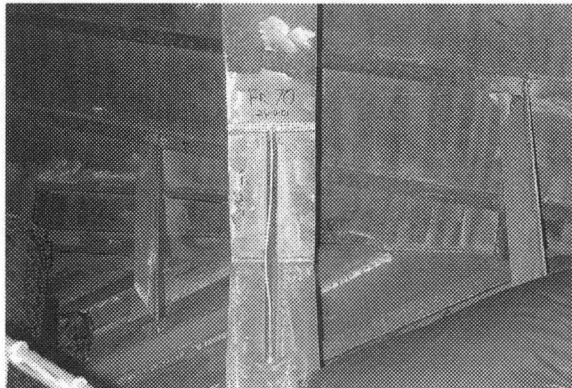


Figure 1-9: Tripped C- Bracket due to Slamming



Figure 1-10: Cracking Possibly due to Fatigue

In addition to local and global slamming damage, structural cracking, which is probably due to fatigue, has been found on Incat vessels, as shown in Fig. 1-10. As noted earlier, large high-speed vessels, due to the flexible nature of their hull girders, are especially susceptible to whipping vibrations following slam events. The corresponding vibratory stresses may be of equal order of magnitude to those induced by quasi-static wave bending moments, though they have a higher fundamental frequency. Hence whipping can make a very significant contribution to the total fatigue damage.

Unfortunately slam events on large high-speed catamarans are presently not well understood. Many questions in regard to their character and the effects of their occurrence may only be answered adequately through full-scale measurements on vessels operating in a range of conditions. In comparison to the extensive work conducted on slow and high-speed monohulls (for example [4], [5], [6]), little work has been conducted on full-scale motions and loads measurement of large fast catamarans<sup>1</sup>. Haugen and Faltinsen [7] conducted measurements on a small catamaran (30m in length), with respect to the local structural response, global motions and accelerations due to wetdeck slamming. A set of full-scale measurements was conducted by Steinmann et al. [8] on an 86m high-speed catamaran ferry. Strain gauges, accelerometers, gyroscopes and an on-board wave sensor were used to measure the global wave load hull stresses. The transient response of the vessel to slamming events was also recorded and presented. The present study arises from a joint measurement program, instigated by Incat Tasmania and the University of Tasmania, with the aim of investigating the motions and loads experienced by large high-speed catamarans. Incat Hull 038, an 81m wave piercing catamaran launched in 1995, was the first vessel to undergo strain gauge and vessel motion measurement in sea trials and during a delivery voyage [9]. The shipborne measurement systems used for Hulls 038 and 042 (launched in 1996) were introduced by Watson et al. [10] and preliminary results of vessel response transfer functions presented. A sample strain gauge time trace was shown which illustrated the dramatic increase in strain measurement during a typical slam event and the subsequent whipping behaviour.

Therefore, little has so far been established concerning the nature and influence of slam events of large high-speed catamarans. In particular, the environmental circumstances that give rise to slam occurrence are not known. Also the effect of vessel operating conditions, such as heading angle, speed and relative vertical velocity, on slam occurrence requires investigation.

There are a significant number of analytical tools available for calculating the global loads on a catamaran (examples are [11], [12], [13]). However fewer methods have been developed for the estimation of slamming loads on catamarans. Kvålsvold and Faltinsen [14] solved a two-dimensional boundary value problem in the time domain to determine the slamming pressure on the wet-deck of a catamaran. This method was further developed by Økland et

---

<sup>1</sup>In this chapter some references to previous work by other researchers are introduced. However, more complete reviews of available literature may be found in the introductions to subsequent chapters.

al. [15] and slam load predictions compared with slow-speed model test results. The authors concluded that whilst the calculation method described the physics of the complex problem of slamming correctly it resulted in a conservative slamming load. Haugen and Faltinsen [7] proposed a three-dimensional analysis for estimating wet-deck slamming loads and compared theoretical results with full-scale measurements on a 30m catamaran in wave heights up to 1.9m. Good agreement was found with the theory, although this agreement relied upon the impact velocity being estimated rather than being directly obtained from the measurements. The loads imparted on large high-speed catamarans by slam impacts are therefore not currently quantified satisfactorily. Classification societies do not have sufficient experiential knowledge to provide accurate design load cases to vessel designers. This is due to the rapid development of these novel craft which has tended to outpace the accumulation of full-scale data. It is clear from the incidents of structural damage experienced by a substantial number of high-speed large catamarans that the present design methodology is not adequate. Therefore a new practical methodology for the structural design of large high-speed catamarans in slamming conditions is required.

Knowledge of the dynamic structural response of large aluminium catamarans is also lacking. The whipping of relatively slow-speed monohulls has been investigated by various researchers through towing tank tests ([16], [17], [18]) and full-scale measurements ([4], [19]). Bishop and Price [20] established the basic principles of the hydroelastic theory for flexible beam-like hulls subject to steady state wave-induced loads. The theory was extended to include the response to transient loads such as slamming [21] [22]. Aksu used the impact theory of Stavovy and Chuang [23] to include the slam impact force on the under surface of the vessel and compared results favourably with full-scale trials measurements on a fast patrol boat. Research has been conducted at Marintek and the Norwegian University of Science and Technology into catamaran loads and in particular slam impact forces. The motions prediction theory of Faltinsen and Zhao [24] was generalised for modal analysis by Hermundstad et al. [25] [26] to estimate the whipping response of catamarans. The comparison of whipping frequencies between theory and experiment was found to be good. However the correlation of whipping magnitudes was less satisfactory. Despite this work the mode shapes and frequencies of the whipping behaviour of large high-speed catamarans are not known. A method is required for estimating the mode shapes and frequencies, including the fluid-structure interaction. There is also a paucity of understanding of the components that constitute the whipping behaviour damping, along with the total level of damping. In 1979 Bishop and Price [20] stated that with regard to hull damping 'The simple truth is that knowledge is abysmal'. Since the survey of Betts et al. [27] there appears to have been little progress in increasing knowledge of damping, particularly for modern fast lightweight vessels. Therefore further investigation into the levels of modal damping in ships and the relative magnitudes of its components is overdue.

Slamming and whipping may make a significant contribution to the fatigue [19] [28]. The effect of whipping was found to be significant on the predicted fatigue life of a small fast aluminium patrol boat by Olkinuora et al. [5] and Kannari et al. [29]. Hermundstad et al. [30] noted the importance of whipping behaviour on fatigue life through a study on the hydroelastic response of a high-speed monohull, and a long term statistical analysis was conducted to quantify the influence. Friis-Hansen et al. [31] [32] [33] developed a long-term probabilistic method to investigate the whipping of large fast monohulls. Through a numerical example of this method for a 35 knot 100m long aluminium monohull it was found that slamming and whipping may be an important factor with regard to fatigue life. However, the contribution of slamming and whipping on fatigue life has not yet been quantified for large high-speed catamarans.

### 1.3 Scope of Work

Bearing in mind the problems defined in the previous section, the following aims were proposed:

- Develop a new practical methodology for the structural design of large high-speed catamarans in slamming conditions.
- Improve understanding of slam events for large high-speed catamarans. In particular the nature and influence of slam events with respect to environmental and vessel operating conditions.
- Advance knowledge of the dynamic behaviour associated with the slamming of large high-speed catamarans i.e. the whipping response, in particular to develop and test techniques for estimating the whipping mode shapes and frequencies, including the fluid-structure interaction, and to determine the level of damping of the whipping behaviour and ascertain the magnitude of its various components.

Extensive full-scale hull stress, motion and wave measurements have therefore been conducted on two Incat high-speed catamaran ferries during a delivery voyage and regular service operations. A definition of a slam event for these vessels is proposed and used to identify slam events from the data records. The character and effects of these slamming events are investigated with respect to several factors including structural loading, wave height and length, vessel speed and heading angle, relative vertical velocity and frequency of occurrence. Particular attention is paid to the whipping response of the structure, with the principal structural response frequencies being identified through spectral analysis.

A realistic quasi-static slam load scenario for structural design purposes has been developed using the strain gauge data from the full-scale slam events, including an extreme slam event that caused extensive structural damage. This was achieved by correlating the peak slam stress levels with results obtained through finite element modelling. The global wave loading,

used as an input into the finite element model, is derived from a Froude-Krylov wave-induced load model. A method for scaling the design load case for use with new designs is also proposed and an example of its use presented.

A method for predicting the mode shape and frequency of the whipping behaviour using finite element analysis including the fluid-structure interaction is presented. The hydrodynamic added mass of the surrounding fluid was calculated using a two-dimensional panel method for a range of speeds. The effect of vessel loading on the whipping frequencies is also examined. The calculated whipping modes are then compared with those found through full-scale measurements and exciter experiments, and the results discussed. The level of damping of the whipping behaviour is investigated through full-scale results and exciter experiments. Methods for evaluating the various hydrodynamic components which constitute the damping are also presented including wavemaking damping, viscous damping and acoustic damping. The inherent damping capacity of the aluminium material, used to construct the high-speed catamarans, is also investigated experimentally.

The effect of slamming and whipping on fatigue life is estimated for a large high-speed vessel. Use is made of data from the full-scale trials to determine the influence of slam events, significant wave height, frequency of occurrence and slam maximum stress. Idealised slam events are also used to investigate the effect of whipping damping, rate of occurrence and slam peak stress.

A dynamic extreme slam design load case is developed using knowledge of the dynamic slamming response. This load case is based on time-varying loads and responses and is an extension of the quasi-static load case. This dynamic load case more realistically simulates the dynamic structural response of the vessel to a slam and is the core component of the practical methodology for the structural design of large high-speed catamarans for slamming.

## Chapter 2

# Full-Scale Trials Measurements

### 2.1 Introduction

Full-scale trials have been used extensively for the measurement of motions of conventional slow-speed monohulls when operating in seaways (for example [34], [35], [36], [37]). Such tests have been used predominantly to validate model test results and theoretical predictions. The measurement of loads on such vessels has also been far reaching, usually with the aim of rationalising hull structural design (examples are [38], [39], [40], [41]). The slamming of conventional monohulls has been the focus of a large number of full-scale measurement studies, including the work of Sellers [42], Nagai [43] and Aertssen [4]. For example, Aertssen used pressure transducers and strain gauges to measure slamming data in rough seas of four monohull cargo ships ranging in length from 130m to 230m. The data was used to estimate the effect of slamming on ship performance and predict slam induced stresses.

High-speed craft tend to experience increased wave encounter frequencies and greater motions than slow-speed vessels and are therefore more susceptible to slamming [2]. The majority of full-scale motions and loads measurement studies on high speed monohulls have thus focussed on slamming behaviour. The following studies are typical examples of full-scale measurements on high speed monohulls. Olkinuora et al. [5] and Kannari et al. [29] reported on sea trials of a 40m aluminium monohull patrol boat. Accelerations and stresses were measured with respect to wave height, ship speed and heading angle in order to evaluate the structural design, and conduct comparisons with simulated global stresses derived from a non linear strip theory. Full-scale motion, pressure transducer, strain gauge and wave measurements were made on a high-speed 9.5m monohull by Rosen and Garne [44]. Particular attention was paid to slamming events, which for this vessel were found to occur for virtually every wave encounter. Typical slamming pressures were found to exhibit short duration peaks and very short rise times, and the statistical distributions of the peak pressures were found to be different for the low level peaks (approximately a Rayleigh distribution) and the high level

peaks (approximately an Exponential distribution). An extensive monitoring system to collect structural, motion and wave data on-board the 128m high-speed monohull ferry “MDV Aries” was described by Grossi and Dogliani [45] and Iaccarino et al. [6]. The monitoring was used to assess design loads in terms of vertical accelerations, vertical bending moment and impact pressures and derive long term values for local and global loads. Racing yachts are also prone to slamming when sailing in exposed waters, as noted by Joubert [46]. A comprehensive set of measurements was recently conducted by Manganelli and Wilson [47] on-board two Open’60 and one Open’50 ocean racing yachts. These yachts are capable of sustaining steady speeds of more than 20 knots while sailing in rough seas. An array of accelerometers was used to give information on the rigid body motions and structural deformations. The use of pressure transducers was rejected due to the difficulty of providing adequate hull surface area coverage and the reluctance to have transducers fitted through the hull. Strain gauges were considered to be too hard to mount since the test boats were constructed of composite materials. Plots were derived from the collated data of peak accelerations versus wind angle and number of peak acceleration occurrences. Since no wave sensor was fitted to the yachts the encountered wave field was obtained by combining results from a computational wave model and satellite altimeter measurements.

By comparison little work has been conducted on full-scale motions and loads measurement of large fast catamarans. Haugen and Faltinsen [7] reported on measurements conducted on a small catamaran (30m in length) with respect to wetdeck slamming. Strain measurements were carried out to investigate the local structural response of the wetdeck, along with global motions and accelerations. The classification society DNV regulations stated that the tunnel height (vertical distance between the wetdeck and the design waterline) of the catamaran should be 1.81m in order to avoid wetdeck slamming in sea states of up to significant wave height of 3m. This tunnel height requirement was satisfied for the vessel though slamming was found to occur in significant wave heights equal to half of the maximum operational significant wave height with stress levels close to half of the yield stress being recorded. Typical strain time histories were presented and the stress levels compared with those predicted through hydroelastic plate theory. Good agreement was found, although this agreement relied upon the impact velocity being estimated, by combining the vessel speed and the vertical velocity of the bow, rather than being directly obtained from the measurements. A set of full-scale measurements was conducted by Steinmann et al. [8] on an 86m high-speed catamaran ferry constructed by Austal Ships, Western Australia. Strain gauges, accelerometers, gyroscopes and an on-board wave sensor were used during a delivery voyage from Australia to Turkey. The primary objective of the study was the measurement of global wave load hull stresses, however the transient response of the vessel to slamming events was also captured. The preliminary analysis of the results showed that there were significant differences between some current design loads, as stipulated by classification societies, and the results of the full-scale

measurements. In particular the transverse split load towards the aft of the vessel was found to be small. Sample stress time traces of slam events for various strain gauge locations were presented and these clearly illustrated the whipping nature of the dynamic response of the hull girder. The frequencies of the whipping responses were derived through spectral analysis and it was proposed that the principal modal frequency of the vessel identified at 2.8 Hz was due to global longitudinal bending. These presented examples of full-scale measurement programs are indicative of the limited data available on which classification society rules for large high-speed catamarans are based. Jensen et al. [48] conducted a series of full-scale measurements on a 47m long twin hull surface effect ship using fibre optic strain sensors. Whilst operating in head seas in sea state 6-7 the vessel experienced impacts which were described as being “like something between bow flare slamming and frontal/wet-deck slamming”. During such an impact the measured global sagging moment amidships exceeded the DNV design value by a factor of 2.1.

The present study arises from a joint measurement program, instigated by Incat Tasmania and the University of Tasmania, with the aim of investigating the motions and loads experienced by large high-speed catamarans. Incat Hull 038, an 81m wave piercing catamaran, was the first vessel to undergo strain gauge and vessel motion measurement in sea trials and during a delivery voyage. Roberts et al. [9] presented preliminary results of longitudinal bending and split load measurements, and concluded that stresses may increase by 500% over the global load stresses during slam events. The conservative nature of the split load as prescribed by the classification society DNV was addressed and a reduction of the design split load of 50% was proposed. The shipborne measurement systems used for Hulls 038 and 042 were introduced by Watson et al. [10] and introductory results of vessel response transfer functions presented. A sample strain gauge time trace was shown which illustrated the dramatic increase in strain measurement during a typical slam event and the subsequent whipping behaviour. Work by Yakimoff [49] and Roberts et al. [50] used the Hull 042 full-scale data to develop a wave sagging load case which was approximately 63% of the DNV rule moment. Preliminary fatigue analysis results were also presented which showed that slamming made a large contribution to accrued fatigue damage.

The paucity of full-scale information on the slamming of large high-speed catamarans is therefore apparent, particularly with respect to evaluating the effect of slamming on the structural design and the overall nature and influence of slam events. Analysis of extensive full-scale hull stress, motion and wave measurements from Incat Hulls 042 and 050 has therefore been conducted with regard to slamming events. The primary aim was to provide detailed information which may be used in the development of a practical methodology for the structural design of large high-speed catamarans when operating in slamming conditions. Therefore factors which may influence the structural design of such craft when exposed to slamming, in terms of ultimate strength and fatigue life, are of specific interest. In particular issues

addressed include:

- What environmental and vessel operating conditions give rise to slam occurrence?
- How do slam events affect the vessel's structure?
- What is an extreme slam event?
- What is the frequency of slam occurrence?
- What is the frequency and damping of the whipping behaviour?

A definition of a slam event for these vessels was therefore developed and this was used to identify slam events from the data records. Key outcomes from the subsequent analysis of the slam events included identifying the influence of the encountered wave conditions, vessel operating conditions and the resulting stresses at various structural locations. This data gives valuable information for estimating the influence of slamming on the ultimate strength and fatigue life of large high-speed catamarans. Results from an extreme slam event, which caused extensive structural damage, are reported and provide the basis for development of quasi-static and dynamic load cases.

Particular attention was also paid to the dynamic response of the vessels' structures, with the principal structural response frequencies being identified through spectral analysis and the decay coefficients of the whipping behaviour being estimated. In addition to giving fundamental details on the dynamic behaviour of this novel type of craft, these results contribute towards the development of a dynamic slam load case and the estimation of the influence of slamming and whipping on fatigue life.

Whilst not central to the principal aim of this study, further aspects of the slamming behaviour reported on include: the number of waves encountered between slam events and their relative magnitude; the timing of the change of direction of bow vertical movement during a slam event and the identification of slam events that are a result of wave impact with the vessel wet-deck.

## 2.2 Vessel Details, Measurement Systems and Location of Trials

### 2.2.1 Vessel Details

Incat Hulls 042 and 050, pictured respectively in Figs. 2-1 and 2-2, are high-speed aluminium ferries constructed by Incat Tasmania. They are wave piercer catamarans with prominent centre bows. The principal parameters of the vessels are shown in Table 2.1.

Although 10m longer overall than Hull 042, Hull 050's lightship increased by only 20 tonnes whilst its deadweight increased by 425 tonnes. This gives Hull 050 a significantly greater ratio of deadweight to lightship, 97.5% compared with 49.5% for Hull 042. There are several reasons for this improvement. Firstly, the resiliently mounted superstructure of Hull 050 is a compact design with only one full level and a small bridge deck; secondly, the forward section of the vehicle deck is an open structure removing the need for a foredeck; thirdly, the use in construction of an aluminium with a high magnesium content assisted in reducing the structural mass. Hull 050 has the same overall beam as Hull 042 whilst there are increases of hull beam and draft.

	<b>Hull 042</b>	<b>Hull 050</b>
Length overall	86.6 m	96.0 m
Length waterline	76.4 m	86.0 m
Beam overall	26.0 m	26.0 m
Draft	3.50 m	3.70 m
Hull beam	4.33 m	4.50 m
Lightship	840 tonnes	860 tonnes
Deadweight	415 tonnes	840 tonnes
Speed, fully loaded condition	40 knots	40 knots
Main engines	Four Alstom/Ruston 20RK270 marine diesel engines. 7080kW each @ 1030rpm.	Four CAT 3618 marine diesel engines. 7200kW each @ 1050rpm.
Propulsion	Water Jets - 4 Lips LJ145 D waterjets	Water Jets - 4 Lips 150 D waterjets

Table 2.1: Hulls 042 and 050 - Principal Parameters

### 2.2.2 Monitoring System Instrumentation and Data Acquisition

#### 2.2.2.1 Hull 042

A single monitoring system was fitted to the vessel. The system was designed primarily to measure the motions and global loads experienced by the vessel. However, the data gathered was also suitable for the analysis of slamming events. The monitoring system for Hull 042 was designed and installed by Mr. Glen Mayhew and Mr. Nigel Watson of the University of Tasmania.



Figure 2-1: Incat Hull 042, 86m Catamaran



Figure 2-2: Incat Hull 050, 96m Catamaran

The system comprised strain gauges fitted at 16 locations around the vessel. Drawings of the exact locations of the strain gauges are shown in Appendix 1. A guide to the strain gauge locations is also shown in Fig. 2-3. The general purpose CEA series 350 ohm strain gauges were set up in a quarter bridge with a three wire connection. Bridge completion resistors were fitted to the DBK43 strain gauge module of the IOTECH hardware and an excitation voltage of 5 volts utilised. Each channel was individually calibrated using the shunt resistor method to  $\pm 5$  volts full scale. Minimal drift was found to occur through the service life of the strain gauges since they were located in temperature steady locations within the structure. Dynamic strain measurements do not require compensation for drift since the dynamic range is being investigated not absolute values.

An on-board radar based wave meter, supplied by TSK, was fitted to the bow of the vessel on the centreline, to give a reading of instantaneous distance to the water surface and (by using differences with ship motion) the absolute wave height (the sign convention for the TSK is positive vertically upwards). Accelerometers were fitted at the bow, centre of gravity and transom of the vessel to measure vertical accelerations whilst inclinometers were used to measure roll and pitch motions. The speed of the vessel was also measured using an on-board GPS. The installation of pressure transducers to indicate when a slam event occurred was considered. However the large number that would be required to ensure that an impact was measured, due to the wide spatial variation in impact pressure during a slam, precluded their use.

The data channels were recorded at 20 Hz using an IOtech Daqbook controlled by a PC. This sampling frequency was chosen because the main emphasis of the Hull 042 monitoring program was on the data collection of lower frequency global loads as opposed to high frequency slamming loads. Whilst this frequency was deemed sufficient to capture the slam events, an increased sampling frequency was subsequently utilised for the monitoring system on Hull 050.

The Daqbook was programmed to start recording when the vertical acceleration reading at the bow exceeded a preset threshold of 1.35g. Each record was for 4096 samples which gave a data segment of 204 seconds length. The details of each data channel are shown in Table 2.2. Although the vessel was monitored for a period of 10 months including the delivery voyage and services across the English channel, only the initial four days of the delivery voyage data has been analysed in detail. This part of the voyage was non stop, during which time a total of 787 data files were recorded. These data files were numbered Dec11 to Dec988. Further details on the data collected may be found in Thomas [51].

On-board observations were made by the crew during the monitoring trials of the swell heading relative to the vessel heading.

Channel Number	Description
0	Bow vertical accelerometer
1	LCG vertical accelerometer
2	Aft vertical accelerometer
3	Pitch inclinometer
4	Roll inclinometer
5	TSK wave meter: ship displacement
6	TSK wave meter: relative wave height
7	TSK wave meter: instantaneous wave height
8	TSK wave meter: instantaneous wave height derived
9	TSK wave meter: significant wave height
10	Strain Gauge: Fitted to port steel chevron brace at frame 2
11	Strain Gauge: Fitted to starboard steel chevron brace at frame 2
12	Strain Gauge: Fitted to aft transverse box, top, at frame 14
13	Strain Gauge: Fitted to aft transverse box, bottom, at frame 14
14	Strain Gauge: Fitted to inner cross brace at frame 14
15	Strain Gauge: Fitted to bat wing on cross brace at frame 17
16	Strain Gauge: Fitted to longitudinal girder at frame 24, 4600 off CL
17	Strain Gauge: Fitted to port portal top at frame 24
18	Strain Gauge: Fitted to longitudinal girder at frame 32, 4600 off CL
19	Strain Gauge: Fitted to transverse girder at frame 35
20	Strain Gauge: Fitted to keel plate at frame 24.5
21	Strain Gauge: Fitted to keel plate at frame 35.5
22	Strain Gauge: Fitted to keel plate at frame 41.5
23	Strain Gauge: Fitted to starboard steel post at frame 54
24	Strain Gauge: Fitted to port steel post at frame 54
25	Strain Gauge: Fitted to cross bridge web at frame 24
26	Roll inclinometer
Note: There are 68 frames in total, numbered from the transom	

Table 2.2: Hull 042 Instrumentation

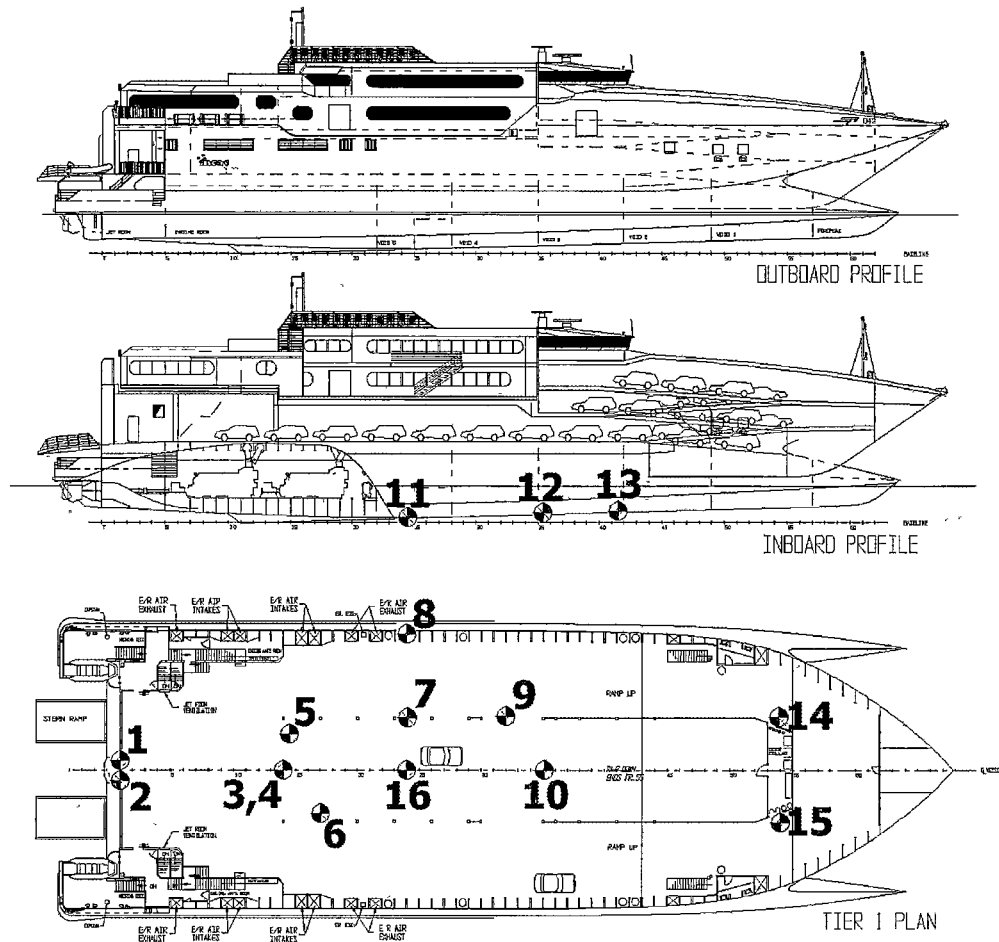


Figure 2-3: Hull 042 - Strain Gauge Locations

**KEY**

Number	Location	Number	Location
1	Port steel chevron brace at frame 2 on CL	9	Longitudinal girder, 4600mm off CL, at frame 32
2	Stb. steel chevron brace at frame 2 on CL	10	Transverse girder at frame 35 on CL
3	Top aft transverse box at frame 14 on CL	11	Stb. hull keel at frame 24.5
4	Bottom aft transverse box at frame 14 on CL	12	Stb. hull keel at frame 35.5
5	Inner x-brace at frame 14	13	Stb. hull keel at frame 41.5
6	Bat wing on x-brace at frame 17	14	Port steel post at frame 54
7	Longitudinal girder, 4600mm off CL, at frame 24	15	Std. steel post at frame 54
8	Port portal top at frame 24	16	Cross bridge web at frame 24 on CL

### 2.2.2.2 Hull 050

Two monitoring systems were fitted to Hull 050. The aim of System 1 was to measure the response of the vessel to slam events, whilst System 2 was designed primarily to gather information on the global loads and motions experienced by the vessel. Data collected using System 2 was also incorporated into the slam event analysis. The monitoring systems for Hull 050 were designed and installed by Mr. Tim Roberts and Mr. David Harcourt of Incat Tasmania.

**System 1** System 1 comprised strain gauges fitted at 8 locations in the forward part of the vessel. These gauges were identical to those utilised on Hull 042 and similar set-up and calibration techniques were employed. Drawings of the exact locations of the strain gauges are shown in Appendix 1. A guide to the strain gauge locations is also shown in Fig. 2-4. An on-board radar based wave meter, supplied by TSK, was fitted to the bow of the vessel on the centreline, to give a reading of instantaneous absolute wave height. Two ultra sonic wave sensors, supplied by the University of Tasmania, were also fitted to the vessel. However their data was not used in the analysis process.

The 11 data channels were recorded at 100 Hz using an IOtech Daqbook controlled by a PC. This sampling frequency was chosen to provide an increased number of data points surrounding the slam peak than was possible with the 20 Hz sampling rate utilised in the Hull 042 monitoring system. This sampling rate proved to give enhanced definition of the slam peaks and it is recommended that all future monitoring of full-scale slam events use this rate as a minimum.

The Daqbook was programmed to start recording when the instantaneous TSK wave height reading exceeded a preset threshold of 2.5m. After one month of monitoring this threshold was increased to a wave height of 3m in order to reduce the amount of collected data. Each record was for 1800 samples which gave a data segment of 18 seconds length, including 6 seconds of data from before the threshold was reached, which was stored in the buffer. The details of each data channel are shown in Table 2.3.

**System 2** System 2, used primarily for the measurement of global loads and motions, comprised strain gauges fitted at 8 locations around the vessel. These gauges were identical to those utilised on Hull 042 and similar set-up and calibration techniques were employed. Again detailed drawings are shown in Appendix 1, with a guide to the strain gauge locations in Fig. 2-4. The TSK on-board radar based wave sensor was also incorporated into this system giving readings of instantaneous wave height, ship vertical displacement, relative wave height and running significant wave height. The TSK calculated significant wave height was based on a six minute running average. A tri-axial accelerometer was fitted close to the centre of gravity of the vessel to measure heave, surge and sway accelerations. The speed of the vessel was also

measured using an on-board GPS.

The 16 data channels were recorded at 20 Hz using an IOtech Daqbook controlled by a PC, located in the electronics room close to the bridge. The Daqbook was programmed to start recording at the same thresholds as System 1. Each record was for 1800 samples which gave a data segment of 90 seconds length. The details of each data channel are shown in Table 2.4.

**Summary of Data Collected** System 1 data was collected between April and November 1999. System 2 data collection also commenced in April 1999 but continued on until January 2000. It should be noted that the two systems had different logging rates and were triggered and operated independently so the records were not synchronised. However, characteristic features of the records did make it possible to establish an approximately common time origin. The systems were not linked since they were originally designed for different purposes: system 1 was designed to collect data on slam loadings whilst system 2 was designed to measure global loads and motions. Further details on the data collected may be found in Thomas [52]. The slam analysis was only conducted for the time period for which both systems were operating.

**On-board Observations** Intermittent on-board observations were made by the crew during the monitoring period. These observations included: sea height and period, swell height and period, combined wave height, engine rpm, vessel speed, wind speed and direction, swell heading relative to vessel heading and significant wave height.

Channel Number	Description
0	Strain Gauge: Fitted on frame 68 on the top rider in the centrebow, on the centreline
1	Strain Gauge: Fitted on frame 67 on the top rider in the centrebow, on the centreline
2	Strain Gauge: Fitted on frame 66 on the top rider in the centrebow, on the centreline
3	Strain Gauge: Fitted on frame 65 on the top rider in the centrebow, on the centreline
4	Strain Gauge: Fitted on forward diagonal on starboard side, approximately at frame 62.
5	Strain Gauge: Fitted on aft diagonal on starboard side, approximately at frame 59.
6	Strain Gauge: Fitted on forward diagonal on port side, approximately at frame 62.
7	Strain Gauge: Fitted on aft diagonal on port side, approximately at frame 59.
8	TSK wave meter
9	University of Tasmania wave meter 1
10	University of Tasmania wave meter 2
Note: There are 70 frames in total, numbered from the transom	

Table 2.3: Hull 050 - System 1 Instrumentation

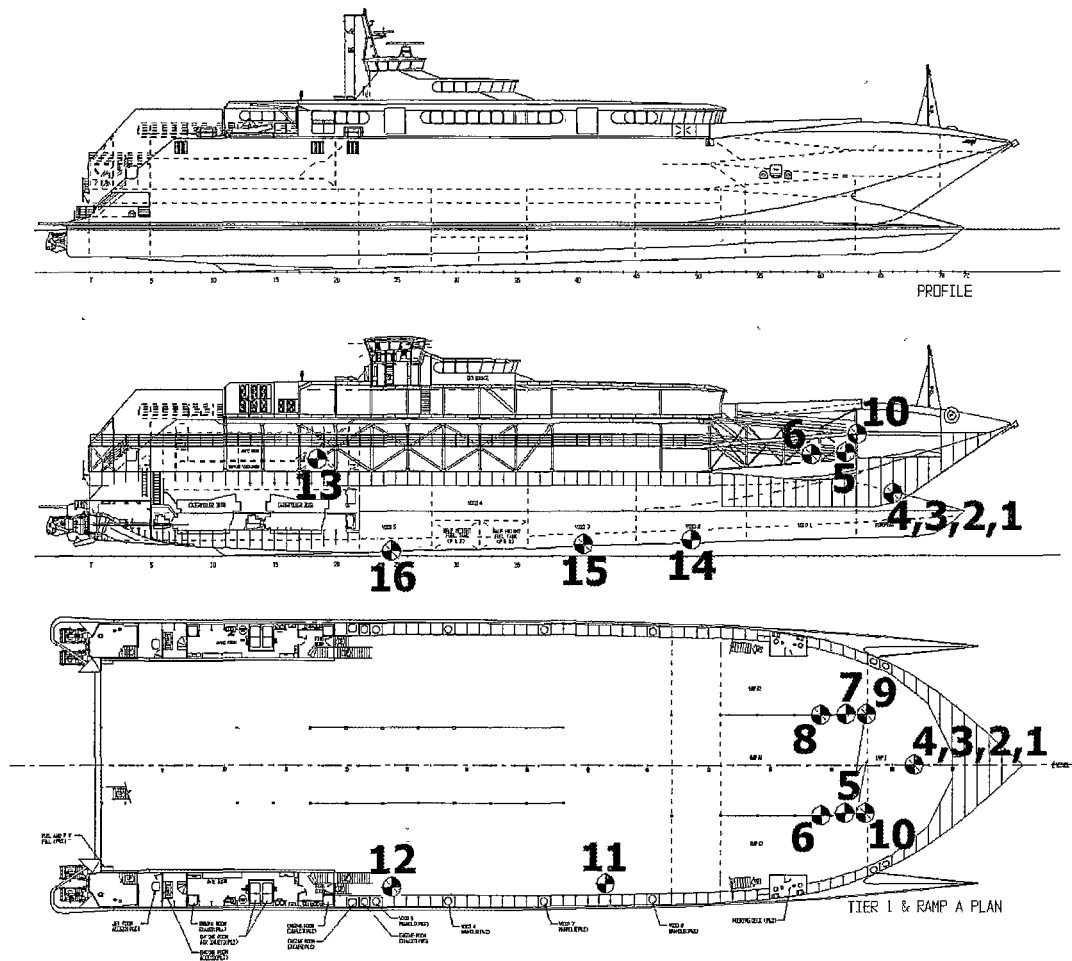


Figure 2-4: Hull 050 - Strain Gauge Locations

**KEY**

SYSTEM 1		SYSTEM 2	
Number	Location	Number	Location
1	Top rider at frame 69 on CL	9	Port lower steel post at frame 63
2	Top rider at frame 67 on CL	10	Stb. lower steel post at frame 63
3	Top rider at frame 66 on CL	11	Stb. portal x-brace at frame 41
4	Top rider at frame 65 on CL	12	Stb. portal x-brace at frame 23
5	Stb. fwd diagonal at frame 62	13	X-brace vehicle deck
6	Stb. aft diagonal at frame 59	14	Stb. hull keel at frame 49.5
7	Port fwd diagonal at frame 62	15	Stb. hull keel at frame 40.5
8	Port aft diagonal at frame 59	16	Stb. hull keel at frame 24.5

Channel Number	Description
0	Strain Gauge: Fitted on port lower steel post at frame 63
1	Strain Gauge: Fitted on starboard lower steel post at frame 63
2	Strain Gauge: Fitted on starboard portal cross brace at frame 41
3	Strain Gauge: Fitted on starboard portal cross brace at frame 23
4	Strain Gauge: Fitted on starboard vehicle deck cross brace at frame 19
5	Strain Gauge: Fitted on starboard keel at frame 49.5
6	Strain Gauge: Fitted on starboard keel at frame 40.5
7	Strain Gauge: Fitted on starboard keel at frame 24.5
8	Accelerometer: z axis
9	Speed log
10	Accelerometer: x axis
11	TSK wave meter: instantaneous wave height
12	Accelerometer: y axis
13	TSK wave meter: significant wave height
14	TSK wave meter: vertical ship displacement
15	TSK wave meter: relative wave height
Note: There are 70 frames in total, numbered from the transom	

Table 2.4: Hull 050 - System 2 Instrumentation

## 2.2.3 Location of Trials

### 2.2.3.1 Hull 042

Full-scale measurements were conducted on Hull 042 for the complete delivery voyage from Sydney, Australia to Portland, United Kingdom (via Fremantle, Western Australia) and for 10 months of service operations across the English Channel. During the portion of the trip from Fremantle to Portland several of the strain gauges malfunctioned which resulted in the data not being suitable for slam analysis, whilst the service operation data tended to be for small wave heights and thus few slams were found in the data. Therefore the detailed slam analysis was carried out on the portion of the delivery voyage from Sydney, New South Wales to Fremantle, Western Australia. The route from Sydney to Fremantle is predominantly through open ocean and is likely to expose a vessel to rough sea conditions. Indeed Hull 042 encountered a large southerly swell which resulted in severe conditions whilst travelling south down the New South Wales coast from Sydney.

### 2.2.3.2 Hull 050

The full-scale measurements of Hull 050 were conducted during normal scheduled ferry crossings across Cook Strait between the North and South Islands of New Zealand. Two return crossings were scheduled daily between Wellington and Picton, with the duration of each crossing approximately 100 minutes. As can be seen in Fig. 2-6, which shows a map of the route, the location is open to swell action from both the north and the south.

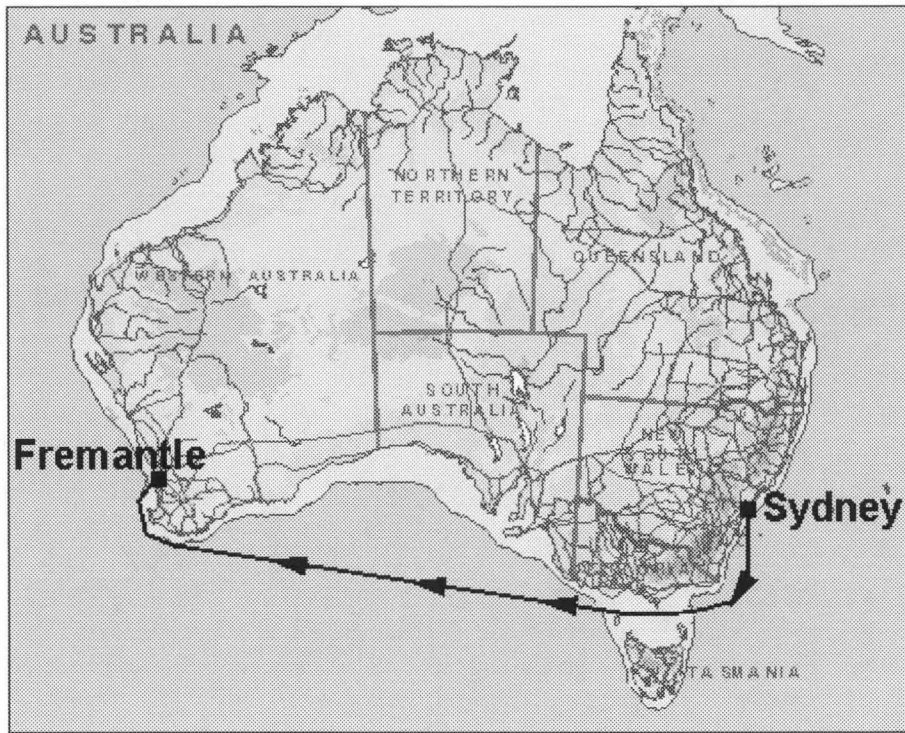


Figure 2-5: Map of Hull 042 Delivery Route between Sydney and Fremantle

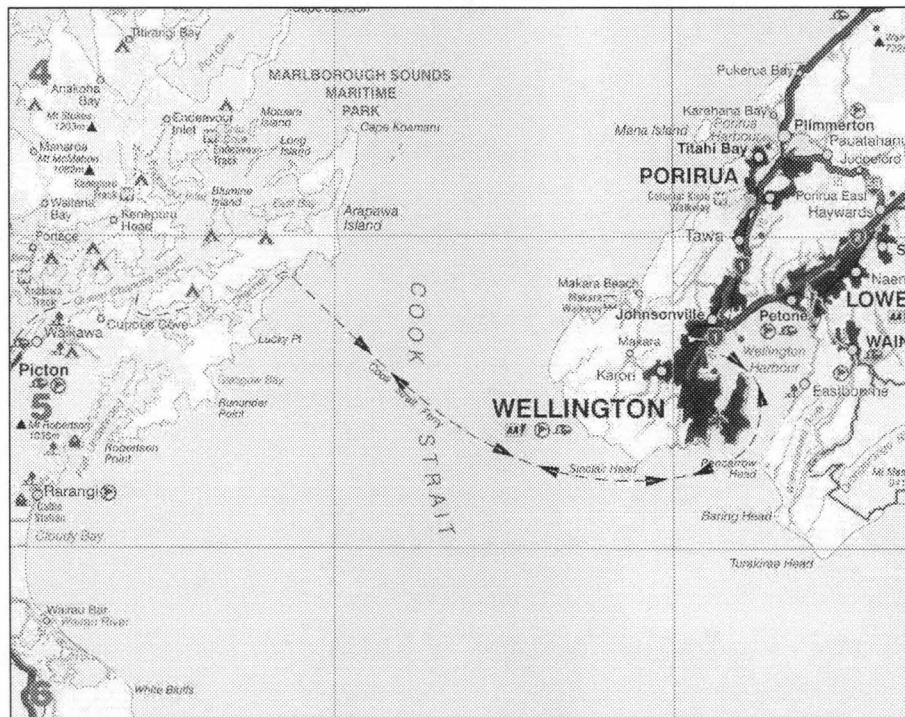


Figure 2-6: Map of Hull 050 Service Route between Wellington and Picton

## 2.3 Data Analysis

### 2.3.1 Slam Definition

Samples of the raw data from the Hull 042 strain gauges during a slam event are shown in Fig. 2-7 which clearly illustrate the initial dynamic impact loading due to a slam event, at time = 167 seconds, and the subsequent whipping of the structure. Whipping is the vibratory response of the hull girder induced by a slam event. It is interesting to note the different whipping behaviour for a variety of strain gauge locations: the steel chevron brace and the inner cross brace appear to have particularly high levels of whipping stress compared to their steady state global loading fluctuation. The underlying global loads due to the waves can also be clearly seen.

Similar behaviour may be seen in the sample strain gauge traces from Hull 050 during a slam event shown in Fig. 2-8. Again the different whipping behaviour for the gauges should be noted; the cross brace at frame 41 appears to have particularly high levels of whipping compared to its steady state global loading fluctuation. In fact this gauge picked up large levels of whipping even when slam events did not occur. This can be seen in Fig. 2-9(a) which shows a complete time record for this gauge with only one slam event occurring at 30 seconds (the same slam event as shown in Fig. 2-9(d)). Occasionally the gauges did not display whipping behaviour after a slam event, as can be seen by the frame 67 top rider raw data shown in Fig. 2-9(b). For this particular slam event none of the strain gauges located in the centrebow exhibited whipping, however whipping was found in gauges located further aft in the vessel. The reason for the absence of whipping behaviour in certain structural locations after some slam events is not known, however it may be due to changes in the fluid added mass distribution of the surrounding water altering the damping of the vessel structure. This would vary according to the hull immersion.

In order to clearly differentiate the slam events from the global sea loads, and allow slam events to be identified irrespective of the underlying global loading, the raw data records were highpass filtered at 0.6 Hz. A value of 0.6 Hz was chosen to ensure that the global wave load signal at approximately 0.2 Hz was removed from the data whilst the high frequency slam data was preserved. The effect of this process on the data records can be seen with the corresponding filtered signal for the strain gauge on the top rider at frame 67 of Hull 050 shown in Fig. 2-10.

A slam is a rapid application of load on a vessel due to bottom impact, bow flare impact or wet-deck impact of the vessel with the water [53]. In order for slam events to be identified in the data records it was necessary first to define what constituted a slam event for this vessel. The strain gauge data was used to define a slam since it ensured that only events which had an appreciable effect on the vessel structure were included in the definition.

The practical difficulty of identifying slam events may be seen by examining Fig. 2-11.

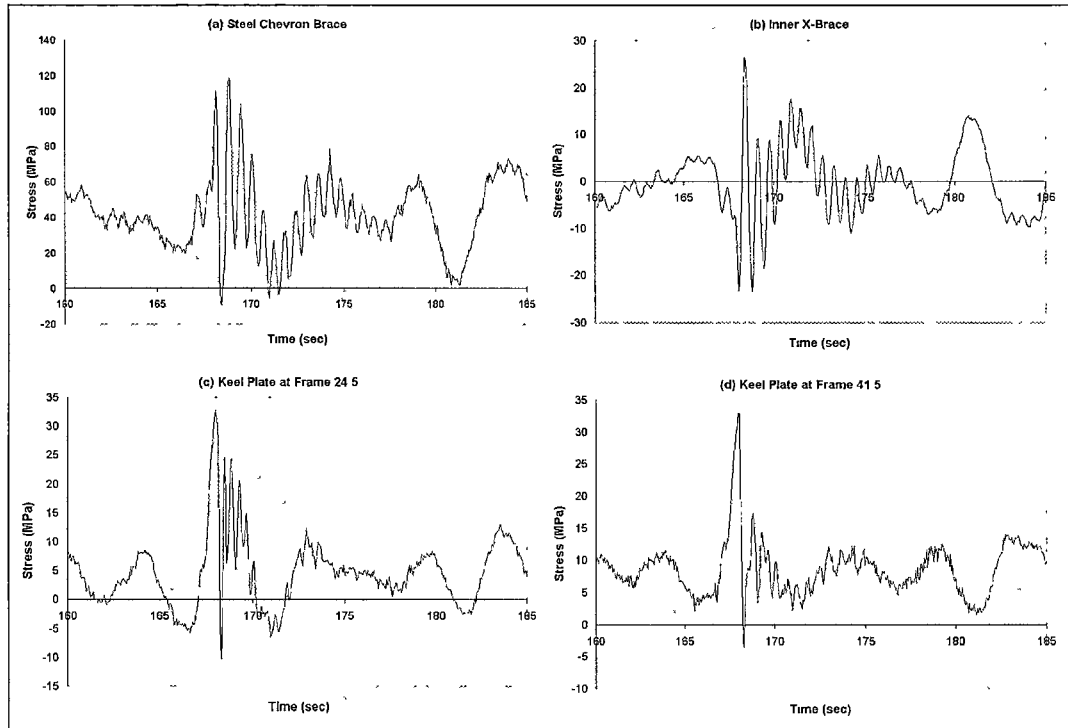


Figure 2-7: Hull 042 - Typical Raw Strain Gauge Data Traces

Slam A is clearly a slam event and would be easy to identify with a large number of different definition techniques. However, whilst it is proposed that slam B is also a slam event, due to its small peak size it may be difficult to classify as a slam using certain definitions. There are many possible methods that may be used to define a slam event each with their own advantages and disadvantages. For example the simplest identification method would be to use a maximum stress criterion, where peaks with stress levels above this criterion are classified as slam events. The drawback with using a stress level criterion is that stress peaks with low rates of change of stress (as may be for example be present in the global underlying wave loading in large waves) would be identified as slams, whilst small slam events, with peaks less than the threshold, may not be identified. Another possible method for identifying slam events is to compare the stress level of a stress peak to the standard deviation of the global loading stress. However, this method means that the criterion changes as the sea conditions change and small slams in large global loading conditions are precluded from identification. It was therefore decided that a definition orientated towards identifying stress peaks with high rates of change of stress prior to the peak would be used. This would enable all events where the loading, as measured by the strain gauges, increased at a rate greater than a specified threshold rate limit would be identified as slam events. This measure was applied to the filtered signal to ensure that slam events with small maximum stress levels that may occur in large sea states, but which are dominated by the global loads, may be identified. For example

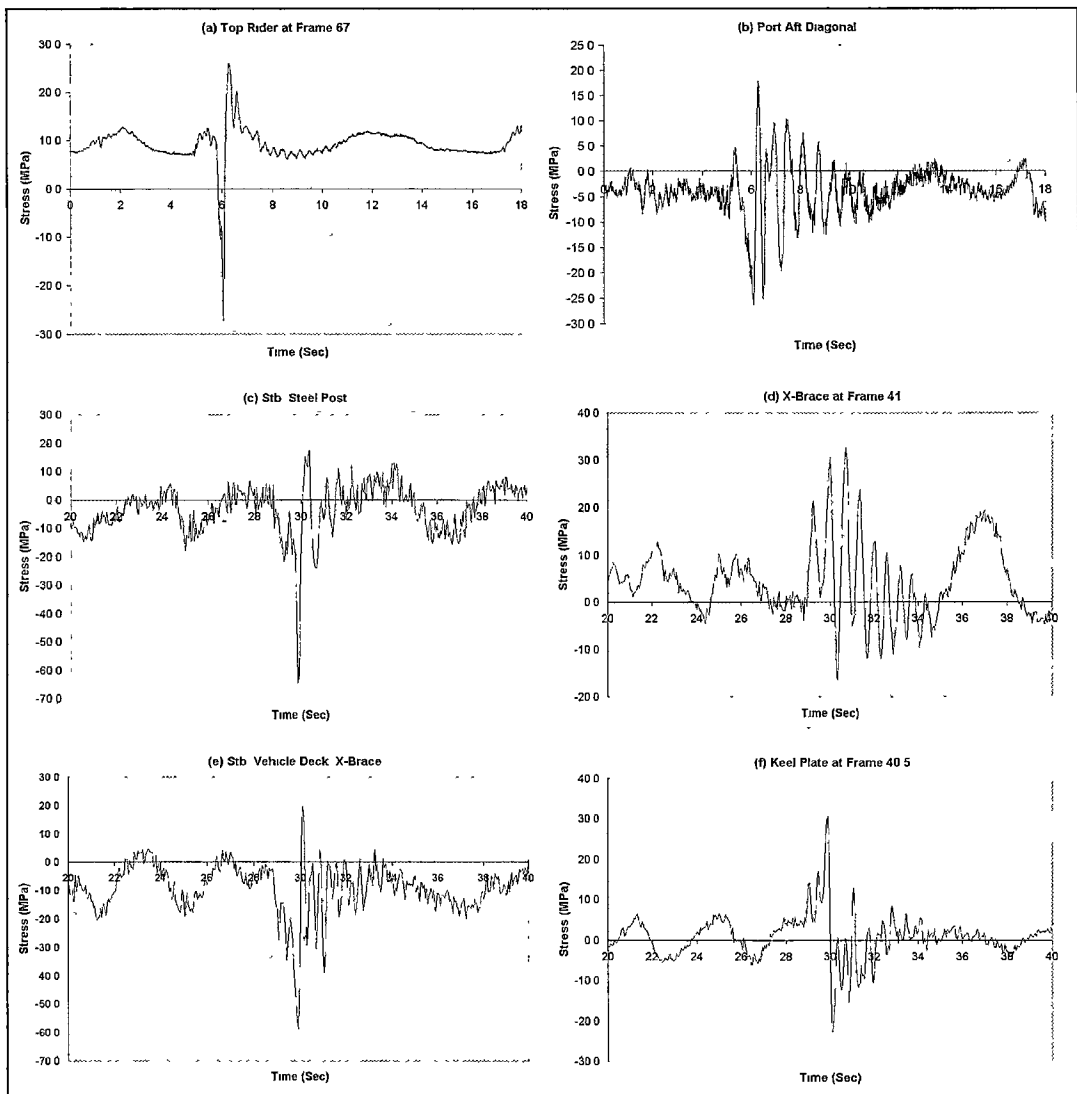


Figure 2-8: Hull 050 - Typical Raw Strain Gauge Data Traces

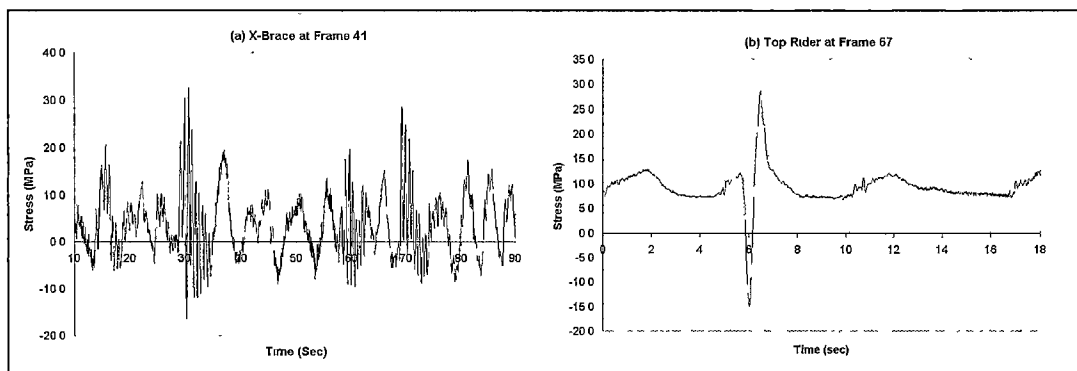


Figure 2-9: Hull 050 - Typical Raw Strain Gauge Data Traces

in Fig. 2-10(a) the event which occurs at time = 42 seconds, although having a maximum stress only equivalent to the cyclic global loading range, has been identified as a slam event due to its rapid rate of loading. The use of a solely rate based criterion for the slam definition ensured that all high rate loading events were identified independently of the maximum stress level reached during the event.

A slam was therefore defined as having occurred if a peak in the stress record occurred with

$$\left(\frac{d\sigma}{dt}\right)_c \geq R_c \times \text{yield stress} \quad \text{MPa/s} \quad (2.1)$$

where  $\left(\frac{d\sigma}{dt}\right)_c$  is the maximum rate of change of stress prior to the peak and  $R_c$  is the rate constant which has the units  $\text{sec}^{-1}$ . Note that for this analysis the yield stress of aluminium  $\approx 100$  MPa. The original intention was to normalise the rate threshold by the stress peak of the individual slam, since generally it appeared that the rate of change of stress for the larger slams was greater than for the smaller slams. However, using such a criterion meant that some large slams, which did not increase in rate as rapidly as their peak suggested, fell outside the slam definition. It also meant that a very large number of very small events were defined as slams since the rate criterion was too easily complied with for small peak stress events.

The next applied problem was selecting an appropriate value of the rate constant,  $R_c$ . Firstly the number of slams identified in the data records was determined as the value of rate constant was systematically altered. Fig. 2-12 shows the normalised number of slam events identified versus the rate constant (the number of slam events is normalised by the number of slam events identified using a rate constant in Eqn. 2.1 of  $0.05 \text{ s}^{-1}$ ) for the Hull 042 strain gauge located on the transverse girder at frame 35. The rate constant of  $0.05$  appears to be a natural cut off point in the curve as the gradient changes markedly at this point. The number of slam events identified can be seen to increase rapidly as the slope criterion tends to zero, since for the threshold levels below  $0.05 \text{ s}^{-1}$  the peaks due to noise in the signal are being incorrectly identified as slam events. Secondly the rate of change of stress of peaks other than slam events in the stress signals were investigated to ensure that the rate constant value of  $0.05 \text{ s}^{-1}$  did not incorrectly identify them as slam events. Lastly an extensive visual examination of the data records was conducted to investigate whether slams were correctly identified for the differing rate constants, especially ensuring that small slams were included in the analysis but noise peaks were excluded. A rate constant of  $0.05 \text{ s}^{-1}$  was therefore adopted, which gave a maximum rate of change of stress prior to the peak of  $5 \text{ MPa/s}$ . The boundary between a slam being defined as occurring and not occurring will always be nebulous. The presented approach is appropriate, particularly when it is borne in mind that changes in rate constant affect the number of small, rather than large, slam events being identified since it is inclusive

in defining stress peaks as slams.

The rate constant,  $R_c$ , will need to be determined for each investigated vessel to ensure that the slams are identified correctly. An identical process was used to determine the appropriate rate criterion for the strain gauge at the top rider at frame 67 for Hull 050. This again resulted in the rate criterion being set at 5MPa/s. Returning to the example slams shown in Fig. 2-11, the adopted rate constant of  $0.05 \text{ s}^{-1}$  ensured that both of these slam events were identified for Hull 050: slam A and slam B. Slam B is a small slam event whose peak slam stress is not as great as the underlying global wave load. This indicates that the slam identification process was successful in classifying a range of impact events as slams.

### 2.3.2 Slam Identification and Analysis

Since the raw data files were recorded in binary format they were first converted to ASCII files using a Daqview program. The slams within the data records were identified using a search routine programmed in LabView according to the slam definition described in the previous section. For Hull 042 this was conducted primarily for the strain gauge located on the transverse girder at frame 35, although the response levels of other gauges were checked to ensure that all slams had been correctly identified. The strain gauge on the transverse girder at frame 35 was chosen as the reference strain gauge for the slam analysis since it was the strain gauge positioned foremost on the vessel's centreline thereby negating any possible asymmetry in the results. Asymmetry would have been a problem if the strain gauges in either of the forward steel posts had been used since they were positioned off the centreline and slam impacts with either a port or starboard bias would have led to inconsistencies in the data analysis if either of them were used as the base strain gauge.

The strain gauge located in the centre bow at frame 67 was selected as the reference for Hull 050 since it was the foremost strain gauge on the centreline (the strain gauge on the top rider at frame 69 ceased to work after three months of operation). Again the response levels of other gauges were checked to ensure that all slams were correctly identified. For Hull 050 the System 2 data runs that corresponded to the System 1 slam events were identified by comparing the file creation times and applying a slam event search routine. The final matching was carried out by comparing the instantaneous wave height signals, which were common in channels to both data acquisition systems. Due to difficulty in matching up slams identified in System 1 data traces with System 2 data traces, some slam events were not able to be included in all the data analysis, for example vessel speed information was only logged in System 2 and thus was absent if matching of the traces was not achieved.

#### 2.3.2.1 Slam Occurrences

**Wave Conditions** The peak stresses of the slam events were determined from the time records and a normalised peak stress,  $(\bar{\sigma}_p)$ , was calculated for each slam as the actual peak

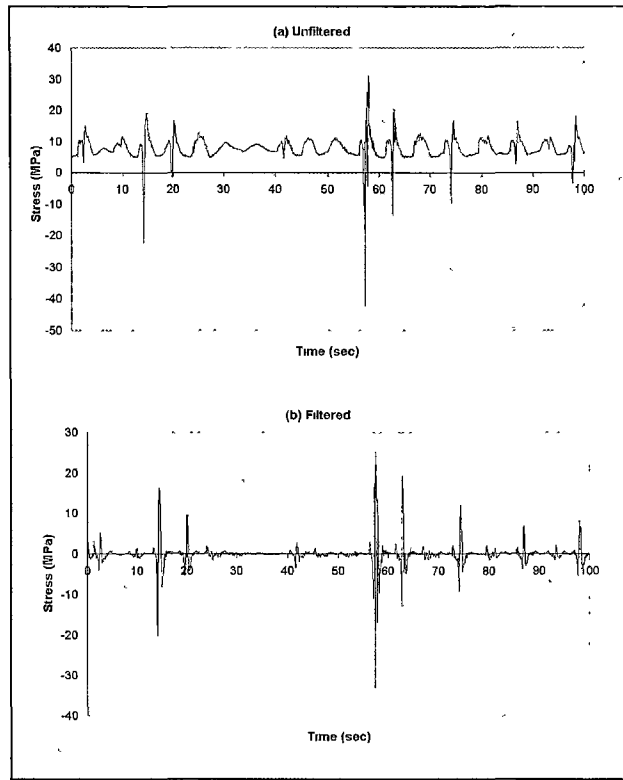


Figure 2-10: Effect of Filtering Raw Strain Gauge Data

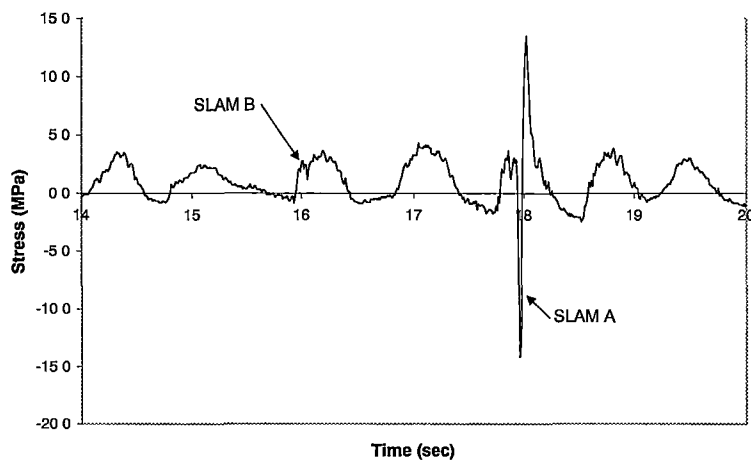


Figure 2-11: Hull 050 - Raw Strain Gauge Data Trace showing Two Identified Slam Events

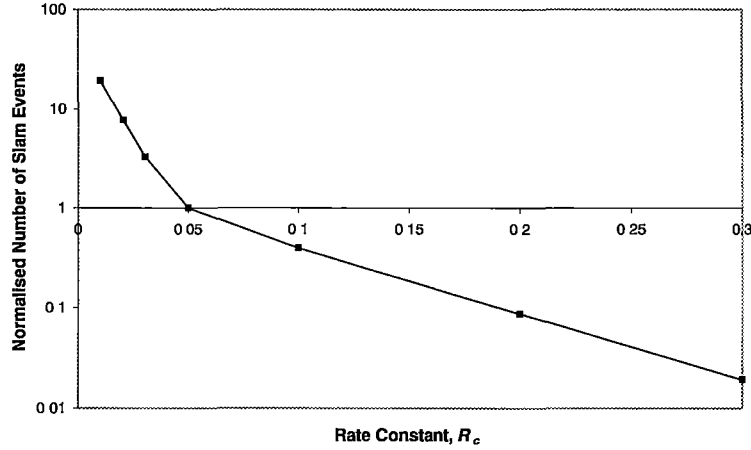


Figure 2-12: Normalised Number of Slam Events versus Rate Constant

stress in the event divided by the mean of the slam peak stress of all the identified slam events for each vessel

$$\text{normalised slam peak stress, } \bar{\sigma}_p = \frac{\sigma_p}{\sigma_{pm}}. \quad (2.2)$$

It should be noted that the quoted stress is based on a uni-axial strain measurement and ignores the Poisson effect from other strain components. Therefore the quoted stress results are defined as an equivalent stress as follows

$$\sigma = E\varepsilon \quad (2.3)$$

where  $E$  is the Young's modulus of elasticity and  $\varepsilon$  is the measured component of strain.

The significant wave height was determined from the instantaneous wave height records. It is recognised that the recording period, of 204 seconds in length, falls well short of that recommended [54] as being of about 20 to 30 minutes duration. However this was the maximum length of continuous data recorded and it was considered that this gave a good indication of encountered wave height at the actual time of the slam event. The encountered wave energy spectrum corresponding to the irregular encounter wave time history was derived from the discrete Fourier transform of the wave height record,  $S_\zeta(\omega_e)$ , where  $\omega_e$  is the encounter frequency. Converting from a moving platform reference system to a fixed platform reference system for the known vessel speed,  $U$ , and heading,  $\mu$ , the wave energy spectrum in a fixed spatial frame was found from the deep water wave relation as

$$S_{\zeta}(\omega) = S_{\zeta}(\omega_e) \left( 1 - 2 \frac{\omega U}{g} \cos \mu \right). \quad (2.4)$$

The spectral moments  $m_0$  and  $m_2$ , the variances of the irregular wave time history and acceleration respectively are then

$$m_0 = \int_0^{\infty} S_{\zeta}(\omega) d\omega \quad (2.5)$$

$$m_2 = \int_0^{\infty} \omega^2 S_{\zeta}(\omega) d\omega. \quad (2.6)$$

The significant wave height, assuming a narrow band spectrum, was found from

$$\bar{H}_{\frac{1}{3}} = 4.00 \sqrt{m_0} \quad (2.7)$$

whilst the mean zero crossing period,  $\bar{T}_z$ , was determined as follows

$$\bar{T}_z = 2\pi \sqrt{\left( \frac{m_0}{m_2} \right)}. \quad (2.8)$$

For deep water waves the average wave length,  $\bar{\lambda}_z$ , was defined in terms of the zero crossing period as

$$\bar{\lambda}_z = \frac{g \bar{T}_z^2}{2\pi}. \quad (2.9)$$

Of course some encountered wavelengths will be shorter and some longer than this average value which is introduced here to indicate the relative scale of encountered waves to the ship length.

**Vessel Operating Conditions** The average vessel speed was determined from the GPS data for each individual data run in which a slam event was identified. The vertical velocity of the vessel's bow relative to the water surface was estimated from the TSK wave sensor data. The vertical bow displacement,  $x_{3b}$ , is calculated by the TSK wave sensor by double integrating the measured vertical acceleration. The vertical ship displacement values at the bow were subtracted from the wave height,  $x_{3w}$ , and then differentiated to give the relative

vertical velocity as

$$\frac{dx_{3r}}{dt} = \frac{d|(x_{3w} - x_{3b})|}{dt}. \quad (2.10)$$

**Extreme Slam Event** A slam which caused extensive structural damage on Hull 050 was identified and defined as an extreme event. The data from this event was analysed in respect to providing data as the basis for the development of quasi-static and dynamic load cases.

**Dynamic Features of Slamming Response** The times between the slam peak occurring at the various strain gauges located along the vessel and at the strain gauge at transverse girder at frame 35 for Hull 042 and the strain gauge at the top rider at frame 67 for Hull 050 were determined for a significant number of slam events. The slam peak for each strain gauge was defined as occurring when the stress reached a maximum value during the slam event.

Spectral analysis was conducted on the raw data traces of the slam events to investigate the dynamic structural response. The raw data was highpass filtered at 0.04 Hz to remove low frequency drift, and windowed using a Hanning window to reduce spectral leakage (the records at 100 Hz were highpass filtered at 0.8 Hz). The Hanning window was chosen since it achieves a good balance between spectral leakage and resolution. The power spectra for the strain gauge records, for a window of 5 seconds surrounding the slam event, were then determined. These spectra were used to identify the various modal response frequencies of the vessel.

The lower frequency global loads were also investigated using a similar technique: the strain gauge signals were lowpass filtered at 4 Hz and then highpass filtered at 0.04 Hz before the power spectra were calculated. This was conducted for a time period of 30 seconds that did not include a slam event.

The decay coefficient of the structural response was also determined from the strain gauge records. The decay coefficient was estimated from the decaying oscillation by determining the ratio between pairs of successive amplitudes. The decay coefficient, as defined in Fig. 2-13, is given in terms of successive stress peak values as

$$\eta = \frac{1}{\pi} \log_e \left( \frac{\sigma_j}{\sigma_{j+1}} \right). \quad (2.11)$$

The determination of decay coefficients is a complex area with a large number of available methods, for example that proposed by Li [55]. Whilst a relatively simple approach has been adopted in this study, it is proposed that it is appropriate in order to achieve the level of accuracy required.

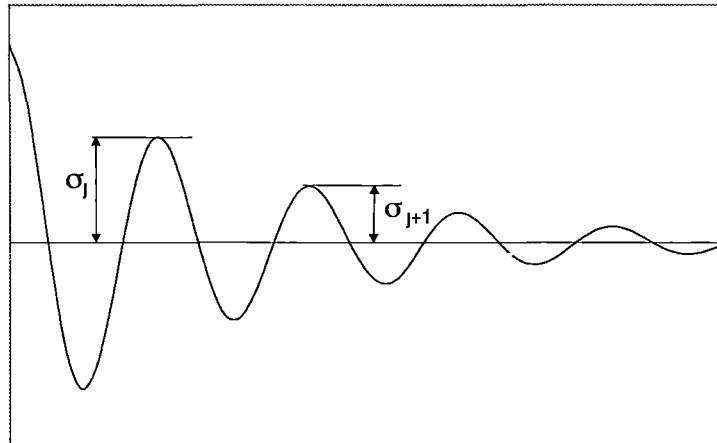


Figure 2-13: Definition of Decay Coefficient

**Additional Slam Analysis** By studying the encountered wave cycles between slam events, if multiple events were identified in a single data record, the number of waves encountered between each consecutive slam event was determined. For slams which were separated by a single wave encounter the relative resultant stress levels were obtained.

From the ship displacement reading from the TSK the point in time at which the bow of the vessel changed direction from moving downwards to upwards was determined. The time when the slam stress attained its maximum level during the slam event for the strain gauge on the top rider at frame 67 was also found. The time between these two occurrences was then calculated.

In order to distinguish between slams that comprised wave impact on the wet-deck as opposed to hull bottom or hull flare slamming, the height of the water surface on the vessel at the point of impact was investigated. The TSK relative wave height value gave the distance between the water surface and the sensor. However the wave sensor was located 10 frames forward of the centre bow archway. In order to estimate the water level in the archway region the change in wave height due to the longitudinal distance was determined based on the wave length of the encountered wave.

## 2.4 Results and Discussion

### 2.4.1 Slam Occurrences

#### 2.4.1.1 Wave Conditions

Several important outcomes were established through the analysis of the slam events with respect to the sea conditions in which they occurred. For example it will be shown that the derived slam peak stress distributions indicate that whilst very severe slams occur they do so rarely, whereas small slams tend to dominate the distributions in all significant wave heights. Analysis of the rate of occurrence of slam events revealed that the frequency of occurrence tends to increase as the significant wave height, of the sea in which the vessel is operating, increases. Such findings have significant implications for the determination of the effect of slam events on the ultimate strength and fatigue life of large high-speed catamarans.

Using the slam definition outlined, a total of 565 slam events were identified in the data records for Hull 042 and 125 slam events for Hull 050. The normalised slam maximum stress of each slam event was determined, divided into bins and plotted against the percentage of the total number of occurrences, as shown in Figs. 2-14 and 2-15.

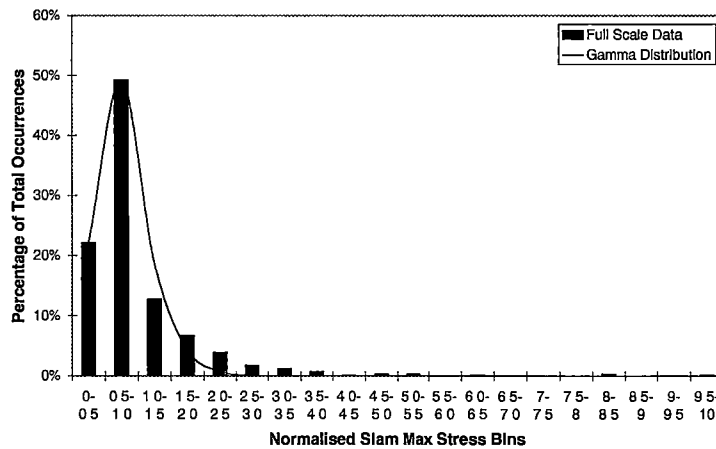


Figure 2-14: Hull 042 - Distribution of Slam Peak Stress for Slam Events

The distribution for Hull 042 shows that the number of slam events initially increases and then reduces rapidly as the normalised peak stress level increases. Approximately 70% of the slam events are in the two bins which correspond to the slam attaining a maximum stress value less than the average peak stress. Only 20% of the slams are in the next two bins for a range of  $1.0 < \text{normalised maximum stress} < 2.0$ . The rate of decline of slam occurrences then tends to reduce as the slam peak stress increases. The distribution of the slam occurrences may be adequately approximated by the Gamma probability density function, as given by

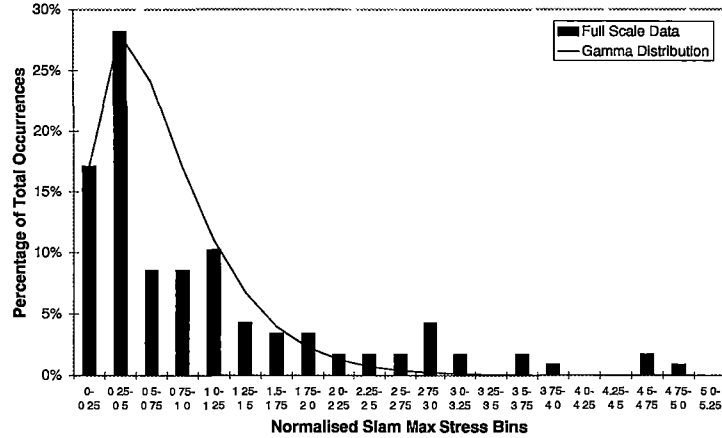


Figure 2-15: Hull 050 - Distribution of Slam Peak Stress for Slam Events

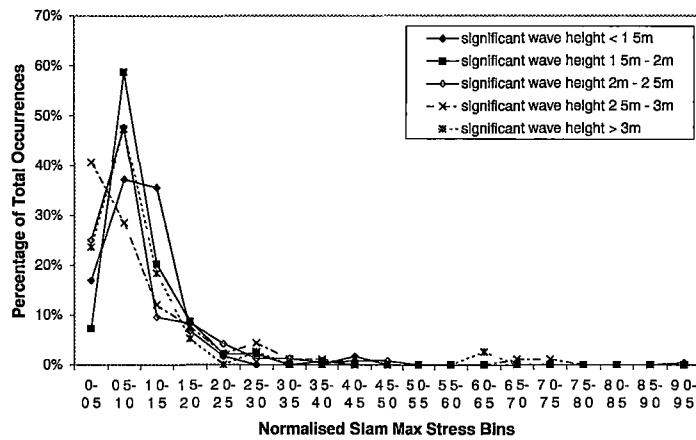


Figure 2-16: Hull 042 - Distribution of Slam Peak Stress for Slam Events for varying Significant Wave Height

$$f(x) = \left(\frac{x}{\beta}\right)^{\alpha-1} \frac{e^{-(x/\beta)}}{\beta\Gamma(\alpha)} \quad (2.12)$$

where  $\alpha$  and  $\beta$  are parameters to the distribution ( $\alpha = 4.0$  and  $\beta = 0.2$ ). The Gamma probability density function is also plotted in Fig. 2-14.

Due to the smaller number of identified slam events and consequently reduced range of slam maximum stresses smaller bin widths were used for the Hull 050 distribution. The distribution for Hull 050, Fig. 2-15, can be seen to be similar to that of Hull 042. The distribution of Hull 050 slam occurrences may be approximated by the Gamma probability density function ( $\alpha = 2.1$  and  $\beta = 0.35$ , see Eqn. 2.12), which is also plotted in Fig. 2-15.

The slam events were divided into ranges of the significant wave height in which they

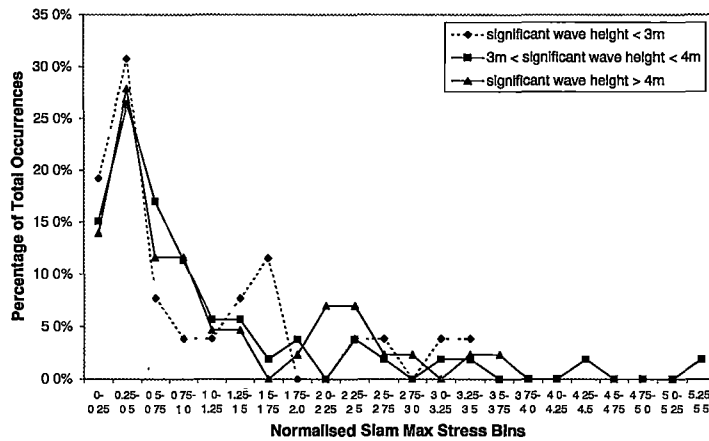


Figure 2-17: Hull 050 - Distribution of Slam Peak Stress for Slam Events for varying Significant Wave Height

occurred and the distribution of occurrences against slam peak stress plotted for each wave height as shown in Figs. 2-16 and 2-17. These plots show that the distributions are similar for the different wave height environments, indicating that relatively smaller slam events predominate in all the sea conditions experienced.

These distributions of the slam peak stresses indicate that whilst very severe slams occur they do so rarely, whereas small slams tend to dominate the distributions in all significant wave heights. The finding that severe slam events occur infrequently has important implications for the ultimate strength of large high-speed catamarans. Whilst the domination of the distributions by small slams may be significant when estimating the fatigue life of such vessels.

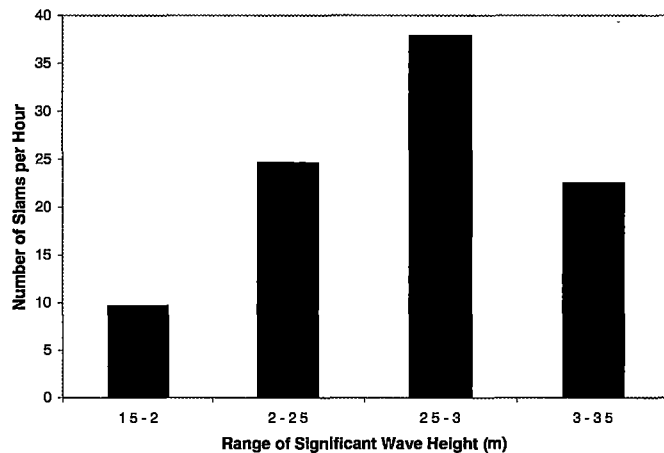


Figure 2-18: Hull 042 - Number of Slams per Hour vs. Significant Wave Height in Head Seas (Vessel Speed = 10 -15 knots)

For a set of consecutive data records, for which Hull 042 was continuously encountering

head seas, the frequency of occurrence of slams for a range of significant wave heights was determined. The results, as shown in Fig. 2-18, were for slam events with a normalised stress value greater than 1.0. This plot shows that as the significant wave height increased the frequency of slam occurrence also tended to increase. For a significant wave height range of 1 to 1.5m, a slam occurred on average every 6 minutes whereas as the wave height rose to 2.5 – 3m the time gap between slams reduced on average to 95 seconds. The reason for the drop in the frequency of occurrence in the significant wave height range 3 – 3.5m is unclear. It is possible that the waves with a larger wave height were also longer in length, with smaller steepnesses, so that the vessel tended to contour the wave more readily. However it may also be due to a reduced amount of data available in the 2.5 – 3m significant wave height range, compared to the other wave heights, giving an unrepresentative value for that range (see Table 2.5). The encountered wave spectrum in all the seas had a fairly consistent average wave period,  $\bar{T}_z$ , varying from approximately 6.0 seconds to 8.0 seconds and the vessel speed range for this data was 10 to 15 knots.

Such data will be invaluable for estimating the effect of slams on fatigue life. Unfortunately the data collected for Hull 050 did not contain a set of consecutive data records for which the vessel was continuously encountering head seas. This meant that the frequency of occurrence of slams could not be determined for Hull 050.

Significant Wave Height (m)	Number of Slams Recorded	Amount of Time in Wave Environment (mins)	Slam Rate (slams/hour)
1.5 - 2	30	186	9.7
2 - 2.5	196	477	24.7
2.5 - 3	24	38	37.9
3 - 3.5	41	109	22.6

Table 2.5: Slam Frequency of Occurrence Data for Head Seas, 10 - 15 knots

The peak stress of each slam was plotted against the measured significant wave height and average wave length of the record that included the corresponding slam, see Figs. 2-19 and 2-20. The peak stress for Hull 042 was found for the strain gauge located on the transverse girder at frame 35, whilst the strain gauge on the top rider at frame 67 was used to find the peak stress of each slam for Hull 050. The resulting plots show that the slams only occurred when the significant wave height was greater than 0.9m for Hull 042 and 1.95m for Hull 050. As expected the envelope of peak stress in a slam appears to increase with increasing wave height. It is apparent that when the vessel is operating in large sea states the slams are not exclusively severe, but rather range in severity from small to large stress levels. For both vessels the slam events occurred in seas with an average wave length which ranged between 40m and 130m, which is comparable to the hull length. For Hull 042 the preponderance of waves (78%) were in the range of wavelengths between 60m and 90m whereas Hull 050's slams occurred for a wider spread of wavelengths. This difference was probably due to the broader range of

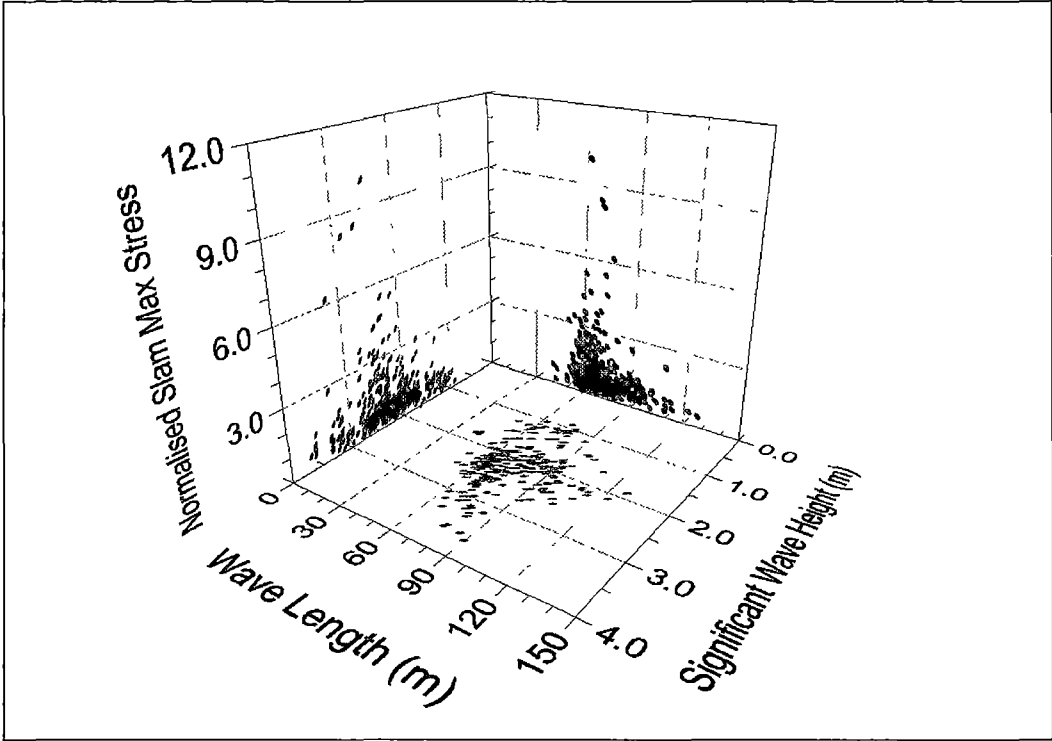


Figure 2-19: Hull 042 - Normalised Slam Peak Stress for varying Significant Wave Height and Wave Length

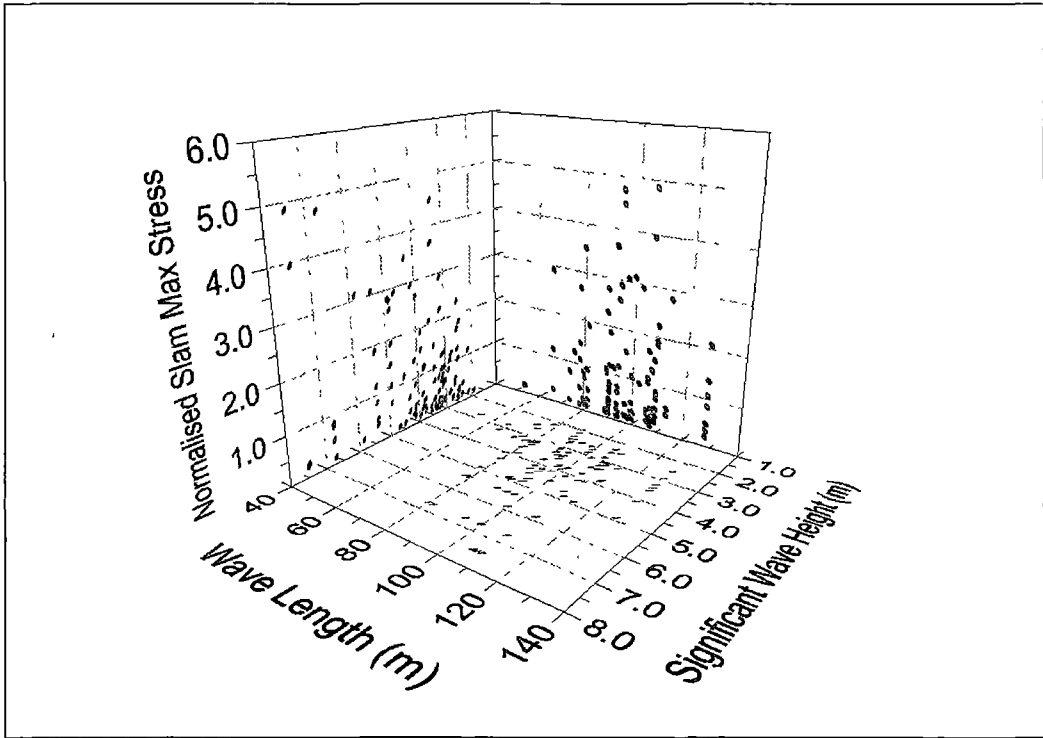


Figure 2-20: Hull 050 - Normalised Slam Peak Stress for varying Significant Wave Height and Wave Length

conditions that 050 encountered over the longer monitoring time of 10 months compared to the period of 4 days analysed for Hull 042 which concentrated on head sea conditions. These results provide an important overview of the sea conditions required to cause slamming in large high-speed catamarans. They also show the influence the wave length and height have on the severity of slam events.

The majority of slam events occurred when the vessels were encountering waves in the range of non-dimensional encounter frequency of  $\omega_e^* = 4.5$  to  $5.5$  (where  $\omega_e^* = \omega_e \sqrt{L/g}$ ) for Hull 042 and  $\omega_e^* = 4.0$  to  $5.0$  for Hull 050 (Figs. 2-21 and 2-22). The range of non-dimensional encounter frequency for Hull 042 corresponds to the location of the resonant peaks of the heave and pitch motions for this vessel [56]. Whilst the motion transfer functions for Hull 050 have not been calculated, the motion peaks are expected to be at approximately the same non-dimensional encounter frequency. This result suggests that slams predominantly occur when the vessel motions are greatest in relation to the encountered wave height. This suggests that measures taken to reduce vessel motions will have also aided the reduction of slam occurrences.

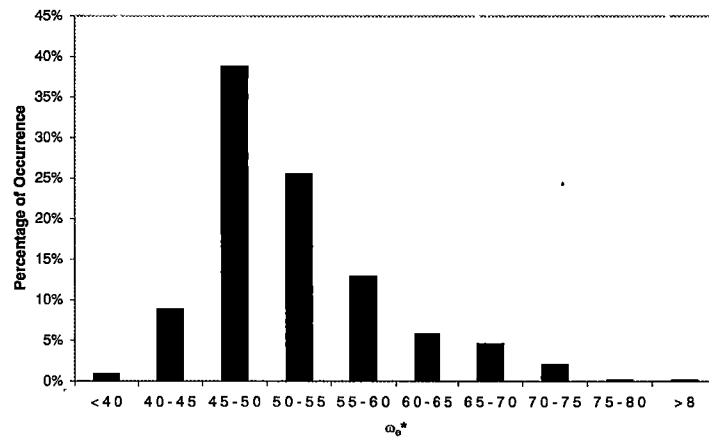


Figure 2-21: Hull 042 - Percentage of Slam Occurrence for varying Non-Dimensional Encounter Frequency

The distributions of identified slam events for both vessels are similar in that they both decay significantly, in terms of slam occurrences, as the slam peak stress increases and the distributions follow similar patterns for varying sea states. A major difference in the slam results is that slam events were experienced by Hull 042 in significant wave heights as low as 0.9m whilst for Hull 050 the minimum significant wave height for slam occurrences was 1.95m. There are two major factors which may account for these differences. The first factor is the difference in tunnel height for the two vessels as shown in Table 2.6, where the tunnel height is the vertical distance between the calm water surface and the top of the wet-deck archway (see Fig. 2-23). The operational tunnel height during measurements was 2.34m for

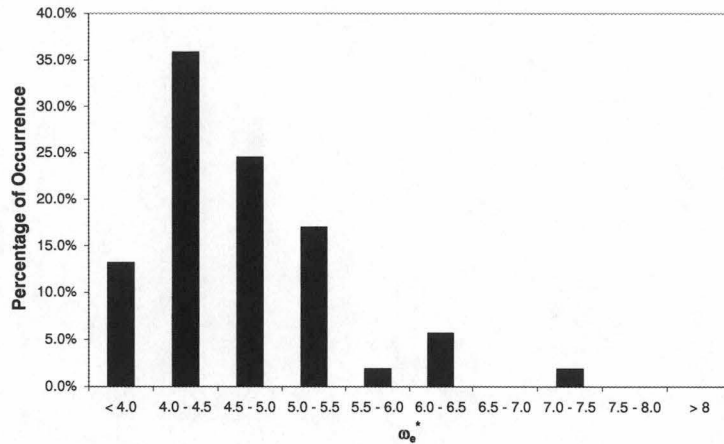


Figure 2-22: Hull 050 - Percentage of Slam Occurrence for varying Non-Dimensional Encounter Frequency

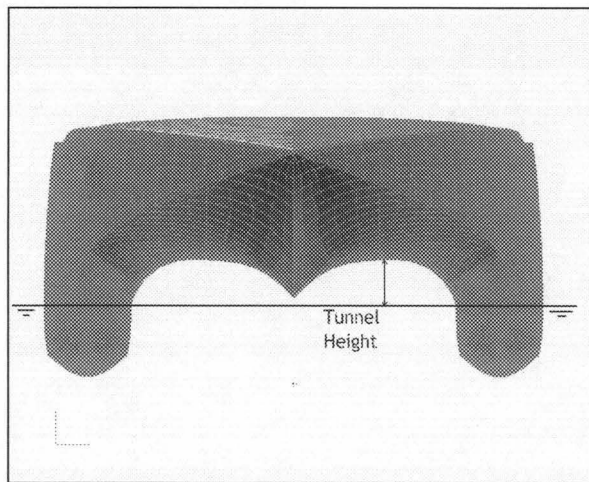


Figure 2-23: Definition of Tunnel Height

Hull 042 compared with 2.97m for Hull 050, i.e. a difference of approximately 0.6m in tunnel clearance which may be expected to have a significant effect on wet-deck slam occurrence rates in smaller waves. Although the tunnel heights were different, the centrebow configurations for both vessels were similar as is demonstrated by the body plans shown in Figs. 2-24 and 2-25. The second factor is the motions of the two vessels. Although the vessels are generally similar in design they are different in overall size and will therefore exhibit different motion characteristics in similar wave environments with the motions of the smaller vessel, Hull 042, being more severe [57]. In addition, during its delivery voyage Hull 042 did not have a fully functioning ride control system to aid the reduction of vessel motions. Thus its motions are likely to have been significantly greater than those of Hull 050. The aft flaps were fitted and operational, however the forward T-foils were not fitted. The T-foils are the

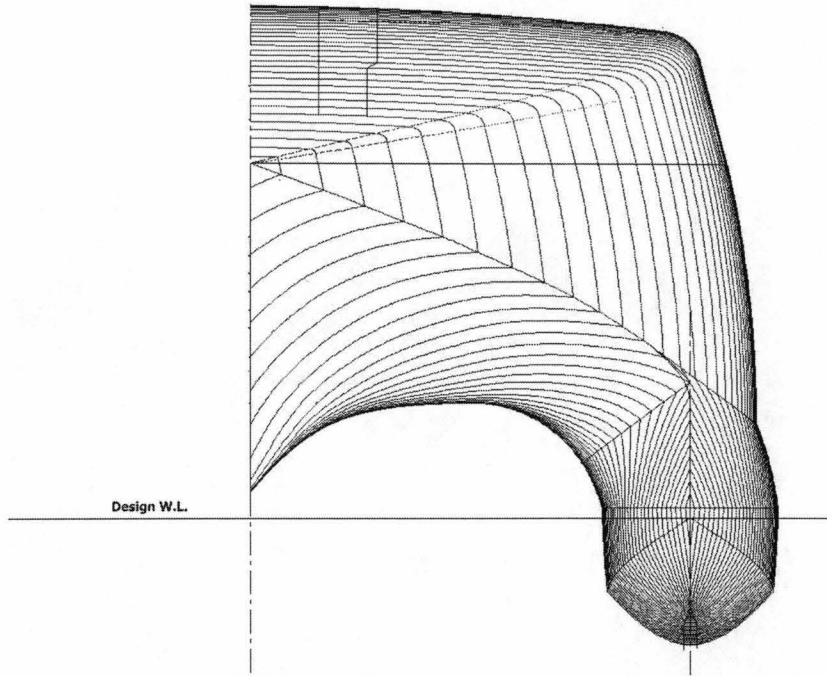


Figure 2-24: Hull 042 Body Plan showing Centrebow Configuration

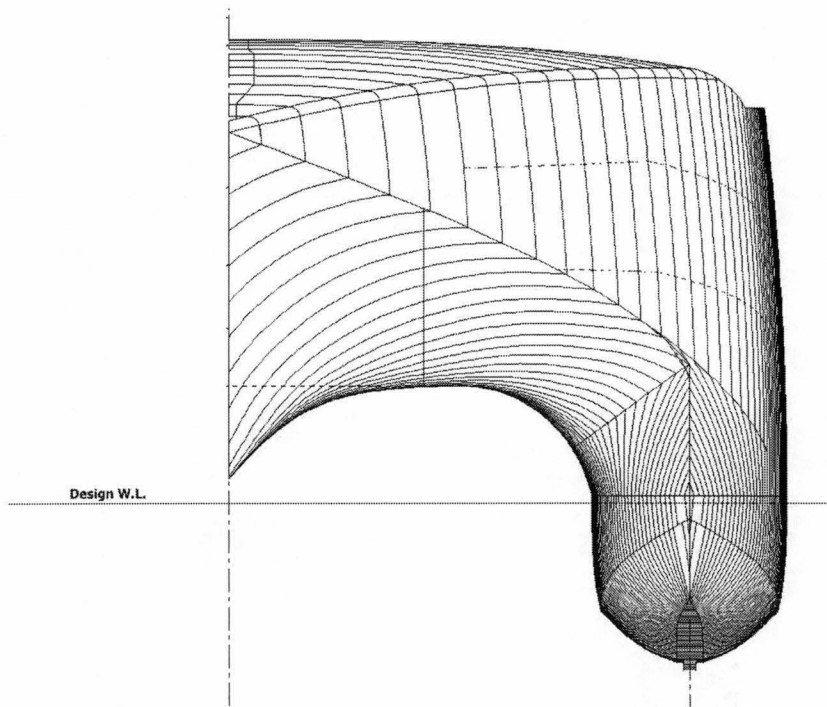


Figure 2-25: Hull 050 Body Plan showing Centrebow Configuration

dominant mechanism of the system for motion reduction and their absence would have had a major impact of the vessel's heave and pitch motions since ride control systems may reduce motions by up to 50% [58]. Again this effect would be more obvious in smaller waves, as ride control systems become relatively less effective in larger waves. Other factors may have also contributed to differences in the slam distributions including that the environmental and operating conditions for both sets of trials were not identical and sea direction may have been a consideration with the Hull 042 data being predominantly for head seas. Also, whilst the same definition for a slam event was used for each vessel, the strain gauge locations were different.

	<b>Tunnel Height Design</b>	<b>Tunnel Height Operational</b>
<b>Hull 042</b>	2.29m	2.34m
<b>Hull 050</b>	2.37m	2.97m

Table 2.6: Tunnel Heights - Hull 042 and Hull 050

Using the on-board observations the heading angle for each of the slam events was determined, as shown in Figs. 2-26 and 2-27. Fig. 2-26 shows that slams occurred in starboard bow quartering, starboard aft quartering, head seas and port bow quartering conditions. It also suggests that a slam was more likely to occur for Hull 042 with a vessel heading of 180 degrees (head sea) and 225 degrees (port bow) than other heading angles. However the vessel route south down the east coast of Australia and across the Australian Bight from east to west produced predominantly head and port bow quartering conditions and therefore not only did the vessel spend the majority of its time operating in these headings, these headings also subjected the vessel to the roughest sea conditions. The Hull 042 data analysed was therefore predominantly for head and bow sea conditions with the vessel spending little time in following or stern quartering seas meaning that the data samples was heavily skewed and little information was available on other sea conditions. Fig. 2-28 shows that the slam events in the head and bow headings were more severe than those in the stern quartering seas. The Hull 050 data (Fig. 2-27) indicates that slams occurred when the vessel was operating in starboard bow quartering, starboard aft quartering and port aft quartering conditions. That slams occurred in the stern quartering conditions is interesting to note since it is often assumed that slams only occur in head or bow sea headings. Slams occurred most frequently with a vessel heading of 135 degrees (starboard bow). This was probably due to the vessel route, as shown in Fig. 2-6, which when combined with the prevailing south to north wave direction, will create mainly quartering conditions. The influence of heading angle on the severity of slam was investigated for Hull 050, as shown in Fig. 2-29 which indicates that the bow heading angle resulted in generally more severe slam events than the stern quartering headings.

These results are important since they indicate that slam events occur for a range of vessel headings, including stern quartering seas, whilst the most severe slams appear to occur predominantly in head seas. These findings will aid the process of estimating of the effect of

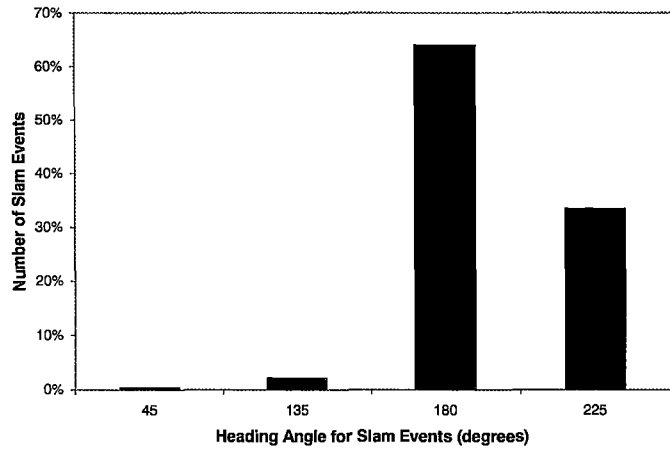


Figure 2-26: Hull 042 - Number of Slam Events for varying Heading Angle

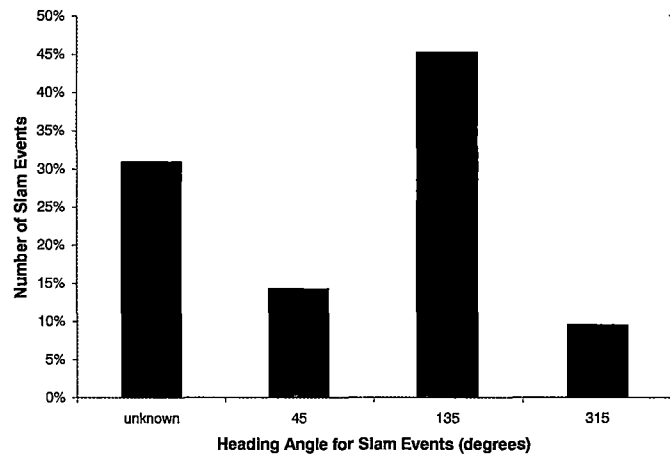


Figure 2-27: Hull 050 - Number of Slam Events for varying Heading Angle

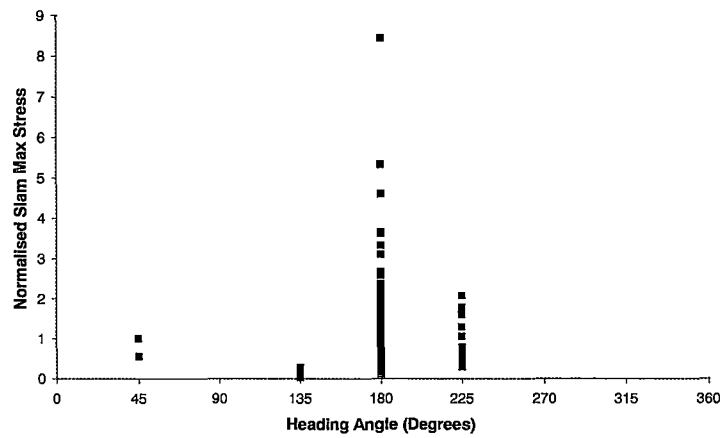


Figure 2-28: Hull 042 - Normalised Slam Max Stress for varying Heading Angle

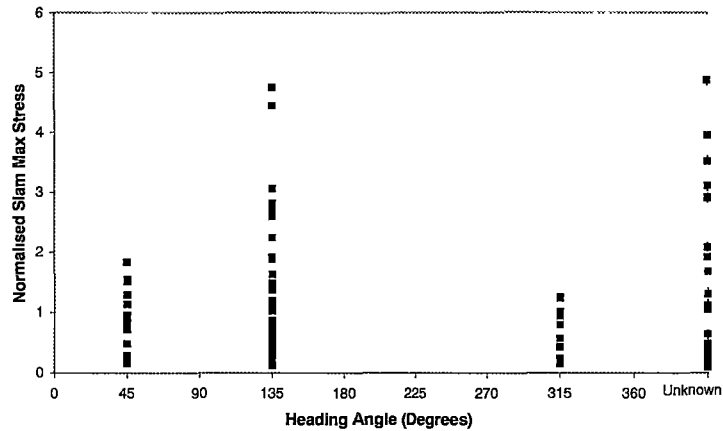


Figure 2-29: Hull 050 - Normalised Slam Max Stress for varying Heading Angle

slam events on fatigue life through providing preliminary data on the effect of vessel heading. However, in order to fully identify the effect of heading angle on slamming, slam occurrence rates would need to be determined for different heading angles. To achieve this the vessels would have been required to operate for a specified time period in each of the wave headings of interest for a range of wave heights.

#### 2.4.1.2 Vessel Operating Conditions

The effect of vessel operating conditions on the nature of slam events was also investigated. In particular the vessel operating speed and maximum relative vertical velocity at the time of slam occurrence were studied. The results of this analysis provide significant information on the conditions that contribute to large high-speed catamarans experiencing severe slam events. For example, although it would be suggested intuitively that a reduction in speed will ensure that severe slams do not occur, this was not found to be the case. The findings are important for determining the effect of slam events on the ultimate strength and fatigue life of large high-speed catamarans, through contributing information on which operating conditions increase the likelihood of severe slams occurring.

The slam events occurred for a range of speeds for both vessels, as can be seen in Figs. 2-30 and 2-31 where each point represents a single slam event, with some of the most severe slams occurring at the lower end of the speed ranges. This was due to a trend of decreasing vessel speed for increasing significant wave height as the masters of the vessels reduced speed in the most severe seas, as may be seen in Figs. 2-32 and 2-33. Whilst reducing speed might be thought to reduce the incidence of slam occurrence, due to a reduction in vessel motions with reduced speed, these results do not confirm such an effect. Rather, reduced speed is associated with larger wave heights for operational reasons and thus with more severe slams.

The maximum relative vertical velocity during each slam event of the bow of the vessel to

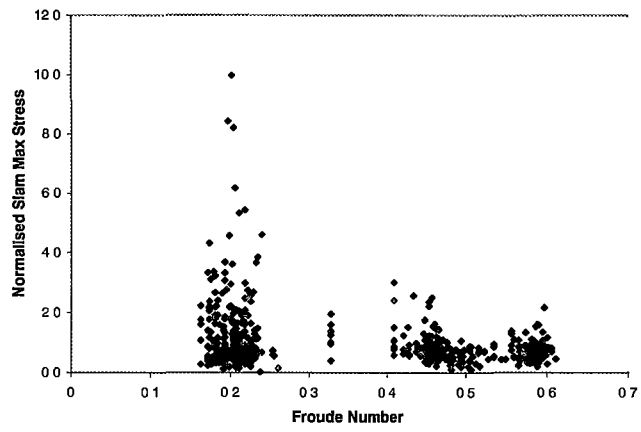


Figure 2-30: Hull 042 - Slam Peak Stress as a function of Froude Number

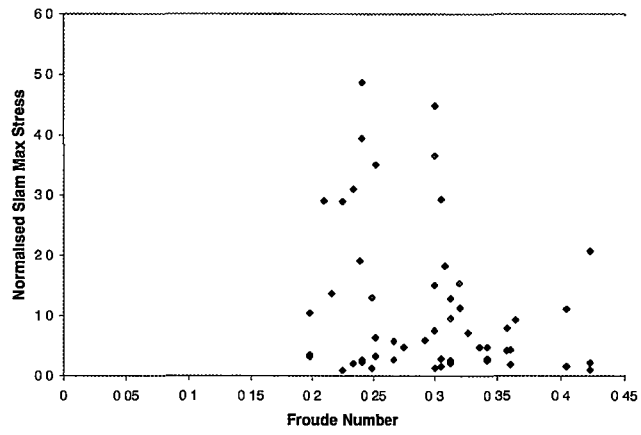


Figure 2-31: Hull 050 - Slam Peak Stress as a function of Froude Number

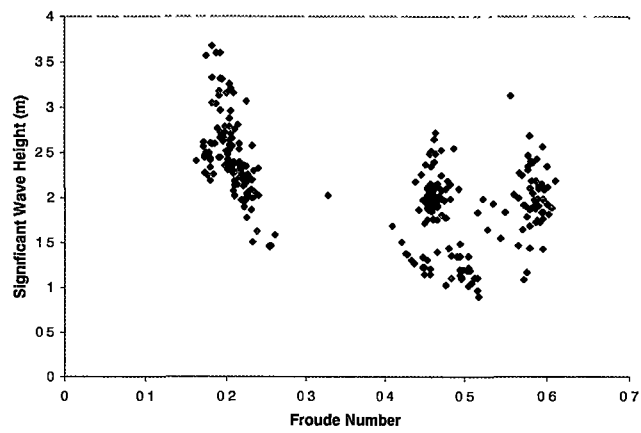


Figure 2-32: Hull 042 - Froude Number for Operating Significant Wave Height

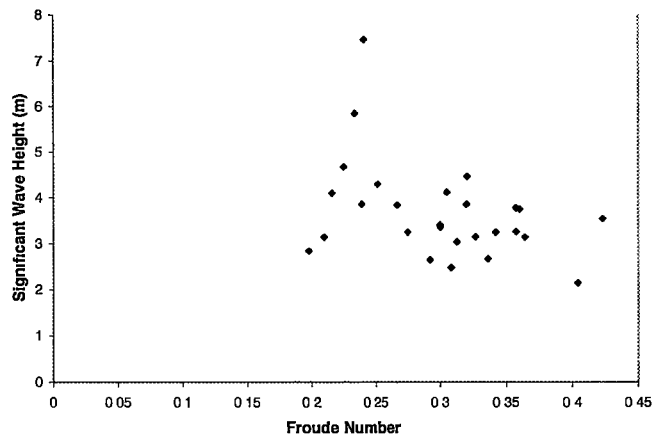


Figure 2-33: Hull 050 - Froude Number for Operating Significant Wave Height

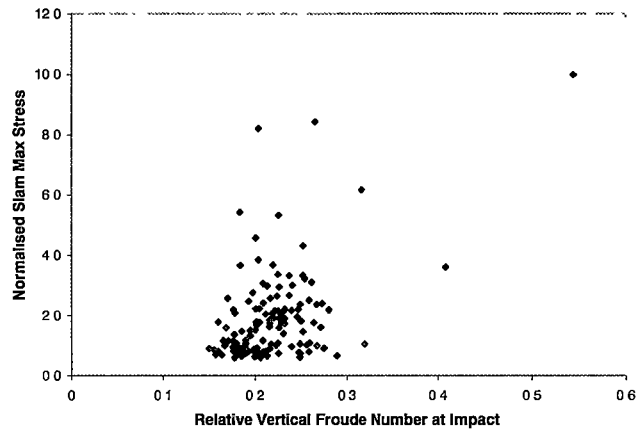


Figure 2-34: Hull 042 - Slam Peak Stress for varying  $Fn_{rel\ vel}$

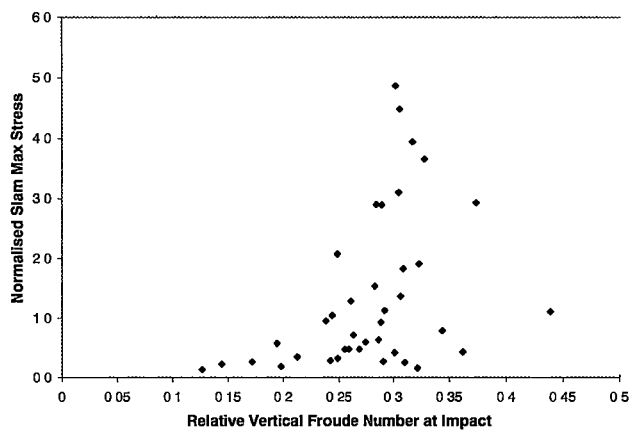


Figure 2-35: Hull 050 - Slam Peak Stress for varying  $Fn_{rel\ vel}$

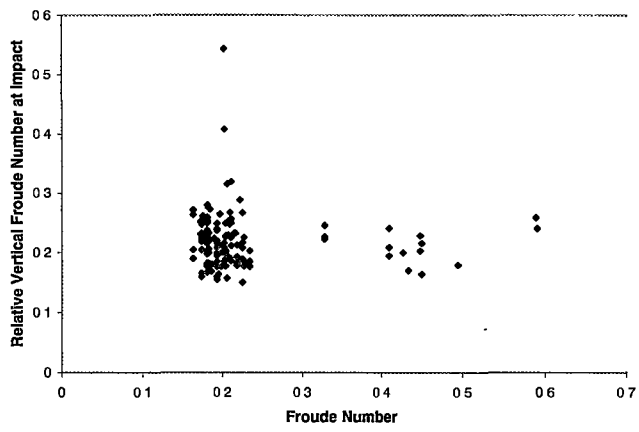


Figure 2-36: Hull 042 -  $F_{n_{rel\ vel}}$  for varying Froude Number

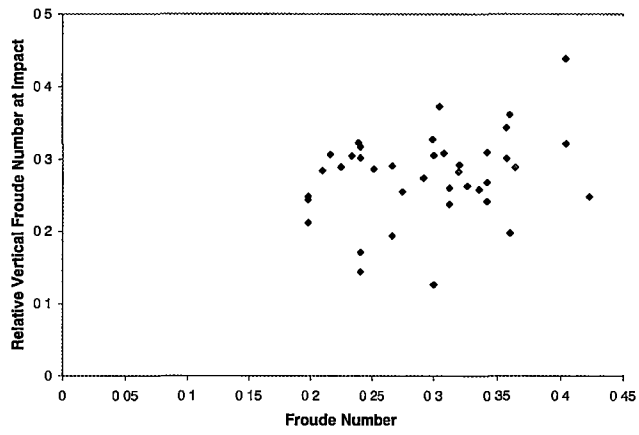


Figure 2-37: Hull 050 -  $F_{n_{rel\ vel}}$  for varying Froude Number

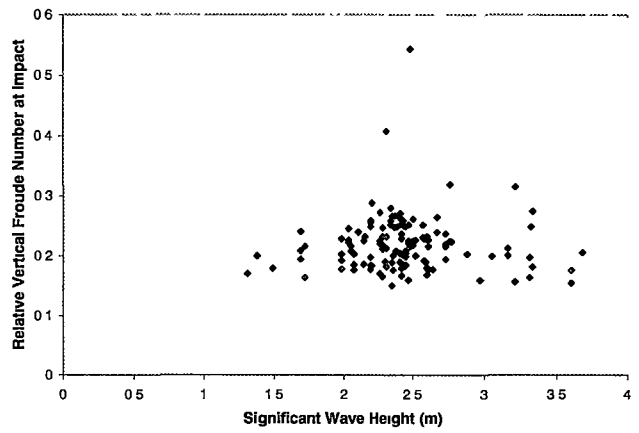


Figure 2-38: Hull 042 -  $F_{n_{rel\ vel}}$  for varying Significant Wave Height

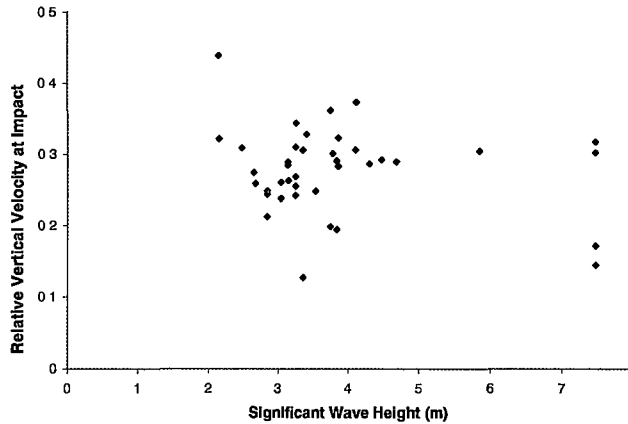


Figure 2-39: Hull 050 -  $F_{n_{rel\ vel}}$  for varying Significant Wave Height

the water surface in a ship based reference frame,  $\frac{dx_{3r}}{dt}$ , was determined using Eqn. 2.10 and converted to relative velocity Froude Number,  $F_n$ , using

$$F_{n_{rel\ vel}} = \frac{\frac{dx_{3r}}{dt}}{\sqrt{gL}} \quad (2.13)$$

Where vessel length,  $L$ , was utilised in the Froude Number definition since it provides a clear indication of vessel size. This was plotted against the peak stress during a slam event as shown in Figs. 2-34 and 2-35. These plots indicate that a relative velocity Froude Number of 0.15 was required for a slam to occur for Hull 042 (this equates to a relative vertical velocity of 4.35m/s), whilst a relative velocity Froude Number of 0.125 was required for a slam to occur for Hull 050 (this equates to a relative vertical velocity of 3.7m/s). The upper envelopes of the plots also show that the maximum severity of the slam tended to increase as the relative vertical velocity increased. Although the Hull 042 slam data indicated that there was no significant relationship between relative vertical velocity at the bow and vessel speed (see Fig. 2-36), Fig. 2-37 indicates that there is a slight trend for the relative vertical velocity to increase with vessel speed for Hull 050. This plot tends to back the actions of the vessel's master to reduce speed in order to reduce the relative vertical velocity at the bow and hence attempt to reduce the severity of a slam. Figs. 2-38 and 2-39 indicate that there is no apparent relationship between relative vertical impact velocity at the bow and wave height. This is possibly because slams are due to rogue or extreme waves in a random train, rather than the underlying or average waves.

#### 2.4.1.3 Slam Relative Stresses

In order to determine the relative influence of the slam events on the different sections of the vessel, the peak slam stresses for a significant number of slam events were normalised about a

single gauge. This analysis will provide input for the development of structural load cases for slamming events by highlighting locations that are significantly affected by slamming.

For Hull 042 slams with a non-dimensional peak value greater than 4.0 were analysed. The gauges were normalised using the values from the strain gauge located on the transverse girder at frame 35 and the results shown in Fig. 2-40. This gauge was chosen since it was mounted on the vessel's centreline and thus should highlight any influence of asymmetry in vessel heading when compared with the other gauges. The results indicate that the strain gauges on the aft transverse box, inner cross brace, cross bridge web and keel plate at frame 41.5 all responded to the slam events in a similar manner. However the strain gauges on the port and starboard steel posts and steel chevron brace were subjected to relatively higher stress levels than the gauge on the transverse girder during the slams. Although all these slam events took place in the nominally head sea direction, some variation of directionality of the sea conditions can be seen in the stress levels, with the relative severity of the port and starboard steel post stresses changing. This suggests that any change in relative heading from direct head seas is detected in the steel post stress levels: i.e. it appears that slam events 3, 6 and 7 are slightly starboard bow quartering whilst slam events 4 and 8 are slightly port bow quartering and slam events 1, 2 and 9 are virtually direct head sea events. Fig. 2-40 indicates that the gauge at frame 24.5 on the keel experienced very similar relative stresses in the slams to the gauge at frame 35.5 on the keel, but relatively more than the gauge further forward on the keel at frame 41.5.

Slams with a non-dimensional peak stress of greater than 1.0 underwent analysis for Hull 050. The gauges from System 1 were normalised using the values from the strain gauge located on the top rider at frame 67 and the results shown in Fig. 2-41. This gauge was chosen as it was mounted on the vessel's centreline for the same reason as above. System 2 did not have a gauge mounted on the vessel centreline so the gauge located on the keel at frame 41 was used for normalisation, see Fig. 2-42.

The results for System 1 indicate that the strain gauges on the top riders of frames 65 to 68 all responded to the slam events in a similar manner, which was to be expected since they are located in close proximity. For some slam events the gauges on the top riders at frames 65 and 66 exhibited higher levels of stress than the top rider at frame 67, whereas for other slams the gauges at frames 65 and 66 exhibited lower levels of stress than at frame 67. This may have been due to the actual location of the slam impact in relation to the strain gauges, i.e. the further aft the impact the greater the dominance of the stress at the aft frames. The directionality of the sea conditions can be clearly seen to have a strong influence on the stress levels. In particular Fig. 2-41(b) shows the changing dominance of the starboard and port diagonal's stress levels. The slam events where the port diagonals show greater stress levels than the starboard gauges were when the vessel was operating in a port bow seaway. For System 2, Fig. 2-42(b) indicates that the gauge at frame 25 on the keel experienced higher relative stresses in the slams than the gauges further forward on the keel, with the gauge at

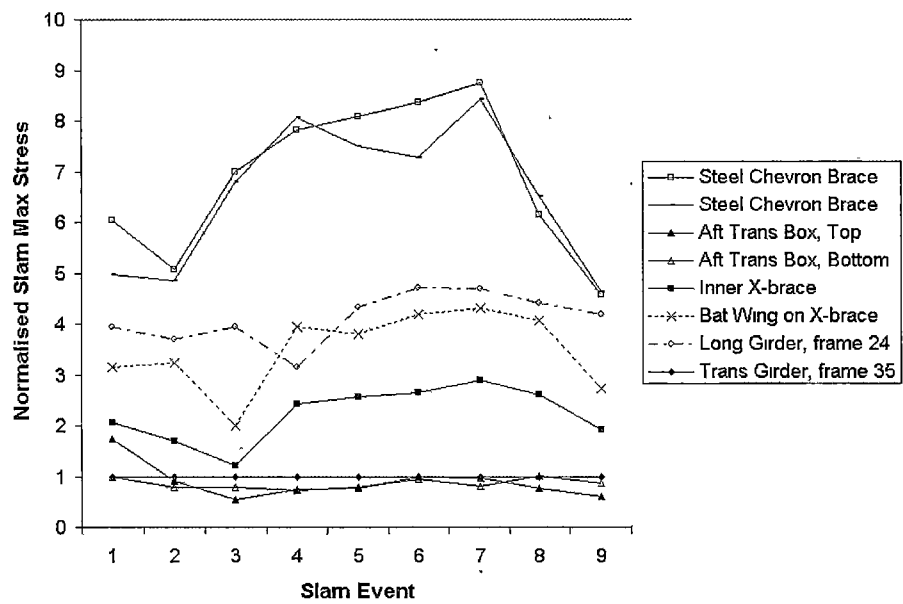
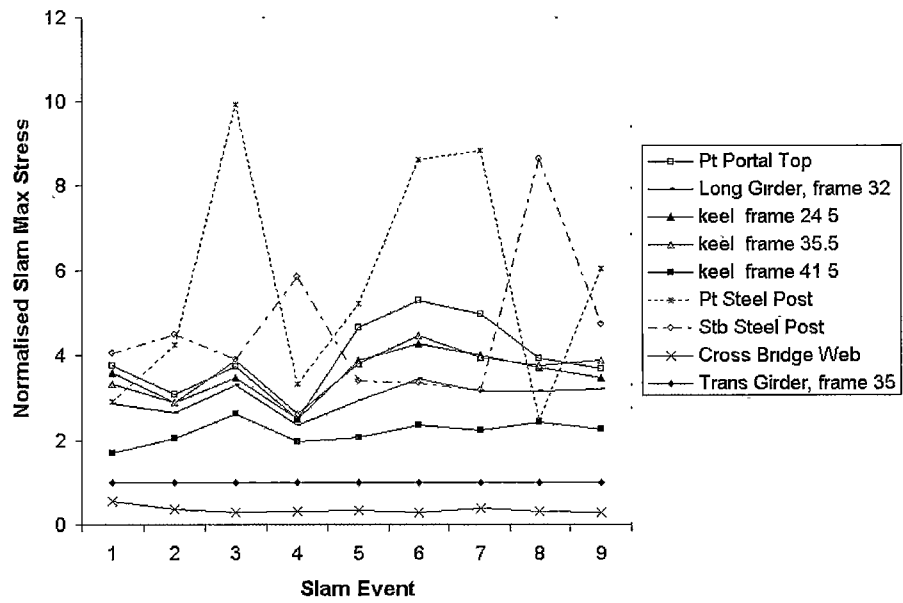


Figure 2-40: Hull 042 - Normalised Strain Gauges

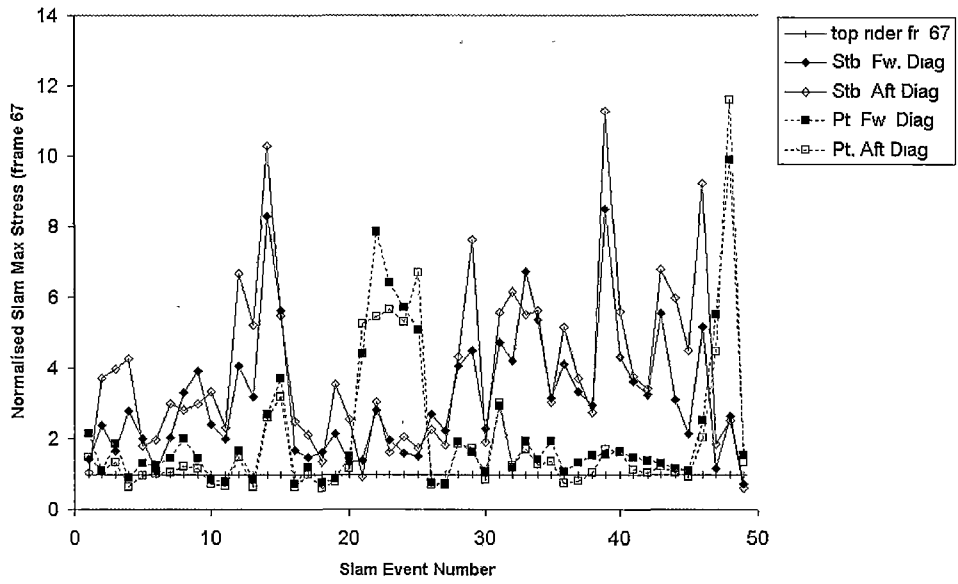
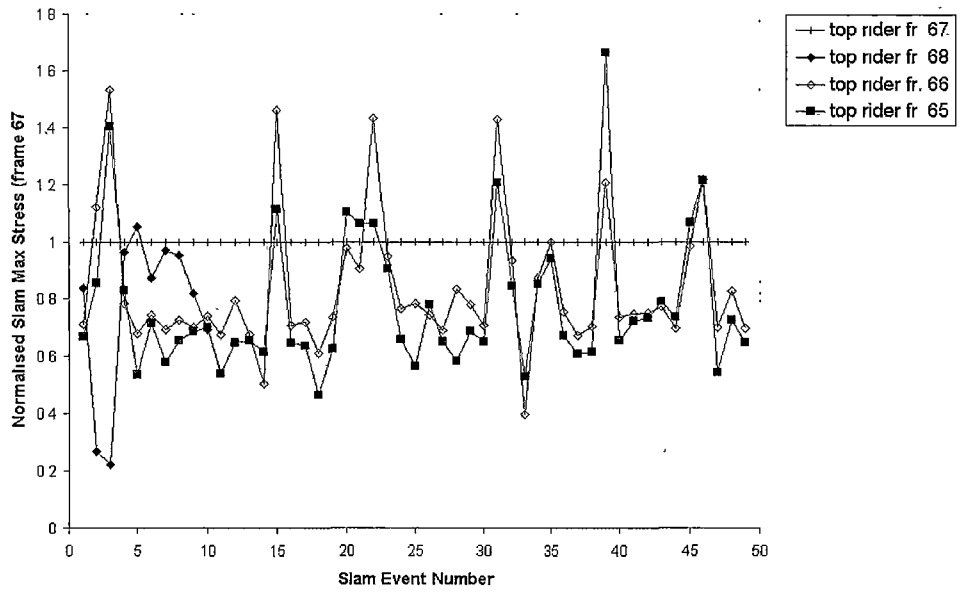


Figure 2-41: Hull 050 - System 1 Normalised Strain Gauges

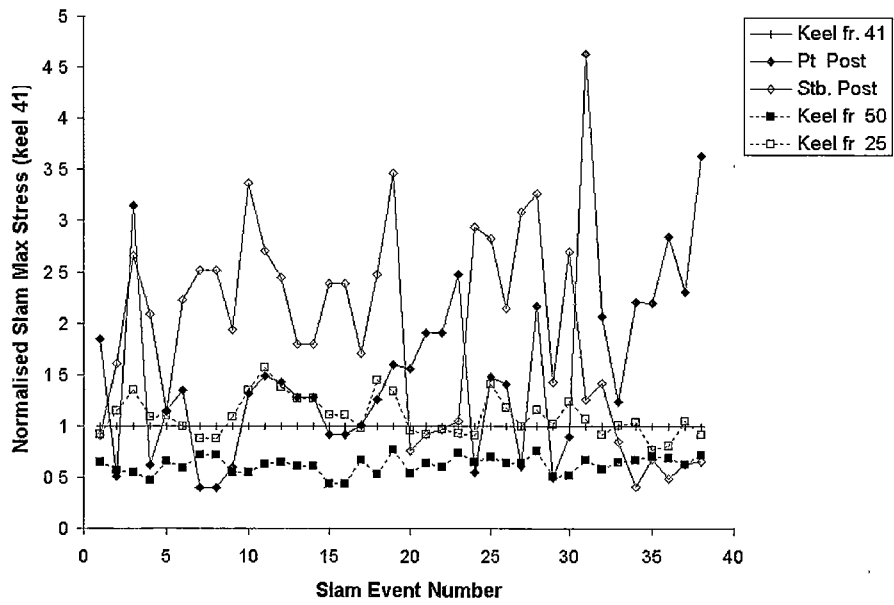
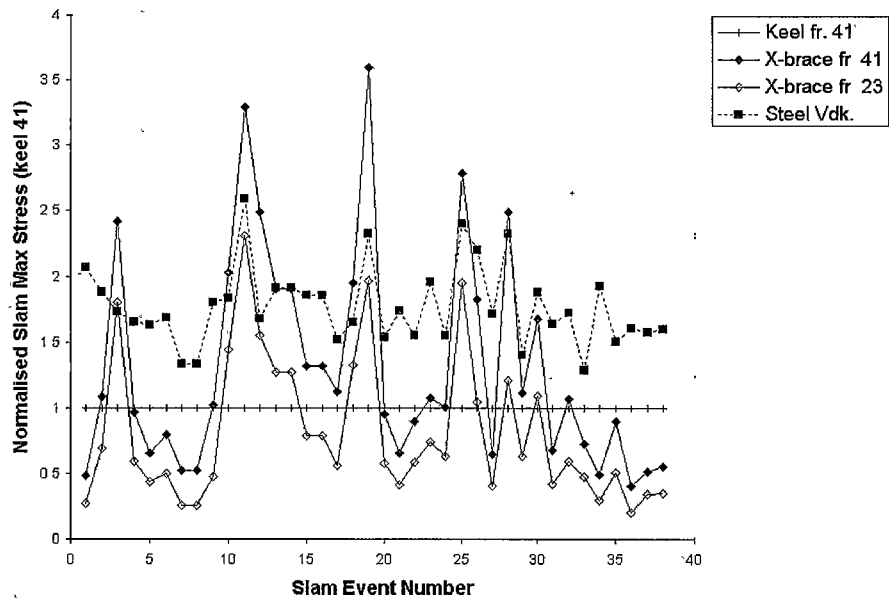


Figure 2-42: Hull 050 - System 2 Normalised Strain Gauges

frame 50 showing the lowest levels. The cross braces and forward posts were subjected to higher levels of stress than the gauges located on the keel, as can be seen in Fig. 2-42(a). The influence of the wave directionality can again be seen when comparing the relative levels of the strain gauges on the port and starboard posts. Since the stress levels recorded may be a function of the local structural design a simulation of a slam loading case, using a finite element model of the vessel, needs to be conducted before conclusions may be drawn on the relative effect of slam events on different parts of the vessel's structure.

#### **2.4.2 Extreme Slam Event**

The severity of extreme slam events and the damage they can cause to a large high-speed aluminium catamaran was demonstrated during the Hull 050 sea trials. The vessel experienced a very severe slam event that will be used as the basis for the development of quasi-static and dynamic load cases to simulate the extreme loads a slam event may impart on a large high-speed catamaran. The data collected during this slam event is therefore crucial for generating a practical methodology for the structural design of such vessels for slamming.

At 17.08 (NZ summer time) on November 21st 1999 whilst Hull 050 was travelling from Picton to Wellington into a large southerly swell it experienced a severe slam event which caused extensive structural damage. The wave impact was great enough to twist the bow slightly to port and cause external plate buckling as well as severe internal distortion to several frames, as shown in Figs. 2-43 to 2-45.

The slam event occurred with a vessel heading of 140 degrees and it was determined from the data records that the wave height was approximately 5m and the encounter wave length 80m. The vessel speed at the time of impact was 19 knots. The vertical acceleration at the LCG during the slam was 1.9g, whilst at the bow it was 3.0g (although no dedicated accelerometer was fitted to the bow, the TSK wave sensor readings allowed the vertical acceleration at the bow to be calculated). Whilst these values of vertical acceleration are high the vessel was only subjected to them for a short instant of time, i.e. a vertical acceleration of above 1.2g for a time of approximately 0.15 seconds. Unfortunately the strain gauges from System 1 were not operating on the day of the extreme slam occurrence, thus analysis could only be conducted for the System 2 strain gauges. The raw data from the measurements are shown in Fig. 2-46.

The on-board stress measurements for the extreme slam will be able to be used in inferring the loads that were experienced by the vessel during the event. These loads may then aid the optimisation of the structural design of such vessels by providing realistic loading data. Whilst it is imaginable that a more severe slam event may be experienced by such a vessel it is proposed that this slam event was close to the worst possible. Two reasons for this are provided: the vessel was operating in a seaway with a significant wave height measured as 3.7m which is slightly above the upper limit of its maximum allowable operational significant wave height of 3.5m as prescribed by classification society Det Norske Veritas; from the extensive

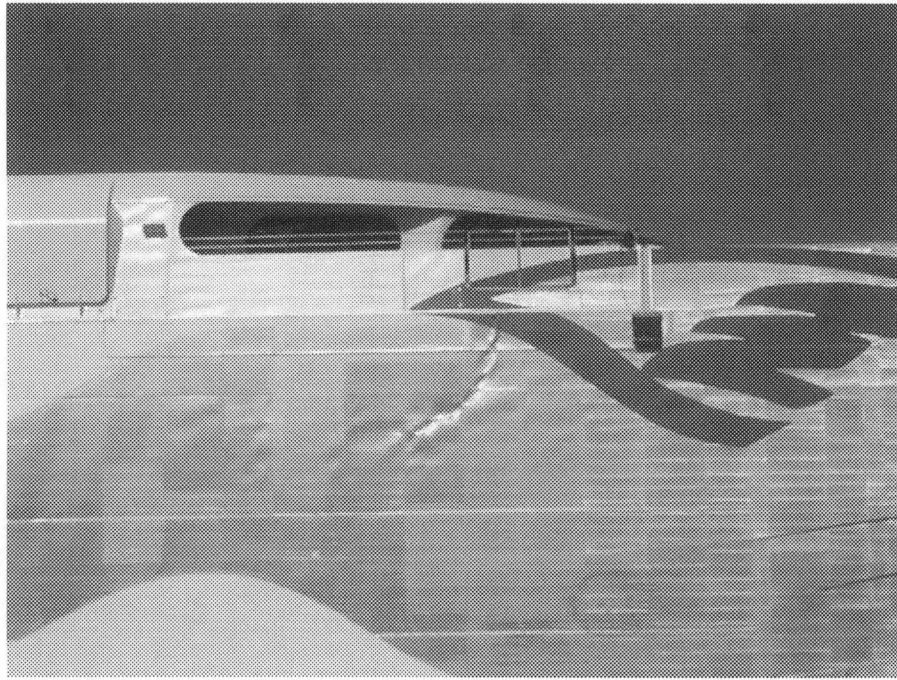


Figure 2-43: Hull 050 Extreme Slam Damage - Buckling of External Plating

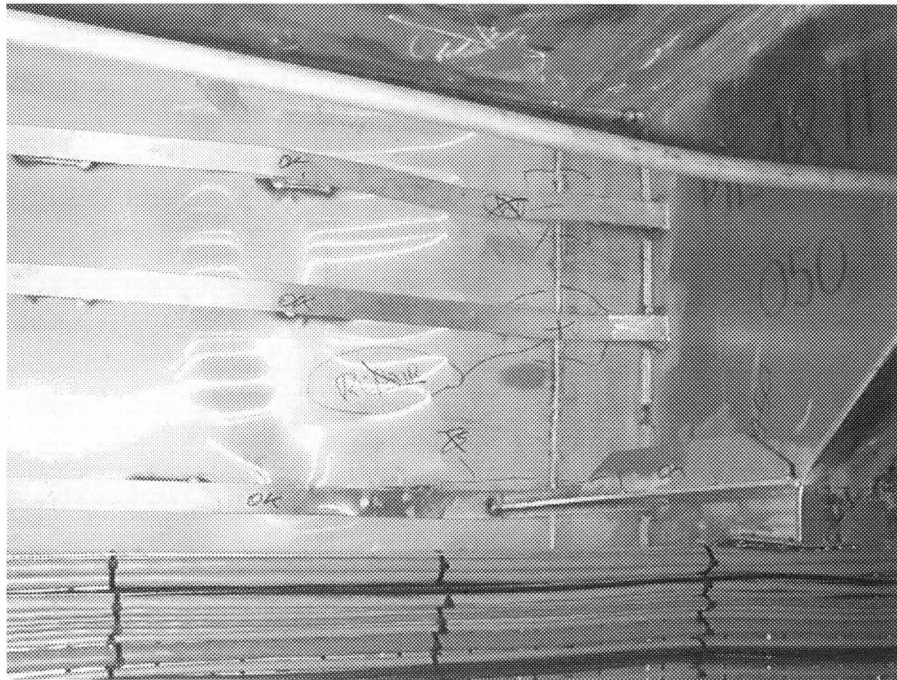


Figure 2-44: Hull 050 Extreme Slam Damage - Internal Structure at Frame 60 showing Bending of Longitudinals and Plate Buckling



Figure 2-45: Hull 050 Extreme Slam Damage - External Plating at Frame 60. View to Waterline down Outer Surface of Hull showing Buckled External Plating and Sponson

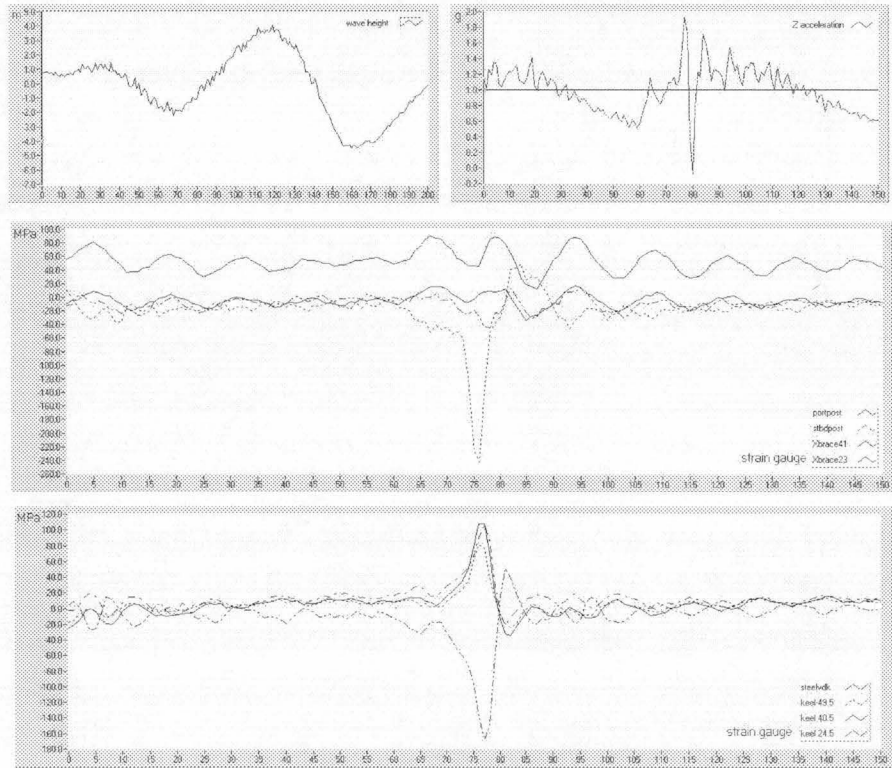


Figure 2-46: Hull 050 - Extreme Slam Event Raw Data

monitoring regime, which provided a combined total of twenty months of data for Hulls 042 and 050, this was the severest slam event recorded by a large extent.

It is not clear why an extreme slam event such as this occurs when in similar operating conditions all the slams are of a considerably smaller magnitude. One possibility is that an extreme slam event will only occur when during impact the profile of the surface of the water matches closely with that of the archway causing a close-fit and complete closure of the archway, in a manner similar to a flat plate being dropped parallel onto calm water so that the impact is not softened by the presence of a compressible pocket of air. The majority of slam events therefore occur when complete matching of the surfaces does not happen ensuring a range of impact loads are experienced.

### 2.4.3 Dynamic Features of Slamming Response

The samples of the raw data from the strain gauges (see Section 2.3.1) clearly show the dynamic nature of the vessel's structural response to a slamming event. In particular the vibratory whipping of the structure after the initial impact can be seen. Since the dynamic response of the vessel's structure may have significant ramifications for both the ultimate strength and fatigue life of a large high-speed catamaran, several facets of the dynamic response of the structure were investigated. In particular the timing of the initial response propagation through the structure, the principal modal frequencies and the level of damping of the modal responses were investigated.

For a selection of slam events, where the slam peak stress levels were greater than a normalised value of 3.0, the time between the slam peak occurring at a forward located strain gauge and at the other strain gauges located along the vessel were determined. The forward reference strain gauge was on the starboard steel post at frame 54 for Hull 042 and on the top rider at frame 67 for Hull 050. The times were averaged for each strain gauge location and are shown in Figs. 2-47 and 2-48.

A trend is apparent that the further aft the strain gauge was located the greater the time delay for the slam peak to be registered, although this time interval was always small. It indicates that there was a delay in the global response (time to initiate whipping) compared to the local impact effect. The maximum time period of approximately 0.25 seconds for Hull 042 and 0.4 seconds for Hull 050 appears to be the time required for the transference of energy from the initial slam impact zone to other locations throughout the structure. These plots clearly show that the slam impacts occurred in the bow region of each of the vessels. For Hull 050 the impact appears to have been forward of frame 67 since the time value is negative for frame 69. These findings are significant, particularly in providing information for the development of quasi-static and dynamic slam load cases.

Examples of the spectra derived from the spectral analysis of the Hull 042 slam events are shown in Figs. 2-49(a) and (b). The response spectrum for the strain gauge on the keel at

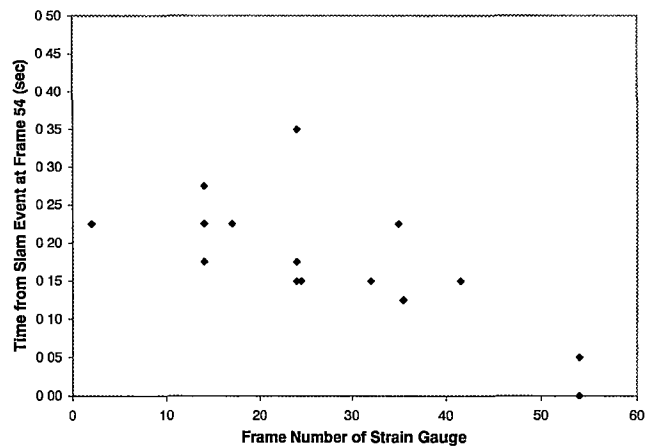


Figure 2-47: Hull 042 - Time from Slam Event registering at Frame 54 and registering at other Strain Gauges, plotted against varying Strain Gauge Longitudinal Location

frame 24 clearly shows two response frequencies present in the signal at approximately 1.5 Hz and 2.5 Hz. In contrast the signal for the strain gauge on the inner cross brace at frame 14 appears to contain a single frequency at approximately 1.5 Hz. An example encounter wave spectrum, for an individual data record, is shown in Fig. 2-49(c) which illustrates a peak wave encounter frequency of 0.2 Hz. The spectral analysis was conducted for slam events whose slam peak stress levels were greater than a normalised value of 4.0. The principal frequencies identified from the spectral analysis were averaged for each strain gauge and are plotted in Fig. 2-50. The range of data which was averaged is indicated by the range bars shown for each point. The global load frequency appears to be consistent across all the gauges at approximately 0.15 Hz to 0.2 Hz which corresponds to the underlying encountered wave frequency. For all the gauges, except those located on the steel chevron, inner cross brace and bat wing on the cross brace, two whipping frequencies were apparent during the slamming event: at approximately 1.5 Hz and 2.6 Hz. It is proposed that these two frequencies correspond with major modes of the hull structure. Some gauges, such as those on the cross bracing of both vessels, probably exhibit only the lower modal frequency because their local structural behaviour is dominated by this mode; these locations appear to whip even when slam events have not occurred, as was shown in Fig. 2-9.

Figs. 2-51 and 2-52 show the data for Hull 050 corresponding to Figs. 2-49 and 2-50. From Fig. 2-51 it can be seen that the response spectrum for the strain gauge on the top rider at frame 67 clearly shows two response frequencies present in the signal at approximately 1.0 Hz and 2.8 Hz, while the signal for the strain gauge on the cross brace at frame 41 appears to only contain a single frequency at approximately 1.5 Hz and the encounter wave spectrum shows a peak wave encounter frequency of 0.18 Hz. Results of spectral analysis conducted for all the gauges for slam events whose slam peak stress levels were greater than a normalised value of

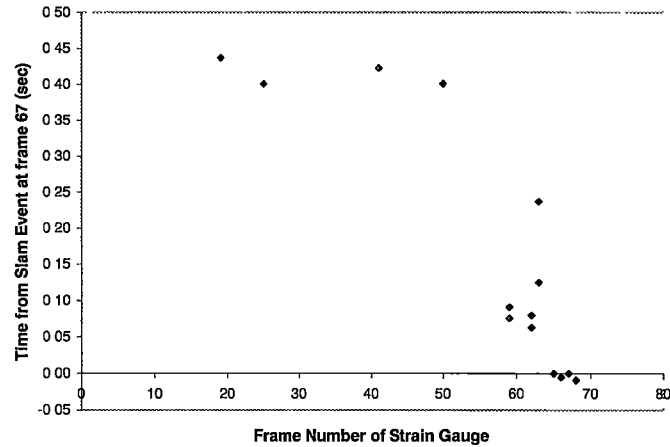


Figure 2-48: Hull 050 - Time from Slam Event registering at Frame 67 and registering at other Strain Gauges, plotted against varying Strain Gauge Longitudinal Location

2.0 are plotted in Fig. 2-52. The global load frequency appears to be consistent across all the gauges at approximately 0.15 Hz to 0.2 Hz which corresponds to the underlying encountered wave frequency. For all the gauges, except those located on the steel posts and cross braces, two whipping frequencies were apparent during the slamming event: at approximately 1.0 to 1.5 Hz and 2.6 Hz. As for Hull 042 it is proposed that these two frequencies correspond with major modes of the hull structure.

The average decay coefficients (defined in Fig. 2-13) were determined for the signals from four Hull 042 strain gauges: inner cross brace at frame 14, transverse girder at frame 35 and frames 24.5 and 41.5 at the keel, see Fig. 2-53 where the average values are shown with range bars (analysis was conducted on slams with a non-dimensional peak stress greater than 3.0). The response frequency for which the decay coefficient was determined was 1.5 Hz for the inner cross brace at frame 14 and 2.5 Hz for the other gauges. The decay of the whipping response for the inner cross brace strain gauge at frame 14 appears to be fairly constant across the number of detectable cycles with an average value of 0.07. The decay coefficient for the transverse girder strain gauge at frame 35 tends to start at a higher level of approximately 0.25 and then slowly decreases until the 7th cycle when the coefficient turns negative before growing rapidly so as to diminish the whipping response - it has an average value of 0.13. The gauge at frame 24.5 at the keel appears to have three distinct parts: the large decay coefficient (between 0.3 and 0.4) for the first cycle due to the transfer of local energy to the rest of the ship; a negative coefficient for the 2nd cycle as the energy from the rest of the ship is reflected back to the local member and then a relatively steady lower coefficient (between 0.05 and 0.2) for the subsequent cycles, as the steady state whipping mode shape is approached, until the signal becomes indistinct. The decay coefficient for the keel gauge at frame 41.5 appears to behave in a similar manner; the values for average decay coefficient for the two keel gauges are

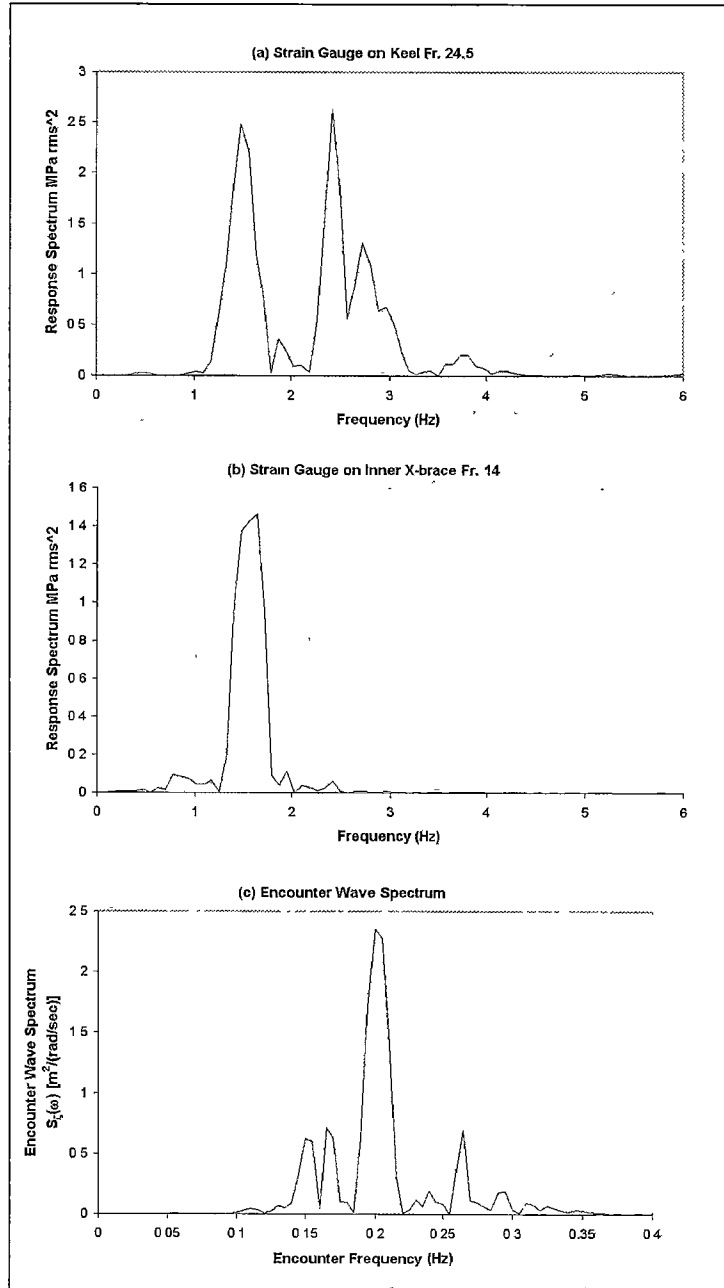


Figure 2-49: Hull 042 - Strain Gauge and Wave Spectra

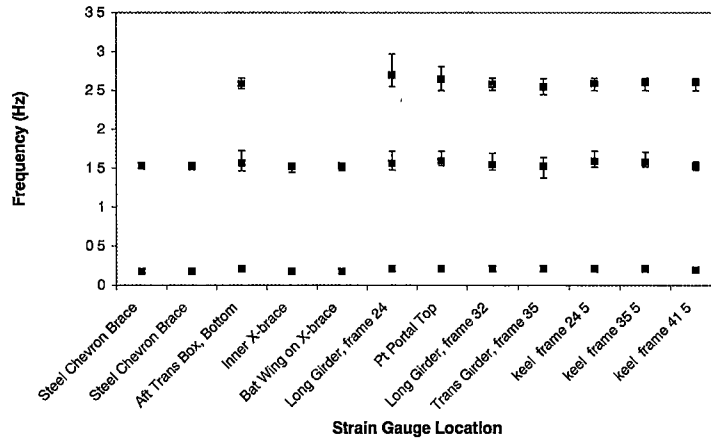


Figure 2-50: Hull 042 - Principal Frequencies for Strain Gauges

0.11 at frame 24.5 and 0.13 at frame 41.5. It should be noted that a negative decay coefficient means simply that the signal amplitude of the subsequent cycle increases.

The average decay coefficients are shown in Fig. 2-54 for the signals from four strain gauges for Hull 050: frame 67 in the centre bow, frame 41 at the keel, frame 25 at the keel and frame 23 on the starboard portal cross brace (analysis was conducted on slams with a non-dimensional peak stress greater than 2.0). The response frequency for which the decay coefficient was determined was 1.5 Hz for the cross brace at frame 23 and approximately 3.0 Hz for the other gauges. The decay of the signal at frame 67 has two parts: the large decay coefficient (between 0.3 and 0.4) for the first 2 cycles and then the steady lower coefficient (less than 0.15) for the subsequent cycles until the signal becomes indistinct. Since this strain gauge was situated in the centre bow, and was very close to the slam impact region on the hull, the initial large decay value was most likely to be due to transient energy transfer in the beam like structure towards the aft of the vessel in order to set up the modal vibration. This effect is borne out further in the strain gauge results from further aft in the vessel where the initial decay factor is negative (see the second cycles in Figs. 2-54(c) and (d)), meaning an increase in oscillation strength, as the energy is transferred aft. After this initial effect the decay coefficient for the gauges at frames 23, 25 and 41 are consistently low at less than 0.15.

The determination of the principal response frequencies and the decay coefficient of these frequencies gives significant information on the dynamic response of a vessel to slam impacts. The results will be valuable in determining the influence of slamming and whipping on the fatigue life of large high-speed catamarans.

#### 2.4.4 Additional Slam Analysis Results

Additional characteristics and effects of the identified slamming events were investigated. Whilst not central to the principal aim of this study they provide further information on the

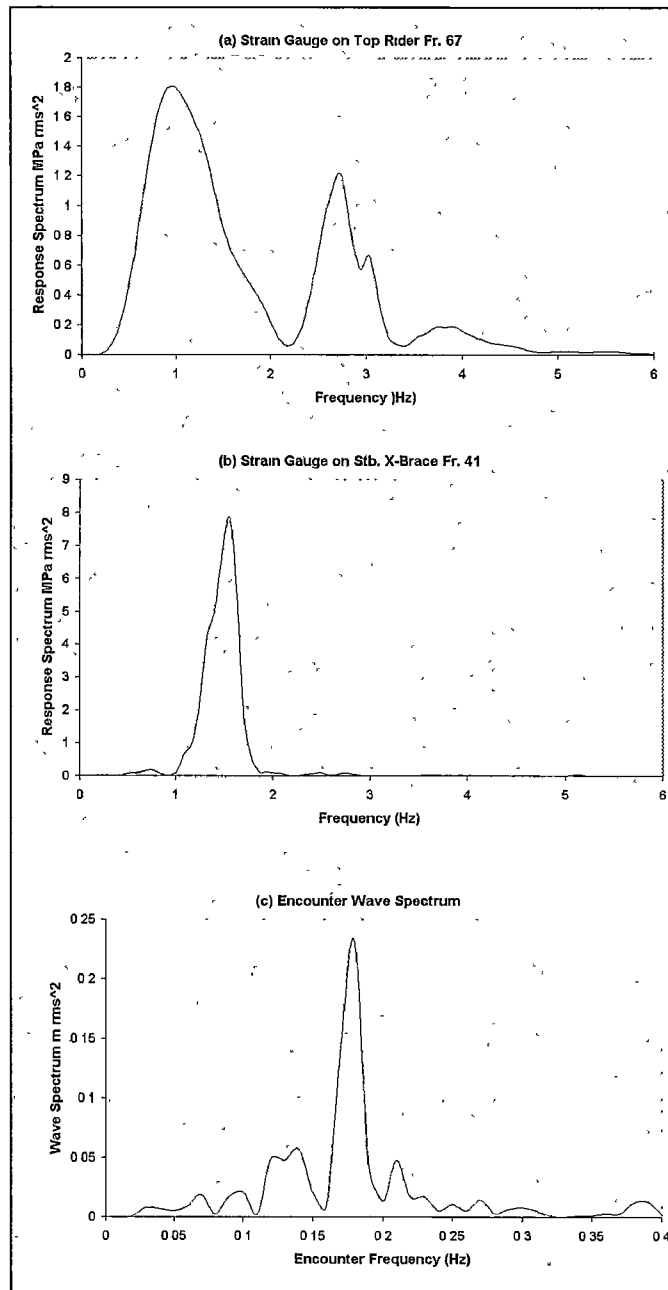


Figure 2-51: Hull 050 - Strain Gauge and Wave Spectra

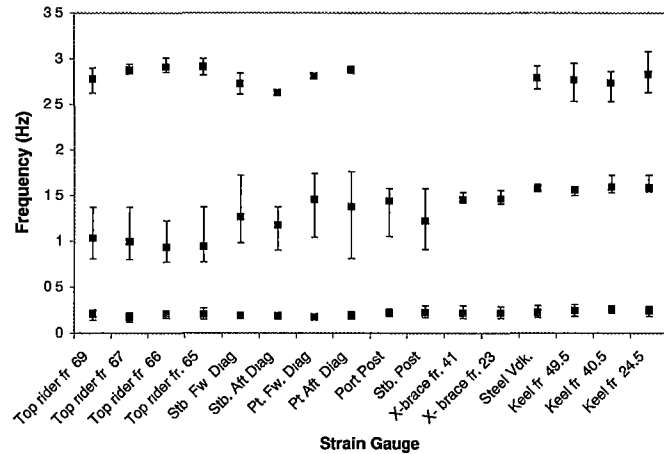


Figure 2-52: Hull 050 - Principal Frequencies for Strain Gauges

nature and influences of slam events of large high-speed catamarans. The results for both vessels were found to be similar. Therefore for the sake of brevity only the plots of Hull 042 results are shown here.

The number of waves encountered by the vessel between each slam occurrence, when more than one slam occurred in a data record, was determined and plotted against the number of occurrences, as shown in Fig. 2-55. The results show that when slams occurred in a series, they predominantly occurred with only one wave separating them. This may have been due to the phenomenon of ocean waves travelling in groups or sets so that the vessel encountered groups of large waves which caused it to slam in groups. The relative severity of slams that occurred on consecutive waves was investigated and it was found that the first slam of the two tended to be more severe than the second slam (see Fig. 2-56); this may have been due to the influence of the first slam reducing the vessel motions, thereby reducing the harshness of the subsequent slam for the same wave height. It should be noted that the strain gauge and wave data make it clear that the consecutive slam events are bow impacts on separate waves and not impacts on the same wave with the wave first hitting the forward and then the aft part of the vessel.

For a representative set of slam events of varying slam peak stress levels (approximately twenty events for each vessel), the time between the instant at which the bow of the vessel changed direction from moving downwards to moving upwards and the slam peak stress was found. These times were converted into the number of boat lengths travelled at the given vessel speed and are plotted in Fig. 2-57. The results show that for the slam events with large slam peak stresses the change in bow direction occurred a fraction of a second prior to the slam event as recorded, the maximum time was found to be 0.05 seconds for Hull 042 and 0.2 seconds for Hull 050. For the slam events with smaller peak stresses the change in direction of

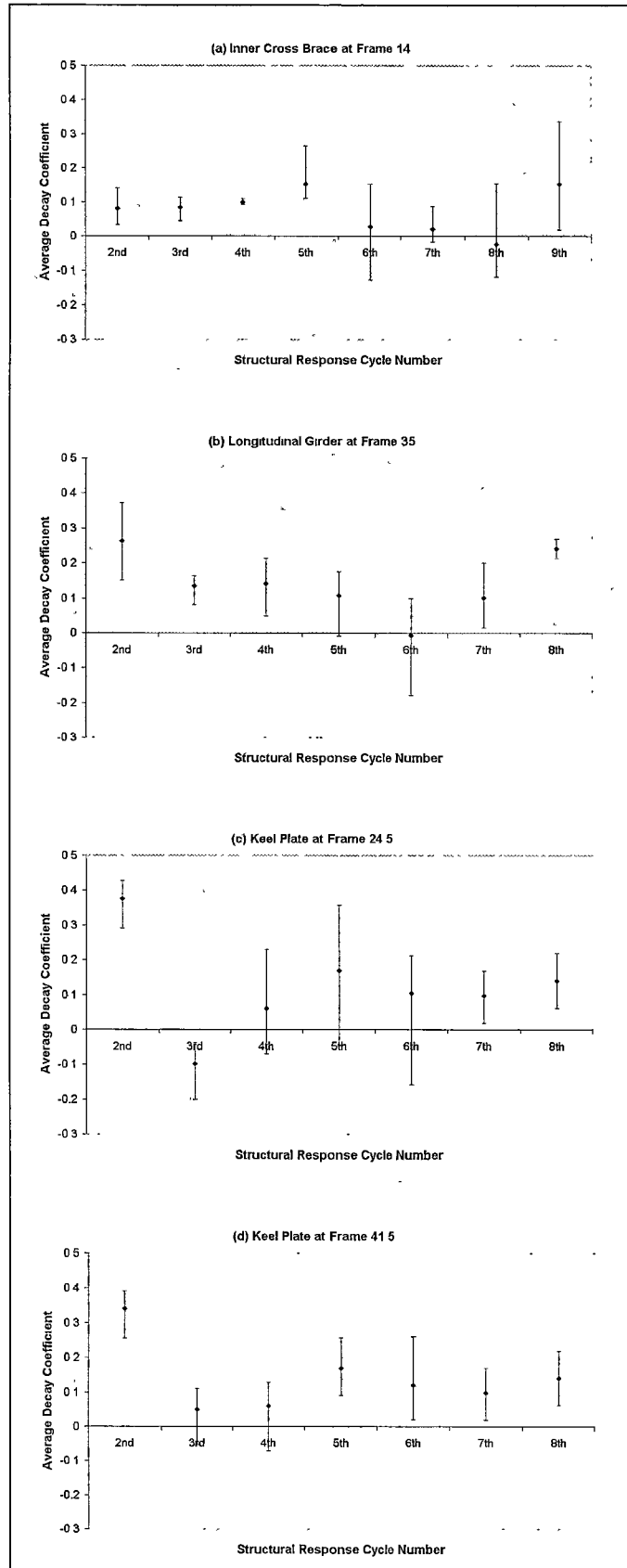


Figure 2-53: Hull 042 - Average Decay Coefficient for varying Cycle Number for Strain Gauges

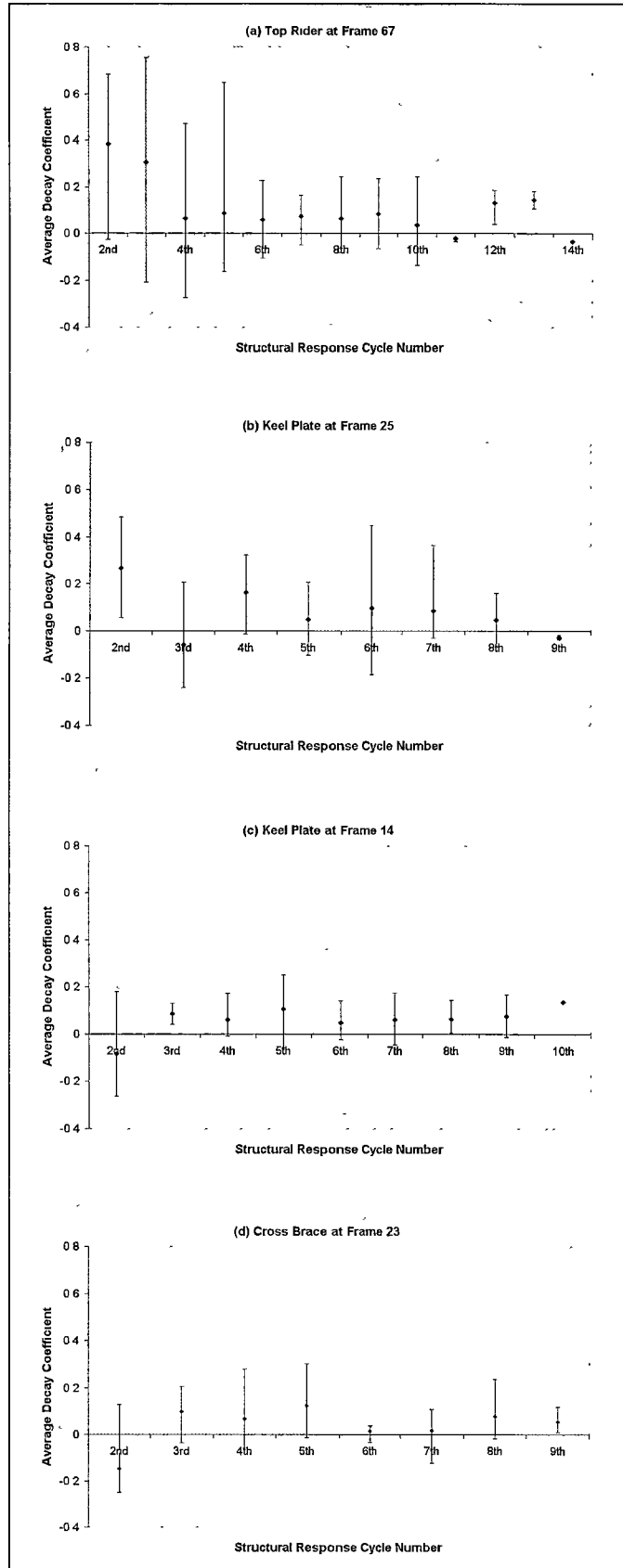


Figure 2-54: Hull 050 - Average Decay Coefficient vs. Cycle Number for Strain Gauges

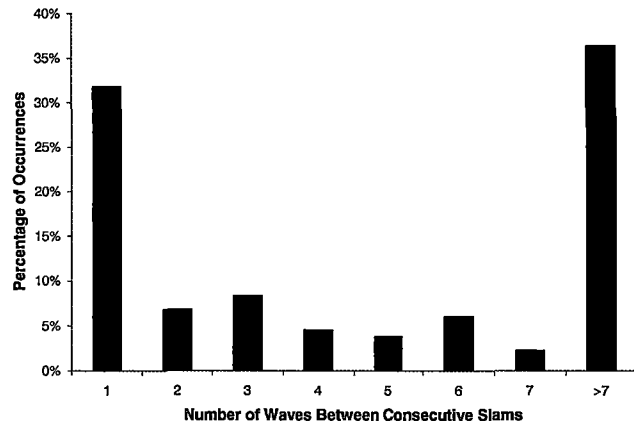


Figure 2-55: Hull 042 - Number of Slam Occurrences as a function of Number of Waves Encountered between Slams

bow movement occurred for a range of times up to 0.6 seconds prior to the recorded slam. It is thus suggested that the severe slam events were wet-deck slams and occurred when the bow of the catamaran pitched down into a wave at a high relative velocity. This motion caused the centre hull archways to be filled with water leading to a change in bow motion direction and a severe impact on the wet-deck. The less severe slam events appear to have been wet-deck slams, bottom impact slams or hull flare slams with impacts which were not large enough to change the vertical direction of travel of the vessel.

In order to further distinguish between slams that comprised wave impact on the wet-deck as opposed to bottom impact or hull flare slamming, the height of the water surface on the vessel at the point of impact was investigated. Fig. 2-58 shows the estimated water surface at the centrebow archway obtained from the TSK relative wave height values with the change in wave height due to the longitudinal distance aft from the sensor being accounted for. The tunnel height for this vessel was 2.34m. Therefore each slam event with a water height greater than 2.34m at frame 55 has been designated as a wet-deck slam. Obviously water heights above 2.34m at frame 55 are not actually possible but this plot demonstrates that the more severe slams appear to be wet-deck slams.

## 2.5 Conclusions

The following conclusions may be drawn from the results for Hull 042 and Hull 050 when operating in the conditions experienced during full-scale trials:

- The slam events could be clearly identified on all the strain gauge records with the existence of a large impulsive response followed by a whipping response.
- The slam events only occurred when the significant wave height was greater than 0.9m

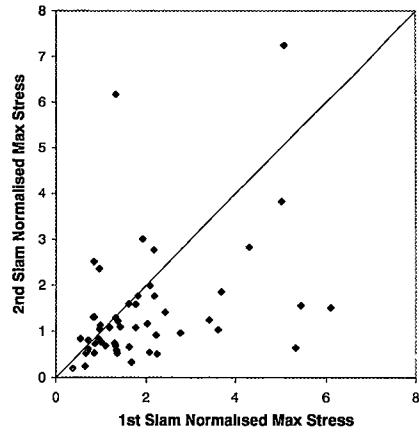


Figure 2-56: Hull 042 - Ratio of Slam Peak Stress for Consecutive Slam Events

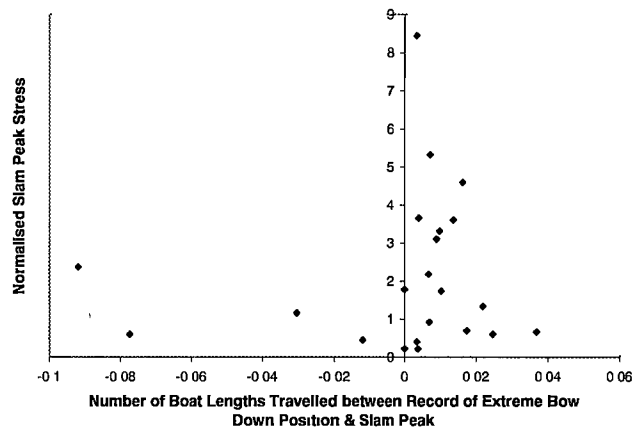


Figure 2-57: Hull 042 - Number of Boat Lengths Travelled between Record of Extreme Bow Down Position & Slam Peak for varying Slam Peak Stress

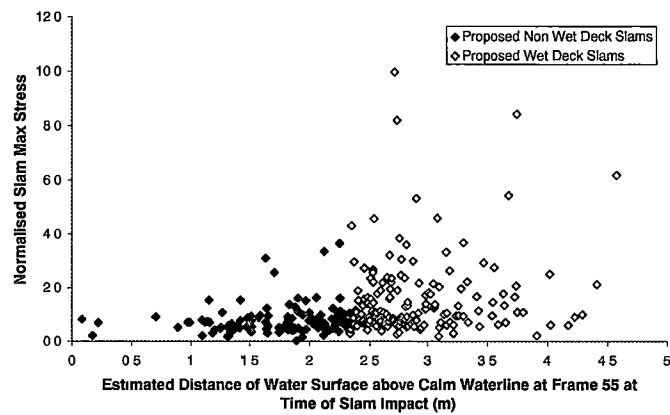


Figure 2-58: Hull 042 - Normalised Slam Peak Stress for varying Estimated Distance of Water-Surface above Calm Waterline at Frame 55 at Time of Slam Impact

for Hull 042 and 1.95m for Hull 050. The envelope of peak stress in a slam increases with increasing wave height. However, as the wave height increases smaller slam events still occur.

- The distribution of slam event peak stress against occurrences showed that the majority of slams (70% for Hull 042 and 65% for Hull 050) occur at peak stress levels less than the average peak stress value for all events. The distribution of the slam occurrences may be approximated by a Gamma probability density function.
- The slam occurrence distributions were similar for different wave height environments, indicating that relatively smaller slam events predominate in all the sea conditions experienced.
- A relative vertical velocity of  $F_{n_{relvel}} = 0.15$  for Hull 042 and  $F_{n_{relvel}} = 0.125$  for Hull 050 at the bow is required for a slam to occur.
- Slams occurred at vessel speeds as low as  $F_n = 0.16$  for Hull 042 and  $F_n = 0.18$  for Hull 050.
- The severity of the slam tended to increase with increasing relative vertical velocity at the bow.
- For Hull 050 the relative vertical velocity at impact in a slam at the bow tended to increase slightly as vessel speed increases. Such a relationship was not apparent for Hull 042.
- The relative stress levels in gauges positioned off the centreline were influenced by the sea directionality.
- Extreme slam events may occur that cause significant structural damage.
- By conducting spectral analysis on the slam data records three dominant frequencies were found for Hull 042: the global loads at 0.15 to 0.2Hz and then two associated with the whipping response at 1.5 Hz and 2.6 Hz. Three main frequencies were also found for Hull 050: the global loads at 0.15 to 0.2 Hz and then two associated with the slam impacts at 1.0 to 1.5 Hz and 2.5 to 3.0 Hz.
- The level of Hull 050 whipping was most severe for the starboard portal cross brace at frame 41, with whipping being apparent when no slams had taken place. Occasionally whipping was not exhibited by certain gauges after a slam event; this may be due to the effect of a change in fluid added mass distribution.
- The decay coefficient of the average Hull 042 whipping response tended to vary for the strain gauges investigated between -0.1 and 0.3.

- For Hull 050 the decay coefficient of the structural response signal in the strain gauge at the centrebow was large for the first two cycles (between 0.3 and 0.4) and then reduced rapidly to a steady lower level (less than 0.15) until the signal became indistinct. The decay coefficient of the signal at the keel at frame 25 had a consistently low value (less than 0.15) for all cycles.
- When slams occurred in a series, they predominantly occurred with only one wave separating them. For slams which occurred on consecutive waves the first slam tended to be more severe than the second slam.
- The large slam events were wet-deck slams as opposed to bow impact or bow flare impact slams.

## 2.6 Summary: Full-Scale Trials

The current paucity of full-scale information on the slamming of large high-speed catamarans has been outlined, particularly with respect to the nature and influence of slam events. Therefore analysis of extensive full-scale hull stress, motion and wave measurements from two large high-speed catamarans, Incat Hulls 042 and 050, has been conducted. A definition of a slam event for these vessels was proposed and used to identify slam events from the data records. The character and effects of these slamming events were investigated with respect to several factors including structural loading, wave height and length, vessel speed and heading angle, relative vertical velocity and frequency of occurrence. Particular attention was paid to the whipping response of the structures, with the principal structural response frequencies being identified through spectral analysis.

During the measurement regime Hull 050 suffered an extreme slam event which led to extensive structural damage. The data recorded during this slam event may be used to estimate the loads experienced by such vessels. This will provide the basis for the development of quasi-static and dynamic load cases which simulate extreme slam events. Key additional outcomes, such as the distribution of slam event stresses and frequency of occurrence data in varying significant wave heights, also provide valuable information for developing a structural design methodology accounting for slamming for both the ultimate strength and fatigue life estimation of large high-speed catamarans.

The slamming behaviour for both vessels was similar. Slam events only occurred once a certain significant wave height was reached, 0.9m for Hull 042 and 1.95m for Hull 050. The difference being mainly due to a variation in wet-deck tunnel height clearance and motions behaviour as a result of ride control operability. The distributions of slam peak stress against occurrences showed that the majority of slam events were less than the average peak stress for all events and that the distributions were similar for different wave environments. It was clear

that the master of both vessels slowed down as the significant wave height increased, although severe slams still occurred at the slower speeds. The slam peak stress tended to increase as relative vertical velocity increased and although a trend of increasing relative vertical velocity with vessel speed was found for Hull 050, no such trend was apparent for Hull 042. When a slam occurred, for both Hull 042 and 050, the further aft the strain gauge was located the greater was the time delay for the slam peak to register. The whipping responses of both vessels were similar with two response frequencies at approximately 1.0 to 1.5 Hz and 2.5 to 2.8 Hz and the encounter wave frequency at 0.15 Hz to 0.2 Hz. Whilst the average decay coefficient for the vessels was approximately 0.09. For both vessels when multiple slam events occurred within a single data record they were separated by only one wavelength with the second usually resulting in a smaller slam peak stress. Large slam events appeared to be wet-deck slams which could change the direction of vertical bow movement.

## Chapter 3

# Quasi-Static Slam Loads

### 3.1 Introduction

In order to optimise the structural design of lightweight high-speed vessels knowledge is required of the effect of sea loads on their structure [59], [60]. As demonstrated by the damage experienced by Incat Hull 050 after the extreme slam event, wet-deck slams can impart a large global load onto a vessel's structure and are thus of particular importance for high-speed catamarans [61], [7]. Full-scale stress data such as that collected on Incat Hulls 042 and 050 are extremely valuable for providing slam loading data which may be used in validating slam load prediction techniques, such as the method currently under development at the University of Tasmania [62] and others including Kvålsvold and Faltinsen [14] and Økland et al. [15], as well as enabling correlation with drop test and model slamming experiments (for example [62], [26] and [63]). One of the aims of the present study was therefore to develop a realistic slam load case that may be used in the structural design of large high-speed catamarans and provide data for the validation of theoretical and experimental prediction techniques of slam loads.

#### 3.1.1 Load Types

The global loads experienced by high-speed monohulls are similar to those encountered by conventional slow-speed monohulls [2], although impact or slamming loads are usually more pronounced [5], [64]. High-speed catamarans experience two major additional loading categories when compared with monohulls. As outlined originally by Nordenstrøm et al. [65] these are the global transverse load known as split and the antisymmetric global loads with opposite phase on each hull known as the pitch connecting moment (PCM), see Fig. 3-1. All loads must be accounted for in the structural design of catamarans since there are no general rules governing which will be decisive in determining the structural scantlings. Wet-deck slamming can cause significant global loads on catamarans [61], [7], in particular the longitudinal global

loads may be exacerbated by slamming effects. Slamming can also produce critical local loads for catamarans structures (local loads are defined as forces or pressures which are applied directly to a structural element). This study focuses on the global longitudinal loads imparted on a catamaran by a slam event in extreme seas.

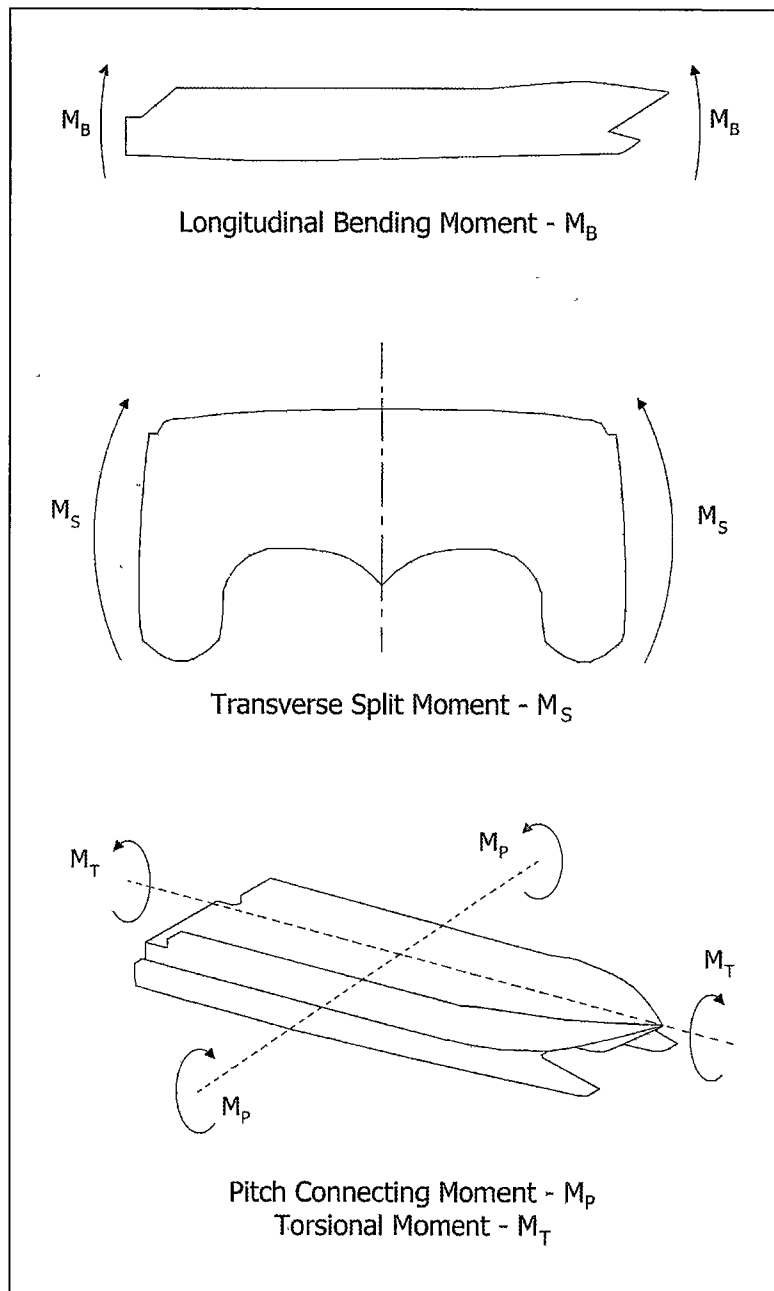


Figure 3-1: Definition of Principal Catamaran Global Loads

### 3.1.2 Load Calculation Techniques

The definition of applicable loads for a vessel during the design process is usually carried out by classification societies. Historically for conventional slow-speed monohulls, classification societies have used an empirical approach using operational experience to determine the structural rules [66]. These rules use parametric formulae to determine the structural loads, with the nature of the formulations prohibiting the use of complex descriptions of the vessel. Classification societies have been forced to respond to the rapid development of high-speed vessels over the last two decades by extending their rules to encompass the structural design of high-speed craft. However the operational experience upon which the new rules are based has been accumulated more slowly than the evolution of the craft to higher speeds and larger sizes has occurred. Therefore in addition to the empirically based rules, direct calculation methods have been introduced, as outlined by Pettersen and Wiklund [67] and Humphrey and Nybø [66] to supplement the standard rules, although these direct calculation techniques have not yet been used exclusively for the structural design of a large high-speed catamaran. Currently there are four sets of rules issued by classification societies that cover high-speed craft:

- Det Norske Veritas (DNV): *Rules for Classification of High Speed, Light Craft and Naval Surface Craft* [68].
- Lloyd's Register (LR): *Rules and Regulations for the Classification of Special Service Craft* [69].
- American Bureau of Shipping (ABS): *Guide for Building and Classing High Speed Craft* [70].
- Germanischer Lloyd, Bureau Veritas & Registro Italiano Navale (UNITAS): *Rules for the Construction and Classification of High Speed Craft* [71].

Comparisons have been conducted by authors on the variability of the different rules; Fan and Pinchin [72] concluded that there were major differences in the derived loads with the UNITAS rules giving the lightest resultant scantlings. These differences are due to variations in the parametric formulae and the methods used for accounting for service restrictions. The Det Norske Veritas rules are used in this study when comparisons are made with loads prescribed by classification societies since they are employed by Incat Tasmania during the design and construction of their vessels. Further details of DNV load requirements may be found in Section 3.2.

There are many methods available for calculating the global loads on a catamaran. The work of Holloway [73], [12] has resulted in the development of a high Froude number strip theory method which calculates the loads and motions of multihulls as well as monohulls. The high-speed strip theory of Faltinsen et al. [11] was proposed as a method for estimating global loads on high-speed catamarans. Satisfactory agreement was achieved in comparisons with

model test results except for the vertical shear forces. The values of long term load predictions were lower than those recommended by existing classification rules and it was concluded that the procedure for establishing design values needed further development. This method was further developed by Hermundstad et al. [26] to include the hydrodynamic interaction between the hulls of a catamaran and favourable comparisons were made with model tests of a flexible catamaran. A three-dimensional, non-linear, Rankine panel program, SWAN, was used by Kring and Scлавounos [74] to investigate the motions and global loads of multihulls. This program has undergone subsequent development [13] and is used by DNV as part of their direct calculation method [75]. Weems et al. [76] developed a method (Large Amplitude Motion Program - LAMP) which uses the three dimensional Green function method in the time domain. A 30m super slender twin hull (SSTH) vessel was investigated by Ito et al. [77] with its motions and loads calculated using a strip theory and compared with full-scale measurements. For a speed of 24 knots in significant wave height of 0.75m reasonable agreement was found when comparing the predictions and measurements. A three-dimensional linearised potential theory with a cross-flow approach for taking viscous effects into account was presented by Chan [78] [79] for predicting the motions and loads of catamarans. Comparisons were conducted with a SWATH model operating at zero speed [80] and reasonable agreement was found. The same model tests results were used by Reilly et al. [81] to test their linear seakeeping theory where the hydrodynamic interaction between the twin hulls was included. The correlation of the calculated and measured loads was found to be generally good. Another investigation on SWATHs was conducted by Cheung et al. [82], where three methods of analysis of their primary structure were examined. Quasi-static and rigid-dynamic approaches gave similar predictions of deformation and stress. However due to the elastic response, the hydroelastic approach gave consistently higher stress predictions. In summary, global load prediction for high-speed craft is reasonably well developed, with many analytical tools available that give acceptable predictions of underlying wave loading for design purposes.

Fewer methods are available for estimating the slamming loads on catamarans. Kaplan [83] used a simple momentum consideration to determine the slamming load on multihulls. Considering rigid body modes only, the structural response was found by integrating the forces acting on the cross deck structure, including the inertia force due to the vessel's heave and pitch motions. A two-dimensional boundary value problem was solved by Kvålsvold and Faltinsen [14] in the time domain to determine the slamming pressure on the wet-deck of a catamaran. The effect of structural elasticity was included in the solution and was found to influence the slamming load. This method was further developed by Økland et al. [15] and slam load predictions compared with slow-speed model test results. The tests on a flexible model showed that the slamming force was very sensitive to small changes in wave profile and vessel motions. The authors concluded that the calculation method described the physics of the complex problem of slamming but resulted in a conservative slamming load. Haugen and

Faltinsen [7] proposed a three-dimensional analysis for estimating wet-deck slamming loads and compared theoretical results with drop tests on a sample panel. Comparisons were also made with full-scale measurements on a 30m catamaran in wave heights up to 1.9m. Good agreement was found with the theory, although this agreement relied upon the impact velocity being estimated rather than being directly obtained from the measurements.

It is not clear how applicable these methods are for predicting the global and slamming loads of large high-speed catamarans, particularly with a centre bow configuration as used by Incat, as few comparative studies have been conducted with full-scale measurements. The development of a realistic slam load case from the Hull 050 full-scale data will therefore give valuable information for theoretical validation, as well as providing structural design information.

### 3.1.3 Finite Element Methods

The use of finite element (FE) techniques for the analysis of ship structures was first introduced by Paulling in 1964 [84]. Finite element analysis (FEA) involves replacing the continuous ship structure with a discrete model of small elements of known geometry and elastic properties. The conditions of compatibility of deflections and equilibrium of forces at the intersections of the elements of the approximating structure are applied, and a set of simultaneous equations generated. By solving these simultaneous equations the stress distribution in the structure may be estimated. Naval architects have adopted FE modelling as a standard tool for the structural analysis of ship structures, and in particular the structures of multihull vessels as demonstrated by several authors: [85], [49], [86] and [87].

The validity of using FEA for carrying out the structural design of ships has been confirmed by a small number of researchers over the last thirty years. Tanaka et al. [39] compared measurements from full-scale torsional testing of a newly built container ship with FEA of the same ship. Good agreement between the FE numerical results and full-scale testing was achieved, even though some idealisation of the model was conducted e.g. the bridge structure and some longitudinal frame members were neglected. Primarily in order to investigate hull deflections in way of the machinery space, Kaldjian et al. [88] compared FEA results with full-scale measurements of two Great Lakes bulk carriers. The full-scale deflection measurements were made using taut wire stretched between two frames whilst the vessel was loaded in still water at two different displacements. The FEA was carried out for the port side of the aft portion of the hull only with beam, truss and membrane elements being used. Good agreement was found between the measured and calculated deflections, so it was concluded that the validity of using FEA for ship structures was confirmed. Herrington and Latorre [89] constructed a 4.5m by 1.8m aluminium panel, as proposed for use in the construction of a 36m high-speed catamaran. The panel was instrumented with strain gauges and a dial gauge was used to measure deflections. Loads of up to 26.7 kN were applied and measurements compared

with FEA predictions. While the FE results obtained were sensitive to the coarseness of the mesh, the correlation with the measured results was good. A more ambitious verification of FE modelling was conducted by Pegg and Gilroy [90] for a 20m SWATH vessel. The vessel was subjected to a static loading while at the dockside using an extendable calibrated strut fitted transversely between the two hulls. A load of up to 67 kN was applied whilst strain gauge measurements were made on a transverse bulkhead and good agreement was found between the measured and calculated strain values.

The comparison of the FEA of the transverse frame of a tanker was carried out by nine members of Technical Committee II.1 of the ISSC '91 using different FE methods [91]. The analyses were all linear and elastic though the mesh design, boundary conditions and load modelling were all chosen by the individual researchers. The significant variation in stress and deflection results found was mainly due to the adoption of different boundary condition as opposed to changes in mesh density, modelling of local reinforcements and methods for accounting for self-weight. These differences highlight the need for extreme care to be taken when conducting FEA of a complex structure. Basu et al. [92] addressed the issue of assuring the quality of FEA of ship structures by proposing a standard, though flexible, methodology. A series of checks at all stages of the FEA can help eliminate errors, for example a check on the displacement results of a model can ensure that no discontinuities exist within the model. The above validations of course relied on the structure being subjected to known or measurable loads. However in ship design it is the loading (in particular wave loading) that introduces the greatest degree of uncertainty into the FEA. To improve the effectiveness of FEA in design it is therefore important to have more knowledge of the wave loads that a ship might encounter during service.

FEA has been used previously to reverse engineer load information from full-scale measurements. Stredulinsky et al. [41] measured vertical bending moment loads on a 71.6m monohull during sea trials using an array of 18 strain gauges. An FE model was developed for the vessel to determine the strain to bending moment scaling factors which were used to enable the comparison of measured loads with those predicted by two-dimensional and three-dimensional seakeeping codes. After sea trials were conducted on a US naval vessel, Hay et al. [93] applied a known load to an FE model so that the resulting strains could be calculated. Calibration factors were then obtained for the strain gauge locations on the ship so that the strain gauge readings could be translated into corresponding hull girder bending moments.

The present project uses a similar technique to determine the applied loads from the Hull 050 extreme slam event by applying known loads to the FE model of Hull 050 until the stresses derived at the strain gauge locations match those measured during the sea trials.

### 3.1.4 Summary

Classification societies prescribe the required loads for structural analysis of large high-speed craft during the design process. These loads are based mainly on minimal operational experience data, though direct calculation methods have recently been introduced. A significant number of techniques have been developed for estimated the global and slamming loads of high-speed catamarans, though very little full-scale validation work has been conducted and no validation appears to have taken place in severe weather conditions during which extreme slam events are likely to take place. Finite element analysis has been verified as an applicable method for predicting deflections and stresses of ship structures subjected to known loads by several authors, although it is important that good analysis procedures are used to ensure authentic results. An aim of this study was therefore to develop a realistic extreme slam load case. This was achieved by applying global wave and slamming loads to an FE model of Hull 050 until the results correspond with the stress results from the extreme slam data collected during the sea trials. This load case was compared with the design load case as defined by Det Norske Veritas. Additional slam load cases for other slam events were also derived. A method was developed for scaling the load cases for use with other large catamaran designs and an example of this method in use is given. The load cases will provide data for the validation of theoretical and experimental prediction techniques of extreme wave loads on large high-speed catamarans.

The full-scale results showed that slams are a dynamic event and therefore it is important to note that the development of quasi-static load cases is an approximation. The dynamic nature of the slam events and in particular the whipping behaviour are investigated in detail in Chapter 4 of this thesis, where a dynamic finite element load case method is also presented.

## 3.2 Det Norske Veritas Classification Rules

Det Norske Veritas first published rules for light craft in 1972 [94] which were followed by '*Rules for Classification of High-Speed Craft*' in 1985 [95]. The rules are now fully harmonised with the IMO HSC Code and are published in electronic format [68]. A classification note was issued in 1996 for the strength analysis of hull structures in high-speed and light craft [96]. This note gives guidelines which attempt to set a standard for various types of direct strength calculations performed as specific rule requirements. For vessels greater than 50m in length the note states that a three-dimensional finite element analysis is to be undertaken with regard to global strength analysis. Advice is given on various aspects of the FEA, for example the Classification Note states '*If four noded elements are used, a typical element size is maximum three elements per frame spacing in the longitudinal direction*'.

The global analysis of a multihull vessel shall include the following quasi-static load conditions:

- Still water condition
- Longitudinal bending moment - hogging
- Longitudinal bending moment - sagging
- Transverse split moment
- Pitch connecting moment (PCM)
- 80% longitudinal sagging moment + 60% PCM combination
- 80% PCM + 60% longitudinal sagging moment combination
- 100% longitudinal sagging moment + 100% transverse split moment combination

The applicable longitudinal bending moment may be calculated from the DNV formulation and then applied to the three-dimensional FE model to ensure that the resultant stresses are within the allowable range. This method assumes the dynamic wave loads can be reduced to quasi-static loads that are representative of the typical dynamic loading regime. This approach has been validated against service experience over many years and has the benefits of being consistent and reasonably easy to apply. The results of this quasi-static analysis give information on typical extreme stress values which are suitable for comparison against permissible design stress values.

The longitudinal sagging moment is also known as the hollow landing condition since it simulates the vessel being supported at the bow and stern by wave crests whilst the vessel midships is in a wave trough. A global inertia load is also incorporated into this case to account for the dynamic nature of the wave loading. This load case is the closest simulation of a bow slamming event and was used as a comparison with the derived extreme slam event load case.

### **3.3 Extreme Slam Events Details**

As outlined in Chapter 2 Hull 050 experienced an extreme slam event during the full-scale measurements. The extreme slam event occurred at 17.08 (NZ summer time) on November 21st 1999 whilst the vessel was travelling from Picton to Wellington into a large southerly swell. On-board weather observations were recorded at the time of the slam and are given in Table 3.1. The loading condition of the vessel at the time of the slam event was also noted and is shown in Table 3.2. The slam event occurred with a vessel heading of 140 degrees (bow quartering) and it was determined from the data records that the wave height was approximately 5m and the encounter wave length 80m. The vessel speed at the time of impact was 15 knots. The vertical acceleration at the LCG during the slam was 1.9g, whilst

at the bow it was 3.0g. Whilst these values of vertical acceleration are high the vessel was only subjected to them for a short instant of time.

Unfortunately the strain gauges from System 1 were not operating correctly on the day of the extreme slam occurrence, thus the FE correlation work for the extreme load could only be conducted for the System 2 strain gauges.

Parameter	Observed Value
Beaufort Sea Scale	4
Beaufort Swell Scale	SSE 5
Heading Direction	Waves 40 degrees on starboard bow
Significant Wave Height	3.7 m
Vessel Speed	Engine 700rpm and 15 knots

Table 3.1: Hull 050 Extreme Slam Event On Board Observations

Item	Number	Location
Large Bus	2	Fwd of amidships
15m Truck	1	Fwd of amidships
Car	40	Centre to outboard at amidships
Passengers	562	Superstructure
Crew	23	Superstructure
Fuel	71.636 tonnes	(assumed tank level = 9/10 full)

Table 3.2: Hull 050 Loading at Extreme Slam Event

### 3.4 Additional Slam Event Details

In addition to the extreme slam event, four supplementary slam events from the full-scale trials were also investigated to give a broader indication of the longitudinal loading during slam events. These slam events were also of a severe nature, although not as extreme as the slam that caused the structural damage. Details of all the slam events investigated are shown in Table 3.3. Slam events 3, 4 and 5 were from the same voyage as the extreme slam event so the mass distribution shown in Table 3.2 was also used for these events. No loading information was available for the voyage during which slam event 2 occurred so the same loading configuration as the extreme slam was used except that the truck and two buses were removed and the fuel tanks set at half full.

### 3.5 Finite Element Model

The original FE half model of Hull 050 was constructed in NASTRAN 4 Windows by importing the geometry from CADKEY in order to position the nodes at their correct offset [97]. The model, including element and material properties, was converted to PATRAN/NASTRAN. The model consisted of predominantly plate and bar elements with the exception of laminate

Slam #	1	2	3	4	5
Monitoring System in Operation	System 1 only	System 1 & System 2	System 1 only	System 1 only	System 1 only
Wave Length	80m	70m	100m	85m	90m
Wave Height	5.0m	4.3m	5.7m	4.4m	4.4m
Wave Heading	140 degrees	220 degrees (assumed)	140 degrees	140 degrees	140 degrees
LCG Vertical Acceleration	1.9g	1.3g	1.75g	1.5g	1.6g
Bow Vertical Acceleration	3.0g	2.0g	2.6g	2.3g	2.3g
Comments	Largest slam event in data records. Extreme slam event that caused structural damage.	Severe slam	2nd largest slam event in data records	Severe slam	Severe slam

Table 3.3: Hull 050 Slam Event Details

elements used to model the honeycomb material in the mezzanine ramps. The frame webs and shell plates were modelled as plate elements and the riders and posts as bar elements. However in high stress areas the riders were modelled as a combination of bar and plate elements to enable more accurate stress predictions. All cross-bracing members, longitudinal stiffeners and steel work were modelled as bar elements. The model included the superstructure which was connected to the main hull via elements modelling the connecting rubber mounts.

Two significant changes had been made to the structural design of Hull 050 since the original FE model was developed by Incat Tasmania. Firstly the model did not contain the full rider set-up in the bow void, in particular frames 66 to 69. Secondly a series of longitudinal members had been retro-fitted between the top riders of frames 63 to 69, on the centreline, in order to strengthen the area after some localised shell plate distortion was observed after the delivery voyage. The new bow void design geometry was imported from CADKEY and meshed in a similar manner to the existing structure. The new longitudinal members were also added as 100mm x 100mm box sections (thickness = 5mm) with offsets at each end, see Fig. 3-2.

The FE model was then refined in the areas of the strain gauge locations to achieve enhanced stress resolution and enable improved model correlation with the full-scale data. In order to achieve a suitable level of refinement the DNV longitudinal sagging moment rule load case was analysed after each mesh size reduction. Once no change in the stress result for the strain gauge location was observed from a previous refinement the mesh size was deemed suitable. This iterative process was also used to investigate the extent of mesh refinement as a function of distance from the strain gauge location. Figs. 3-3 and 3-4 show an example of

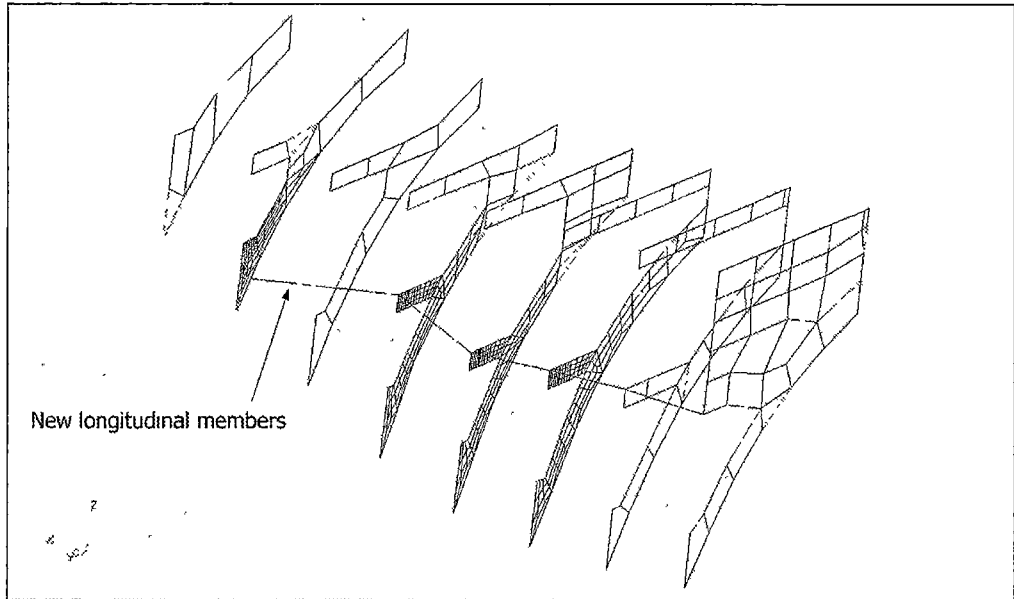


Figure 3-2: Hull 050 - Refined FE Mesh on Frames 65, 66, 67 and 69

the changes to the mesh due to refinement in the strain gauge location at Frame 24.5 on the keel.

In order to carry out an asymmetric analysis the finite element model needed to be extended to a full model. The half model was therefore mirrored about the vessel centreline to produce a full model consisting of 63628 elements, see Fig. 3-5. The element properties and load cases were also transformed during the mirroring process.

The mass distribution of the FE model was then modified to simulate the configuration of the vessel during the extreme slam event. The loading condition outlined in Table 3.2 was used. This involved removing the existing truck and car loads and reloading according to Fig. 3-6. A mass of 43 tonnes was used for the truck and buses (spread over 12 load points for each vehicle) whilst a mass of 1.25 tonnes was used for the cars (spread over 4 load points for each vehicle). The number of passengers and crew on-board (562 passengers plus 23 crew) closely matched the total of 600 used in the original development of the FE model, therefore no change was made to the passenger and crew loading in the FE model. The passenger and crew masses were represented in the model by increasing the density of the material used in the superstructure as opposed to using point loads.

### 3.6 Wave-Induced Load Model

In order to provide load information for the finite element model a method for estimating the wave-induced load of the underlying wave that the vessel encountered during the slam event was needed. Since a simple yet effective method was required the Froude-Krylov exciting force

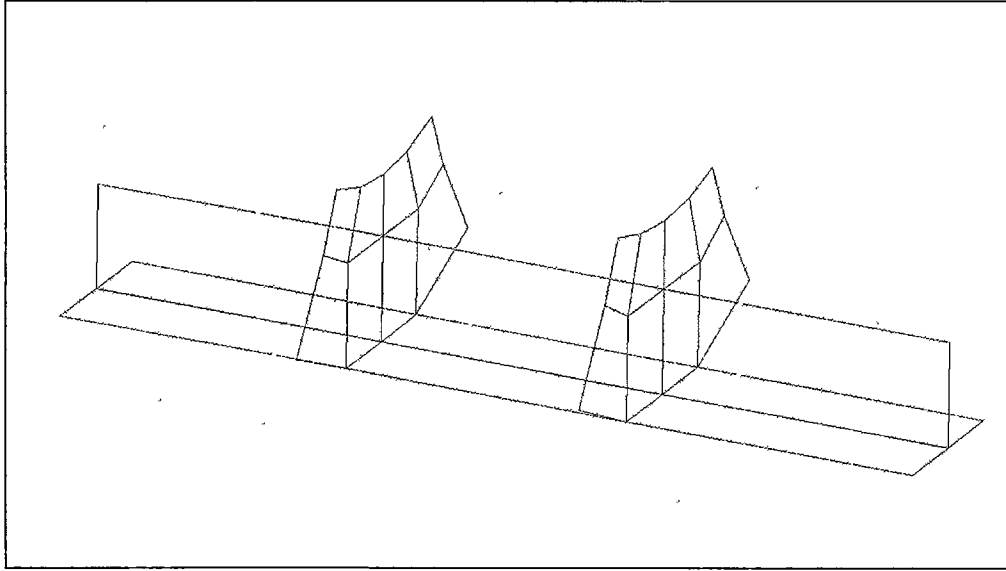


Figure 3-3: Hull 050 - Original FE Mesh on Keel at Frame 24.5

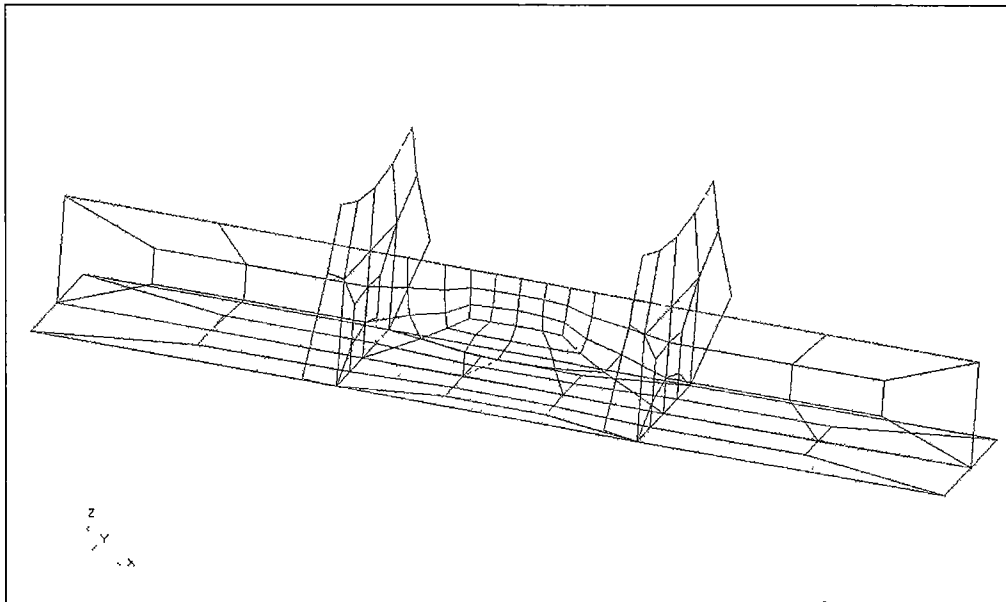


Figure 3-4: Hull 050 - Refined FE Mesh on Keel at Frame 24.5

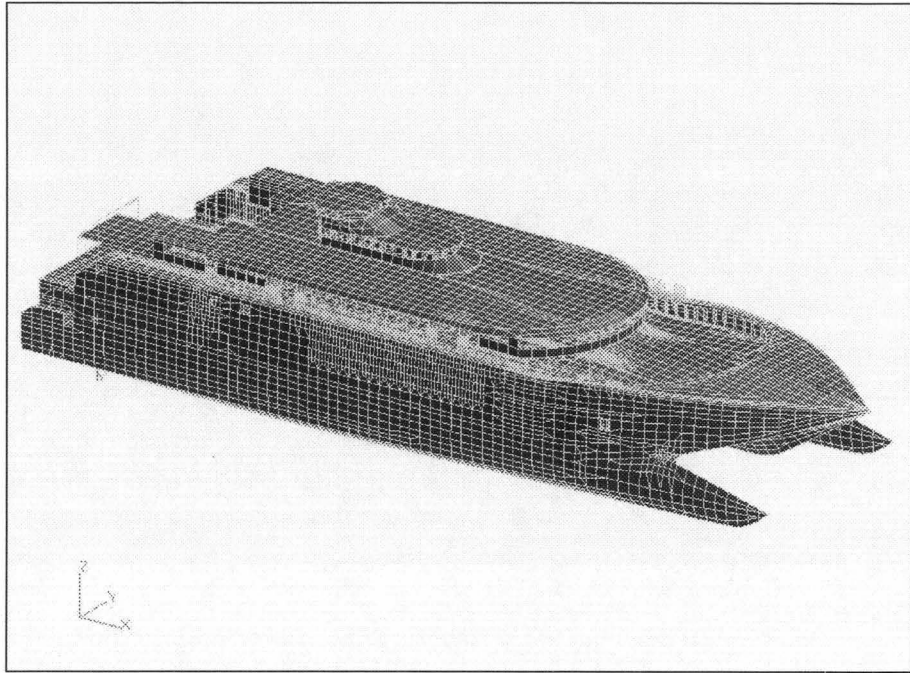


Figure 3-5: Hull 050 - Full FE Model

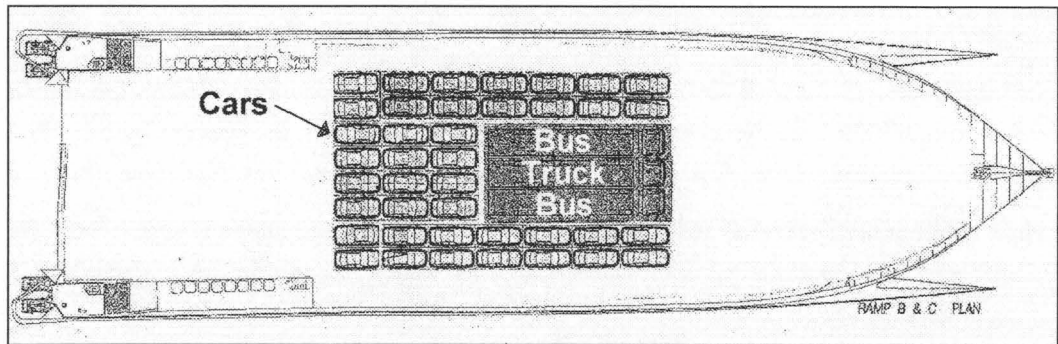


Figure 3-6: Hull 050 - Vehicle Layout on Tier 1

was used to determine the vessel's heave and pitch in a regular wave and consequently the vessel loading. The Froude-Krylov force results from the integration over the vessel's surface of the underwater pressure, assuming that the presence of the hull has no effect on the waves [54]. An advantage of this method over linear strip theory is that it allows the underwater pressures, including the hydrostatic pressures, to be determined up to the instantaneous waterline. The Froude-Krylov approximation uses only the incident wave potential in estimating the total wave exciting force and the effect of wave diffraction by the body is therefore not included. The appropriateness of this approximation increases in accuracy as the incident wave wavelength increases relative to the length of the vessel [98]. In their study on catamaran motions and loads Lee et al. [99] found that for wave lengths greater than four times the overall vessel beam the inclusion of the diffracted wave force had little effect. Since the vessel length to wavelength ratio for the extreme slam condition was close to 1.0, this makes the use of the Froude-Krylov method appropriate in this instance. The motions of the vessel are taken into account in the proposed model by including, in the weight of each section of the vessel, an additional dynamic inertia component. This component is determined from the measured full-scale vertical accelerations at the longitudinal centre of gravity and forward perpendicular and has the effect of increasing the weight of the vessel in the load model causing vertical sinkage. That the hydrostatic portion of the wave-induced loading is dominant may be seen as the reconciliation is good when the model was tested by comparing the measured strain gauge stress readings with those predicted by FEA for a purely global wave loading situation.

The model was developed to consider regular sinusoidal waves at all heading angles. The vessel's hulls were modelled through Bonjean curves representing the immersed area of each transverse section for the local draft. A Bonjean curve is a curve of area for a transverse section, i.e. for a given draft the curve provides the immersed sectional area. The moment generated in the single hulls by the asymmetry of the wetted transverse area was neglected and the draft was considered to be equal on both sides of the same hull. However, for a non-head or non-following sea condition the draft at the same longitudinal position on each hull was different and accounted for.

In the quasi-static approach the vessel is balanced on the wave, for a given wave length, wave height and heading angle, with the vessel's weight forces and moments balanced by the vessel's effective buoyancy forces and moments.

$$F_{bw}(T, v) = F_m \quad (3.1)$$

$$M_{bw}(T, v) = M_m \quad (3.2)$$

where:

$F_{bw}$	Buoyancy force in the wave
$M_{bw}$	Buoyancy moment in the wave
$T$	Sinkage
$v$	Trim
$F_m$	Weight force
$M_m$	Weight moment

The sinkage and trim of the vessel are iteratively varied until the equilibrium position is determined according to Equations 3.1 and 3.2. The vessel is assumed to maintain a zero heeling angle in the wave environment. Although in oblique seas a catamaran would be expected to exhibit an angle of heel, the effect on the buoyancy forces was assumed to be small. The buoyancy force at each frame may thus be calculated using the wave-induced load model. Since the mass distribution for the vessel is also known the bending moment and shear force curves may also be found:

### 3.7 Hull 050 Slam Load Case

An extreme slam load case was developed equivalent to the slam event which caused the structural damage on Hull 050. Slam load cases were also developed for the four other severe slam events listed in Table 3.3. The wave-induced load model and the method of correlating the full-scale stress measurements to the vessel loading were first tested for a purely global wave loading situation with no slam impact on the vessel. Whilst the asymmetry of all the investigated slam events was apparent from the full-scale strain gauge results which indicated differing levels of stress in the port and starboard steel posts, it was not possible to accurately determine the extent of asymmetry of the slam or the sea direction, beyond the information available from the on-board observations. Therefore two load cases were developed: in the first the slam was assumed to be symmetric about the vessel centreline with the vessel operating in head seas and in the second the asymmetry of the slam was determined from the gauges positioned to indicate asymmetry and the vessel was assumed to have a wave heading of 140 degrees (as was observed during the event). In this way extremes of interpretation of the measured data were encompassed and bands could be placed on the magnitude of the slam force as determined from the data records.

The extreme slam load case was compared with the DNV longitudinal sagging moment to ascertain whether the slam event imparted a greater load on the vessel than prescribed by the classification society.

#### 3.7.1 Global Loads Correlation

The first stage of the analysis was to simulate the FE model in typical longitudinal bending conditions and compare the model output with the full-scale strain gauge data. If good cor-

relation was achieved this would give confidence in both the wave-induced loading model and the FE model to extend the process to simulating a slam impact event. This was carried out firstly for a symmetric global loading scenario whereby the vessel was assumed to be operating in head seas and the results for port and starboard location strain gauges were averaged. The results from the symmetric global loads correlation showed reasonable comparison between the measured and calculated on-board stresses, as shown in Thomas et al. [100]. The global loads correlation was then extended to include the asymmetry of the vessel heading. Two separate data runs were used for longitudinal bending correlation purposes as defined in Table 3.4. The full-scale results for the global longitudinal bending scenario 1 are shown in Fig. 3-7. The wave loadings were determined by the wave-induced load model using the wave details and mass distribution from the full-scale measurements. Note that on-board observations, including mass distribution and vessel heading, were not available for scenario number 2.

<b>Longitudinal Bending Scenario Number</b>	<b>1</b>	<b>2</b>
<b>Monitoring System in Operation</b>	System 1 only	System 1 & System 2
<b>Wave Length</b>	90m	70m
<b>Wave Height</b>	2.2m	2.5m
<b>Wave Heading</b>	140 degrees	220 degrees
<b>LCG Vertical Acceleration</b>	1.2g	1.05g
<b>Bow Vertical Acceleration</b>	1.85g	1.7g

Table 3.4: Hull 050 Longitudinal Bending Details

For the analysis the FE model was subjected to a set of buoyancy forces distributed along each demihull (acting at 3 nodes for each frame) and centrebow (acting at 4 nodes for each frame) plus a vertical inertial force equivalent to that determined from the full-scale data. Any model imbalance in the full six degrees of freedom was accounted for by NASTRAN's inertial relief technique [101].

The results for the sagging condition for scenario 1 are shown in Fig. 3-8. This shows that there was good correlation, with the average error in the stress between the FEA and full-scale results being 15.8%. The majority of this error was for the strain gauges situated on the portal top cross bracing where the FE analysis under predicted the stress as measured in full-scale. This may have been due to the presence of some split hull loading which was not included in the FE loading condition. The comparison for scenario 2, as shown in Fig. 3-9, did not achieve the same level of correlation with an average error of 35.2%. This was probably due to the lack of information for the mass distribution of the vessel during the particular voyage which meant that the mass distribution from scenario 1 was used (except that the truck and two buses were removed and the fuel tanks were set at 1/2 full). A sensitivity study showed that a change in mass distribution could have a significant effect on the stress levels derived from the FE analysis, as shown in Fig. 3-10. This plot shows that an increase in fuel loading at amidships, from a base level of 39.8 tonnes, predominantly affects the strain gauges situated on the keel and the steel diagonal on the vehicle deck, whereas the influence on the forward

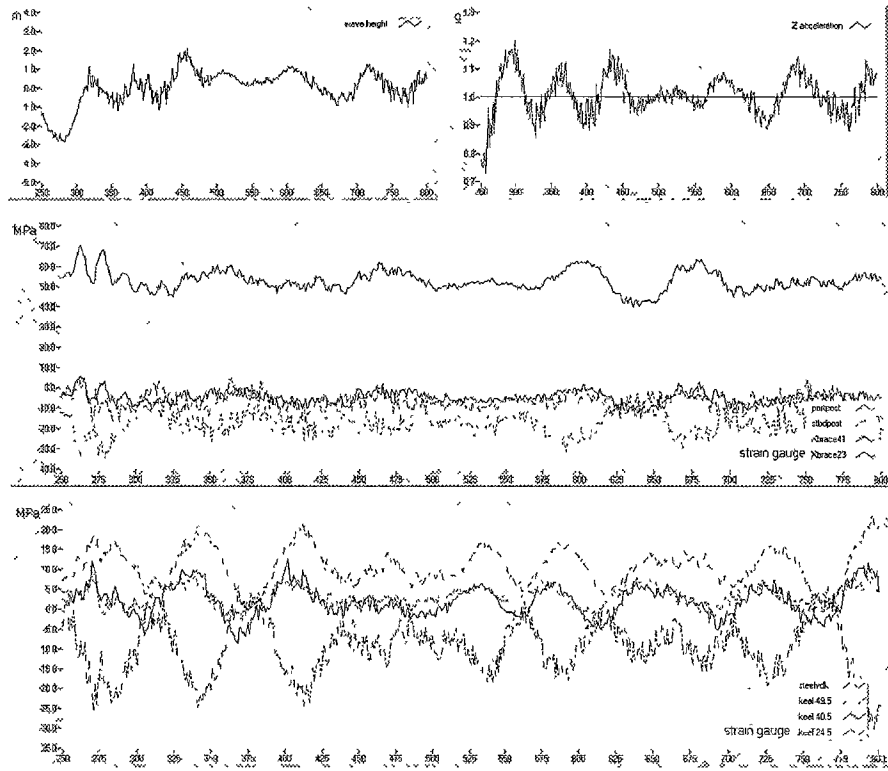


Figure 3-7: Hull 050 - Global Longitudinal Bending Full-Scale Results, Scenario 1

steel posts and cross bracing is small. Also a heading angle of 220 degrees was assumed for the FEA results of Fig. 3-9 in the absence of any on-board observations for this voyage. It was concluded that these two sets of results showed sufficiently acceptable levels of correlation between the full-scale results and the FE analysis to proceed with developing realistic load cases of slam events.

### 3.7.2 Slam Correlation

#### 3.7.2.1 Extreme Slam Correlation

The underlying wave loading for the extreme slam event was determined by using the wave-induced load model (Section 3.6) for a wave of length 80m and height 5m, with a vessel heading of 140 degrees. It is important to note that the wave length of the wave is close to the vessel length and hence near to the worst sagging case during a slam impact of the bow. The vertical acceleration of the vessel was also taken into account when calculating the buoyancy forces using the acceleration levels of 1.9g measured at the LCG and 3.0g measured at the bow during the slam event. In addition to the underlying global load, a load was required to simulate the slam impact force on the bow of the vessel. Unfortunately the size and distribution, both longitudinally and transversely, of this load were unknown. Therefore the load magnitude

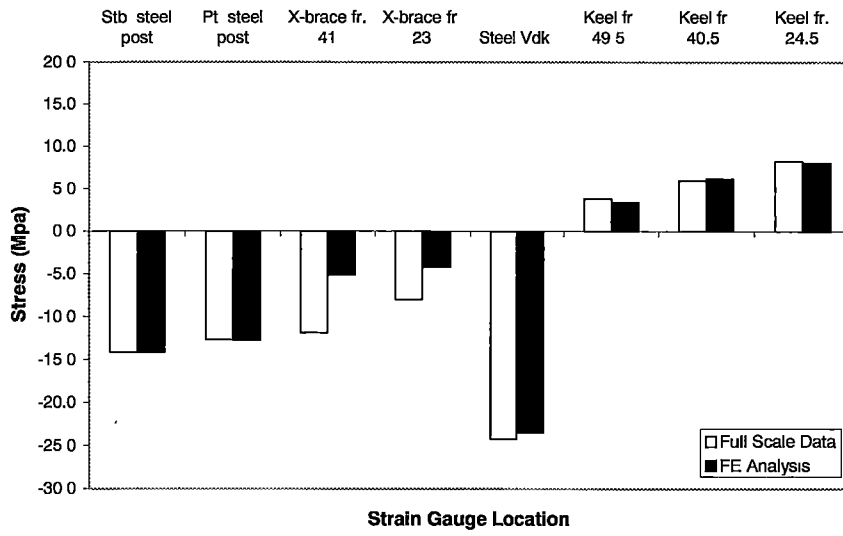


Figure 3-8: Comparison of FEA and Full-Scale Data for Longitudinal Bending Scenario 1

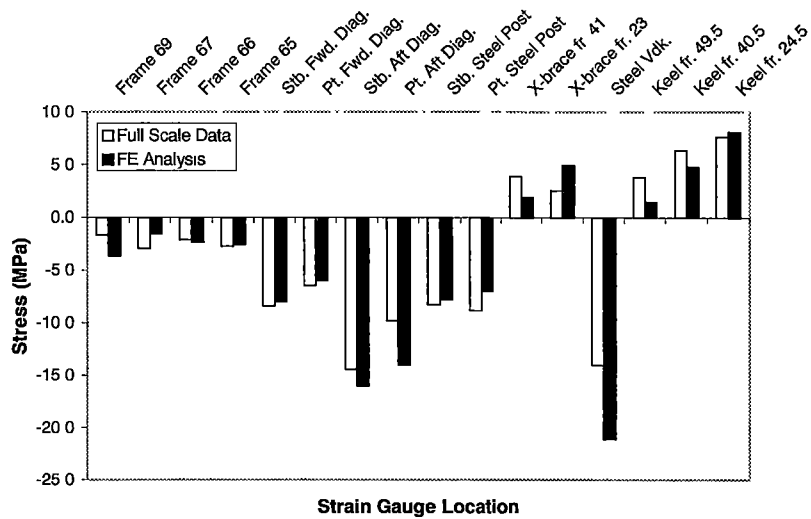


Figure 3-9: Comparison of FEA and Full-Scale Data for Longitudinal Bending Scenario 2

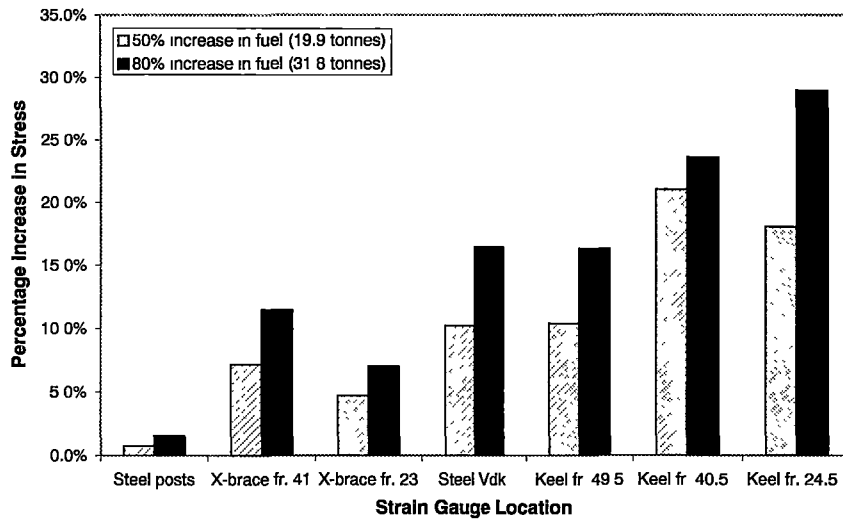


Figure 3-10: Increase in FEA Stress due to Increase in Fuel Loading

and distribution were systematically altered until an acceptable correlation with the full-scale strain gauge data was achieved. The maximal strain gauge values used are shown in Table 3.5. The only port/starboard asymmetry in the strain gauge results was the data for the forward port and starboard steel posts, which were located towards the bow of the vessel at frame 63. These gauges locations were very sensitive to the slam load magnitude and distribution, and were therefore the most productive guides for determining the impact force. The other gauges along the vessel were more sensitive to the slam load magnitude than its distribution, although the gauges on the portal top cross bracing gave some indication of the transverse distribution of the load. The result of the correlation study was that an additional load of 1280 tonnes was distributed over the starboard side of the centrebow and archway to account for the impact force. The distribution of the slam impact load on the centrebow is shown in Fig. 3-11. The centre of this distribution is further forward along the vessel than may have been expected, with the lowest and flattest centre archway sections being at the aft end of the centrebow (frame 52). The longitudinal distribution of the buoyancy for each hull and centrebow plus the slam impact applied forces are shown in Fig. 3-12. Note that the frames are numbered from the transom.

For the analysis the FE model was again subjected to a set of buoyancy forces distributed along each demihull (acting at 3 nodes for each frame per hull) and centrebow (acting at 4 nodes for each frame per hull) plus a slam impact force which was applied to each node on the affected centrebow and archway area. The model was also subjected to a vertical inertial force equivalent to 1.9g.

Examples of the output from the FE analysis are shown in Figs. 3-13 and 3-14. The exaggerated plot of the deflection of the hull in Fig. 3-13 shows the dominance of distortion

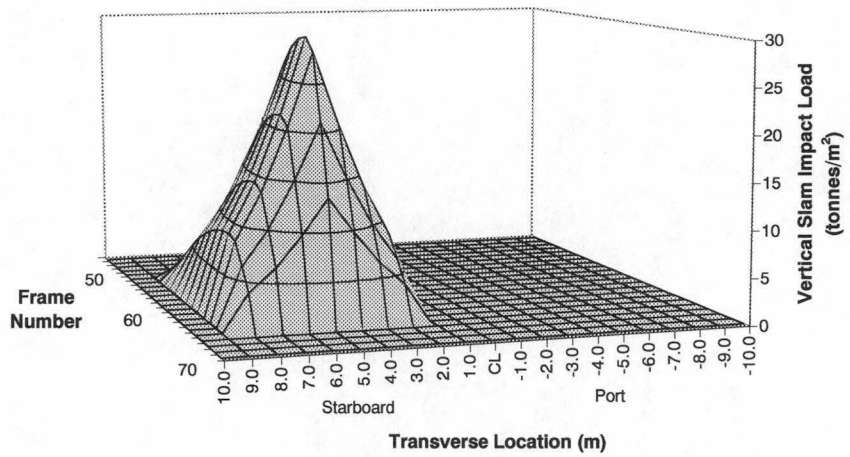


Figure 3-11: Distribution of Slam Impact Load for Extreme Slam Event

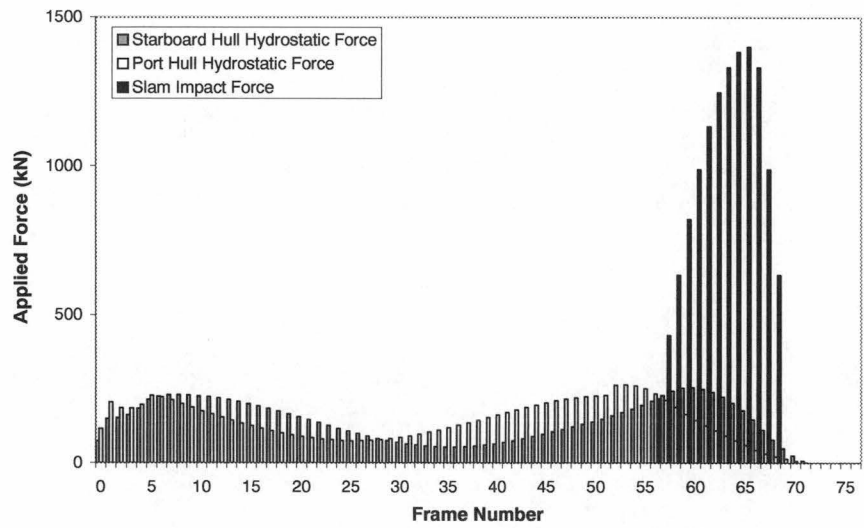


Figure 3-12: Longitudinal Distribution of Applied Force for Extreme Slam Event

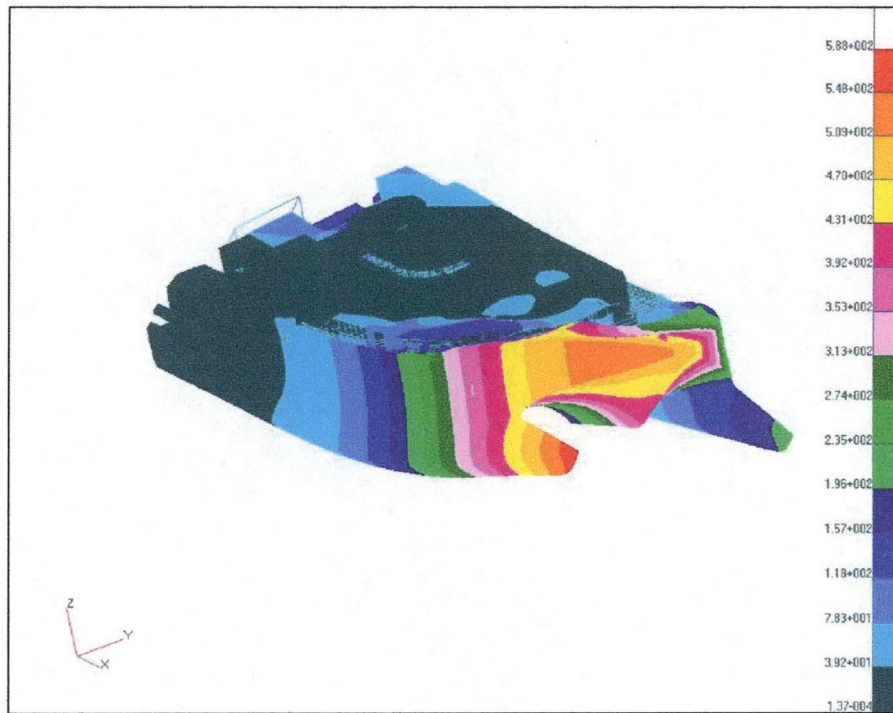


Figure 3-13: Exaggerated Deflection Plot (units in mm) for Extreme Slam Load Case

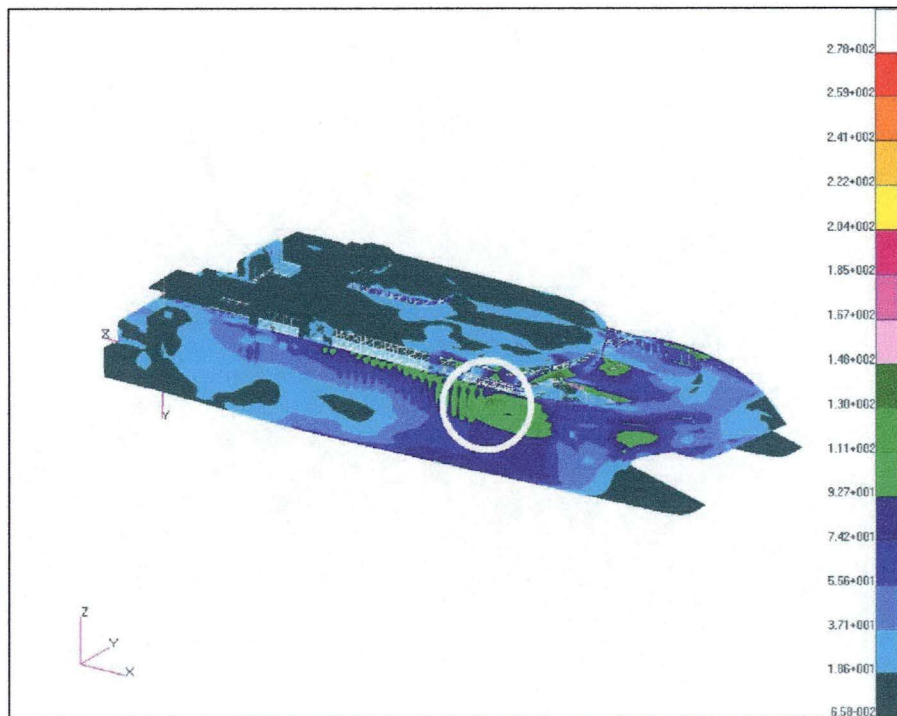


Figure 3-14: Stress Plot (units in MPa) for Extreme Slam Load Case. The zone identified by the circle highlights the area of external damage as indicated in Chapter 2.

Strain Gauge Location	Full Scale Data (MPa)	Scale Stress	FE Analysis Axial Stress (MPa)	% Difference
Starboard Steel Post	-223.5		-232.0	-3.8%
Port Steel Post	-34.2		-51.8	-51.7%
X-brace fr. 23	-36.9		-30.4	17.7%
X-brace fr. 41	-28.2		-27.0	4.3%
Steel Vehicle Deck	-162.7		-142.0	12.7%
Keel fr. 49.5	75.3		83.3	-10.6%
Keel fr. 40.5	101.9		102.0	-0.1%
Keel fr. 24.5	93.7		86.3	7.9%

Table 3.5: Comparison of FE Analysis and Full-Scale Data for Extreme Slam Impact

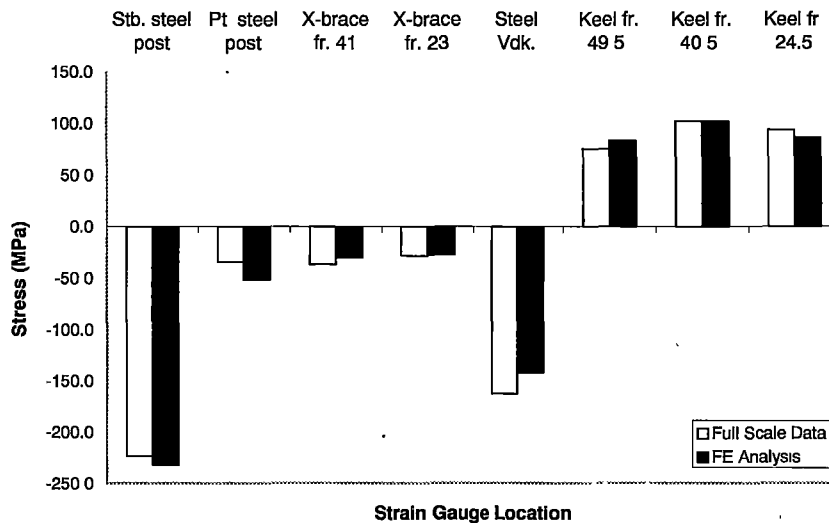


Figure 3-15: Hull 050 - Comparison of FEA and Full-Scale Data for Extreme Slam Impact

in the starboard bow region due to the slamming impact force. The image showing Von Mises stress, Fig. 3-14, illustrates the concentration of stress in the region where damage was experienced by the vessel following the extreme slam event (compare with the photographs of the damage to Hull 050, Figs. 2-41 to 2-43, shown in Chapter 2). A buckling analysis was conducted, as prescribed by DNV rules [102], which revealed that the maximum allowable buckling stresses were exceeded for the shell plating in this region. Fig. 3-15 shows that good correlation was achieved for the strain gauges when compared with the FE analysis for the extreme slam event, with the strain gauge readings being within 17.7 % of the full-scale measurements except for the gauge on the port steel post, and the average error for all the strain gauges was 13.6%. The major discrepancy in the results is the level of stress in the port steel post. It was difficult to reduce the level of stress in this structure whilst maintaining sufficient load to retain the required stress levels at the other strain gauge locations and the steel posts were very susceptible to the localised slam loading. It is noted that while the relative error here is high, it is not significantly different from the error at other locations in

absolute terms. The slam loading increased in magnitude very rapidly during a slam event, particularly in the forward region of the vessel, and since the sampling rate for these strain gauges was only 20 Hz the peak for the port steel post may have been missed which could account for the disparity in results for this location. Also, local effects, or other types of loading not considered may have contributed, for example the accuracy of the heading angle, which was an on-board visual observation, and the lack of information on wave spreading may have affected the underlying global wave loading and account for a portion of the disparity in the correlation with the strain gauge results.

The extreme slam event load condition, as outlined in Table 3.6, is therefore proposed as a realistic slam load case for Hull 050.

Wave Length	80m
Wave Height	5m
Wave Heading	140 degrees
Vertical acceleration at LCG	1.9g
Vertical acceleration at FP	3.0g
Impact Force on Starboard Centre Bow and Archway	1280 tonnes for full vessel

Table 3.6: Proposed Extreme Slam Load Case for Hull 050

As mentioned previously in Section 3.7 the correlation of the extreme slam event was also conducted for a symmetric loading scenario. In this case the heading of the vessel was assumed to be 180 degrees and the slam impact load was taken to be symmetric about the vessel centreline. In comparing the FEA results with the full-scale data the strain gauge readings for the port and starboard steel posts were averaged to give a mean reading. In addition to the underlying global wave load a load of 1600 tonnes was applied to the centrebow and archway region (between frames 52 and 69) to simulate the slam impact force. Whilst full details of this analysis are given in Thomas et al. [100] the results of the comparison between the FEA and full-scale results are shown in Fig. 3-16. This plot shows that good correlation was achieved for the strain gauges when compared with the FEA, with an average error across the strain gauges of 10.9%. The determined slam force for the symmetric load case was therefore significantly greater than that found when the asymmetry of the vessel heading and slam impact were accounted for. Although the symmetric analysis is a simplification, because of the uncertainty in the vessel heading from the on-board observations and the asymmetric nature of the slam impact force it enables extremes of interpretation of the measured data to be encompassed and bands may be placed on the magnitude of the slam force as determined from the data records. It was thus a useful preliminary study to the asymmetric case.

A search was conducted of the full-scale strain gauge results for Hull 050 in order to identify the largest global load due to the time varying wave load. It was found that the bending moment due to the extreme slam event exceeded this maximum global wave load by approximately 700%. This clearly indicates that the structural loading on this type of vessel due to extreme slam events is very severe when compared to wave global loadings.

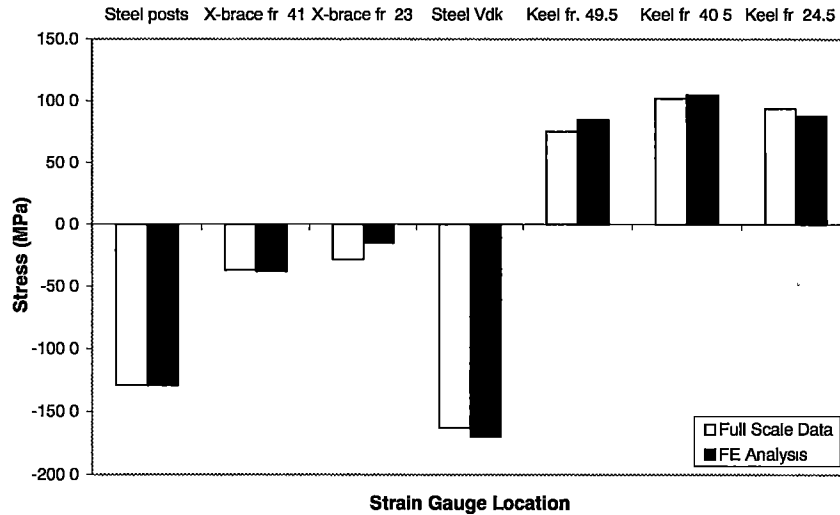


Figure 3-16: Hull 050 - Comparison of FEA and Full-Scale Data for Extreme Slam Impact (Symmetric Analysis)

### 3.7.2.2 Additional Slam Event Correlation

The same correlation process was conducted for the four other identified slam events. The conditions shown in Table 3.3 were used for the underlying global loads, whilst the derived slam loads are shown Table 3.7.

For slam event number 2 the correlation was carried out for both System 1 and System 2 strain gauges, and the results are shown in Fig. 3-17. The agreement between the FE and full-scale results was not as good as was achieved for the extreme slam event with an average error of 27.9%. Whilst still acceptable, this diminished level of agreement may be attributable to the lack of on-board observations for this crossing which meant that neither the vessel's actual mass distribution nor its heading relative to the wave field were known. In particular, the first five locations shown account for the majority of the error, while agreement for the remainder is good, indicating a discrepancy in the distribution of the loading. The correlation for slam number 3 was good with an average error of 11.3% between the FEA and full-scale results, see Fig. 3-18. Figs. 3-19 and 3-20 show that reasonable correlation was achieved for the other slam events, with average errors of 23.1% and 27.7% respectively. In the latter only one location showed a significant absolute error while the two cross braces, due to their small stress levels, showed large relative errors.

Using the slam load cases developed a plot of slam impact load for varying relative vertical velocity at impact has been produced and is shown in Fig. 3-21. This plot gives an indication of the increase in slam impact force as the relative vertical velocity increases. Reference is made however to the complete set of full-scale results for Hulls 042 and 050 in Chapter 2 where it can be seen that whilst there is a trend of increasing strain gauge stress levels with

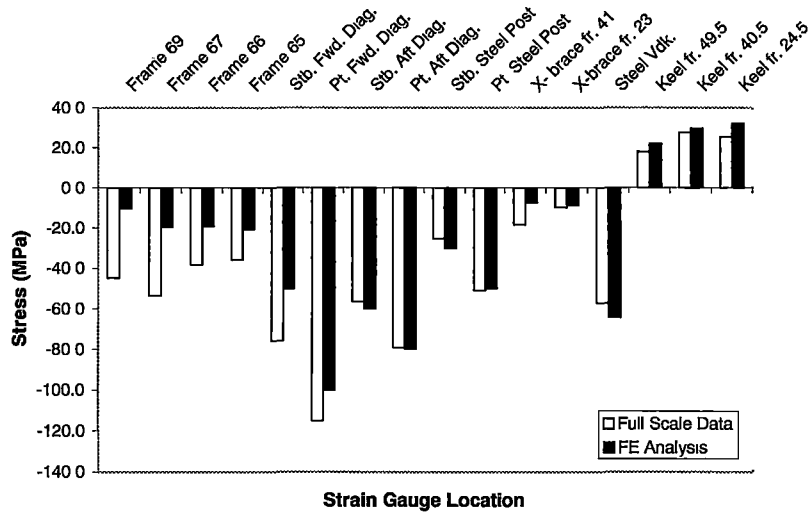


Figure 3-17: Hull 050 - Comparison of FEA and Full-Scale Data for Slam Number 2

increasing relative vertical velocity, a large relative vertical velocity does not always equate to a large impact force.

It appears that the proposed extreme asymmetric slam load case corresponds to a very severe slam with a slam impact load over 2.5 times larger than the next largest slam event found in the data records. This suggests that there may be an additional factor, as well as relative vertical velocity, wave height, vessel speed etc., that precipitates such an extreme event. It is suggested that the extent to which the wave surface matches in with the hull surface during a slam may be such an additional factor.

The range of slam impact force for the extreme slam event due to uncertainty in the vessel heading and asymmetry of the slam event may be seen by comparing the slam impact force of 1280 tonnes for the asymmetric analysis and 1600 tonnes for the symmetric analysis (an increase of 25%).

Slam Number	Asymmetric or Symmetric Load	Total Slam Impact Load
1 (Extreme Slam)	Asymmetric	1280 tonnes
1 (Extreme Slam)	Symmetric	1600 tonnes
2	Asymmetric	240 tonnes
3	Asymmetric	480 tonnes
4	Asymmetric	370 tonnes
5	Asymmetric	290 tonnes

Table 3.7: Hull 050 Slam Event Impact Loads

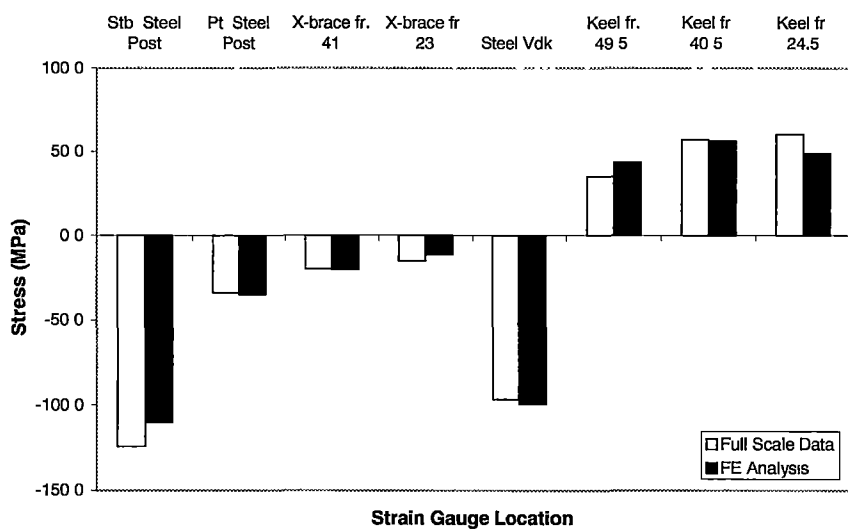


Figure 3-18: Hull 050 - Comparison of FEA and Full-Scale Data for Slam Number 3

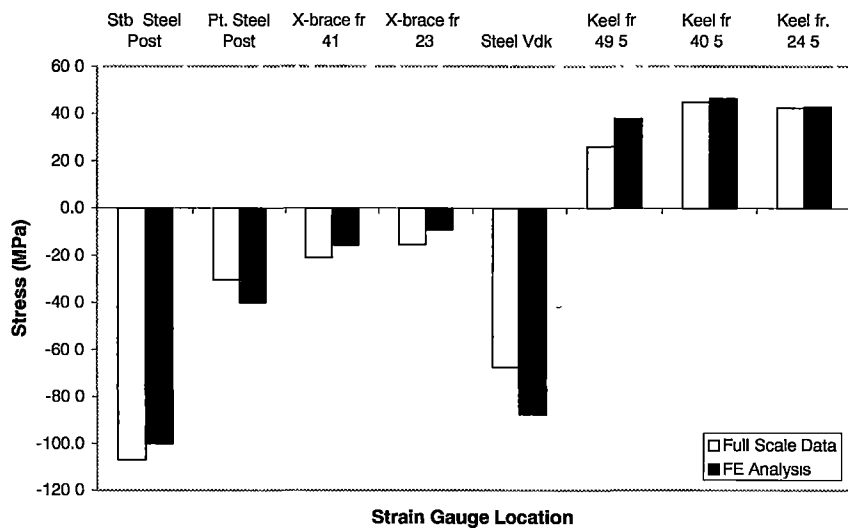


Figure 3-19: Hull 050 - Comparison of FEA and Full-Scale Data for Slam Number 4

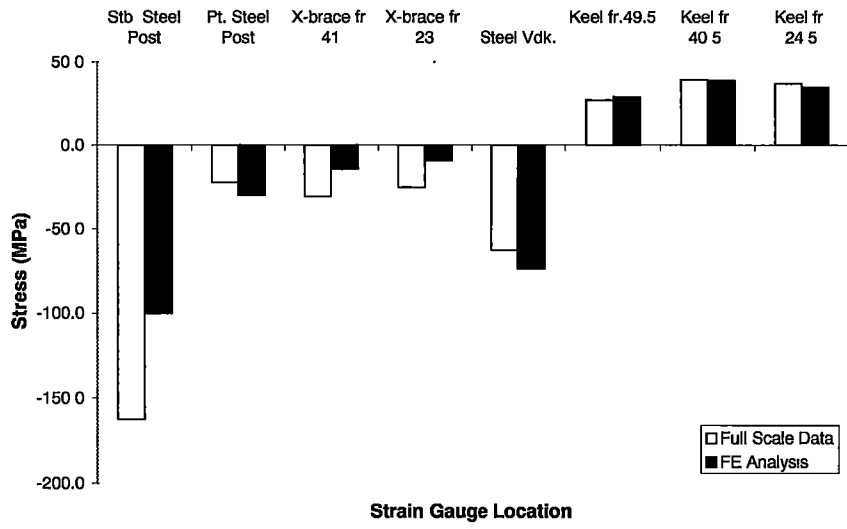


Figure 3-20: Hull 050 - Comparison of FEA and Full-Scale Data for Slam Number 5

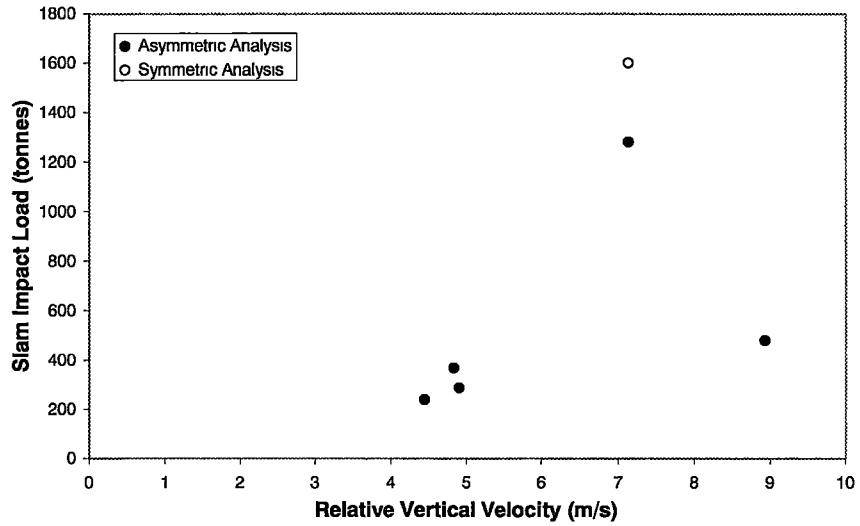


Figure 3-21: Hull 050 - Slam Impact Load for varying Relative Vertical Velocity for Slam Load Cases

### 3.7.3 Comparison of Extreme Slam Load Case with DNV Classification Rules

The results from the proposed extreme slam load case have been compared with those from the DNV longitudinal sagging moment, and are shown in Fig. 3-22. The longitudinal sagging moment was used for comparison since it simulates a hollow landing situation and is thus the closest DNV loading to a bow slamming event. The vessel, for both load cases, was in the full design load condition with a complete complement of trucks, cars and passengers along with full fuel tanks. To achieve the required DNV longitudinal sagging moment the vessel was hydrostatically balanced on a wave of length 81.5m and height 9m with an LCG acceleration of 2.1g. Fig. 3-22 shows that the axial stress levels at the strain gauge locations were greater for every location for the slam load case FEA than the DNV longitudinal sagging moment, except for the steel diagonal on the vehicle deck. This is borne out by the bending moment and shear force curves shown in Figs. 3-23 and 3-24, where the bending moment and shear force curves have been normalised respectively by the maximum values determined from the DNV longitudinal sagging moment. It can be seen that the starboard hull bending moment for the extreme slam load case has a greater maximum value and its peak is further forward than for the DNV longitudinal sagging moment. This trend is strengthened by the starboard hull shear force curve for the extreme slam load case which has a strong forward bias due to the slam impact load on the centrebow and archway region. The port hull bending moment and shear force curves have smaller peak values than the DNV longitudinal sagging moment though its peak occurs further forward along the vessel.

Whilst it is recommended that such an extreme slam load case be used in the structural design process along with the standard DNV load cases to ensure structural integrity in conditions when extreme slams may occur, it is important to place the likelihood of such a slam occurring into perspective. The probability of exceeding the proposed load case is the combined probabilities of experiencing such a slam and of being fully loaded at the time. There are 34 Incat catamarans, of over 70m in length, in operation throughout the world which have been in operation for a total of approximately 240 service years. The extreme slam event recorded on Hull 050 was the most severe slam event experienced by a large Incat vessel. This may be concluded since, although few vessels have undergone monitoring programs such as those carried out on Hulls 042 and 050, no other vessel has incurred such a high level of damage following a slam event and the structural scantling design of the vessels has not been reduced. Therefore the extreme slam event analysed may be proposed as approximately a 1 in 240 years of service event. However it is likely that the probability of occurrence of such an extreme slam would increase if a greater number of vessels operated in sea areas more prone to large wave heights such as Hull 050's route across Cook Strait.

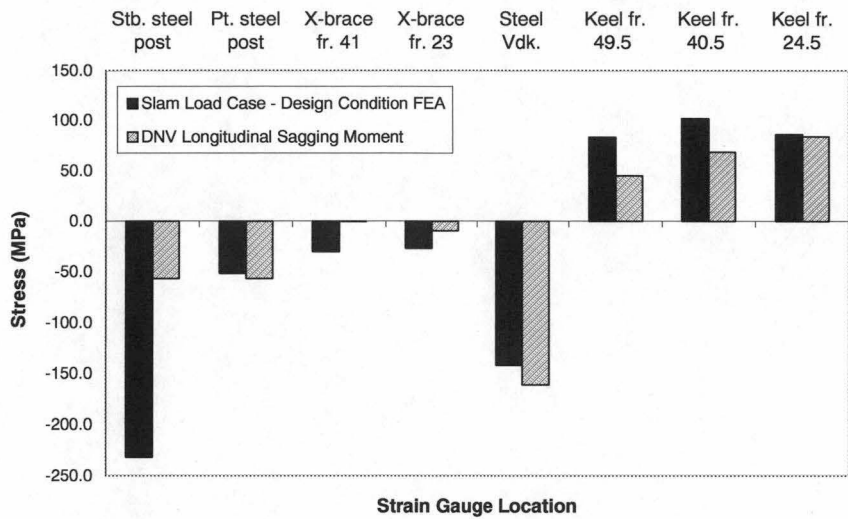


Figure 3-22: Hull 050 - Comparison of Slam Load Case FEA (Fully Loaded Design Condition) and DNV Longitudinal Sagging Moment

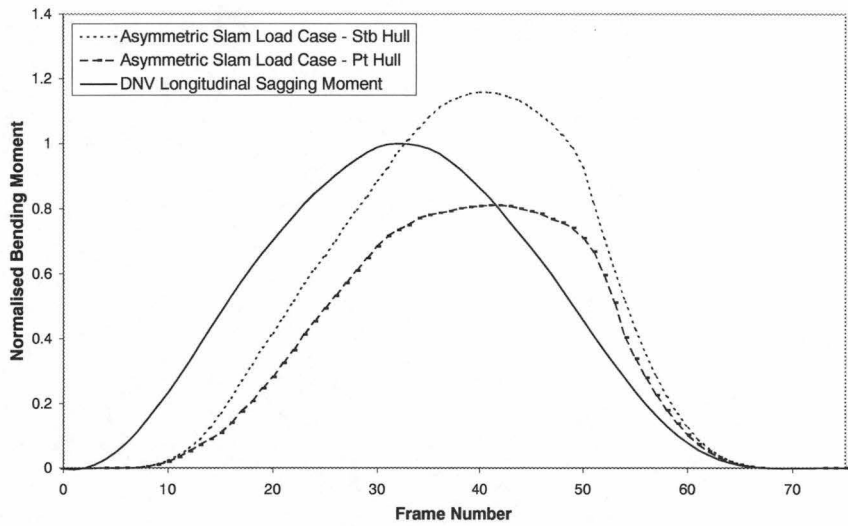


Figure 3-23: Hull 050 - Comparison of Bending Moment Curves for Slam Load Case FEA (Fully Loaded Design Condition) and DNV Longitudinal Sagging Moment

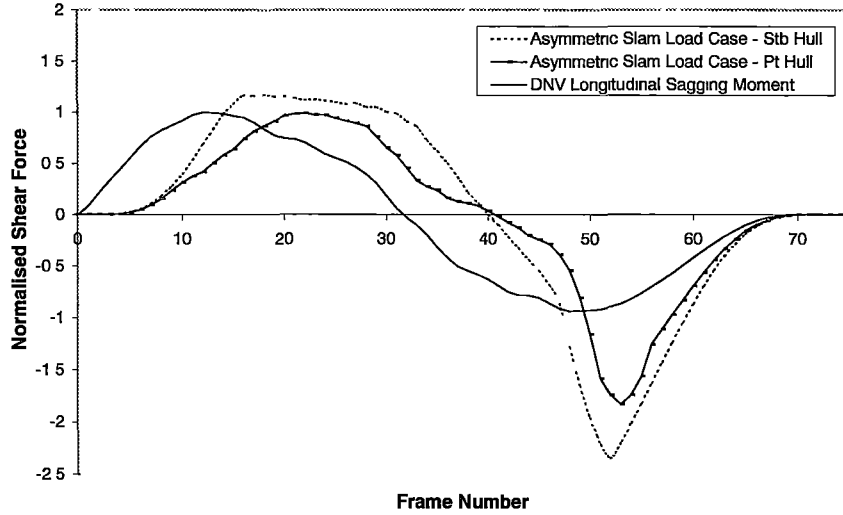


Figure 3-24: Hull 050 - Comparison of Shear Force Curves for Slam Load Case FEA (Fully Loaded Design Condition) and DNV Longitudinal Sagging Moment

## 3.8 Slam Load Case Application

### 3.8.1 Proposed Slam Load Scaling Method

The extreme asymmetric slam event that was experienced by Incat Hull 050 provided an effective design load case for that particular vessel design. However, in order to use the slam load case successfully with other wave piercing catamaran designs a method for scaling the loads is required. Such a method for scaling the extreme slam load case is proposed.

The data required by the wave-induced loading model is scaled assuming Froude scaling based on a scale factor  $R$ . The design wave-induced loading parameters are based purely on the scaled extreme slam load case and do not account for specific conditions that the vessel may encounter in service. If the new design is not a geosim of Hull 050 this scale factor may be derived by averaging the scaling factor of several principal parameters, i.e. overall length, waterline length, displacement, hull beam, overall beam and design draft. For example,

$$R = \frac{\left(\frac{LOA_{des}}{LOA_{050}}\right) + \left(\frac{LWL_{des}}{LWL_{050}}\right) + \left(\frac{(\Delta_{des})^{1/3}}{(\Delta_{050})^{1/3}}\right) + \left(\frac{T_{des}}{T_{050}}\right) + \left(\frac{B_{des}}{B_{050}}\right) + \left(\frac{BOA_{des}}{BOA_{050}}\right)}{6} \quad (3.3)$$

where the subscripts *des* and 050 denote the new design and Hull 050 respectively.  $LOA$  is the length overall,  $LWL$  is the waterline length,  $\Delta$  is the displacement,  $T$  is the design draft,  $B$  is the hull beam and  $BOA$  is the overall beam. These specific factors were chosen since they represent a range of vessel parameters which provide a clear indication of a change in vessel size. The sensitivity of the scale factor,  $R$ , was found to be small in relation to the choice of

vessel parameters.

Therefore the parameters required by the wave-induced loading model may be found as follows

$$\lambda_{des} = \lambda_{050}R \quad (3.4)$$

$$h_{des} = h_{050}R \quad (3.5)$$

$$\ddot{z}_{des} = \ddot{z}_{050} \quad (3.6)$$

The slam impact force is determined by scaling the slam load case force as follows:

$$F_{des} = F_{050} \left[ \left( \frac{LWL_{des}}{LWL_{050}} \right) \times \left( \frac{BOA_{des}}{BOA_{050}} \right) \times \left( \frac{TH_{050}}{TH_{des}} \right) \right] \quad (3.7)$$

where  $TH$  is the tunnel height. The tunnel height is defined as the vertical distance between the design waterline and the top of the centrebow archway. This formulation was adopted since it follows the principle of Froude scaling  $F_{des} = F_{050} \times R^3$ . However instead of using the average scale factor,  $R$ , it makes use of parameters which are likely to have an influence on the slam impact magnitude. The scaling factors for waterline length and overall beam were included since they are guides to the overall change in vessel size. The tunnel height was included as an indication of susceptibility to slamming and severity of slamming load. The height of the tunnel above the design waterline is likely to have a significant influence on wet-deck slam occurrence. For a particular vessel with given motion characteristics the prospect of water impacts on the wet-deck will reduce as the tunnel height is increased. If the ratio of tunnel height of Hull 050 to the design vessel reduces it is proposed that archway closure slams are less likely to occur.

Another two techniques were investigated for scaling the slam force from Hull 050 to new designs:

- Alternative method 1 used Froude scaling on the total slam force as follows:

$$F_{des} = F_{050}R^3$$

where  $F$  is the impact force. This is a straightforward method which scales the slam force according to the average scaling factor and then applies the force over an equivalent area on the design vessel.

- Alternative method 2 was based on scaling the slamming impact pressure over the slam

region according to Froude scaling as follows:

$$P_{des} = P_{050}R$$

where  $P$  is the impact pressure. One difficulty with this method is determining how the slam footprint, i.e. the projected area over which the slam impact pressure acts, will change with vessel design. It could be assumed that the slam area will scale according to Froude scaling. However since the centrebow length may actually decrease with a larger vessel the required footprint area may not be available on the centrebow and archway.

The proposed technique was favoured over both of these alternative methods since it gives an indication of the predisposition of a design to slamming through the inclusion of tunnel height.

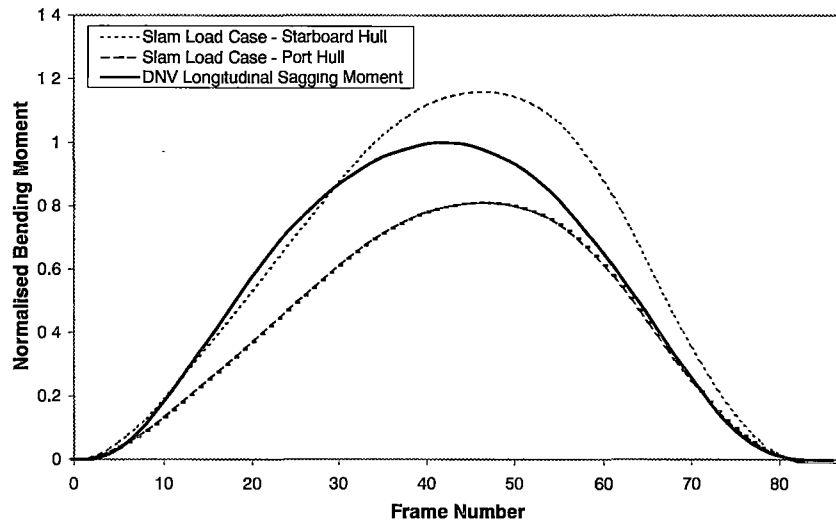


Figure 3-25: Comparison of Bending Moment Curves for Extreme Slam FE Load Case and DNV Sag Rule Moment for 112m Design

### 3.8.2 Slam Load Scaling Example

This scaling method was used to develop a slam load case for a new 112m Incat wave piercer catamaran design, with the resulting impact load of 1660 tonnes. In contrast, alternative method 1 resulted in a slam load of 2100 tonnes whilst the slam load according to the second alternative method was 1640 tonnes if the slam footprint size was kept constant for the two vessels. A comparison of the bending moment curves for the new slam load case and the DNV sagging rule moment is shown in Fig. 3-25. This plot, where the bending moment curves have been normalised by the maximum values determined from the DNV longitudinal sagging moment, shows that the starboard hull maximum bending moment for the extreme

slam load case has a greater maximum value and its peak is further forward than for the DNV longitudinal sagging rule moment due to the slam impact load on the centrebow and archway region. It is interesting to note that the slam impact load accounts for approximately 50% of the total bending moment, whilst the underlying global wave load and vessel mass distribution accounts for the other 50%. This is similar to the result for Hull 050 where the slam load constituted 55% of the total bending moment.

In general it can be seen that the increase in vessel length from 96m to 112m has not greatly altered the comparability of the extreme slam load case with the DNV longitudinal sagging rule moment. However, it does appear that for the larger vessel the location of the maximum bending moment in the DNV case is closer to that for the extreme slam load case than for the smaller vessel, since for the 112m vessel the slam load is relatively smaller, when compared with the underlying global wave loading, than was the case for the smaller vessel.

The extreme slam event that was experienced by Hull 050 has therefore provided an effective design load case that may be applied in future design scenarios by using the proposed scaling method.

### **3.9 Summary**

Slam load cases, including an extreme slam load case, have been developed for Incat Hull 050 by correlating full-scale strain gauge data with stress results from finite element analysis. These realistic slam load cases may be used in the structural design process of large high-speed catamarans and also provide data for the validation of theoretical and experimental prediction techniques for slam impact loads. The extreme slam load case was found to be greater than the rule longitudinal sagging moment as defined by Det Norske Veritas with a larger maximum bending moment and a peak value forward of amidships. The bending moment due to the extreme slam event exceeded the maximum global wave loading found in the Hull 050 strain gauge records by approximately 700%. A method was proposed for scaling the load cases for use with other large catamaran designs and this technique was demonstrated for a 112m design catamaran.

The full-scale results showed that slams are a dynamic event and therefore the development of quasi-static load cases is an approximation. The following chapter of this thesis investigates in detail the dynamic nature of the slam events and in particular the whipping behaviour. A dynamic finite element load case method is also presented.

## Chapter 4

# Dynamic Slamming Response

### 4.1 Introduction

When a large high-speed catamaran experiences a severe wet-deck slam event it exhibits a dynamic response, as was illustrated by the full-scale results for Incat Hulls 042 and 050. This induced vibration of the hull girder, which may be felt on-board as a shudder after a slam impact, is known as whipping. The whipping behaviour constitutes components of the natural frequencies of the vessel's structure including the effect of the added mass of the surrounding water and has an inherent level of damping. One of the major aims of this study was to investigate this whipping behaviour and in particular develop methods suitable for estimating the whipping frequencies, mode shapes and levels of damping. Predictions from these theoretical methods are compared favourably with results from both the full-scale slam measurements and exciter tests.

#### 4.1.1 Whipping Behaviour

Work in the 1970s highlighted that structural damage may occur due to the whipping behaviour of large monohulls when operating in rough weather [103] and a small number of authors began to investigate the phenomenon. Hoffman [104] emphasised the consequences of whipping or vibratory stress after a slam and proposed that the critical condition for the ship bottom was when the global wave bending moment builds up to a sagging peak and the whipping stress is superimposed, with the converse hogging situation being critical for the deck structure. A formula for estimating the exciting forces of whipping vibration for a ship hull, based on the pressure-time relation of waves measured at the bow of a tanker, was proposed by Kumai and Tasai [105]. In order to reduce the whipping response they suggested that the ballast load should be arranged so that the vibrational amplitude at the bow was minimised in the first longitudinal mode of vibration of the hull. Yamamoto et al. [106] used a strip theory to calculate the motions and longitudinal strength in regular waves of two tankers

and a container ship. They concluded that the whipping behaviour depends largely upon the emergence of the bottom, weight distribution and the phase difference of impacts due to bottom and bow-flare slamming, or successive bottom slamming. A simple method for estimating the sag-increasing whipping stress was presented by Ochi and Motter [107], and they determined that only the fundamental hull mode is appreciable because higher-mode vibrations die out very quickly because of strong damping characteristics. The short-term distribution of whipping vibration stresses due to slamming was predicted, by adopting the generalised Rayleigh probability density function, by Kawakami and Tanaka [108]. Good agreement was found when the predicted results were compared with model tests on a container ship in irregular waves and it was concluded that the method may be applicable for use for long-term predictions for full-scale vessels.

The whipping of relatively slow-speed monohulls has since been investigated by various researchers through towing tank tests and full-scale measurements. For experimental investigations of vibration phenomena such as whipping, elastic or segmented models are used whereby the global structural stiffness may be correctly scaled. Fukasawa et al. [16] conducted a series of towing tank tests on an elastic ship model in simulated slamming conditions. The self-propelled 3m long container ship model was tested in a variety of wave headings, heights and lengths. Time histories presented of the strain measurements showed the presence of whipping behaviour for the large slamming events, however the frequencies and damping levels of the whipping were not quantified. Comparisons of the deck strain amplitudes with the theoretical method of Yamamoto et al. [106] showed good agreement. A similar set of experiments was conducted by Watanabe and Sawada [17] and significant values of longitudinal bending moment were found when slamming and whipping occurred, with shallow fore drafts resulting in the severest bending moments. Favourable comparisons were made with a modified strip theory which takes into account the instantaneous waterline due to the wave and vessel motions. McTaggart et al. [18] used a model with a composite flexible backbone to investigate the motions and loads of a frigate. The whipping loads in regular waves due to the first longitudinal bending moment were determined from the model results using spectral analysis. It was found that the whipping moment increases significantly with both wave amplitude and ship speed. At the highest wave steepnesses tested ( $h/\lambda = 1/15$ ) the magnitude of maximum whipping moment approached that of the wave-induced moment which indicated the importance of whipping effects in ship design.

With regard to full-scale measurements, Aertssen [4] analysed full-scale strain gauge data from four large cargo vessels and used the data to estimate the long-term whipping stresses of the vessels. Two Royal Navy frigates underwent full-scale rough weather trials during which data was measured on their slamming response [19] [35], with the whipping frequencies and damping values being extracted from transient slam signals. Favourable comparisons were made between the full-scale slamming responses and predictions using Bishop and Price's

hydroelastic theory.

Bishop and Price established the basic principles of the hydroelastic theory for flexible beam-like hulls subject to steady state wave-induced loads [20]. Traditionally for seakeeping studies the vessel is treated as a rigid body with motions in six degrees of freedom: heave, pitch, roll, sway, yaw and surge. However hydroelastic theory takes into account the flexibility of the hull structure so that these motions are a subset of a larger group of motions as the flexible structure is capable of distorting in an infinite number of ways. Two- and three-dimensional methods have been developed and applied to a variety of craft including bulk carriers [109], yachts [110] and SWATHs [111]. These methods were extended to include the response to transient loads such as slamming [21] [22]. Aksu used the impact theory of Stavovy and Chuang [23] to include the slam impact force on the under surface of the vessel. Results from this method were compared with full-scale trials measurements on a fast patrol boat operating in heavy winter seas south of the Isle of Wight. Good agreement was found when comparing the distributions of the number of strain peak exceedences for locations on the keel and deck.

The formulation presented by Evans [112] endeavoured to provide a semi-empirical method for estimating the influence of whipping on bending moments. The method was based on a combination of data obtained through full-scale measurements of a bulk carrier and dynamic load factor theory. Jiao [113] developed a probabilistic model for the prediction of extreme stress for slamming ships. The model, which assumes correlation between the wave-induced and whipping stresses, was recommended for use in predicting extreme stress and fatigue damage. The large amplitude motion program (LAMP) system developed by Weems et al. [76] uses a potential flow boundary element method in a three-dimensional time domain program to predict ship motions. The slam load predictions are calculated using a generalised two-dimensional Wagner approach [114] in a post processor with the assumption that the impacts do not affect the vessel motions. It was proposed that the system will also provide an interface with a structural finite element program so that the structural response including whipping may be calculated. Ramos and Guedes Soares [115] used the strip theory method of Salvesen, Tuck and Faltinsen [98] to determine the relative vertical motion of a ship and then the methods of Ochi and Motter [107] and Stavovy and Chuang [23] to estimate the slamming force. A simplified beam-like structural model, containing 25 elements, was set up to estimate the structural response to this slamming force. An example was presented for a 270m long container ship and very large differences in the vertical wave induced bending moments were found depending on the slamming force calculation method adopted.

High-speed craft tend to operate close to their structural design limits [2]. They are constructed using materials such as aluminium alloys, high tensile steels and composite materials in order to obtain an effective lightweight structure. This will generally reduce the stiffness of the hull structure. In addition these vessels may encounter large waves at high frequen-

cies, therefore the dynamic structural response such as the whipping behaviour may become more pronounced. Takahashi and Kaneko [116] conducted towing tank experiments on a 3.6m long elastic backbone model of a semi-displacement high-speed craft. As well as the low frequency wave loads, the higher frequency whipping loads were measured and presented. It was concluded that the first longitudinal mode of vibration was the dominant whipping mode. Experiments were also conducted by Chou et al. [117] on an elastic backbone model of a fast monohull with the results being compared with theoretical predictions. The theory was based on a combination of a modified strip theory method and Wagner's impact theory with an idealised beam representation of the vessel. The comparison of the longitudinal bending moments provided reasonable correlation for the whipping loads. An extensive set of full-scale sea trials has recently been completed by Iaccarino et al. [6] on a 128m long high-speed monohull. Results from the trials indicated the presence of whipping behaviour following slam events.

In catamarans, wet-deck slamming may cause global whipping of the entire ship hull [7]. Research has been conducted at Marintek and the Norwegian University of Science and Technology into catamaran loads and in particular slam impact forces, as noted in the introduction to Chapter 3. The motions prediction theory of Faltinsen and Zhao [24] was generalised for modal analysis by Hermundstad et al. [25] [26] to estimate the global loads and whipping response of catamarans. Comparisons were made with experimental results from tests on a flexible high-speed catamaran model. The comparison of whipping frequencies between theory and experiment was found to be good, however the correlation of mode shapes was less satisfactory.

Little work has been conducted on the whipping of large fast catamarans, though both Watson et al. [10] and Steinmann et al. [8] presented full-scale stress results of large catamaran ferries which showed severe whipping behaviour after slam impact events. Whelan et al. [62] at the University of Tasmania are currently developing a wet-deck slamming impact prediction method which may eventually be combined with the seakeeping prediction program 'BESTSEA' [73] to provide slam loading data for realistic sea conditions. These loads may in the future be combined with dynamic finite element modelling techniques to enable whipping stresses to be estimated for large high-speed catamarans.

Therefore whilst several methods are available for the estimation of whipping stresses, there is a paucity of knowledge on the whipping of large high-speed catamarans. The nature and influences of the whipping behaviour of such vessels are not well understood. In particular, the magnitude of their natural frequencies and damping, and the factors that may affect them such as mass distribution and vessel speed require investigation.

### 4.1.2 Whipping Mode Prediction

Structural finite element analysis has been used by several authors to determine the natural modes of monohulls and multihulls. The dry modes simulate a vessel as though it is unsupported in-vacuo, whereas the wet modes are for a vessel in its natural condition supported by water. Kannari et al. [29] used a half FE model to calculate the symmetric wet natural modes and frequencies of an aluminium patrol boat. Louarn and Temarel [110] used a full FE model to estimate the modes of a Whitbread 60 yacht as part of an investigation into the structural dynamics of a racing yacht. The wet and dry natural frequencies of a SWATH were determined through FE analysis using Guyan's reduction method by Price et al. [111]. Results for dry natural frequencies from FE analysis of a catamaran were compared with measurements on a segmented model by Hermundstad et al. [26]. Good agreement was found between the calculated and measured frequencies.

Various techniques have been used for incorporating the fluid-structure interaction whereby the natural modes and frequencies in-water may be calculated. For example, Kannari et al. [29] used the method proposed by Hakala [118] by which the surrounding water was also modelled by finite elements. Both Louarn and Temarel [110] and Price et al. [111] used a three-dimensional Green function method to determine the influence of the surrounding fluid. Nestegård and Mejlænder-Larsen [119] used a symmetric boundary integral equation method for the fluid flow, coupled with a finite element method to determine the eigen-frequencies of floating structures. Numerical examples of the method included the frequency analysis of a steel rudder and a large cruise vessel.

Riska and Kukkanen [120] also used the method of Hakala [118] during a study of the structural response of a vessel to ramming an ice floe. The impact of a vessel with an ice floe may be considered to be comparable to a slamming event (although the time from initial impact to maximum vertical force, at approximately 1 second, is significantly longer than a slam event [121]) and the structural response is likely to be similar. Following exciter tests on a segmented model, Riska and Kukkanen proposed that forward speed may have some influence on the vessel added mass and hence on the dynamic behaviour of the hull girder.

There are unfortunately few comparisons of the results from using normal mode analysis with full-scale measurements available. However one exception is the work of Oei [122] from 1976. The added mass of the surrounding fluid was calculated using the work of Landweber and Macagno [123] and the natural frequencies found using a coarse finite element model. A mechanical exciter with out-of-balance masses was used to promote vibration on a 165m cargo vessel to enable comparisons between predicted and measured natural frequencies to be made. Reasonable agreement was found for the first longitudinal mode, with the predicted value being within 10% of the measured frequency.

The use of finite element techniques appears to be a valid approach in order to conduct normal mode analysis, however there are few comparisons with full-scale data available. Positive

correlation of normal mode analysis predictions with full-scale measurements will therefore provide additional confidence in the use of finite element techniques for predicting whipping modes of large high-speed catamarans. The effect of vessel speed and loading on the whipping frequencies may also be examined.

### 4.1.3 Damping

The rate at which the whipping behaviour decays after a slam is due to the damping within the system. As well as conducting a series of vibration measurements on a large tanker, Kumai [124] collated the first longitudinal mode (two-node vertical vibration) damping factors of seven additional steel monohulls determined by other investigators. For these vessels the damping factors were found to be approximately inversely proportional to their length. Betts et al. [27] conducted a survey of available full-scale results and found that values of hull damping varied widely. The damping was proposed to consist of two components: hydrodynamic damping and structural damping. The hydrodynamic damping was presumed to be small, however no evidence was provided to support this assumption. In 1979 Bishop and Price [20] stated that with regard to hull damping ‘The simple truth is that knowledge is abysmal’. In an analysis of the hydroelastic response of a high-speed monohull, Hermunstad et al. [30] concluded that the internal hull damping had a negligible effect on the response of the first vibration mode. They suggested that the damping was dominated by hydrodynamic damping due to the forward speed. Sunnersjö and Janson [125] used finite volume calculations to study damping due to sound radiation. The results indicated that the hydrodynamic damping due to very low frequency pressure wave radiation contributes a significant part of the total modal damping. Since the survey of Betts et al. [27] there appears to have been little progress in increasing knowledge of damping, particularly for modern fast lightweight vessels. For example the method for estimating the structural response of a vessel to wave induced loads of Ramos and Guedes Soares [115] uses the work of Kumai [124] in the absence of more recent data. Therefore further investigation into the levels of modal damping in ships and the relative magnitudes of its components is overdue.

### 4.1.4 Summary

It is apparent that whipping behaviour is a significant structural response to slamming events. It is clear that large fast catamarans, due to their aluminium construction, are likely to be comparatively flexible and hence susceptible to whipping. However, whilst extensive research has been conducted into the whipping of slow-speed steel monohulls, little work has been carried out on the whipping of high-speed craft. This chapter therefore reports on an investigation into the whipping behaviour of large, high-speed catamarans.

In addition to the full-scale whipping data presented in Chapter 2, exciter tests were conducted on two vessels whilst stationary in calm water and out of the water in order to

further examine the modes, frequencies and damping of the whipping behaviour. A theoretical investigation of the whipping behaviour of the vessels using finite element normal mode analysis including the fluid-structure interaction was conducted. The hydrodynamic added mass of the surrounding fluid was calculated using a two-dimensional panel method for a range of speeds. The effect of vessel loading on the whipping frequencies was also examined. The calculated whipping modes are then compared with those found through the full-scale measurements and exciter experiments. The whipping investigation includes an examination of the components that contribute to the damping of the system. Estimates were made of the relative magnitude of the various hydrodynamic components including: wavemaking damping, viscous damping and acoustic damping. The total calculated damping was then compared with the levels of damping found through the full-scale measurements and exciter tests.

## 4.2 Exciter Tests

In order to investigate the whipping behaviour of large high-speed catamarans exciter tests were conducted on two vessels. The vessels were excited using the anchor to simulate a slam impact at the bow. The frequency, modal shape and damping of the primary symmetrical (longitudinal) mode of vibration were then determined. The vessels for which these tests were conducted were Incat Hulls 045 and 050. Unfortunately Hull 042, for which in service strain data had been obtained, was not available for testing and hence Hull 045, an identical sister ship, was used instead.

### 4.2.1 Experimental Details

These tests were carried out in controlled conditions with the vessels being stationary in calm water. An out-of-water test was also conducted on Hull 050 in an endeavour to isolate the effect of hydrodynamic damping. For this test the vessel was supported on wooden blocks set on steel beams (18 per hull) under the keel line whilst in dry dock. The vessels' anchors (050 mass = 1.8 tonnes, 045 mass = 1.4 tonnes) were used to excite the longitudinal mode of vibration. Three methods of using the anchor were adopted: firstly releasing the anchor and then applying the brake a couple of seconds later, secondly stopping the anchor abruptly whilst it was being winched up and lastly dropping the anchor and then instantaneously restraining it with the electric winch (called the down/up instantaneous technique). It was this down/up instantaneous technique that provided the best excitation of the hull girder. Unfortunately, due to practical constraints, it was not possible to conduct exciter tests for the torsional modes as the anchor was mounted on the vessel centreline at the bow.

	Displacement (tonnes)	Draft (m)
Hull 045	880	2.88
Hull 050	1100	3.10

Table 4.1: Exciter Test Vessel Loading Conditions

Four accelerometers, distributed along the length of the vessel on the centreline, measured the structural response. For the tests on Hull 045, accelerometers were also positioned 10m to port off the centreline to obtain further information on the mode shape. The accelerometer locations are shown in Figs. 4-1 and 4-2 and Tables 4.2 and 4.3. The data was sampled at a rate of 100 Hz for 2048 samples and logged on a notebook PC.

The fore and aft draft marks were recorded to obtain the vessel displacements, see Table 4.1. Hull 045 was in the lightship condition whilst the displacement of Hull 050 was close to that recorded from the full-scale trials.

## 4.2.2 Data Analysis

Spectral analysis was conducted on the raw data traces to investigate the dynamic structural response. The 100 Hz raw data was highpass filtered at 0.6 Hz to remove low frequency drift and windowed using a Hanning window to reduce spectral leakage. The power spectra for the accelerometer records were then determined and used to identify the modal response of the vessel. The decay coefficient of the structural response was also determined from the accelerometer records. The decay coefficient was estimated from the decaying oscillation by determining the ratio between pairs of successive amplitudes (the Hull 045 raw data was lowpass filtered at 5 Hz prior to determining the decay coefficient). The decay coefficient, as defined in Fig. 2-13, is given in terms of successive stress peak values as

$$\eta = \frac{1}{\pi} \log_e \left( \frac{\sigma_j}{\sigma_{j+1}} \right). \quad (4.1)$$

As noted in Chapter 2, the determination of decay coefficients is a complex area with a large number of available methods, for example that proposed by Li [55]. Whilst a relatively simple approach has been adopted in this study, it is proposed that it is appropriate in order to achieve the level of accuracy required. The modal shape of the dominant structural response was found by comparing the response at the four accelerometers distributed along the centreline with regard to magnitude and phase.

## 4.2.3 Results and Discussion

An example of the exciter test raw data is shown in Fig. 4-3. The oscillatory nature of the structural response may be clearly seen, along with the decay of the signal. The response levels on Hull 045 were lower than for Hull 050 in the water which suggests that the anchor excitation method was not as successful at exciting the longitudinal mode of Hull 045. This may have been due to a combination of the lighter anchor and less powerful winch fitted on Hull 045. The dry dock hull supports may have influenced the response levels of Hull 050 out of the water since they were approximately one third of the magnitude of those found when the vessel was in the water.

A typical response spectrum from the in-water tests is shown in Fig. 4-4 which shows the dominance of the response at approximately 3 Hz. Fig. 4-5 shows a response spectrum from the Hull 050 out-of-water tests. It is clear that there was a significant reduction in the magnitude of the main frequency peak and an increase in peak frequency of approximately 0.5 Hz when compared with the in-water tests. The other frequency peaks appear to have increased in relative significance as more higher frequency modes were present. The hull supports seem to have increased the longitudinal natural frequency and reduced the signal

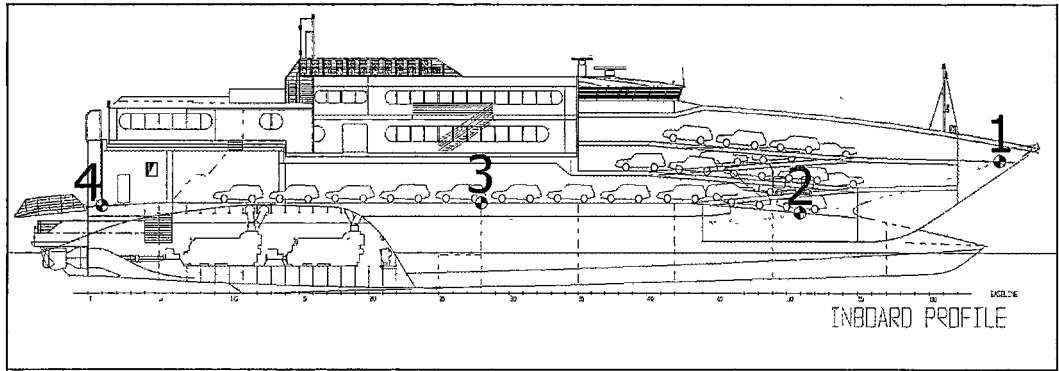


Figure 4-1: Hull 045 - Exciter Test Accelerometer Locations

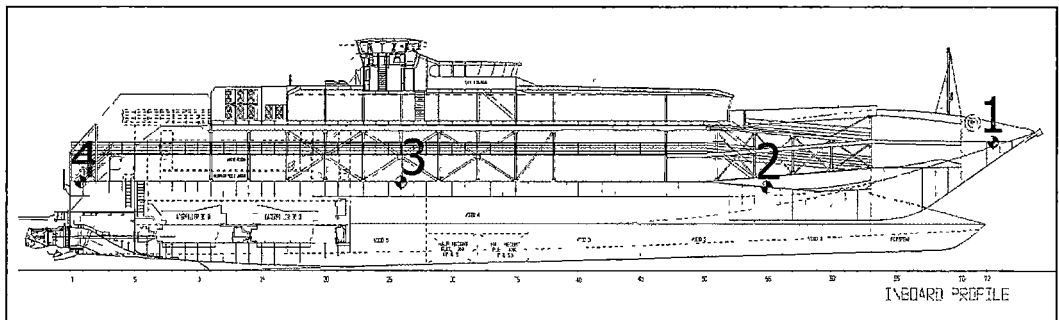


Figure 4-2: Hull 050 - Exciter Test Accelerometer Locations

Accelerometer Number	Location A	Location B
1	Top rider in centrebow at frame 64.5, 600mm off centreline to port	Top rider in centrebow at frame 64.5, 600mm off centreline to port
2	Deck of ramp A1 at frame 51 on centreline	Deck of ramp A at frame 51, 9.8m to port
3	Main vehicle deck at frame 28 on centreline	Main vehicle deck at frame 28, 11.0m to port
4	Main vehicle deck at frame 1 on centreline	Main vehicle deck at frame 1, 9.5m to port

Table 4.2: Hull 045 - Exciter Test Accelerometer Locations

Accelerometer Number	Location
1	Top rider in centrebow at frame 72.5, 600mm off centreline to port
2	Deck of ramp A1 at frame 55 on centreline
3	Main vehicle deck at frame 26 on centreline
4	Main vehicle deck at 300mm aft of frame 1 on centreline

Table 4.3: Hull 050 - Exciter Test Accelerometer Locations

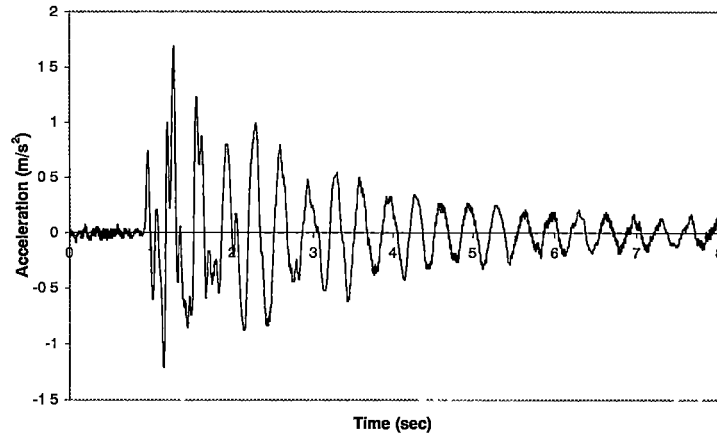


Figure 4-3: Hull 050 - Exciter Test Raw Data, In-Water

level towards the stern of the vessel when compared with the in-water results. The average first longitudinal natural frequencies from all the tests are shown in Table 4.4.

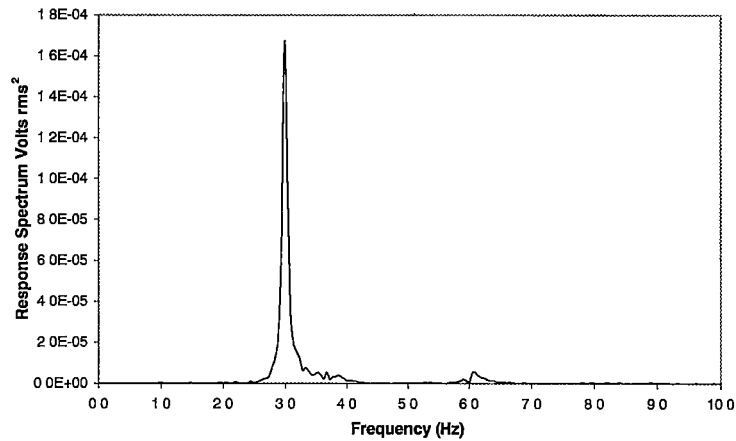


Figure 4-4: Hull 050 - Exciter Test Response Spectrum, In-Water

For Hull 045 the decay coefficient ranged between 0.007 and 0.14 with an average value of 0.069. The Hull 050 in-water results shown in Fig. 4-6, where the average values for each cycle number after the initial impact are shown with range bars, indicate that the decay coefficient was generally in the range of 0.01 to 0.06 with an average decay coefficient for all cycles of 0.035. It should be noted that a negative decay coefficient means simply that the signal amplitude of the subsequent cycle increases. The range of results was smaller for Hull 050 than for Hull 045 which may have been due to the heavier anchor used for the excitation which produced a larger and more clearly defined structural response. This is also borne out by the average number of cycles that the data was able to be analysed for: 19 cycles for Hull 050 and 8 cycles for Hull 045. The damping level recorded for Hull 050 is significantly smaller

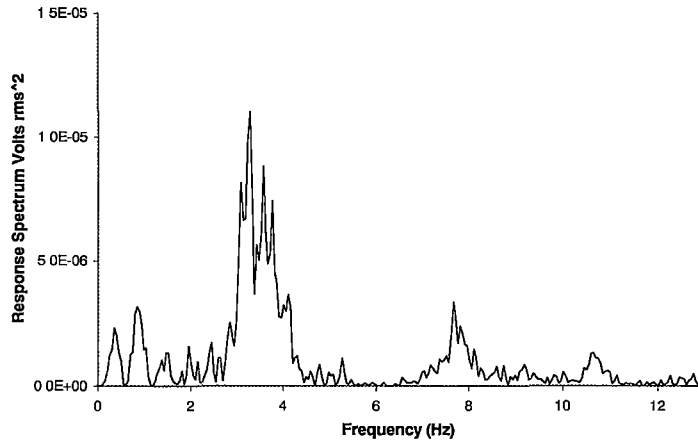


Figure 4-5: Hull 050 - Exciter Test Response Spectrum, Out-of-Water

	<b>Average First longitudinal Natural Frequency</b>
Hull 045	3.01 Hz
Hull 050 in-water	2.89 Hz
Hull 050 out-of-water	3.51 Hz

Table 4.4: Exciter Test Average First Longitudinal Natural Frequencies

than that measured for Hull 045, although it falls within the range measured for Hull 045.

When Hull 050 was tested out of the water the decay coefficient was within the range of 0.05 to 0.115 with an average decay coefficient for all cycles of 0.084. The higher damping values for the Hull 050 test out of the water suggest that the hull supports may have increased the damping. This means that whilst the out-of-water tests did not provide a true picture of the global damping of the structure without the presence of the water, it did provide evidence which suggests that material structure, such as steel supports, can significantly increase damping levels. An additional method for investigating the influence of the surrounding fluid on the frequency and damping may be to carry out the anchor exciter test for a range of vessel drafts. If it is assumed that the structural damping remains constant as the displacement and hence draft is altered, and constant with frequency, any change in measured damping would be due to changes in the hydrodynamic damping. This change in hydrodynamic damping could then be related to the change in immersion of the vessel and an indication of the level of hydrodynamic damping obtained. However there was no opportunity to test at significantly different displacements during the present investigation.

The mode shape of Hull 050, measured on the centreline, is shown in Fig. 4-7. The magnitude of the mode was normalised with respect to the response level of the accelerometer at the bow of each vessel. The mode magnitude at each accelerometer location was averaged for a few exciter tests and the range of data which was averaged is indicated by the range bars shown for each point. The mode was identified as the first longitudinal mode with

the maximum displacement at the bow, whilst on average the displacement at the stern was approximately one half that at the bow. Further results for the mode shapes, including for off the centre line, are shown in Section 4.3.6 where comparisons are made with theoretical predictions.

The values of decay coefficient determined through the exciter tests were compared with those collated by Betts et al. [27], as shown in Fig. 4-8. The comparison shows that the decay coefficient values for the two large high-speed catamarans lie at the lower end of the range of values. It should be noted that all the other vessels were of steel construction.

#### 4.2.4 Conclusions

Exciter tests were successfully conducted on two large high-speed catamarans whilst they were stationary in calm water in order to investigate the first longitudinal mode natural frequency, damping and mode shape. An additional test on a catamaran whilst out of the water in dry dock was also conducted. The results give important information on the nature of whipping behaviour of such vessels. The following conclusions may be drawn:

- The main natural frequencies of the response were at 3.01 Hz for Hull 045 and 2.89 Hz for Hull 050.
- The identified mode at approximately 3 Hz is the first longitudinal mode with the maximum displacement at the bow. On average the displacement at the stern was approximately one half that at the bow.
- The first longitudinal mode was also visible off the vessel centreline in phase with the mode on the centreline, although with a reduced intensity. The maximum displacement was again at the bow, whilst the displacement at the stern was approximately 0.2 times that at the bow.
- The average decay coefficient fell within the range of 0.007 to 0.14 with an average value of 0.069 for Hull 045. For Hull 050 the damping range was 0.01 to 0.06 with an average value of 0.035.
- The response levels on Hull 045 were lower than for similar experiments on Hull 050 which suggests that the anchor excitation method was not as successful at exciting the longitudinal mode of Hull 045, probably due to the smaller anchor on Hull 045.

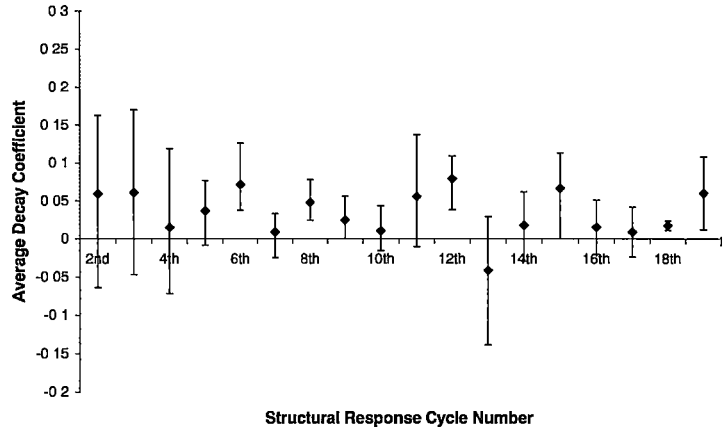


Figure 4-6: Hull 050 - Exciter Test Decay Coefficients, In-Water

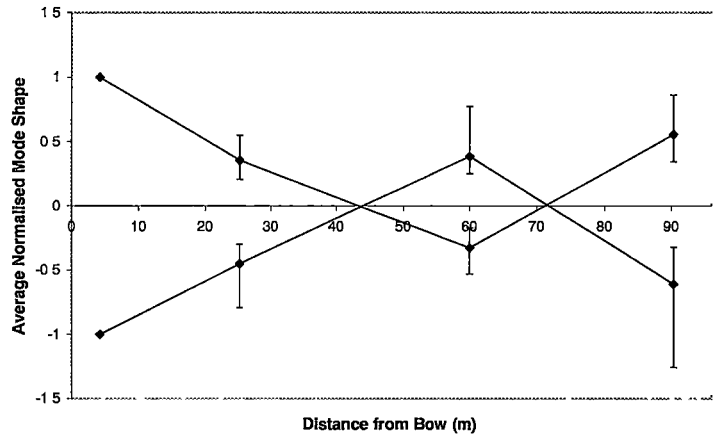


Figure 4-7: Hull 050 - Exciter Mode Shape on Centreline

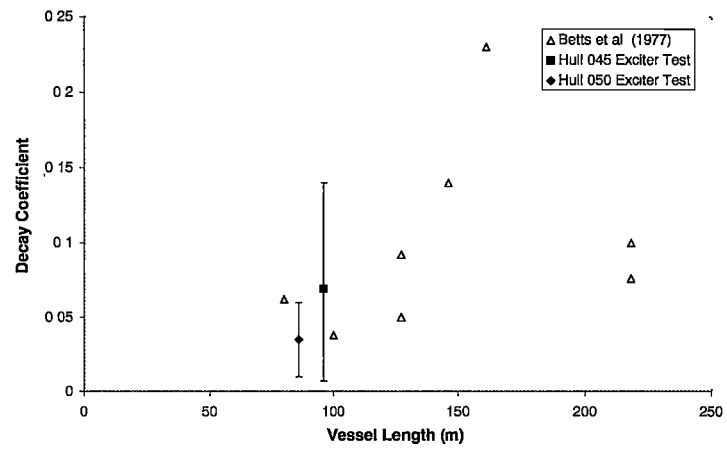


Figure 4-8: Decay Coefficient: Comparison of Exciter Test Results with Betts et al. (1977) Data

## 4.3 Whipping Mode Prediction

Normal mode analysis, using a finite element technique is proposed as a method for determining the natural frequencies and hence the whipping frequencies of large high-speed catamarans. The primary low frequency dry and wet modes may be determined, with the hydrodynamic added mass of the surrounding fluid being calculated by a two-dimensional panel method coupled with a strip theory. In order to test the method, normal mode analysis was conducted on two vessels: Hull 042/045 and Hull 050. The results were compared with the natural frequencies found from the full-scale trials and exciter tests.

### 4.3.1 Normal Mode Theory

The solution of the equation of motion for natural frequencies and normal modes requires a special reduced form of the equation of motion [126]. If there is no damping and no applied loading, the equation of motion in matrix form reduces to

$$[M] \{\ddot{u}\} + [K] \{u\} = 0 \quad (4.2)$$

where

$[M]$  = mass matrix

$[K]$  = stiffness matrix

$\{u\}$  = displacement vector

This is the equation of motion for undamped free vibration. Equation 4.2 may be solved by assuming a harmonic solution of the form

$$\{u\} = \{\phi\} \sin \omega t \quad (4.3)$$

If the assumed harmonic solution is differentiated and substituted into the equation of motion, the following is obtained

$$-\omega^2 [M] \{\phi\} \sin \omega t + [K] \{\phi\} \sin \omega t = 0 \quad (4.4)$$

which becomes

$$([K] - \omega^2 [M]) \{\phi\} = 0 \quad (4.5)$$

Equation 4.5 is called the eigenequation, which is a set of homogeneous algebraic equations for the components of the eigenvector and forms the basis for the eigenvalue problem. There is an eigenvalue which satisfies Equation 4.5 and corresponds to each eigenvector. Therefore, Equation 4.5 can be rewritten as

$$[K - \omega_i^2 M] \{\phi_i\} = 0 \quad i = 1, 2, 3... \quad (4.6)$$

where each eigenvalue,  $\omega_i^2$ , and eigenvector,  $\{\phi_i\}$ , define a free vibration dry mode of the structure.

When the added mass matrix is added to Equation 4.6 in order to account for the surrounding fluid, the solution of the eigenvalue problem becomes:

$$[K - \omega_i^2 (M_s + M_a(\omega_i))] \{\phi_i\} = 0 \quad i = 1, 2, 3... \quad (4.7)$$

where:

$$\begin{aligned} M_s &= \text{ship structure mass} \\ M_a &= \text{hydrodynamic added mass} \end{aligned}$$

Hence the added mass of the surrounding fluid may be included in the finite element model to determine the wet modes of a vessel.

There are several real eigenvalue extraction methods available through NASTRAN [126], including inverse power, Givens, modified Givens and the Householder method. It is suggested [127] that the Lanczos method combines the best features of all of the other solvers and is the recommended method for all medium- or large-sized problems. The Lanczos method is known as a robust method, which does not miss roots, and derives accurate eigenvalues and eigenvectors.

The Lanczos method is implemented as a block shifted method. It is called a block method because it extracts several eigenvectors within a frequency block close to an assumed trial eigenvalue. These trial eigenvalues are referred to as shift points. A Sturm sequence check [127] is made at each of the shift points to determine the number of eigenvalues below that shift point. This information is used to ensure that all of the eigenvalues have been determined.

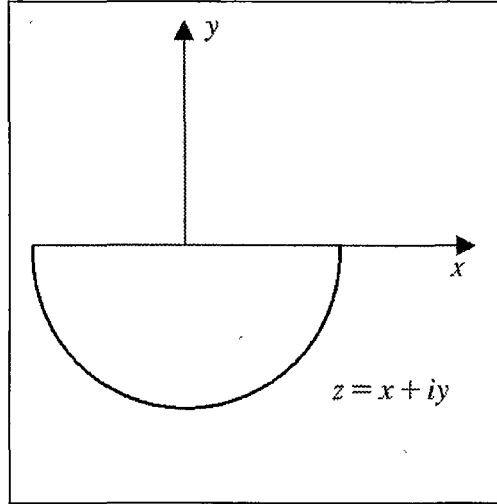


Figure 4-9: Coordinate System 1 in Cross Sectional Plane of the Hull (Equations 4.8 - 4.25)

### 4.3.2 Fluid Structure Interaction - Hydrodynamic Model

In order to determine the wet modes of ships, the added mass of the surrounding fluid needs to be included in the normal mode analysis. The added mass represents the effective inertia of the water surrounding the oscillating hull, and may be defined in terms of the component of force in phase with the body's acceleration exerted by the hull on the water for a unit amplitude acceleration of the hull. It was calculated using a steady periodic Green function panel method proposed by Doctors [128] and further developed by Holloway [73].

The potential function at  $z = x + iy$  for a source of sinusoidally oscillating strength,  $Q$ , in two dimensions located at  $c = a + ib$  (where  $z$  is the complex coordinate of collocation point) is given by Wehausen and Laitone [129] as

$$f(z, t) = \left[ \frac{1}{2\pi} (\ln(z - c) - \ln(z - \bar{c})) - \frac{1}{\pi} \text{PV} \int_0^{\infty} \frac{e^{-ik(z - \bar{c})}}{k - v} dk \right] Q \cos \omega t - \left[ e^{-v(z - \bar{c})} \right] Q \sin \omega t \quad (4.8)$$

where PV indicates the principal value of the integral required to ensure uniqueness of the solution, the overbar represents the complex conjugate in the spatial domain and  $k$  is the wave number variable. The body is assumed to oscillate with angular frequency  $\omega$ , so that it will generate outgoing waves with a characteristic wave number given by  $v = \omega^2/g$  where  $g$  is the acceleration due to gravity. It should be noted that this source function is for a stationary source of pulsating strength. Hence it is assumed that the oscillations are of infinitesimal amplitude, and the body has zero speed. The coordinate system shown in Fig. 4-9 is used.

It is convenient to eliminate the time variable by use of complex notation when solving oscillatory problems, noting that the imaginary part in the space and time domains are represented by  $i$  and  $j$  respectively. The use of the symbol  $\sim$  above a quantity signifies that it is time-complex. These quantities may be converted to the time domain by multiplying by  $e^{j\omega t}$  and taking the time-real part<sup>1</sup>.

The evaluation of the integral  $PV \int_0^\infty \frac{e^{-ik(z-\bar{c})}}{k-v} dk$  is described by Doctors [128], giving

$$PV \int_0^\infty \frac{e^{-ik(z-\bar{c})}}{k-v} dk = -e^{-ik(z-\bar{c})} [\text{Ei}(iv(z-\bar{c})) + \epsilon\pi i] \quad (4.9)$$

where Ei is the exponential integral, defined as  $\text{Ei}(z) = \int_{-\infty}^z \frac{e^t}{t} dt$ , and  $\epsilon = 1$  if  $\text{Re}(z) > \text{Re}(\bar{c})$  or  $\epsilon = -1$  if  $\text{Re}(z) < \text{Re}(\bar{c})$ .

Therefore

$$\begin{aligned} \tilde{f}(z) = & \tilde{Q} \left\{ \frac{1}{2\pi} \left[ (\ln(z-c) - \ln(z-\bar{c})) + 2e^{-v(z-\bar{c})} (\text{Ei}(iv(z-\bar{c})) + \epsilon\pi i) \right] \right. \\ & \left. + j \left[ e^{-ik(z-\bar{c})} \right] \right\} \end{aligned} \quad (4.10)$$

and  $f(z, t) = \text{Re}_j \left( \tilde{f}(z) e^{j\omega t} \right)$  may be recovered if  $\text{Im}_j \left( \tilde{Q} \right) = 0$ .

The complex velocity due to a uniform source of unit strength integrated over an element with end points  $c_1$  and  $c_2$ ,  $\tilde{W}_{i,j}$ , is given by:

$$\begin{aligned} \tilde{W}_{i,j} = & \left\{ \frac{1}{2\pi} \left[ e^{-i\beta} \ln \left( \frac{z-c_1}{z-c_2} \right) - e^{i\beta} \ln \left( \frac{z-\bar{c}_1}{z-\bar{c}_2} \right) \right] \right. \\ & \left. - \frac{e^{i\beta}}{\pi} \left[ e^{-v(z-\bar{c})} (\text{Ei}(iv(z-\bar{c})) + \epsilon\pi i) \right]_{\bar{c}_1}^{\bar{c}_2} \right\} \\ & - j \left\{ e^{i\beta} \left[ e^{-v(z-\bar{c})} \right]_{\bar{c}_1}^{\bar{c}_2} \right\} \end{aligned} \quad (4.11)$$

where the first logarithm is interpreted as  $-i\pi$  when  $i = j$ . The complex coordinate of the source panel end points are  $c_1, c_2$  and  $\beta$  is the source panel slope.

Since the Green function method automatically satisfies the free surface condition only the kinematic boundary condition on the body boundary needs to be satisfied, giving

$$\tilde{A}_{i,j} = -\text{Im}_i \left\{ \tilde{W}_{i,j} e^{i\alpha} \right\} \quad (4.12)$$

---

<sup>1</sup>The subscripts  $i$  and  $j$  on the functions Re and Im are used to indicate the space or time complex domains respectively

where  $\tilde{A}_{i,j}$  is the influence of the  $i$ th boundary condition equation due to the  $j$ th source ( $Q_j$ ) and  $\alpha$  is the slope of the body boundary at the collocation point.

The source strengths are thus obtained by solving for  $\{Q\}$  in the matrix equation

$$[\tilde{A}] \{\tilde{Q}\} = \{\tilde{R}\} \quad (4.13)$$

where  $R_i$  represents the terms in the  $i$ th boundary condition equation independent of the sources. The potentials are then obtained from

$$\{\tilde{\phi}\} = [\tilde{B}] \{\tilde{Q}\} \quad (4.14)$$

where the complex potential at point  $i$  due to a unit source distributed over panel  $j$  is given by

$$\tilde{B}_{i,j} = \text{Re}_i \left\{ \frac{1}{\tilde{Q}_j} \int_{j\text{th panel}} \tilde{f}(z_i) ds \right\} \quad (4.15)$$

From Equations 4.8 and 4.15, and the fact that

$$\int_0^x e^{\pm ax} \text{Ei}(\mp ax) dx = \pm \frac{1}{a} [e^{\pm ax} \text{Ei}(\mp ax) - \ln ax - \gamma] \quad \text{where } \gamma = \text{Euler's constant} \quad (4.16)$$

the following is obtained,

$$\begin{aligned} \tilde{B}_{i,j} = & \text{Re}_i \left( \left\{ \frac{-1}{2\pi} [e^{-v\beta} (z-c) \ln(e^{-v\gamma} (z-c)) - e^{-v\beta} (z-\bar{c}) \ln(z-\bar{c})]_{c_1}^{c_2} \right. \right. \\ & \left. \left. - \frac{ie^{v\beta}}{\pi v} \left( [e^{-v(z-\bar{c})} (\text{Ei}(iv(z-\bar{c})) + \epsilon\pi i)]_{c_1}^{c_2} - \ln \left( \frac{z-\bar{c}_2}{z-\bar{c}_1} \right) \right) \right\} \right. \\ & \left. - j \left\{ \frac{ie^{v\beta}}{v} [e^{-v(z-\bar{c})}]_{c_1}^{c_2} \right\} \right) \end{aligned} \quad (4.17)$$

where  $\gamma = \arg(c_1 - c_2) + \frac{\pi}{2}$  if the source and collocation panels are identical and  $\gamma = \arg(z - \frac{c_1 + c_2}{2})$  if they are not identical.

The total force exerted by the water on the body is the sum of forces on each panel,

$$\tilde{F} = \sum_{i=1}^n \Delta \tilde{F}_i \quad (4.18)$$

where  $\Delta\tilde{F}_i = -\tilde{p}_i ds_i \hat{n}_i$  and  $\hat{n}_i = -\sin(\alpha_i)\hat{i} + \cos(\alpha_i)\hat{j}$ . An element of area on the body surface is denoted by  $ds$  and the symbol  $\hat{\phantom{x}}$  is used to show that the variables have a unit magnitude.

Bernoulli's equation is as follows:

$$\frac{p}{\rho} + \frac{\partial\phi}{\partial t} + \frac{1}{2}\nabla\phi\cdot\nabla\phi + gy = 0. \quad (4.19)$$

If the hull is split up into panels, we have the hydrodynamic component of pressure on a panel, assuming small motions and ignoring the hydrostatic term, as

$$\tilde{p}_i = -\rho j\omega\tilde{\phi}_i. \quad (4.20)$$

the total unsteady force is

$$\tilde{F} = -\rho j\omega \sum_{i=1}^n \tilde{\phi}_i ds_i \cos\alpha_i \quad (4.21)$$

The motion  $X_g$  is considered for the three modes of heave, sway and roll (i.e.  $g = 1, 2$  and  $3$  respectively). This will give the corresponding time-complex amplitudes of the generalised force  $\tilde{F}_h$  for the heave force, sway force and roll moment (i.e.  $h = 1, 2$  and  $3$  respectively). As defined above, the added mass,  $a$ , is the component of force in phase with the body's acceleration exerted by the hull on the water for a unit amplitude acceleration of the hull. The damping,  $b$ , may be defined as the component of force in phase with the body's velocity exerted by the body on the water for a unit amplitude velocity of the body. Noting that  $\tilde{F}$  has been defined as the force exerted by the water on a body,

$$\tilde{F}_h + \left( (j\omega)^2 a_{gh} + (j\omega) b_{gh} \right) \tilde{X}_g = 0 \quad (4.22)$$

giving:

$$a_{gh} = \text{Re}_j \left[ \frac{-\tilde{F}_h}{(j\omega)^2 \tilde{X}_g} \right] \quad (4.23)$$

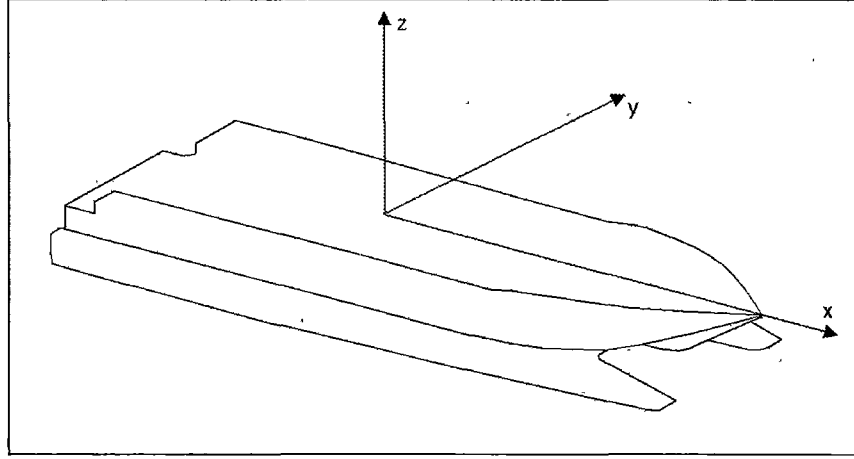


Figure 4-10: Coordinate System 2 (Equations 4.26 - 4.39)

$$b_{gh} = \text{Im}_j \left[ \frac{-\tilde{F}_h}{(j\omega) \tilde{X}_g} \right]. \quad (4.24)$$

Validation of this method is presented in Holloway and Davis [130] where comparisons are made with analytical expressions of Ursell [131] and numerical results of Doctors [128], as well as a transient method of the authors.

It is important to note that the formulations for added mass and damping shown in Equations 4.23 and 4.24 ignore the forward speed of the vessel. Whilst the exciter tests were conducted at zero speed, the results from the full-scale trials were for forward speed. The effect of forward speed should therefore be taken into account. The method of Salvesen, Tuck and Faltinsen [98] is generalised below to express the vertical sectional added mass and damping with forward speed in terms of the local hull deflection, slope and curvature due to hull flexure.

If the flow field is represented by the potential function  $\phi(x, y, z, t)$  then, ignoring the hydrostatic term, the dynamic pressure is given by Bernoulli's equation as  $p = -\rho \left( \frac{\partial \phi}{\partial t} + \frac{1}{2} \nabla \phi \cdot \nabla \phi \right)$ . The global coordinate system shown in Fig. 4-10 is now being used.

Hence in a stationary reference frame

$$F_z = -\rho \int \int_{\text{hull}} \left( \frac{\partial \phi}{\partial t} + \frac{1}{2} \nabla \phi \cdot \nabla \phi \right) n_z dl dx \quad (4.25)$$

where  $l$  is the girth distance from the waterline around the section. Assuming small motions, and noting in a reference frame moving with the ship that  $\frac{\partial}{\partial t}$  must be replaced by  $\left( \frac{\partial}{\partial t} - U \frac{\partial}{\partial x} \right)$ , it follows that

$$\begin{aligned}
\frac{\partial F_z}{\partial x} &= \frac{\partial}{\partial x} \left( -\rho \int \int_{\text{hull}} \left( \frac{\partial \phi}{\partial t} - U \frac{\partial \phi}{\partial x} \right) n_z dl dx \right) \\
&= -\rho \left( p - U \frac{\partial P}{\partial x} \right)
\end{aligned} \tag{4.26}$$

where

$$p = \int_{\text{section}} \frac{\partial \phi}{\partial t} n_z dl, \quad P = \int_{\text{section}} \phi n_z dl.$$

If  $\eta$  is the local vertical displacement of a point on the hull, then  $\phi$  satisfies the boundary condition:

$$\frac{\partial \phi}{\partial n} = \left( \frac{\partial \eta}{\partial t} - U \frac{\partial \eta}{\partial x} \right) n_z \tag{4.27}$$

which, assuming a slender hull (i.e. that  $n_x$  is small),  $\frac{\partial \phi_o}{\partial n} = n_z$ , and  $\eta = \eta_o e^{i\omega t}$  has a solution of the form

$$\phi = (i\omega\eta_o - U\eta'_o) e^{i\omega t} \phi_o \tag{4.28}$$

where  $\eta' = \partial\eta/\partial x$ . If the following is defined

$$a + \frac{b}{i\omega} = z = \rho \int \phi_o n_z dl \tag{4.29}$$

then

$$P = (i\omega\eta_o - U\eta'_o) e^{i\omega t} \frac{z}{\rho} \tag{4.30}$$

hence

$$\frac{\partial P}{\partial x} = \frac{\partial}{\partial x} \left\{ (i\omega\eta_o - U\eta'_o) e^{i\omega t} \frac{z}{\rho} \right\}. \tag{4.31}$$

Therefore since  $p = i\omega P$ , from Equation 4.26:

$$\frac{\partial F_z}{\partial x} = e^{i\omega t} \left\{ z (\omega^2 \eta_o + 2i\omega U \eta'_o - U^2 \eta''_o) + \frac{\partial z}{\partial x} (U i \omega \eta_o - U^2 \eta'_o) \right\} \quad (4.32)$$

and

$$\operatorname{Re} \left\{ \frac{\partial F_z}{\partial x} \right\} = a (\omega^2 \eta_o - U^2 \eta''_o) + b (2U \eta'_o) + \frac{da}{dx} (-U^2 \eta'_o) + \frac{db}{dx} (U \eta_o). \quad (4.33)$$

Hence the added mass accounting for forward speed,  $a_u$ , assuming that there is no phase difference between  $\eta'$ ,  $\eta'_o$ , and  $\eta''_o$  (i.e. the damping is small), is

$$\begin{aligned} a_u &= \frac{\operatorname{Re} \left\{ \frac{\partial F_z}{\partial x} \right\}}{\omega^2 \eta_o} \\ &= a \left( 1 - \frac{U^2 \eta''_o}{\omega^2 \eta_o} \right) + \frac{U}{\omega^2} \left\{ \frac{db}{dx} + \frac{\eta'_o}{\eta_o} \left( 2b - U \frac{da}{dx} \right) \right\} \end{aligned} \quad (4.34)$$

where  $\eta'_o = d\eta_o/dx$  and  $\eta''_o = d^2\eta_o/dx^2$ .

Similarly the damping accounting for forward speed,  $b_u$ , is from

$$\begin{aligned} b_u &= \frac{-\operatorname{Im} \left\{ \frac{\partial F_z}{\partial x} \right\}}{\omega \eta_o} \\ &= b \left( 1 - \frac{U^2 \eta''_o}{\omega^2 \eta_o} \right) - U \left\{ \frac{da}{dx} + \frac{\eta'_o}{\eta_o} \left( 2a + \frac{U}{\omega^2} \frac{db}{dx} \right) \right\}. \end{aligned} \quad (4.35)$$

### 4.3.3 Normal Mode Analysis

To provide a test for the proposed method for estimating the whipping modes, normal mode analysis was conducted on two vessels: Hull 042/045 and Hull 050. The results were then compared with the natural frequencies found from the full-scale trials and exciter tests.

The finite element model described in Chapter 3 was used for the normal mode analysis of Hull 050. A global finite element model of Hull 042 which was initially constructed by consultants Sinclair Knight Mertz using SDRC I-DEAS Master Series MCAE software [49] was converted to PATRAN/NASTRAN, as shown in Fig. 4-11. The model consisted of predominantly plate and bar elements with the exception of laminate elements used to model the honeycomb material in the mezzanine ramps. Rather than a full superstructure, only a superstructure raft was modelled with beam elements for the transverse and longitudinal beams and plate for the flooring. This raft was connected to the main hull using rubber mounts and had the correct mass and stiffness of the superstructure.

In line with the information listed in Section 4.3.3.1, three Hull 042 finite element models were set up with different loading conditions relating to trials conditions 1 and 2 and the

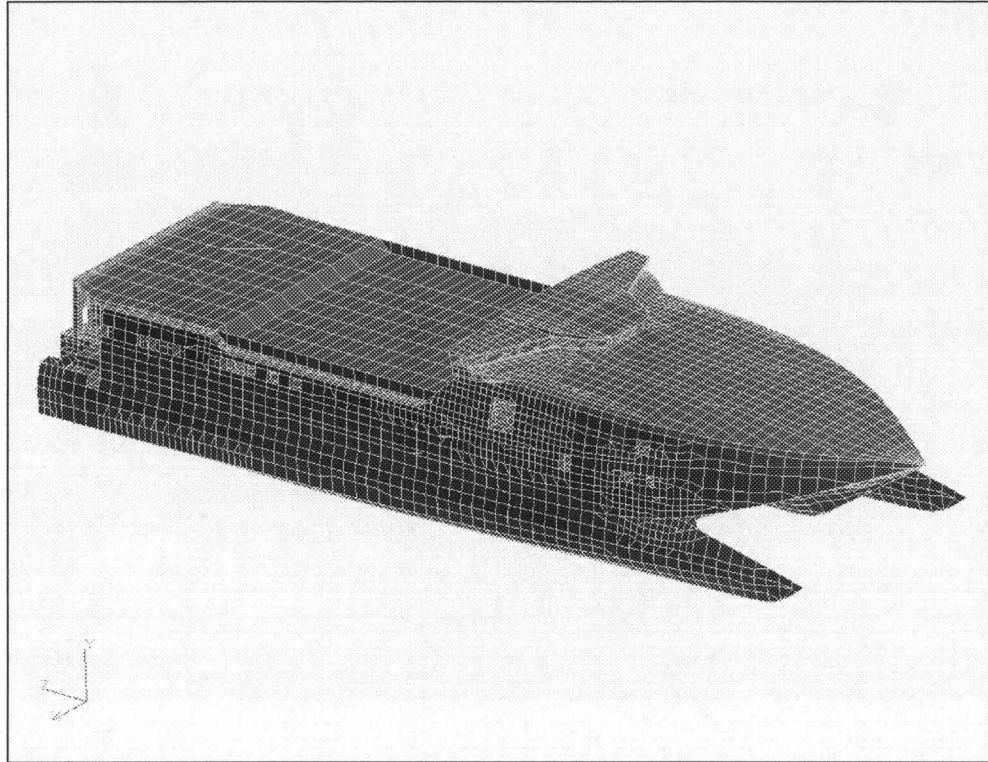


Figure 4-11: Hull 042 Finite Element Model

lightship (exciter test) condition. Only one Hull 050 finite element model was set up for the full-scale trials loading condition.

#### 4.3.3.1 Vessel Loading Conditions

**Hull 042:** During the full-scale measurements, the majority of large slam impacts were recorded on 20th December 1996, when Hull 042 was travelling south down the New South Wales coastline into a large southerly swell. It was recorded that the total fuel on-board at that time was approximately 339,150 litres, with 40,000 litres being maintained in the service tanks. The remaining crew, stores, oil and water masses were assumed to be as per the delivery condition, which gave a total displacement of approximately 1150 tonnes (note that the full displacement of Hull 042 is 1250 tonnes). This condition was identified as trials condition 1.

Further slam events were experienced by Hull 042 two days later (22nd December 1996) on the same delivery voyage. At this time the total fuel on-board was recorded as being 126,000 litres with again 40,000 litres being maintained in the service tanks. The change in the crew, stores, oil and water masses was assumed to be negligible from trials condition 1, which gave a total displacement of approximately 970 tonnes. This condition was identified as trials condition 2.

Since Hull 042 was not available for exciter tests, Hull 045, a near identical sister vessel to

Hull 042, was tested instead. The drafts measured at the time of the exciter test indicated that the displacement was close to the lightship condition at 880 tonnes. This displacement value was significantly different to the full-scale trials loading condition of 1150 tonnes (a change of 21.6% of the full displacement).

**Hull 050:** The full-scale monitoring equipment was on-board Hull 050 for a period of nine months and thus the collected data incorporated a large number of different loading conditions. However on November 21st 1999 the vessel was travelling from Picton to Wellington into a large southerly swell and experienced a large number of severe slam impacts. The loading condition was noted for this crossing and was used in the development of the extreme slam load case. This loading condition corresponded to a displacement of 1100 tonnes and was used for the normal mode analysis (note that the full displacement of Hull 050 is 1700 tonnes).

The exciter tests on Hull 050 were carried out for a vessel displacement of 985 tonnes. Since this displacement value was close to the full-scale trials loading condition of 1100 tonnes (a change of only 6.7% of the full displacement) only one FE model was set up for Hull 050, using the full-scale trials loading condition.

A summary of the vessel loading conditions for Hulls 042 and 050 is shown in Table 4.5.

	Displacement (tonnes)	Draft (m)
Hull 042 Trials Condition 1	1150	3.45
Hull 042 Trials Condition 2	970	3.12
Hull 042/045 Exciter Test Condition	880	2.88
Hull 050 Trials/Exciter Test Condition	1100	3.10

Table 4.5: Hulls 042/045 and 050 Loading Conditions

#### 4.3.3.2 Local Modes

In calculating the normal modes of the models it became apparent that, as well as the existence of the global body modes (e.g. first longitudinal mode), there also existed a large number of local modes due to the localised configuration of plates and beams. When a large number of local modes were present it was difficult to calculate sufficient modes to identify the global modes. This problem was addressed by artificially increasing the bending stiffness of the shell elements by converting the elements from having the properties of standard homogenous plate to those of standard equivalent section plate (SESP). With SESP properties the elements were then given an artificially high bending stiffness value which caused the local plate modes to increase in frequency significantly above the range of frequency of interest for finding the global modes. Changing the plate bending stiffness had the effect of increasing the global mode frequencies marginally; once the approximate location of the global mode frequencies had been determined the original models (without SESPs) were used to determine the global modes. The bending stiffnesses of beam elements were not altered.

On occasions it was difficult to locate a global mode because of the presence of a dominating local mode at the same frequency. The technique used to avoid this problem was to view the eigenvector results for different parts of the structure to isolate the local modes. For example, to locate the first longitudinal mode for Hull 050 the results were viewed for the hull without the superstructure, since the global mode coincided with a local mode of some beam elements in the superstructure which disguised the presence of the longitudinal mode.

#### 4.3.4 Results - Dry Modes

The first two flexible global modes found were the lateral torsion mode and the first longitudinal mode. Only the low frequency global modes were investigated since the aim was to identify the modes which corresponded to the frequencies ascertained through the spectral analysis of the full-scale trials strain gauge results. Examples of these mode shapes, for Hull 050, are shown in Figs. 4-12 and 4-13, with the scale being the translational eigenvector deformation, nominally in millimetres. The lateral torsion mode is similar in shape to the load case known as pitch connecting moment where the hulls of the catamaran rotate against each other about a node close to amidships. The first longitudinal mode has two nodes, approximately  $\frac{1}{3}L$  from the bow and  $\frac{1}{3}L$  from the stern, and is equivalent to the hogging and sagging loading conditions. The dry hull natural frequencies are shown in Table 4.6. Whilst there was only a small change in frequency from trials condition 1 to trials condition 2 for Hull 042, it is apparent that a change in loading condition from delivery to lightship caused a significant increase in the dry hull frequencies of Hull 042. This is to be expected since from Equation 4.5 it is clear that for a constant stiffness the natural frequency will reduce as the mass of the system increases, in proportion to  $\frac{1}{\sqrt{M}}$ . Hull 050 is a similar vessel to Hull 042 and hence the natural frequencies were found to be similar. However, the first longitudinal mode for Hull 050 is approximately 10% higher than the lightship condition of Hull 042 which suggests that Hull 050 is a stiffer vessel longitudinally.

Mode	Hull 042 Delivery Condition 1	Hull 042 Delivery Condition 2	Hull 042 Lightship Condition	Hull 050
Lateral Torsion	2.16 Hz	2.28 Hz	2.56 Hz	2.48 Hz
First Longitudinal	3.29 Hz	3.39 Hz	3.56 Hz	3.97 Hz

Table 4.6: Hull 042 and 050 Dry Natural Frequencies

#### 4.3.5 Results - Added Mass

The two-dimensional sectional added mass coefficients at zero speed were calculated for Hulls 042 and 050 according to the formulation outlined in Section 4.3.2. The input required was a set of single demi-hull offsets, the number of panels per half girth of the section, the calculation frequencies and the hull draft. 64 sections were used for Hull 042 and 72 sections for Hull 050

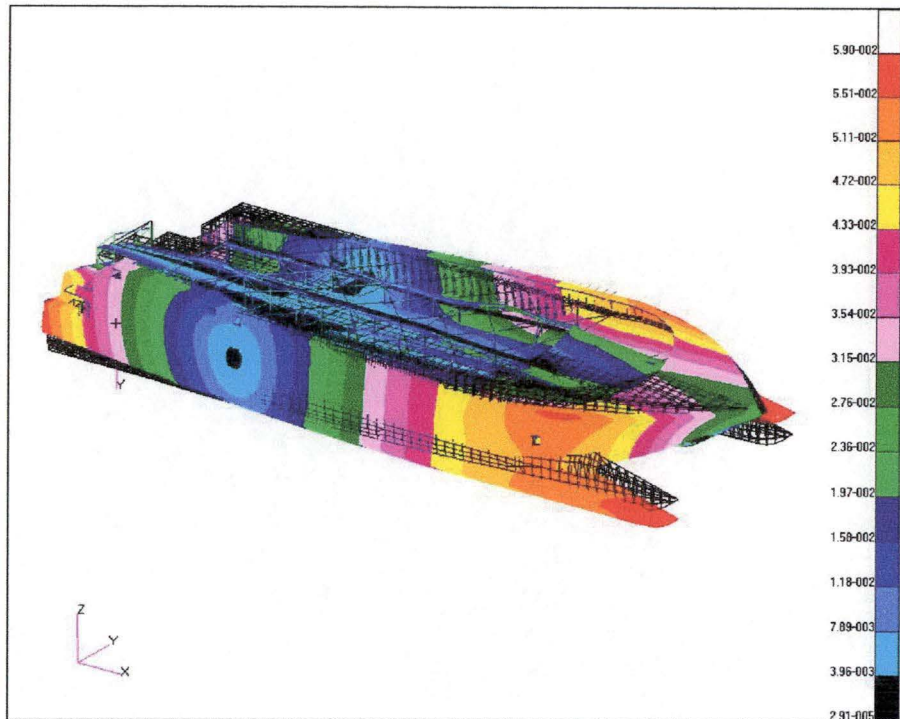


Figure 4-12: Hull 050 - Lateral Torsion Dry Mode (2.48 Hz), units in mm

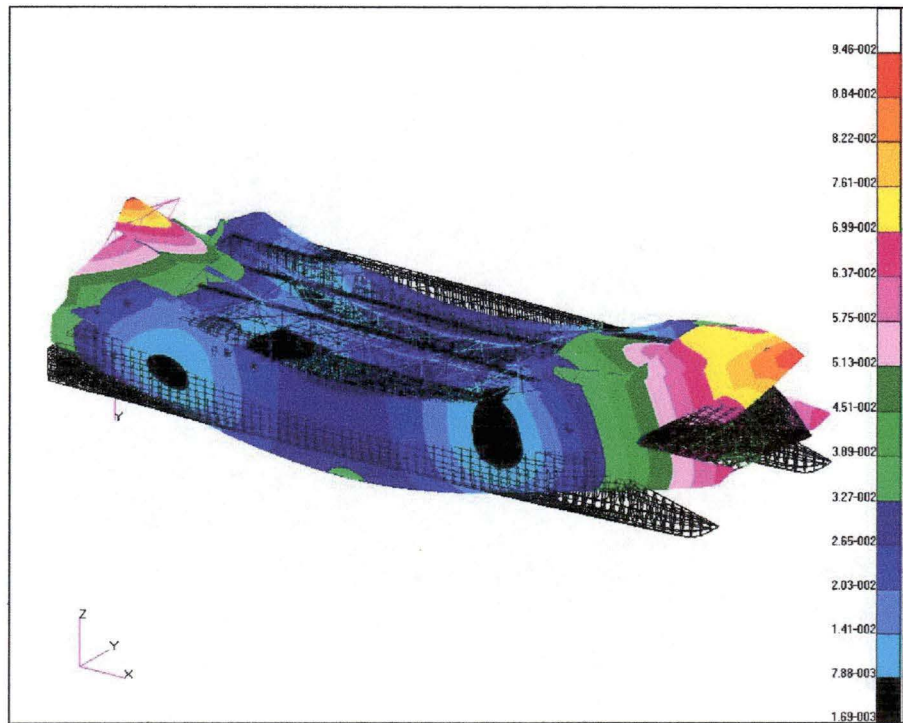


Figure 4-13: Hull 050 - 1st longitudinal Dry Mode (3.97 Hz), units in mm

each at a section spacing of 1.2m. The offsets for Hull 042 and 050 are shown in Figs. 4-14 and 4-15.

#### 4.3.5.1 Zero Speed

The zero speed added mass for each vessel was calculated and the results for Hulls 042 and 050 are shown in Figs. 4-16 to 4-19, where the added mass per unit length,  $a$ , is normalised as

$$\text{Normalised Added Mass, } a' = \frac{a}{\Delta/L}$$

where  $\Delta$  is the total vessel displacement (two hulls for catamaran) and  $L$  is the waterline length. It should be noted that the sections are numbered from the transom and the station spacing for each hull is 1200mm. The plots show that the added mass increases towards the stern of the vessels as the hull sections become fuller. This is further highlighted by Fig. 4-20 which shows a plot of the added mass coefficient against section number, where:

$$\text{Added Mass Coefficient} = \frac{a_{\text{section}}}{\Delta_{\text{section}}} \text{ for unit length of hull}$$

Also apparent is the manner in which the added mass value approaches a steady value by approximately 10 rad/sec, which is comfortably below the lowest natural frequency.

	<b>Displacement (tonnes)</b>	<b>Total Vessel Added Mass (tonnes)</b>
Hull 042 Trials Condition 1	1150	978
Hull 042 Trials Condition 2	970	910
Hull 042/045 Exciter Test Condition	880	875
Hull 050 Trials/Exciter Test Condition	1100	1085

Table 4.7: Hulls 042/045 and 050 Displacement and Added Mass

The values of added mass and displacement for each vessel, see Table 4.7, show that the added mass of each of the vessel configurations is close to the corresponding displacement of the vessel. This was to be expected since the added mass coefficient, as shown in Fig. 4-20, averages out over the length of the vessel to a value close to 1.0.

An investigation was conducted to determine the optimum panel density for calculating the sectional added mass. The results, as shown in Fig. 4-21, indicate that for the section investigated the added mass reduced as the panel density increased until a steady value was achieved at 200 panels per section. This was therefore the panel density used for the added mass calculations.

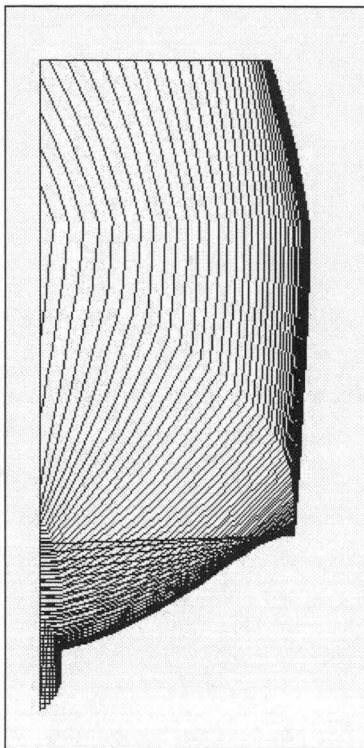


Figure 4-14: Hull 042 Offsets with Design Waterline (DWL) shown

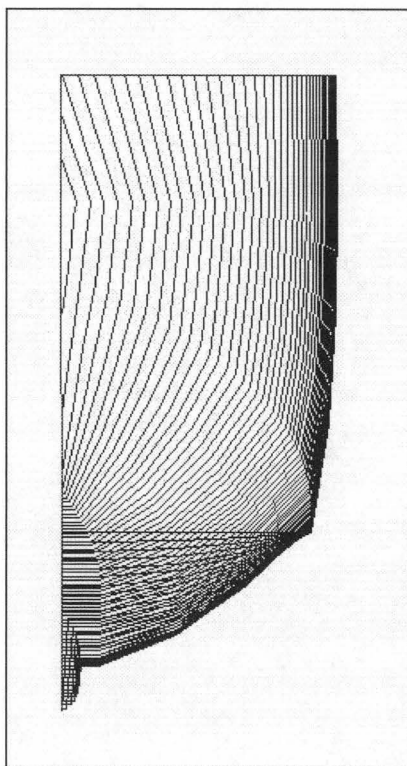


Figure 4-15: Hull 050 Offsets with Design Waterline (DWL) shown

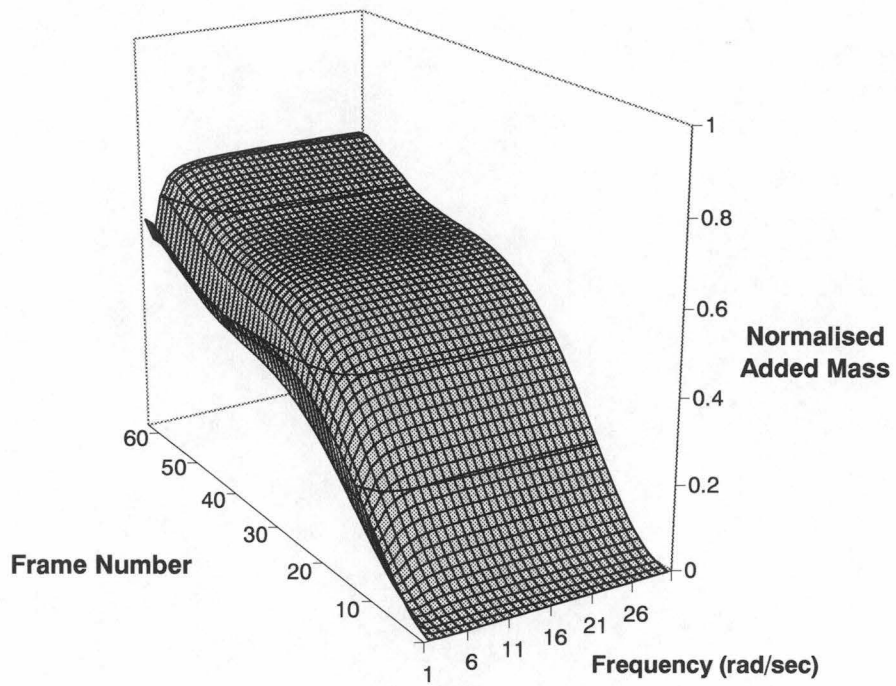


Figure 4-16: Hull 042 - Sectional Added Mass, Trials Condition 1, Draft = 3.45m

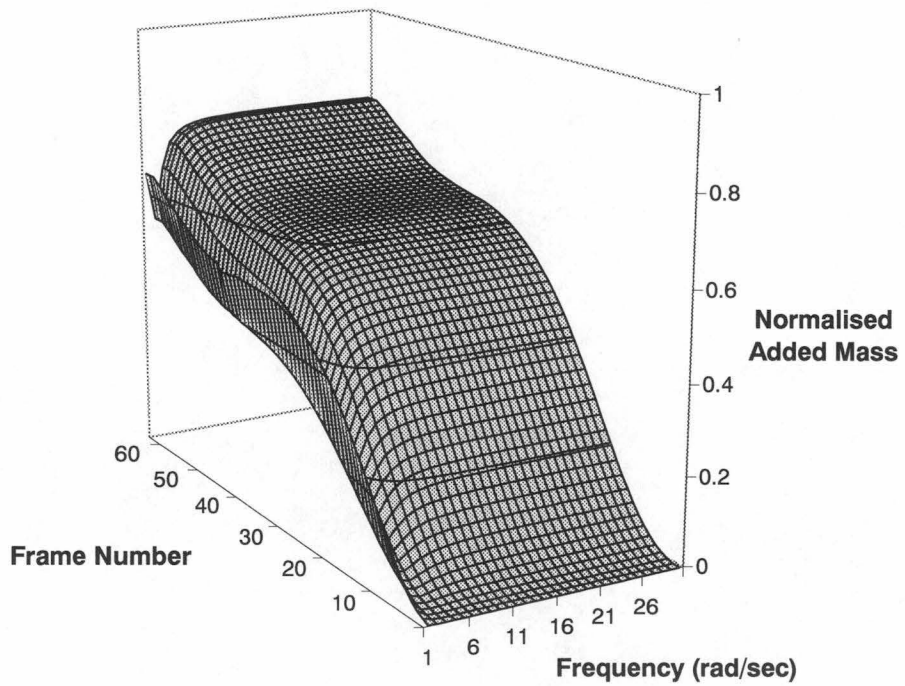


Figure 4-17: Hull 042 - Sectional Added Mass, Trials Condition 2, Draft = 3.12m

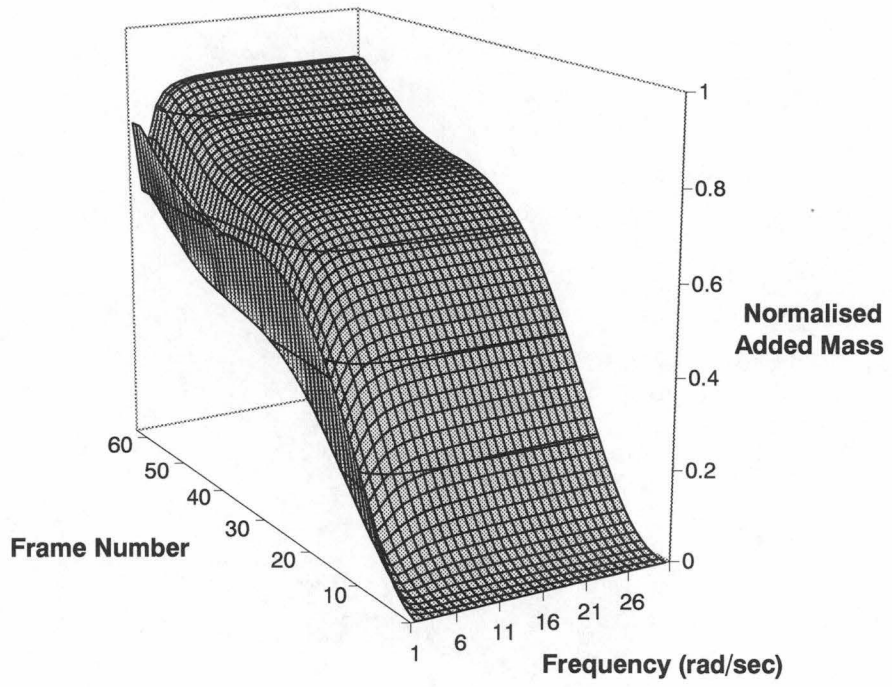


Figure 4-18: Hull 042 - Sectional Added Mass, Exciter Test Condition, Draft = 2.88m

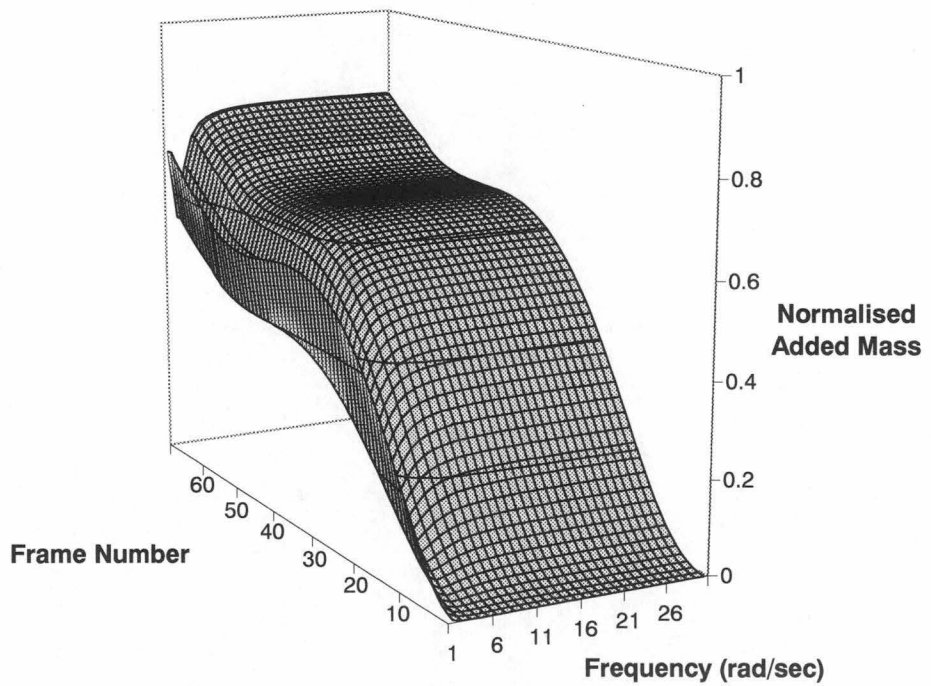


Figure 4-19: Hull 050 - Sectional Added Mass, Trials/Exciter Test Condition, Draft = 3.10m

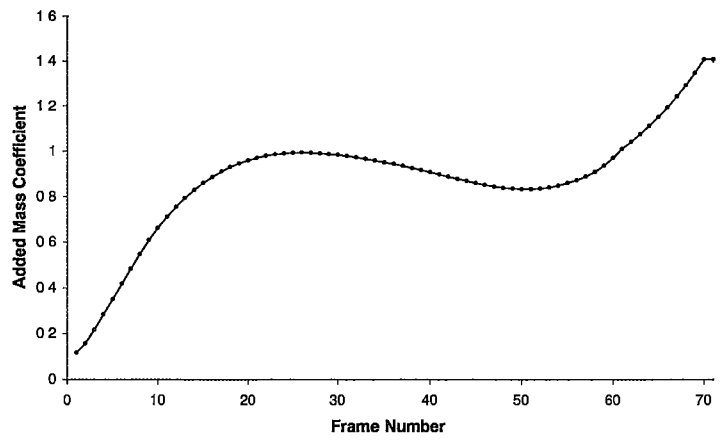


Figure 4-20: Hull 050 - Added Mass Coefficient for varying Frame Number, Frequency = 3.0 Hz

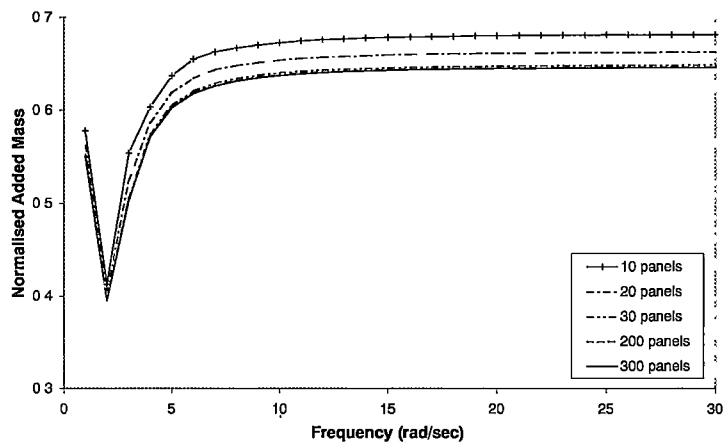


Figure 4-21: Hull 050 - Influence of Panel Density on Sectional Added Mass, Frame 40

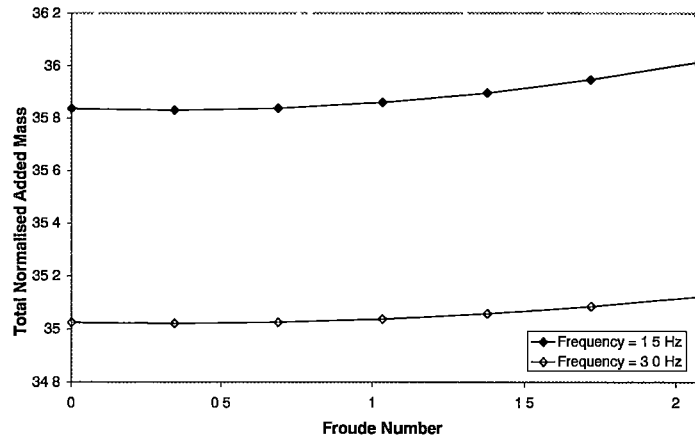


Figure 4-22: Hull 050 - Effect of Froude Number on Total Added Mass

#### 4.3.5.2 Forward Speed Effects

It was found that due to the relatively high frequency the forward speed terms (Eqn. 4.34) were negligible, as is demonstrated in Fig. 4-22 where the effect of forward speed on the total rigid vessel heave added mass is shown for two frequencies. At a Froude number of 0.7, typical for these vessels, the total vessel added mass is less than 0.1% greater than for zero speed.

#### 4.3.5.3 Distribution Tests

To ascertain the influence of different methods of incorporating the added mass into the finite element model on the resulting natural frequencies, a set of tests was conducted on the FE model of Hull 050. The methods investigated were as follows:

- Method 1: Added mass for section included as a single lumped mass at a node at the keel of each section.
- Method 2: Added mass for section included as lumped masses at 7 nodes per hull section, uniformly distributed between the elements at each section.
- Method 3: Added mass for section included as lumped masses at 7 nodes per hull section, non-uniformly distributed between the elements at each section. The added mass was distributed according to the horizontal projected area of the section, or  $\cos \alpha$  distribution, as illustrated in Fig. 4-23. Where  $\alpha$  is the angle between the hull surface and the horizontal baseline.
- Method 4: Added mass for section included as lumped masses at 7 nodes per hull section, non-uniformly distributed between the elements at each section. The added mass was distributed according to the  $\cos^2 \alpha$  distribution to approximate the effect of  $\alpha$  on both the local boundary condition and the vertical force component.

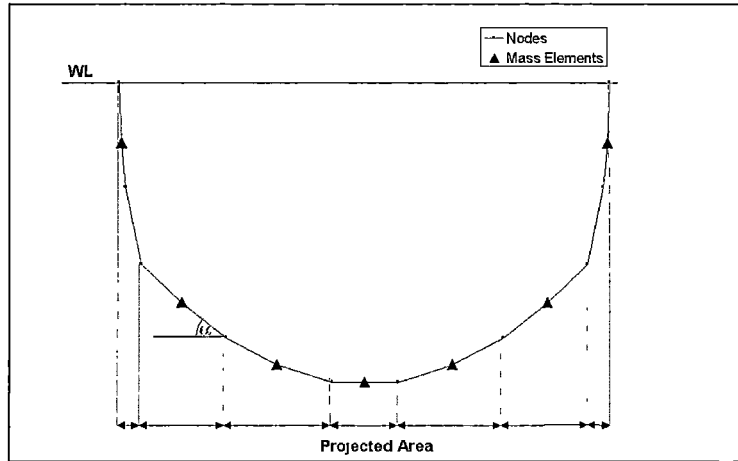


Figure 4-23: Added Mass Distribution according to Horizontal Projected Area around a Hull Section ( $\cos\alpha$  Distribution)

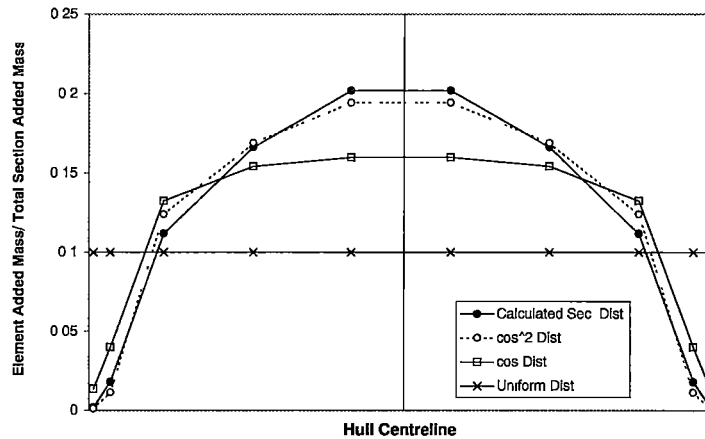


Figure 4-24: Added Mass Distributions

- Method 5: Added mass for section included as lumped masses at 7 nodes per hull section, non-uniformly distributed between the elements at each section. The added mass was distributed according to the actual calculated distribution of the added mass around the section, as illustrated in Fig. 4-24.

The results, as shown in Fig. 4-25 and Table 4.8, indicate that the technique for allocating added mass around a section had a negligible effect on the resulting natural frequencies. This leads to the conclusion that, although a  $\cos^2\alpha$  added mass distribution was used for the subsequent analysis in this study, the technique of locating the added mass as a lumped mass element at the keel will give sufficient levels of accuracy (within 0.3%) in determining the natural frequencies of such vessels.

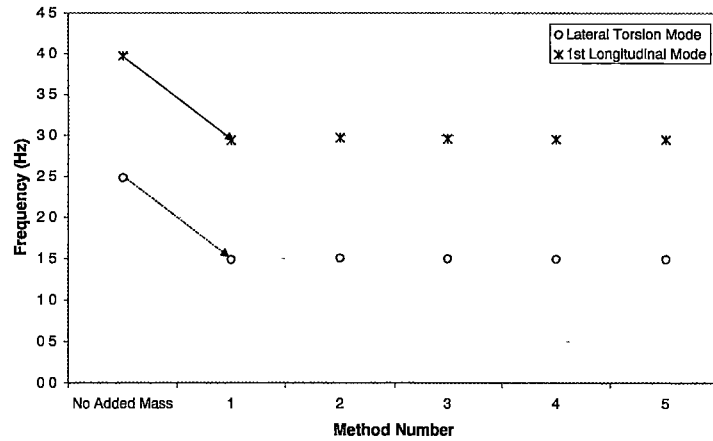


Figure 4-25: Hull 050 - Effect of Added Mass Inclusion Techniques on Natural Frequency

	Lateral Torsion Mode	1st Longitudinal Mode
No Added Mass	2.480 Hz	3.970 Hz
Method 1: 1 Node per Section at Keel	1.489 Hz	2.938 Hz
Method 2: 7 Nodes per Section Uniform Distribution	1.507 Hz	2.968 Hz
Method 3: 7 Nodes per Section Cosine Distribution	1.498 Hz	2.956 Hz
Method 4: 7 Nodes per Section Cosine Squared Distribution	1.495 Hz	2.950 Hz
Method 5: 7 Nodes per Section Actual Distribution	1.493 Hz	2.947 Hz

Table 4.8: Hull 050 - Effect of Added Mass Inclusion Techniques on Normal Mode Analysis Natural Frequencies

#### 4.3.5.4 Frequency Tests

The added mass used to obtain the results shown in Fig. 4-25 was that for the frequency of the corresponding dry mode. The use of an iterative technique was also investigated, whereby the wet mode was initially determined using the added mass at the frequency of the respective dry mode. Then the added mass at this wet mode frequency was used to recalculate the wet natural frequency. The results are shown in Table 4.9, and indicate that there was very little difference (0.1% at 3 Hz increasing to 0.6 % at 1.5 Hz) in the resulting dry modes by using this technique. Therefore the subsequent modal analysis to determine the wet modes used the added mass at the dry mode frequency, with no iteration process being used. However, if there was a significant difference in the added mass for the wet mode frequency and the dry mode frequency (as may be the case at much lower frequencies) then it may be necessary to perform an iterative process.

	Added Mass for Dry Mode Frequency	Iterative Technique: Added Mass for Wet Mode Frequency
Lateral Torsion	1.495 Hz	1.504 Hz
First Longitudinal	2.950 Hz	2.953 Hz

Table 4.9: Hull 050 - Effect of Added Mass Frequency on Natural Frequency

#### 4.3.5.5 Forward Speed Effects

A comparison of the natural frequencies calculated by finite element normal modes analysis with and without the effect of forward speed on the vessel's added mass is shown in Table 4.10. The vessel speed was taken to be 30 knots. There was no significant change in the calculated frequencies due to the incorporation of speed effects on added mass; this was to be expected since the added mass for Hull 050 varied little with speed, as was shown in Section 4.3.5.2.

	Added Mass - Zero Speed	Added Mass - 30 knots
Lateral Torsion	1.495 Hz	1.495 Hz
First Longitudinal	2.950Hz	2.950 Hz

Table 4.10: Hull 050 - Effect of Including Added Mass Speed Influence on Natural Frequency

#### 4.3.6 Results - Wet Modes

As for the dry mode analysis, the first two flexible global wet modes found were the lateral torsion mode and the first longitudinal mode. These mode shapes were similar to those shown for the dry modes in Figs. 4-12 and 4-13. As expected from the form of Eqn. 4.7 the natural frequencies reduced significantly due to the effect of the added mass (by 31-40% for the lateral torsion mode, and 14-25% for the first longitudinal mode), as can be seen in Table 4.11.

	Dry Modes		Wet Modes	
	Lateral Tor-sion	1st Longitu-dinal	Lateral Tor-sion	1st Longitu-dinal
Hull 042 Trials Condition 1	2.16 Hz	3.29 Hz	1.50 Hz	2.56 Hz
Hull 042 Trials Condition 2	2.28 Hz	3.39 Hz	1.58 Hz	2.92 Hz
Hull 042/045 Exciter Test Condition	2.56 Hz	3.56 Hz	1.65 Hz	3.00 Hz
Hull 050 Tri-als/Exciter Test Condition	2.48 Hz	3.97 Hz	1.50 Hz	2.95 Hz

Table 4.11: Hulls 042 and 050 - Wet Natural Frequencies

The output from the normal mode analysis incorporating the fluid structure interaction was compared with the results from the trials measurements and exciter tests. The comparison for Hull 042 in trials condition 1, see Fig. 4-26, shows that the predicted natural frequencies correlate closely with the two main frequencies measured during the full-scale trials. The mode measured at approximately 2.6 Hz correlates with the first longitudinal mode as predicted by the finite element analysis, whilst the mode at approximately 1.5 Hz matches with the calculated lateral torsion natural frequency. Similar correlation may be found in Fig. 4-27 for Hull 042 in trials condition 2, with the first longitudinal mode at approximately 2.9 Hz and the lateral torsion mode at approximately 1.7 Hz, both matching with the finite element results. These results clearly highlight that different vessel loading conditions result in changes in natural frequency, with the frequencies generally increasing as the vessel displacement decreases. The influence of the load distribution is also significant. The long distance fuel tanks were located close to modal nodes for both the identified modes and a change in displacement due to loading/unloading of long range fuel was not as significant as a change in mass at a modal anti-node would have been. For example, if the difference in fuel mass between trials condition 2 and trials condition 1 were loaded evenly at the bow and stern of the vessel, as opposed to the centrally located long range fuel tanks, the finite element modal analysis estimated the lateral torsion and first longitudinal modes as 1.39 Hz and 2.27 Hz respectively. These values are significantly different from those measured and calculated for delivery condition 1 where the fuel is loaded close to amidships.

From the exciter tests on Hull 045 the first longitudinal mode was identified at approximately 3 Hz. This frequency matches closely with that found by the finite element analysis for Hull 042 in the lightship configuration, as seen in Fig. 4-28. This confirms that the mode at approximately 2.6 Hz in the trials results is the first longitudinal mode, and the difference in frequency between the trials measurements and the exciter test is again due to the vessel loading variation.

It should be noted that the added mass formulation is conducted for the vessel's calm wa-

terline. This assumption was applicable for the exciter test measurements where the waterline variation was minimal. However the waterline would have varied significantly when the vessel was operating in waves, particularly in waves large enough to cause slamming. A change in local draft affects the vessel's total added mass value while vessel trim and the presence of waves both affect added mass distribution and these factors may have contributed to the spread in the measured natural frequencies for the full-scale trials.

Fig. 4-29 shows that the first longitudinal mode found from the normal mode analysis of Hull 050, with the added mass incorporated, matches up well with the frequency determined from the exciter test. This confirms that the mode identified from the trials measurements at approximately 2.8 Hz is the first longitudinal mode. It is also evident that the mode at approximately 1.4 Hz in the trials results is the lateral torsion mode since it compares well with the frequency identified by the finite element analysis.

The mode shapes for the first longitudinal mode, as measured on Hulls 045 and 050 through the exciter tests, were compared with the mode shapes as predicted through the finite element normal mode analysis including the added mass, as shown in Figs. 4-30 to 4-32. The magnitudes of the modes were normalised about the response level at the forward accelerometer location from the exciter tests. The comparison for Hull 042/045 on the centreline shows that the finite element prediction tends to underestimate the magnitude of the mode shape towards amidships, but the comparison is good at the stern of the vessel. The difference between the mode shapes predicted on and off the centreline is small when compared to the exciter test results, which may be due to the anchor, which was used to excite the mode, being situated on the centreline rather than on the demi-hulls. The Hull 042/045 prediction of the mode shape off the centreline shows good correlation for most of the length of the vessel except for a slight over prediction towards the transom. The Hull 050 exciter tests were only conducted on the centreline of the vessel and hence a comparison with the finite element results can only be made for those locations; the correlation appears to be satisfactory with the theoretical predictions lying within the range of the measured results along the length of the vessel.

The comparisons of the trials measurements and exciter tests with the theoretical predictions indicate that the method used in this study for determining the whipping modes of large high-speed catamarans including the fluid-structure interaction gives satisfactory results.

### 4.3.7 Conclusions

The use of finite element normal mode analysis has been proposed for estimating the natural frequency of the whipping modes of large high-speed catamarans. In order to test the method dry and wet modes of two Incat catamarans, Hulls 042 and 050, were estimated and compared with results from exciter tests and full-scale trials. The fluid structure interaction was accounted for by calculating the added mass using a steady periodic Green function panel method. The effect of forward speed on sectional added mass was expressed in terms of

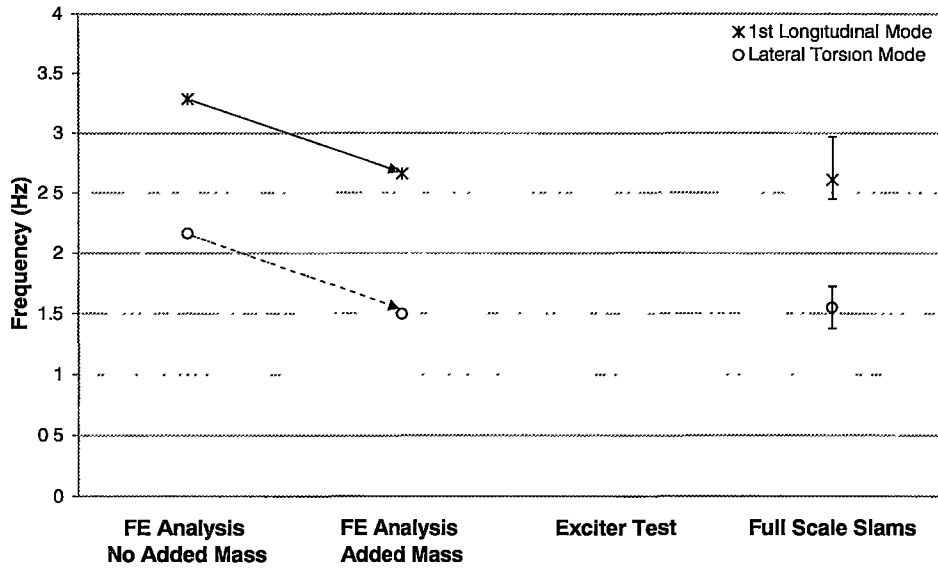


Figure 4-26: Hull 042 - Natural Frequencies, Trials Condition 1

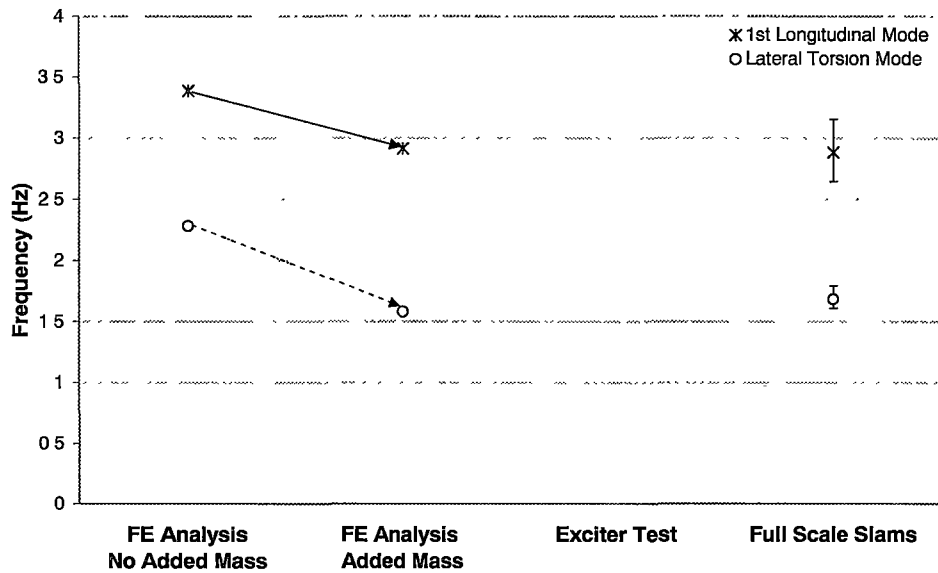


Figure 4-27: Hull 042 - Natural Frequencies, Trials Condition 2

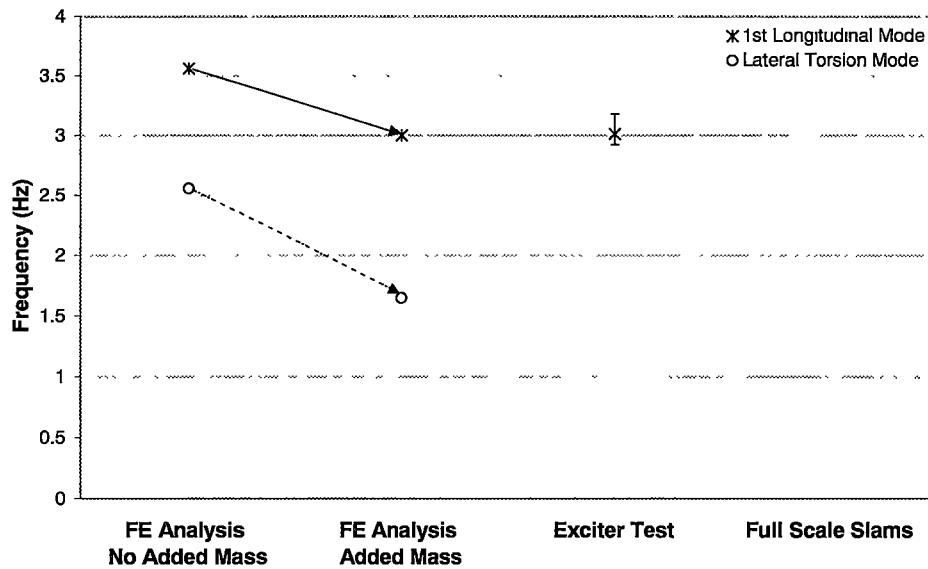


Figure 4-28: Hull 042/045 - Natural Frequencies, Exciter Condition

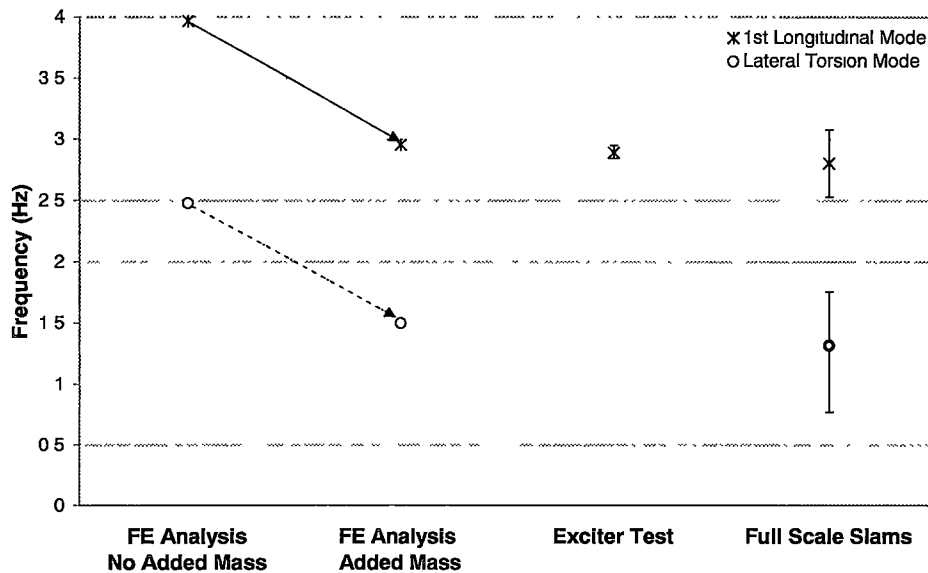


Figure 4-29: Hull 050 - Natural Frequencies, Exciter Test/Trials Condition 1

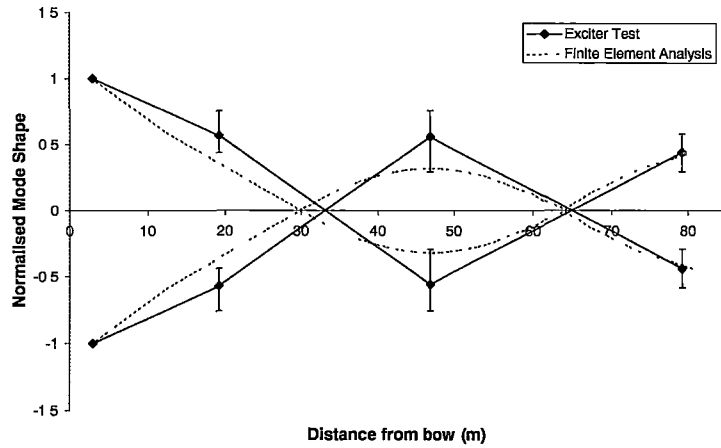


Figure 4-30: Hull 042/045 - First Longitudinal Mode Shape Comparison on Centreline

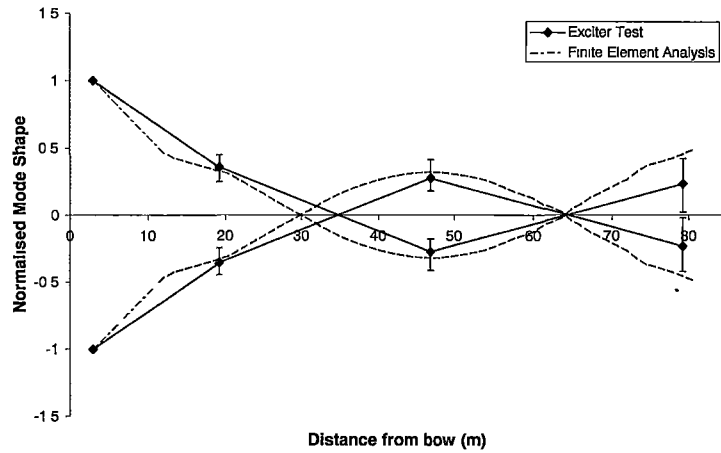


Figure 4-31: Hull 042/045 - First Longitudinal Mode Shape Comparison off Centreline

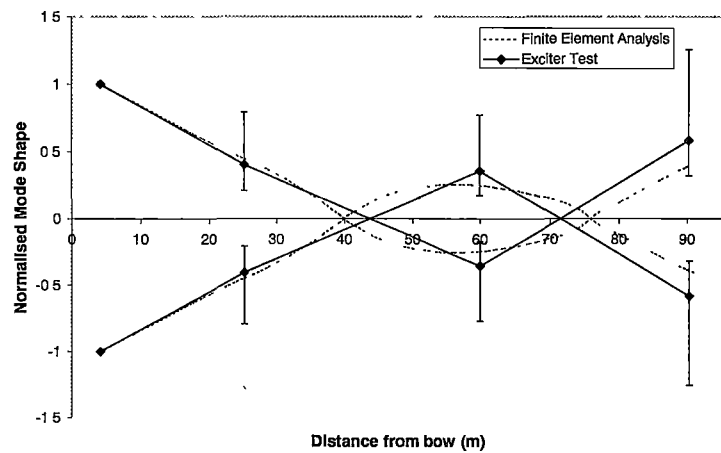


Figure 4-32: Hull 050 - First Longitudinal Mode Shape Comparison on Centreline

the local hull deflection, slope and curvature due to longitudinal hull flexure. The following conclusions may be drawn:

- Good correlation was found between the finite element analysis results for the wet modes and the full-scale and exciter test results which indicate that the method used for deriving the flexible global modes is suitable for this style of vessel.
- Of the two major frequencies identified in the vibratory whipping through the full-scale measurements of slam impacts, the lower frequency (approximately 1.5 Hz) corresponds to the lateral torsion mode whilst the higher frequency (approximately 2.5 - 3 Hz) is the first longitudinal mode.
- The first longitudinal mode frequency for Hull 050 is approximately 10% higher than the lightship condition of Hull 042 which suggests that Hull 050 is a stiffer vessel longitudinally.
- The calculated added mass increases towards the stern of the vessels as the hull sections become fuller.
- The calculated added mass value is essentially independent of frequency above approximately 10 rad/sec.
- The effect of forward speed on added mass and hence natural frequency was found to be negligible at the speeds and frequencies considered.
- In order to incorporate the added mass into the finite element models a  $\cos^2\alpha$  distribution (where  $\alpha$  is the angle of the section surface to the horizontal, see Fig. 4-23) around each hull section was used since this was close to the actual added mass distribution around a section. However it was found that placement of the added mass as a lumped mass on the keel at each section would give satisfactory results.
- An iterative approach to applying the added mass to the finite element model, where the added mass was refined as the natural frequency changed, made no discernible difference to the resulting natural frequencies.
- Significant changes in natural frequency were apparent due to changes in vessel mass loading magnitude and distribution.

These results are important since they show that the proposed method of finite element mode analysis is suitable for estimating the whipping modes of large high-speed catamarans. The technique for accounting for the surrounding fluid to enable wet modes to be determined also appears to be appropriate.

## 4.4 Damping

The rate at which the whipping behaviour decays after a slam is due to the damping within the system. As noted in the introduction to this chapter, there is scarce knowledge available on the damping of the whipping behaviour of ships. The reported analysis of the full-scale slam measurements and exciter test results has enabled estimates to be made for the total damping for large high-speed catamarans. It has been proposed previously [27] that the damping consists of two components: hydrodynamic damping and structural damping. Methods for estimating the various components of hydrodynamic damping, including wavemaking, viscous, appendage and acoustic damping, are now introduced. These methods were used to estimate the hydrodynamic damping of a large high-speed catamaran, Incat Hull 050, for the first longitudinal and lateral torsional modes, and the results are presented. An experimental investigation into the material damping of the aluminium used in the construction of large high-speed catamarans was also conducted. Structural damping may also arise from the fit out of the ship (lining materials, pipe work etc.), methods of connection of components (welds, bolts, rubber mounts etc.) and the response of loads (vehicle suspensions, sloshing of fuel etc.). These sources are difficult to estimate, but unfortunately are likely to account for the majority of the total damping, as argued below.

This work has enabled conclusions to be drawn on the relative importance of the various components of damping, in particular the hydrodynamic and structural damping.

### 4.4.1 Energy Dissipation in the System

For an idealised linear spring, damper system [132] the total force resisting motion may be expressed as

$$F = -kx - b \dot{x} \quad (4.36)$$

where  $k$  is the stiffness and  $b$  the damping. If the motion is assumed to be simple harmonic, then

$$x(t) = X \sin \omega t, \quad (4.37)$$

so that Eqn. 4.36 becomes

$$F = -kX \sin \omega t - b\omega X \cos \omega t. \quad (4.38)$$

The energy dissipated in a complete cycle will be

$$\begin{aligned}
\Delta W &= \int_{t=0}^{2\pi/\omega} Fv dt \\
&= \int_0^{2\pi} kX^2 \omega \sin \omega t. \cos \omega t. \frac{d(\omega t)}{\omega} + \int_0^{2\pi} b\omega^2 X^2 \cos^2 \omega t. \frac{d(\omega t)}{\omega} \\
&= \pi b\omega X^2.
\end{aligned} \tag{4.39}$$

The energy dissipated by each identified damping mechanism, in a complete cycle,  $\Delta W$ , may therefore be found. In order to achieve this the vessel is split into transverse sections (nominally corresponding to the structural frames) and the damping contribution for each section found,  $b_s X_s^2$ ; where  $b_s$  is the sectional damping and  $X_s$  is the sectional amplitude of motion or mode shape displacement. Using the mode shapes, for the first longitudinal and lateral torsion modes, found through finite element analysis, the total damping contribution,  $bX^2$ , may be found by summing the contributions of each section along the vessel as follows

$$bX^2 = \sum_0^L b_s X_s^2 \tag{4.40}$$

and the energy dissipated in a complete cycle found from Eqn. 4.39.

The fraction of the total energy of the vibrating system which is dissipated in each cycle may then be calculated: where the fraction of the total energy of the vibrating system which is dissipated in each cycle,  $\Delta W$ , is divided by the total energy in the system,  $W$ . The total energy in the system  $W$  may be expressed either as the maximum potential energy ( $\frac{1}{2}kX^2$ ) or the maximum kinetic energy ( $\frac{1}{2}mv^2 = \frac{1}{2}m\omega^2 X^2$ ) since they will be equal for low damping levels. It thus follows that

$$\frac{\Delta W}{W} = \frac{\pi b\omega X^2}{\frac{1}{2}m\omega^2 X^2} = 2 \left( \frac{2\pi}{\omega} \right) \left( \frac{b}{2m} \right). \tag{4.41}$$

Again, a "generalised" mass is used where  $mX^2 = \sum_0^L m_s X_s^2$ , analogous to Eqn. 4.40. The total energy in the system may be found from finite element modal analysis which gives the total strain energy in the vessel's structure, for each modal frequency, normalised against the point of maximum deflection in the structure. The damping loss may be defined as follows

$$\frac{\Delta W}{W} = 2\delta = 4\pi\zeta \tag{4.42}$$

where  $\delta$  is the decay factor or logarithmic decrement and  $\zeta$  is the ratio of damping to critical

damping. The loss coefficient is defined as the ratio of the energy dissipated per radian and the total strain energy:

$$\text{loss coefficient} = \frac{\Delta W}{2\pi W} = \frac{\delta}{\pi}. \quad (4.43)$$

Symbol	Name	Definitions	
$\delta$	logarithmic decrement	$\ln \left( \frac{x_1}{x_2} \right)$	$\frac{1}{2} \frac{\Delta W}{W}$
$\eta$	{ decay coefficient loss factor/coefficient }	$\frac{1}{\pi} \ln \left( \frac{x_1}{x_2} \right)$	$\frac{1}{2\pi} \frac{\Delta W}{W}$
$\zeta$	damping ratio	$\frac{1}{2\pi} \ln \left( \frac{x_1}{x_2} \right)$	$\frac{1}{4\pi} \frac{\Delta W}{W}$
-	specific damping capacity	$\ln \left( \frac{x_1}{x_2} \right)^2$	$\frac{\Delta W}{W}$

Table 4.12: Definitions of Damping Measures

#### 4.4.2 Hydrodynamic Damping - Theory

The hydrodynamic damping is defined as the component of force in phase with the vessel's velocity exerted by the body on the water for a unit amplitude velocity of the body. The hydrodynamic damping arises from various mechanisms. The primary component is due to the waves created by the oscillating vessel, called wavemaking damping. Energy may also be dissipated by friction; although these viscous effects are likely to be small [54] they are also calculated, see Section 4.4.2.2. Since the damping due to sound radiation was highlighted as a possible hydrodynamic damping source by Sunnersjö and Janson [125], a technique was also investigated for estimating this form of damping.

The presented techniques were then used to estimate the hydrodynamic damping of a large high-speed catamaran, Incat Hull 050.

##### 4.4.2.1 Wavemaking Damping

The wave making damping arises because the oscillating vessel generates waves which radiate outwards and dissipate energy. It may be calculated using a steady periodic Green function panel method as described in Section 4.3.2. The formulation for estimating damping was extended to account for forward speed as shown in Eqn. 4.35. Given the sectional damping the total damping for each hydrodynamic component was found using the method given in Section 4.4.3.2.

##### 4.4.2.2 Viscous Damping

As the vessel oscillates, water flows past the hull and exerts frictional forces on the hull surface. Since the oscillating flow for whipping will be of fairly high frequency and small amplitude it

is proposed that the flow regime does not fit the typical ship motion solutions [54]. This was confirmed by analysing the exciter test results from Incat Hull 050 where it was found that the vertical amplitude of displacement during a typical first longitudinal modal vibration at the bow was approximately 2.5mm and the maximum velocity was approximately 0.05 m/s.

The oscillating flow therefore has a very low Reynolds Number ( $\sim 220$ ) and will be laminar in nature. The oscillating flow is therefore similar to the flow past a flat plate with sinusoidal oscillations parallel to itself, which is sometimes termed *Stokes's second problem* [133]. If only the steady periodic solution is considered, after the starting transients have died out, there are no initial conditions to satisfy.

Consideration of dynamic equilibrium of a volume element of thickness  $dy$  gives

$$\frac{\partial \tau}{\partial y} = \rho \frac{\partial u(y, t)}{\partial t}. \quad (4.44)$$

Substitution of the shear stress definition

$$\tau = \mu \frac{\partial u}{\partial y} \quad (4.45)$$

gives the governing equation

$$\rho \frac{\partial u}{\partial t} = \mu \frac{\partial^2 u}{\partial y^2}$$

which is subject to

$$u(0, t) = U \cos \omega t \quad (4.46)$$

$$u(\infty, t) = \text{bounded} \quad (4.47)$$

In the steady state, the flow variables must have a periodicity equal to that of the boundary motion. Therefore the solution is of the form

$$u = e^{i\omega t} f(y). \quad (4.48)$$

Substituting this into the governing equation gives

$$i\omega f = \nu \frac{\partial^2 f}{\partial y^2}, \quad (4.49)$$

the solution of which is

$$f(y) = A e^{-(1+i)y/y_0} + B e^{(1+i)y/y_0}, \quad (4.50)$$

where  $y_0 = \sqrt{\frac{2\mu}{\rho\omega}}$ , with  $\mu$  being the dynamic viscosity and  $\rho$  the fluid density ( $\nu = \mu/\rho$ ). The boundary condition, Eqn. 4.47, requires that the solution must be bounded at  $y = \infty$ , needs  $B = 0$ . The solution therefore becomes

$$u = A e^{i\omega t} e^{-(1+i)y/y_0} \quad (4.51)$$

The surface boundary condition, Eqn. 4.46, gives  $A = U$ . Taking the real part of Eqn. 4.51 the velocity distribution for the problem is:

$$u = U e^{-y/y_0} \cos(\omega t - y/y_0) \quad (4.52)$$

The cosine term in Eqn. 4.52 represents the signal propagating in the direction of  $y$ , while the exponential term represents a decay in  $y$ . The shear stress,  $\tau$ , may be found from using the velocity distribution from Eqn. 4.52

$$\begin{aligned} \tau &= -\mu \frac{U}{y_0} e^{-y/y_0} \cos(\omega t - y/y_0) + \mu \frac{U}{y_0} e^{-y/y_0} \sin(\omega t - y/y_0) \\ &= \mu \frac{U}{y_0} e^{-y/y_0} [\sin(\omega t - y/y_0) - \cos(\omega t - y/y_0)] \end{aligned} \quad (4.53)$$

For  $y = 0$

$$\tau = \mu \frac{U}{y_0} (\sin(\omega t) - \cos(\omega t)) \quad (4.54)$$

The work done by the fluid on the plate per cycle per unit area,  $\Delta W$ , may then be found as

$$\begin{aligned}
\Delta W &= - \int_0^{\frac{2\pi}{\omega}} \tau u(0, t) dt \\
&= - \frac{\mu U^2}{\omega y_0} \int_0^{2\pi} (\sin(\omega t) \cos(\omega t) - \cos^2(\omega t)) d(\omega t) \\
&= \frac{\pi \mu U^2}{\omega y_0}
\end{aligned} \tag{4.55}$$

Since  $y_0 = \sqrt{\frac{2\mu}{\rho\omega}}$ , therefore

$$\Delta W = \pi U^2 \sqrt{\frac{\rho\mu}{2\omega}} \text{ per unit area} \tag{4.56}$$

If we assume for a cross section with vertical velocity amplitude  $\omega X_s$  that  $U \simeq \omega X_s \sin \alpha$ , where  $\alpha$  is again the angle between a tangent to the cross section and the horizontal, then the work at a cross section per unit length of hull will be

$$\begin{aligned}
\Delta W_s &= \int_{\text{section}} \Delta W dl \\
&= X_s^2 \pi \omega^2 \sqrt{\frac{\rho\mu}{2\omega}} \int_{\text{section}} \sin^2 \alpha dl,
\end{aligned} \tag{4.57}$$

and for the whole ship

$$\begin{aligned}
\Delta W &= \int_0^L \Delta W_s dx \\
&= \Delta x \Sigma \Delta W_s,
\end{aligned} \tag{4.58}$$

summed for all cross sections, in which  $\Delta x$  is the section spacing.

Using the method outlined in Section 4.4.1 the contribution to the total damping due to the viscous damping may be estimated by comparing the energy dissipated per cycle with the total energy in the system. The results of this calculation are shown in Section 4.4.3. Again, given the sectional damping the total damping for each hydrodynamic component was found using the method given in Section 4.4.3.2.

#### 4.4.2.3 Acoustic Damping

Sound radiated by a vibrating structure transports energy from the structure and thus contributes damping to the system [134]. Sunnersjo and Janson [125] conducted a study into the hydrodynamic inertia and damping of ship hull vibrations. They used a finite volume method to investigate the damping due to sound radiation and found that the hydrodynamic damping

due to this mechanism may contribute significantly to the total modal damping.

Propagation of small amplitude acoustic waves through a homogeneous compressible fluid at constant frequency is governed by the Helmholtz equation,

$$\nabla^2 \phi + k^2 \phi = 0, \quad (4.59)$$

where

$$\phi = \text{Re} \{ \phi_0 e^{-i\omega t} \} \quad (4.60)$$

is the velocity potential, in which pressure is given by

$$p = -\rho \frac{\partial \phi}{\partial t} \quad (4.61)$$

and velocity by

$$\vec{v} = \nabla \phi, \quad (4.62)$$

and  $k = \omega/c$  is the wavenumber, where  $\omega$  and  $c$  are respectively the angular frequency and wave speed.

The acoustic radiation problem is further defined by the boundary conditions of compatibility of velocity on the surface of the radiating source (ship hull)

$$\nabla \phi \cdot \hat{n} = \vec{V} \cdot \hat{n}, \quad (4.63)$$

and zero pressure on the water-air interface

$$\phi = 0. \quad (4.64)$$

The water-air interface is effectively a “pressure-release” surface for acoustic waves in-water due to the great disparity between the densities and speeds of sound in the two media [135]. Furthermore, the free surface may validly be represented as a flat surface if free surface gravity waves are assumed to be short compared with the acoustic waves, enabling efficient modelling of the symmetry using a double body representation of the ship hull.

The fluid domain is also assumed to be infinite, requiring a far-field condition of outgoing waves,

$$\lim_{r \rightarrow \infty} r \left( \frac{\partial \phi}{\partial r} - ik\phi \right) = 0. \quad (4.65)$$

The speed of sound in-water adopted for the present calculations was 1429 m/s (corre-

sponding to salt water of density  $1025 \text{ kg/m}^3$  at  $10^\circ\text{C}$ ), thus with frequencies of interest being around  $3 \text{ Hz}$  it is noted that the corresponding acoustic wavelength of about  $500 \text{ m}$  is large compared with the ship dimensions, hence a three-dimensional analysis is essential.

The problem is modelled using a boundary element method based on that outlined in [136]. The method makes use of the point source function

$$G_k(r) = \frac{1}{4\pi} \frac{e^{ikr}}{r}, \quad (4.66)$$

which is easily shown to satisfy the field equation (4.59) and the far field condition (4.65), noting that  $\nabla^2\phi(r) = d^2\phi/dr^2 + 2/r \times d\phi/dr$  in three dimensions. The body surface is discretised into triangular elements, over which sources of this type were distributed piecewise uniformly, with intensities determined from the matrix equation resulting from application of condition (4.63) to the centroid of each element. In doing so the induced velocity at each point due to a uniformly distributed source over a boundary element was determined by integration of the gradient of (4.66) over that element, which was performed using Gaussian quadrature. This resulted in a set of equations for the (complex) body surface potential magnitudes of the form

$$\left[ M - \frac{1}{2} I \right] \{ \phi_0 \} = [L] \{ \vec{V} \cdot \hat{n}_i \} \quad (4.67)$$

where

$$L_{ij} = \int_{\text{element } j} G_k(r_{ij}) dS \quad (4.68)$$

$$M_{ij} = \int_{\text{element } j} \nabla G_k(r_{ij}) \cdot \hat{n}_j dS, \quad (4.69)$$

$\hat{n}_i$  and  $\hat{n}_j$  are the normals to elements  $i$  and  $j$  respectively,  $r_{ij}$  is the distance between the centroid of element  $i$  and a point on element  $j$ , and  $dS$  is an element of the boundary surface.

The method given by (4.67) becomes singular at certain characteristic frequencies, which by inspection correspond to the eigen values of  $2[M]$ , and ill-conditioned in the vicinity of these frequencies. These are the resonant frequencies of the corresponding interior acoustic problem. Kirkup [136] makes use of a hybrid method in which the equation to be solved is a linear combination of (4.67) and one obtained by differentiating that equation with respect to the normal to the boundary. This is unnecessary for the present problem, due to the long wavelength to ship length ratios involved, and in fact was found to be detrimental to the accuracy of the solution at such low frequencies.

Once surface potentials have been obtained, surface pressures can be calculated from (4.61),

hence power radiated by the body as

$$P = \int \vec{V} \cdot \hat{n} p dS = \sum_{\text{all elements}} \frac{1}{4} i \omega \rho \phi_0 \vec{V} \cdot \hat{n} A,$$

( $A$  = element area). The factor  $\frac{1}{4}$  accounts for the cyclic average, or RMS ( $\frac{1}{2}$ ), and reduction of the double body representation to the actual submerged hull ( $\frac{1}{2}$ ). From this the loss factor is easily obtained in terms of energy radiated per cycle as  $2\pi P/\omega$ .

The above method was used to determine the damping due to acoustic radiation for the longitudinal bending mode and the torsional mode.

#### 4.4.2.4 Other Components of Hydrodynamic Damping

Two other forms of hydrodynamic damping may be present. Eddy making damping is due to the eddies which are shed when relatively sharp corners move through the water; it is proposed that this mechanism of damping may be insignificant for the small amplitude high frequency motion present. Appendages, such as the ride control surfaces, may also contribute a damping force. However the areas of these surfaces are small and the effect is also likely to be very small.

#### 4.4.3 Hydrodynamic Damping - Calculation

The components of hydrodynamic damping were estimated for a large high-speed catamaran, using Incat Hull 050 as an example vessel.

##### 4.4.3.1 Wavemaking Damping Results

As for the added mass, the wavemaking damping of Hull 050 was calculated based on the formulation outlined in Section 4.3.2. The program uses as input a set of offsets of a single hull, the number of panels per section and in the lid, the calculation frequencies required and the hull draft. 72 sections were used at a section spacing of 1.2m.

The wavemaking damping results are shown in Fig. 4-33, where the damping per section is normalised as follows:

$$\text{Normalised Sectional Damping, } b'_s = \frac{b_s}{\Delta \sqrt{g/L^3}}. \quad (4.70)$$

Fig. 4-33 shows that the damping increases towards the stern of the vessel where the section shapes are fuller, and decreases rapidly with frequency. It is clear that for the frequencies of interest for whipping of large high-speed catamarans ( $> 10$  rad/sec) there is little damping due to wavemaking. Some small irregular results were found as the frequency increased which

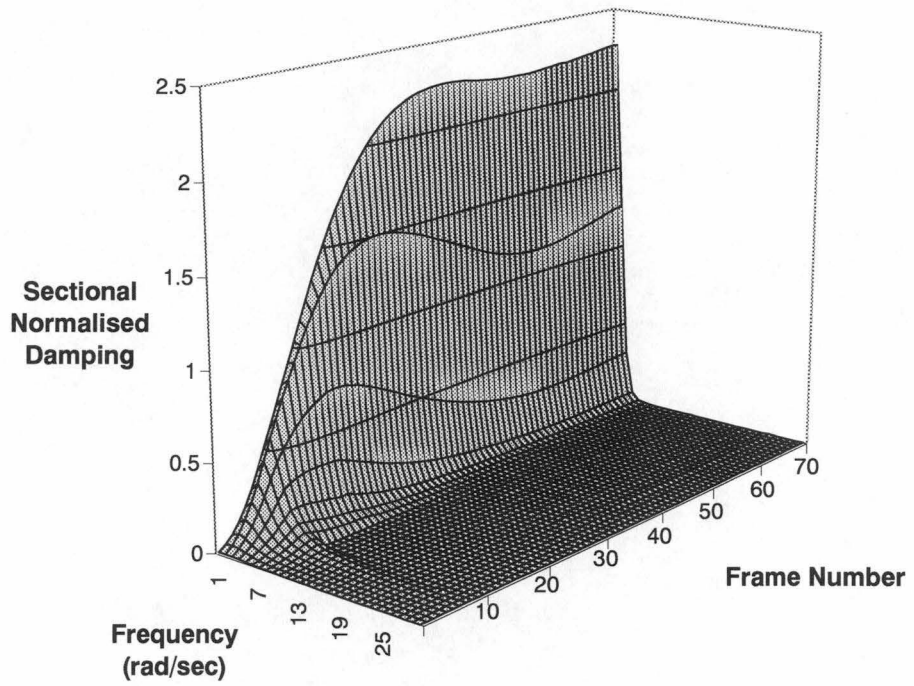


Figure 4-33: Hull 050 - Wavemaking Sectional Damping in Trials/Exciter Test Condition, Draft = 3.10m

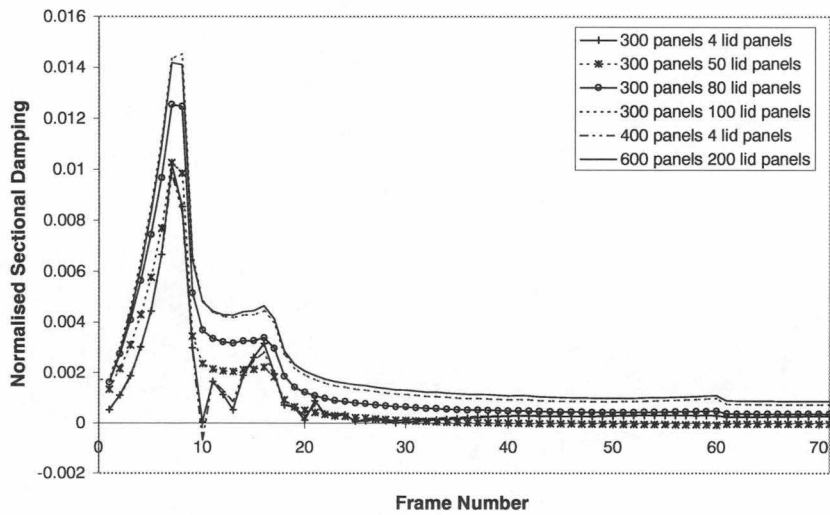


Figure 4-34: Influence of Panel Density on Sectional Damping, Frequency = 18 rad/sec

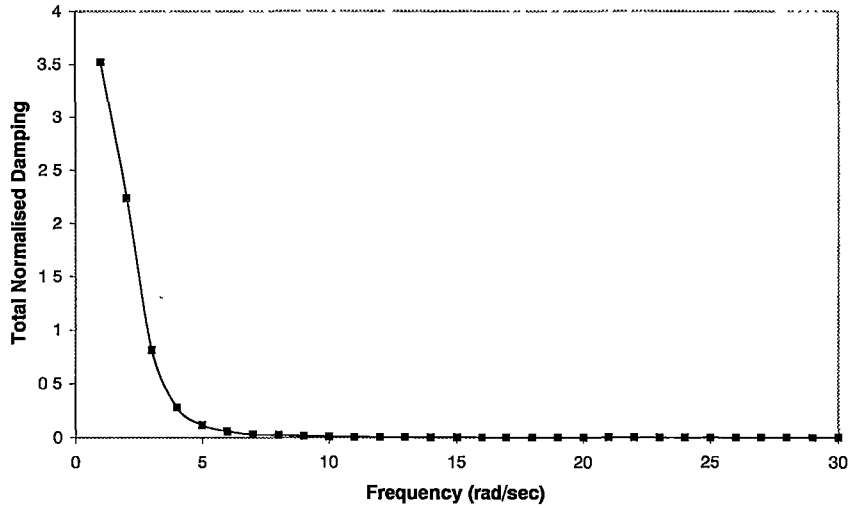


Figure 4-35: Hull 050 - Total Vessel Damping for varying Frequency, in Full-Scale Trials Condition, Draft = 3.10m

were probably due to spurious internal waves. These were eliminated by an increase in lid panel density.

An investigation was conducted to determine the effects of panel density on the calculated sectional damping. The results, Fig. 4-34, show that the magnitudes of the irregularities reduced as the panel density was increased, particularly of the lid panels. A panel density of 300 per section with 100 for the lid appears to be sufficient for an accurate indication of damping without excessive computational time, showing significant improvement over 300 per section and 80 for the lid, but only a small change with the panel density doubled.

The total vessel damping for varying frequency is shown in Fig. 4-35 for Hull 050, where the damping per section is normalised as follows:

$$\text{Normalised Total Damping, } B' = \frac{B}{\Delta\sqrt{g/L}} . \quad (4.71)$$

It can be seen that the level of damping reduces rapidly as frequency is increased, with only very small levels of damping being present at the higher frequencies of interest (first longitudinal mode at 9 rad/sec and lateral torsion mode at 18 rad/sec).

#### 4.4.3.2 Total Hydrodynamic Damping Calculation

The method outlined in Section 4.4.1 was used to estimate the total hydrodynamic damping given the section damping of the various components:

- The vessel was split into 72 sections (corresponding to the structural frames).

- The sectional damping,  $b_s$ , for the wavemaking, viscous and acoustic damping contributions for each section were found according to the formulations outlined in Sections 4.4.2.1 to 4.4.2.3.
- The mode shapes, for the first longitudinal and lateral torsion modes, were calculated for the vessel through finite element analysis to give the sectional mode shape displacement,  $X_s$ , normalised against the point of maximum deflection in the structure.
- The damping contribution,  $b_s X_s^2$ , for each section was found. Where  $b_s$  is the sectional damping and  $X_s$  is the sectional amplitude of motion or mode shape displacement.
- The total damping contribution,  $bX^2$ , was then found by summing the contributions of each section along the vessel according to Eqn. 4.40 and the energy dissipated in a complete cycle,  $\Delta W$ , found from Eqn. 4.39.
- The total energy,  $W$ , in the system was found for the same mode shape  $X_s(x)$  from finite element modal analysis which gave the total strain energy in the vessel's structure, for each modal frequency, normalised against the point of maximum deflection in the structure.
- The fraction of the total energy of the vibrating system which was dissipated in each cycle,  $\frac{\Delta W}{W}$ , was then calculated. The loss factor was thus obtained as  $\eta = \frac{1}{2\pi} \frac{\Delta W}{W}$ , see Eqns. 4.41 and 4.43.

#### 4.4.3.3 Hydrodynamic Damping Results

The hydrodynamic damping results for Hull 050 are shown in Table 4.13. These results show that the wavemaking damping contribution was very low for both modes. This leads to the conclusion that, for vessels such as the one examined, the waves radiated by the vibratory whipping are very small and consequently contain little energy. From the wavemaking damping results it was clear that the frequency of whipping vibration is too high to make the wavemaking damping a large component of the total damping. The frictional damping component is insignificant due to the small oscillation displacements and velocities.

The acoustic damping is also insignificant. At low frequencies (i.e. when the acoustic wavelength is significantly longer than the typical ship dimensions, such as is the case here) the radiated acoustic power in theory is proportional to the 6th power of frequency, hence the energy loss per cycle is proportional to the 5th power of frequency. However, if the frequency increase is a result of increased structural stiffness (with constant mass) then the modal energy increases with the 2nd power of frequency, thus the loss factor will be proportional to the 3rd power of frequency. Acoustic damping therefore may be significant at higher frequencies. With some vessels there may even be particular modes for which the acoustic wavelength is

closely matched to the wavelength of hull deformation, and in such cases the damping may be substantial.

	Loss Factor	
	First Longitudinal Mode	Lateral Torsion Mode
Wavemaking Damping	$0.23 \times 10^{-3}$	$2.31 \times 10^{-3}$
Viscous Damping	$78.6 \times 10^{-6}$	$38.2 \times 10^{-6}$
Acoustic Damping	$24.0 \times 10^{-6}$	$24.0 \times 10^{-9}$
Total Hydrodynamic Damping	$0.23 \times 10^{-3}$	$2.31 \times 10^{-3}$

Table 4.13: Hydrodynamic Damping Decay Factor Values

#### 4.4.4 Structural Damping

Vibrational energy can be dissipated within a volume element of material as it is cyclically deformed [137] [138]. There are a range of mechanisms associated with internal reconstructions of the micro and/or macro structure, ranging from crystal lattice to molecular scale effects which cause material damping.

Xie et al. [139] stated that “there exists little information about damping in commercial aluminium alloys”. They conducted tests that showed the loss factor for three commercial aluminium alloys lay in the range of  $0.2 \times 10^{-3}$  and  $1 \times 10^{-3}$ . The loss factor for aluminium has also been given as ranging between  $5 \times 10^{-5}$  and  $7 \times 10^{-3}$  by White [140] and approximately  $1 \times 10^{-4}$  by Beranek [134].

The total structural damping for a structure will be significantly greater than the material damping property of the material of construction [141] [134]. Nashif [137] stated that built-up structures usually have high initial structural damping, with loss factors as high as 0.05. Depending on the joints used to create the structure the built-up structure may increase the material damping by a factor of 10. White [140] quoted values for structural damping of thin aluminium structures measured experimentally of 0.004 for a model structure and 0.04 for an aeroplane elevator panel. These values are significantly greater than the inherent material damping of aluminium by factors of between 5 and 800. Ungar [142] also gave typical loss factors for materials as  $10^{-4}$  to  $10^{-3}$  and for an aluminium aircraft structure as  $10^{-2}$  due to the effect of joints. These values give increases in damping due to the structure of between 10 and 100 times the loss factor of aluminium. Values for loss factors of 0.016 and 0.018 were given by Clarkson [143] and of 0.017 by Mead [141] for the damping of aluminium aircraft panels. Again these values are significantly greater than the inherent material damping of aluminium by factors of between 2 and 360. It should be noted that most of the data for aircraft structures is for relatively high frequencies that relate to jet noise.

There is considerable uncertainty concerning the mechanism that dominates the damping of built-up structures at low frequencies [142], however various factors are proposed for the increase in damping for a complex structure. Firstly, the damping properties of a metal tend

to increase with increasing stress [138], which might have significant implications for welded aluminium vessels where significant welding residual stresses [27] may be present (other stress concentrations will also be present due to local design and manufacturing influences). Secondly energy dissipation is likely to occur at the structural joints [134], but how the energy is dissipated, and what parameters this damping obeys, appears to be unknown. For higher frequencies, above 30 Hz, Beranek [134] provided a method for calculating the loss factor for a structure accounting for varying absorption coefficient. The absorption coefficient is dependent upon the type of fastening i.e. rivets, bolts or welds. The type of weld may also affect the damping properties of a welded built-up structure. Betts et al. [27] reported on tests conducted into the damping of a welded beam where it was found that the damping was significantly influenced by the type of weld with the stiffest weld connection having the least damping. This may be significant for aluminium welded vessels since much of the welding is not continuous along the whole length of a join but instead extended spot welding is employed. Grice & Pinnington [144] conducted a series of experiments on plate stiffened beams in order to investigate the vibration analysis of built-up structures. They investigated the typical set-up in a ship machinery foundation where flexible plates (hull and deck), which do not carry much load, are separated by stiff beams (frames), which carry significant loads. They surmised that the speed of the long vibratory waves in the beams is high and the beams form the primary path for vibration transmission. The flexural waves travelling along the stiff beams radiate short wavelength flexural waves into the flexible plates which remove energy from the beams. The relative proportions of the total power carried by the two waves depends on the inherent damping of the long waves (e.g. the material loss factor) and the level of coupling between the two waves at the joints where the stiff and flexible components meet. Therefore built-up structures may increase damping if more energy can be transmitted to the short waves in the more flexible plate. Energy dissipation will also occur due to the non-structural contents of the vessel, i.e. the outfit and on-board cargo. The outfit will include cables, pipes, stowed equipment, carpets, ceiling and wall fittings etc whose attachments will not be perfectly rigid, will allow some relative movements and so will allow energy to be dissipated.

Unfortunately it is difficult to examine and quantify all of these effects on the overall damping of a structure. The aim of the out of the water exciter test on Hull 050 was to measure the total structural damping, by comparing the results with the inherent damping properties of aluminium as measured on simple beams. However the presence of the dry dock vessel supports meant that the measured damping was greater than that measured when the vessel was in-water. This led to the verdict that the results could not be regarded as conclusive.

A method for estimating the structural damping of a complete structure has recently been introduced [145] and used on simple beams. The method initially estimates a loss factor for the structure, then uses finite element analysis to evaluate the stress distribution within the structure and then calculates a refined loss factor based on the stress/loss factor relationship

for the material. The results are then checked for convergence of the stress and loss factor and the calculation iterated until convergence is achieved. With development it may be possible that such a technique could be used on ship structures however it is important to note that the method only accounts for the influence of stress on damping in a built-up structure.

There is therefore no experimental evidence that quantifies the increase in low frequency damping from the inherent material damping to the structural damping for a structure such as a large aluminium catamaran. The only practical solution is to experimentally determine the total damping, calculate the hydrodynamic damping and subtract this from the total damping. This will provide an estimate of the total structural damping of the system. The total structural damping may then be compared with the inherent damping of the material to give an indication of the increase in structural damping due to the built up structure.

#### 4.4.4.1 Measurement of Material Damping

In order to ascertain the damping properties of the commercial grade aluminium, used in the construction of large high-speed catamarans, tests were conducted on extruded beams typical of those used by Incat. Two beams were tested: firstly an I-Beam section of length 6505mm with web 150x6mm and flange 100x10mm, see Fig. 4-36, and secondly a square section beam of length 5913mm with an outside dimension of 47mm and wall thickness 3mm, see Fig. 4-37. Both sections were simply supported at the ends, with the I-Beam being tested for both the weak and strong axes. An accelerometer was fixed to the mid point of the beam and the data logged at a sampling rate of 100 Hz by a notebook PC. The beams were excited by a small impact and then the response allowed to decay. The experimental test was designed to have a frequency similar to that of the ship modes of interest.

An example of the raw accelerometer results is shown in Fig. 4-38. The loss factor for each test was determined and averaged for each beam and the results are given in Table 4.14. When the values for loss factor were averaged for all the beams a value of decay coefficient of  $1.718 \times 10^{-3}$  was obtained. The values for the loss factor appeared to vary slightly for the varying beam section; however the values for material damping fall within the range provided by the literature (see Section 4.4.4).

Beam Section	Decay Coefficient
I-Beam (strong axis)	$1.15 \times 10^{-3}$
I-Beam (weak axis)	$1.55 \times 10^{-3}$
Square Section	$2.18 \times 10^{-3}$
<b>Average</b>	<b><math>1.71 \times 10^{-3}</math></b>

Table 4.14: Beam Section Decay Coefficient Values

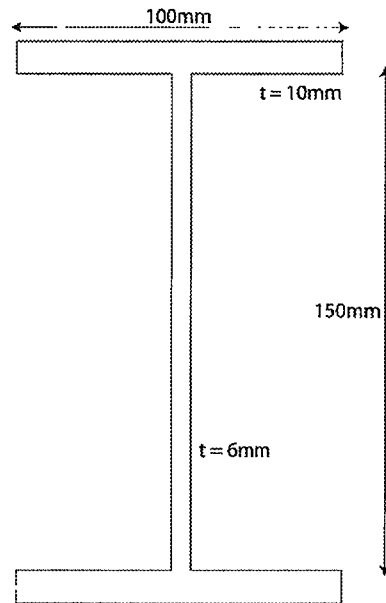


Figure 4-36: Material Damping Experiment - I-Beam Section

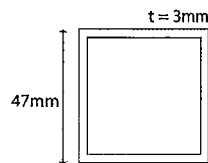


Figure 4-37: Material Damping Experiment - Square Beam Section

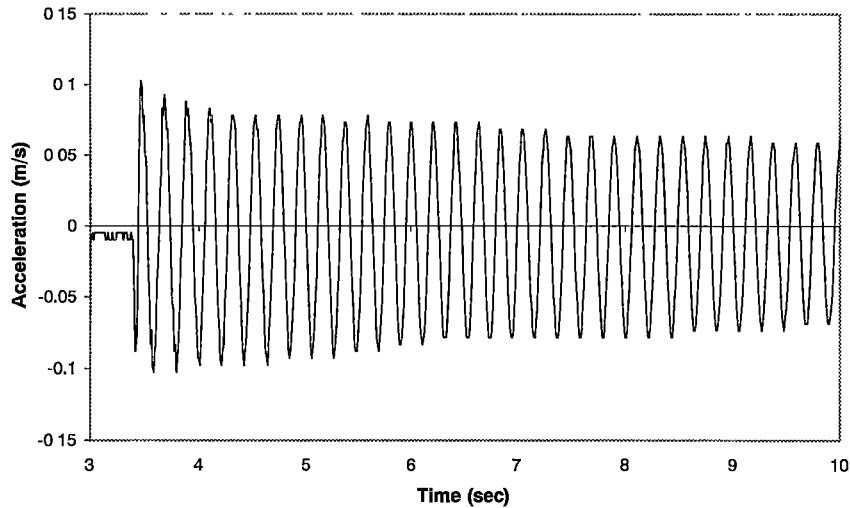


Figure 4-38: Example of Aluminium Material Damping Testing Raw Data

#### 4.4.4.2 Other Structural Damping Contributions

Another factor that has been identified as possible contributor to the overall damping is the effect of the superstructure rubber mounts. On Incat catamarans the superstructure is connected to the main hull structure by way of a series of rubber mounts. The rubber mounts are used to reduce the level of vibration felt by the passengers from sources such as the engines and water jets which is in the range of 25 to 35 Hz. The rubber mounts may also have an effect on the damping of lower frequency vibratory modes of the vessel. The manufacturer's specification for the rubber mounts used, HDA2P, quotes a loss factor of 0.05 [146].

The influence of the mounts may be investigated by estimating the strain energy in the mounts during the modal deflections and then attributing this percentage of the total strain energy to estimate the contribution of the rubber mounts. This exercise was carried out for Incat Hull 050 where it was found that for the first longitudinal mode the rubber mounts are subjected to 2% of the total strain energy. The damping contribution of the rubber mounts may therefore be estimated as a loss factor of  $0.05 \times 0.02 = 1 \times 10^{-3}$ . This suggests that the rubber mounts do not have a significant influence on the total structural damping of the vessel of about 0.035. Although it is significant when compared with the material and hydrodynamic damping.

The influence of the rubber mounts was also investigated by analysing strain gauge data collected on a similar large high-speed aluminium vessel which had the superstructure integrated into the main structure and hence did not use rubber mounts. The raw strain gauge data presented by Steinmann et al. [8] was for an Austal 86m catamaran. The slam events showed similar levels of damping to that for Incat vessels (for the Austal vessel a range of -0.22 to 0.26 compared with -0.15 to 0.38 for Incat Hulls 042 and 050), as shown in Fig. 4-39.

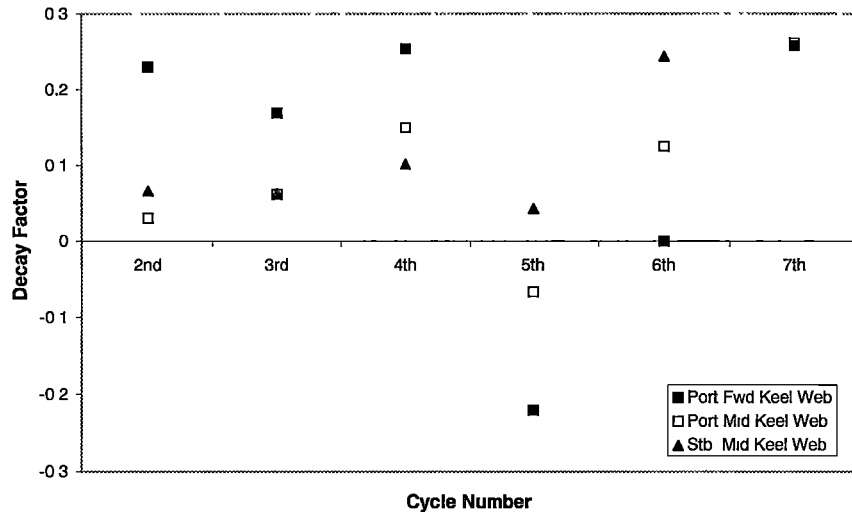


Figure 4-39: Damping for 86m Austal Catamaran

Although the data on the Austal vessel is very limited compared to that available for the Incat vessels, it again suggests that the rubber mounts have little influence on the total structural damping.

#### 4.4.5 Comparison of Predicted and Measured Damping

The predicted damping values, for both hydrodynamic and structural damping, were compared with the measured damping values. The measured total damping used for comparison purposes was that measured during the exciter tests on Hull 050. The exciter test results were chosen, rather than the full-scale trials results, because they were made under more controlled conditions with a predominance of a single frequency of vibration. The Hull 050 results were used rather than the Hull 045 results since the Hull 050 exciter test results appeared to be a much clearer and consistent set of measurements due to the larger anchor. The comparison is shown in Fig. 4-40.

This plot shows that there is a large discrepancy between the total measured damping value and the combined material and hydrodynamic damping found through measurement and calculation. The major factor proposed for this discrepancy is that the total structural damping for a large structure may be considerably greater than the inherent damping of the component material. This structural damping component, due to the built up structure rather than the inherent material damping, has been estimated as being 16 times the inherent material damping. This structural damping component, excluding the inherent material damping, is also shown in Fig. 4-40.

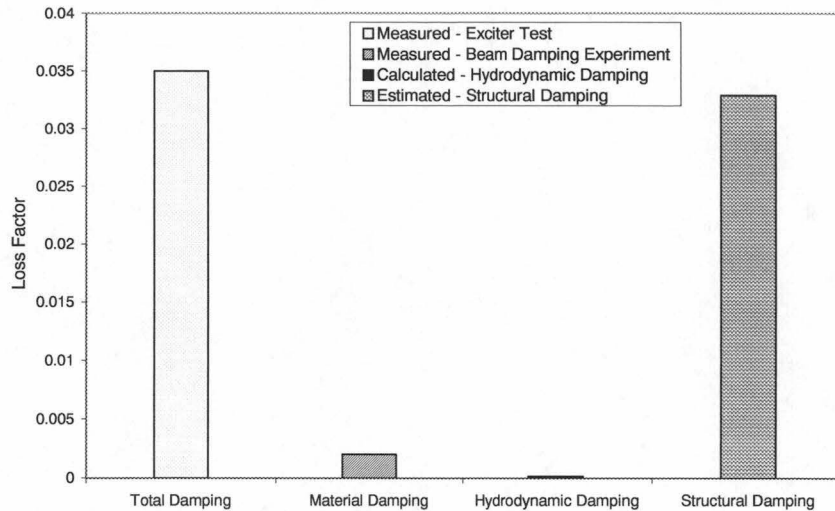


Figure 4-40: Hull 050 - Comparison of Measured, Calculated and Estimated Damping

#### 4.4.6 Conclusions

The damping of the whipping behaviour of large high-speed catamarans has been investigated. Methods for estimating the various components of hydrodynamic damping were presented: wavemaking damping, viscous damping and acoustic damping. These methods were then used to estimate the hydrodynamic damping for the first longitudinal and lateral torsional modes of a large high-speed catamaran, Incat Hull 050. An experimental investigation was conducted into the material damping of the aluminium used in the construction of large high-speed catamarans. Other contributors to damping, such as the superstructure rubber mounts, were also addressed.

The predicted and measured components of damping were compared with the total damping for a vessel measured through exciter tests. The total predicted hydrodynamic and material damping was found to be only a small proportion of the measured total damping. The shortfall can only be presumed to be due to additional structural damping which is estimated to be approximately 16 times the level of the inherent material damping. This ratio is similar to that found in aeronautical and similar structural applications [143] [142] [141] [140]. This additional structural damping is likely to be composed of many items of damping which are not accounted for in a simple structural model, including: fuel and water in tanks, all fittings, soft materials and furnishings, bonded joints, fireproofing and pipe work.

These results are significant since they provide new understanding on the problem of damping of whipping behaviour of large high-speed catamarans.

## 4.5 Summary

A result of the work described in this chapter is an improved understanding of whipping behaviour of large high-speed catamarans. Whipping behaviour is a significant structural response to slamming events which large fast catamarans, due to their aluminium construction, are susceptible to.

Exciter tests were successfully conducted on two vessels for the first longitudinal mode. The modes, frequencies and damping of the whipping behaviour were determined.

The use of finite element normal mode analysis was proposed for estimating the whipping modes. The hydrodynamic added mass of the surrounding fluid was calculated using a two-dimensional panel method for a range of speeds. The effect of vessel loading on the whipping frequencies was also examined. The calculated whipping modes were then compared favourably with those found through the full-scale measurements and exciter experiments. This confirmed that the methods are suitable for use in determining the whipping modes and frequencies.

The investigation also included an examination of the components that contribute to the damping of the system. Estimates were made of the relative magnitude of the various hydrodynamic components including: wavemaking damping, viscous damping and acoustic damping. The total calculated damping was then compared with the levels of damping found through the full-scale measurements and exciter tests. The total predicted damping, due to hydrodynamic and material damping, was found to account for only a small proportion of the measured total damping. It was proposed that the shortfall is due to additional structural damping as a result of the built-up structure. This was estimated to be approximately 16 times the level of the inherent material damping, this ratio being similar to that reported elsewhere in aeronautical and other structural applications

## Chapter 5

# Influence of Slamming and Whipping on Fatigue Life

### 5.1 Introduction

Fatigue is the tendency of a material to break under repeated cyclic loading at a stress considerably less than the tensile strength in a static test [147]. Several factors contribute to make fatigue an important design factor for high-speed aluminium craft [2] [148] [149]. Since the craft are operating at high-speed the wave encounter frequencies are high which leads to relatively high stress cycles in a vessel's lifetime. Also, as mentioned above, when compared to conventional steel vessels the hull structures of high-speed aluminium craft tend to be more flexible which makes dynamic effects such as whipping more pronounced. Also aluminium is a less tolerant material than steel with regard to fatigue life [150].

Following a series of measurements on two frigates Clarke highlighted the influence of whipping behaviour on fatigue life [19] [28]. A method for estimating the fatigue damage produced by whipping, based on British Standard fatigue curves for steel offshore structures, was proposed. In a preliminary study it was found that for frigates and destroyers damage produced by slamming and whipping was less than 5% of the total. Sumi et al. [151] investigated the initiation of low-cycle fatigue cracks by considering wave induced bending stresses combined with whipping stresses of the hull girder. A tentative study of fatigue failure for a container ship was reported on and the fatigue damage per cycle of wave encounter was found to increase logarithmically with ship speed. The effect of whipping was found to be significant on the predicted fatigue life of a small fast aluminium patrol boat by Olkinuora et al. [5] and Kannari et al. [29]. They used the Rainflow method to determine the equivalent stress variations for simulated and measured stress time histories. It was concluded that the simulation method, based on a non-linear strip theory, was not accurate enough to predict fatigue life though it may be used for comparative vessel design studies. Hermundstad et al. [30] noted the im-

importance of whipping behaviour on fatigue life through a study on the hydroelastic response of a high-speed monohull, and a long term statistical analysis was conducted to quantify the influence. Friis-Hansen et al. [31] [32] [33] developed a long-term probabilistic method to investigate the whipping of large fast monohulls. In this method rainflow counting is applied to all wave cycles within a cluster of slamming impacts and then the expected accumulated damage within the short term sea state is found by weighting with the probability density of maximum wave amplitude and frequency. A long term distribution may then be obtained by taking into account the probability of occurrence of various sea states, although no account of different vessel headings is made. Through a numerical example of this method for a 35 knot 100m long aluminium monohull it was found that slamming and whipping may be an important factor with regard to fatigue life.

It appears that slamming and whipping behaviour may have a significant influence on the fatigue life of a vessel when compared to accounting for the wave induced stresses alone. The influence of whipping on the fatigue life of large high-speed catamarans requires further investigation, particularly in respect to the effects of slam occurrence rates, slam peak stresses, significant wave height and the damping of the whipping behaviour.

Estimates have therefore been made for the fatigue life of a large high-speed catamaran with a view to assessing the influence of slamming and whipping. In particular the following issues, with respect to fatigue life, were addressed:

- The presence of slam events compared to no slam events occurring, for similar global wave induced loading scenarios.
- The effect of varying significant wave height in which the vessel operates.
- The effect of slam occurrence rates and slam peak stress.
- The influence of the frequency and damping of the whipping behaviour.

The fatigue investigation has two main components. Firstly fatigue analysis, using strain gauge data from sea trials, was conducted to determine the influence of slam events, their occurrence rates and sea conditions on fatigue life. Secondly idealised stress traces were used to investigate the effect of whipping behaviour, in particular the damping coefficient, slam rate and slam peak stress, on fatigue life. Whilst knowledge of the fatigue strength of large aluminium vessels is crucial in the design process [149], there are several reasons why prediction of a vessel's life span is difficult. The main difficulties are estimating the lifetime sea spectrum and load regime that the vessel will be exposed to. These difficulties were reduced in this study by concentrating on the differences in estimated fatigue life for different slamming and whipping behaviour, rather than attempting to estimate the absolute fatigue life.

The results of this fatigue study are important since they give valuable guidance for designers on the influence of slamming and whipping on fatigue life. For example, it will be shown

that fatigue life is severely reduced by the presence of slamming and that this reduction is most marked in large significant wave heights.

## 5.2 Estimation of Fatigue Life

In order to estimate the fatigue life of a structure it is first necessary to have knowledge of the loadings that the structure will be subjected to during a lifetime. The Rainflow method [147] was used to determine the number of stress cycles for specific stress ranges from time traces of the stress data. The fatigue life was then estimated using the British Standard BS8118 [152], which is based on Miner's Law, which states that failure will occur when

$$\sum \frac{n_i}{N_i} = 1$$

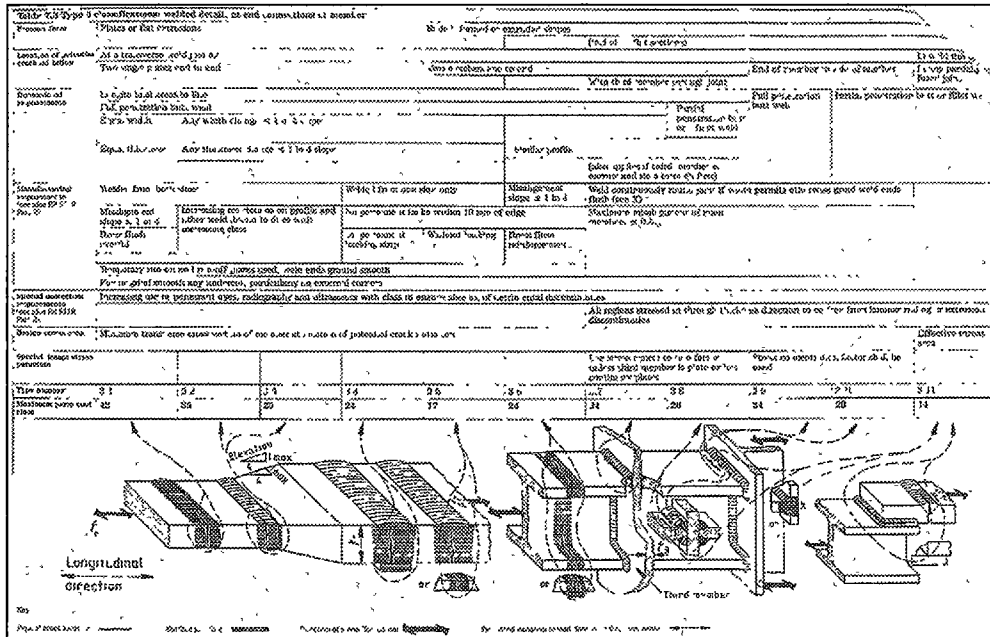
where  $n_i$  is the number of cycles in the  $i$ th stress range and  $N_i$  is the number of cycles to failure at the  $i$ th stress range. The design allowable S-N curves (S-N curves are plots of stress versus life in cycles) given in BS8118 were derived from fatigue tests on both small plate specimens and realistic components. The fatigue life is dependent upon the weld detail and BS8118 gives a large number of possible alternatives for use, see Figs. 5-1 and 5-2. A number 24 weld detail, which corresponds to a typical end fillet weld that might experience the simulated stresses, was used for the fatigue predictions.

The Miner's Law technique is predominantly used by Classification Societies to estimate fatigue life because it is a simple concept. However since the correct assessment of the amount of damage incurred by given stress levels and cycles is not straightforward there is difficulty using it in practice. For example experimental values for Miner's sum at the time of failure often range from approximately 0.6 to 1.6 for quasi-random cyclic stress amplitudes [150]. Nonetheless it is suitable for use in this study in order to give comparative values of fatigue life for differing stress cycle regimes.

In order to predict the fatigue life in years it was assumed that the vessel would operate for 5000 hours per year of life, which is a standard value used within the fast ferry industry and corresponds to approximately 15 hours service per day for 48 weeks of service.

## 5.3 Fatigue Analysis: Influence of Slamming

The aim of the first part of the fatigue study was to investigate the effect of slam events on fatigue life using full-scale strain gauge data. The full-scale data for Hull 042, as described in Chapter 2, was used. Firstly a direct comparison was conducted on the estimated fatigue life when slam events were present in the strain gauge data and when they were not present, for similar underlying global wave loads. Then the influence of significant wave height on fatigue



life was examined. Lastly the influence of slam occurrence rate and slam peak stress on fatigue life was also investigated.

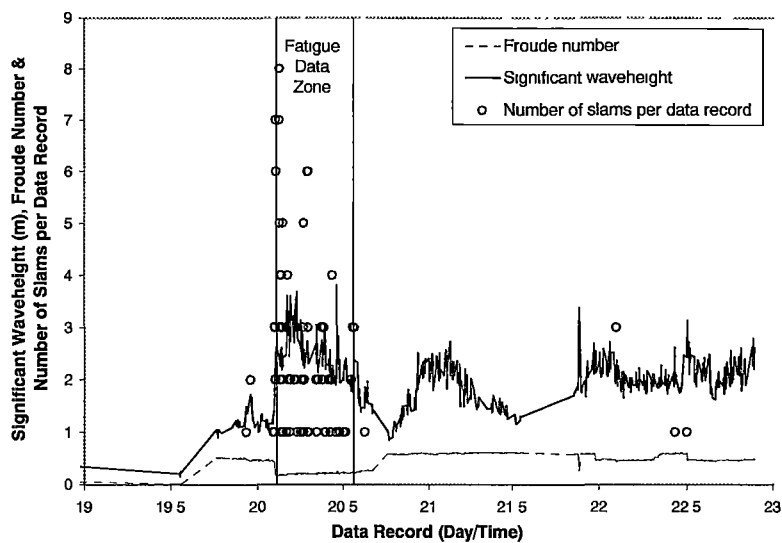


Figure 5-3: Summary of Hull 042 Delivery Voyage showing Fatigue Data Zone. Time period is from 00.00 hours on 19th December to 00.00 hours on 23rd December.

### 5.3.1 Analysis Procedure

A portion of the Hull 042 trials data which corresponded to an extended period of operation for a constant heading angle (head seas) into rough seas was chosen as a base for the fatigue study. The 12 hour portion chosen can be clearly seen in Fig. 5-3 which gives a summary of the Hull 042 delivery voyage data. To investigate the effect of slamming fifty raw data files, each containing only one slam event, were spliced together to make one extended data file. The slams were chosen to represent a realistic distribution of slam peak stresses as per the overall distribution of slams found from all the Hull 042 trials data, as presented in Chapter 2. The combining of 50 raw data files into a single file was conducted for 10 strain gauges. The strain gauges located on steel structure were ignored as were gauges which were close to duplicates, for example only one gauge from the pair fitted to the aft transverse box was used. Another set of 50 data runs were joined together for the 10 strain gauges, although these data files did not include slam events. These files were chosen as being recorded close in time to the files which contained slams to ensure that the wave environment and underlying global wave loads were as similar as possible.

To examine the influence of significant wave height on fatigue life Hull 042 full-scale data for a variety of significant wave heights was used. For each range of significant wave height, found in the fatigue data zone in Fig. 5-3, approximately 20 raw strain gauge data runs for the keel at frame 35.5 were identified and spliced together. This gave approximately one hour of

data per wave height range. The data runs included traces in which slams were both present and not present.

The full-scale data for Hull 042 was also used to investigate the predicted fatigue life for varying rates of slam occurrence and slam peak stress. Hull 042 sea trials data runs for the keel at frame 35.5 which each contained a single slam event were identified. Seven data runs were chosen from those identified with normalised slam peak stresses ranging from 1.38 to 9.98. The data files were then reduced in length so that only the strain gauge trace of the actual slam event remained. The fatigue life was then estimated for varying slam frequencies of occurrence.

### 5.3.2 Results and Discussion

Sample S-N curves are shown for two strain gauges in Figs. 5-4 and 5-5: the bat wing on the cross brace at frame 17 and the keel at frame 35.5 (see Appendix 1 for detailed drawings of strain gauge locations). At lower stress levels there appears to be little difference between the results for slams and no slams. However as the stress range increases the plots clearly show significant reductions in the number of cycles due to an absence of slam events. The fatigue life in years was estimated for 10 strain gauge locations on Hull 042 for the data files with and without slam events, the results are shown in Fig. 5-6. This data was for 100% operation in head seas of between 1.5m and 3.8m significant wave height. The slamming occurrence rate used was 17.5 events per hour. The plot shows that there is a wide range of fatigue life for the various structural locations: for example the transverse girder and cross bridge web both have fatigue lives greater than 1000 years whereas the bat wing on the cross brace has an estimated fatigue life of less than a year. It should be noted that the bat wing on the cross brace suffered cracking during the first year of service and underwent a redesign and refit. The effect of slamming on fatigue life can easily be seen with significant reductions in life when slamming events are included. Fig. 5-7 shows the percentage reduction in estimated fatigue life due to slamming. All structural locations show large percentage reductions due to slamming, ranging between 55% and 98%. This plot should be used in conjunction with Fig. 5-6 to see whether the reduction in fatigue life is critical, for example although the transverse girder has a 98% reduction due to slamming events its fatigue life is still over 100 years. Therefore taking steps to avoid slamming, through either vessel design or operation, is obviously desirable to order to improve the fatigue life of a large high-speed catamaran.

As expected the estimated fatigue life was found to reduce as the significant wave height increased, see Fig. 5-8. If the vessel were to operate in head seas of greater than 2.5m then this structural location (keel at frame 35.5) is predicted to suffer fatigue failure in less than 3 years. This is a significant reduction from the predicted fatigue life of greater than 32 years when operating in seas of less than 2m. This result highlights the importance of knowing the likely operational sea state which will be encountered by a vessel during the design process

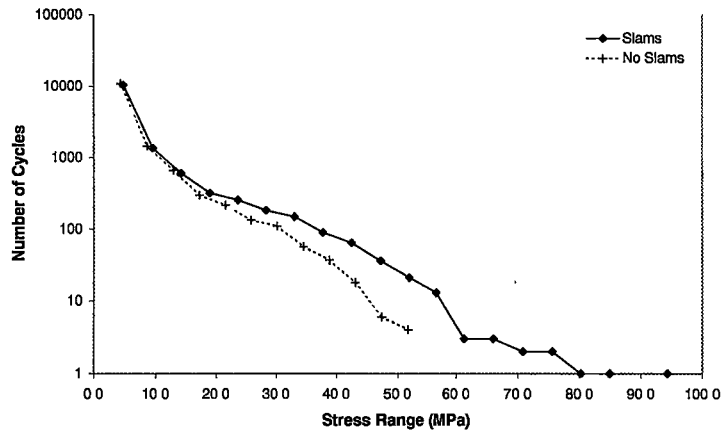


Figure 5-4: S-N Curve for Bat Wing on Cross Brace at Frame 17

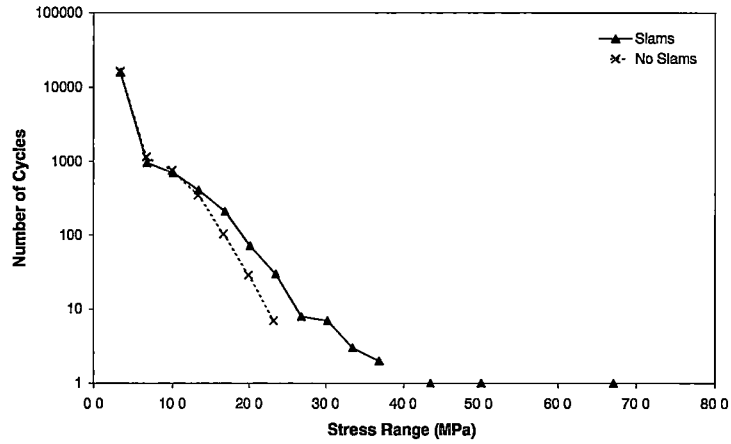


Figure 5-5: S-N Curve for Keel at Frame 35.5

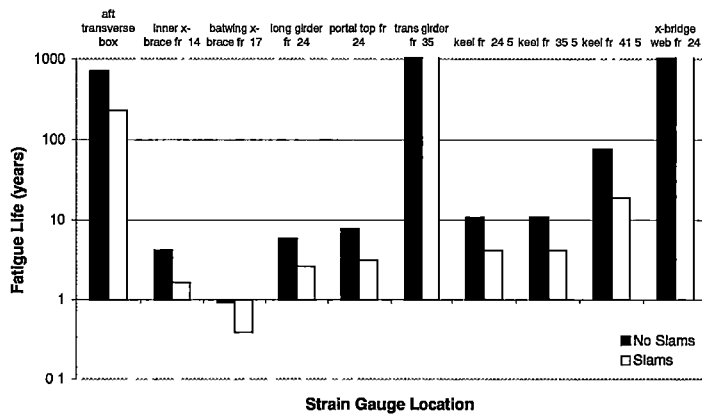


Figure 5-6: Change in Fatigue Life due to Slamming - Hull 042

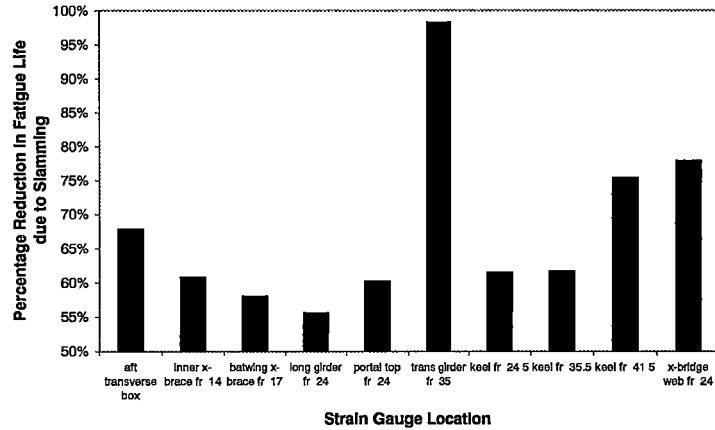


Figure 5-7: Reduction in Fatigue Life due to Slamming - Hull 042

to ensure adequate fatigue life is achieved. It is important to note that this data includes the fatigue damage due to slamming. The number of cycles to failure, for the stress ranges found in the full-scale results, for the significant wave height of 3m to 3.5m are shown in Fig. 5-9. The reduction in cycle number as the stress range increases may be clearly seen. Fig. 5-10 shows the contribution of the various cycles of stress ranges to the predicted damage. The low stress ranges, although they have very large cycle numbers, appear to make no contribution to the failure. However once the stress range is greater than 11 MPa the cycle numbers are sufficient to contribute significantly to the damage. It is interesting to relate these results back to the distributions of slam peak stresses identified from the full-scale data in Chapter 2. The small slam events which predominate the slam peak stress distributions appear to have little or no influence on the fatigue life.

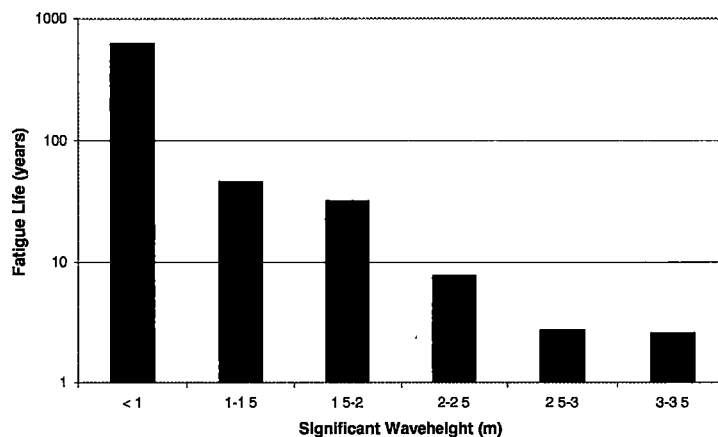


Figure 5-8: Fatigue Life for varying Significant Wave Height - Hull 042

The predicted dependence of fatigue life on frequency of slam occurrence and slam peak

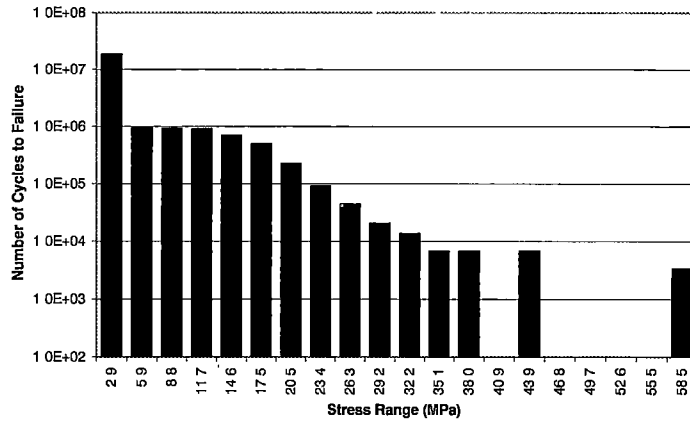


Figure 5-9: Cycle Count to Failure for Significant Waveheight 3m to 3.5m - Hull 042

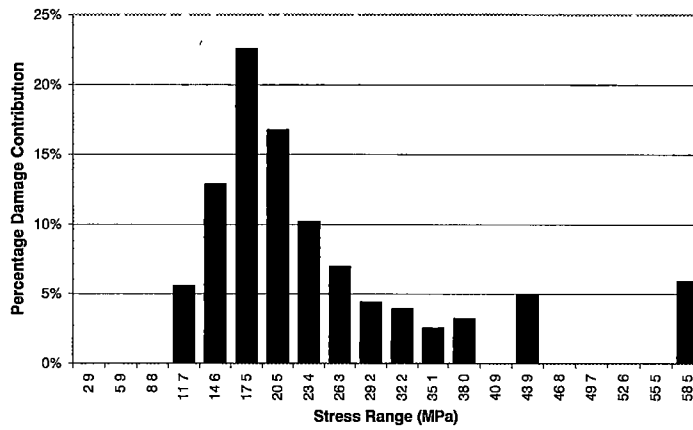


Figure 5-10: Damage Contribution for Significant Waveheight 3m to 3.5m - Hull 042

stress is shown in Fig. 5-11. This plot shows, as expected, that fatigue life reduces as frequency of slam occurrence increases. The fatigue life reduces as the slam peak stress increases. Again it is apparent that small slams contribute little to the consumption of fatigue life with a non-dimensional slam peak of 1.38 at 120 slams per hour giving a fatigue life of 5 years. In contrast 15 slams per hour for a non-dimensional slam peak of 9.98 results in a fatigue life of just over a year, a significant reduction.

## **5.4 Fatigue Analysis: Influence of Whipping**

The influence of whipping behaviour on the expected fatigue life of a large high-speed aluminium catamaran was then investigated. The study focussed on the effect of damping coefficient and slam peak stress on fatigue life using idealised slam events.

### **5.4.1 Analysis Procedure**

A series of realistic simulated stress traces resulting from idealised slam events, for a strain gauge on the keel plate, were developed for various decay coefficients and slam peak stresses, see Fig. 5-12. Slam peak stress and slam frequency of occurrence data gained from the sea trials was used to build up realistic slam scenarios. It should be noted that the stress records took no account of the underlying wave induced global loads, and only the slams and subsequent whipping were included. Again the fatigue life was then estimated for varying slam occurrence rates.

### **5.4.2 Results and Discussion**

For a slam peak stress of 25% of the yield stress the fatigue life was determined for a varying number of slams per hour throughout the vessel's life for a range of decay coefficients. The results, as shown in Fig. 5-13, clearly indicate that as the decay coefficient increases the fatigue life increases. For a slam rate of 7.5 per hour (for the whole operational life of the vessel), a change in decay coefficient from 0.035 to 0.025 brings about a reduction in fatigue life of approximately 25%. It is apparent that there is a strong influence of whipping behaviour on fatigue life. As expected the fatigue life also reduces as the number of slams per hour increases.

For a decay coefficient of 0.035 (which was the value determined for Hull 050 through the exciter test), the fatigue life for varying slam peak stress was found for a range of slam occurrence rates (Fig. 5-14). This plot shows that the fatigue life reduces rapidly as the slam peak stress is increased. For example, at a slam rate of 7.5 per hour, the fatigue life reduces from 56 years to 0.72 years as the slam peak stress is increased from 12.5% to 50% of the yield stress. It is clear that slam events with large peak stress have a significantly greater influence on fatigue life than smaller slam events. It should be remembered though that the Hull 042 and Hull 050 trials data showed that the majority of slam events resulted in low maximum

stress levels. Again an increase in slam occurrence rate is shown to cause a reduction in fatigue life.

## 5.5 Implications of Fatigue Analysis on Slam Definition

The slam definition used in this study was based solely on a rate criterion, as discussed in Chapter 2. A slam was defined as having occurred if a peak in the stress record occurred with the maximum rate of change of stress prior to the peak exceeding a designated value. This ensured that slam events, as opposed to slow time varying global wave loads, were identified. In order to be inclusive in identifying slam events, a stress criterion was not used in conjunction with the rate criterion. Instead an appropriate rate factor was chosen to ensure that signal noise peaks were not included in the defined slams. From the fatigue study results it is apparent that very small stress cycles have no effect on the cumulative damage due to fatigue, as shown in Fig. 5-10. Obviously these small stress cycles do not have implications with respect to the ultimate strength of the vessel's structure, problems of this nature are due to the very large slam events. Therefore it may be applicable to use a two stage slam definition process in future work:

1. Firstly the slams would be identified using the existing method based on a rate criterion, since this will enable all the slam events to be located.
2. Then a fatigue analysis would be conducted on typical full-scale data to obtain the contribution of the various stress ranges to the predicted damage. The minimum stress cycle which has an effect on the fatigue damage would then be defined. The fatigue analysis would need to be conducted for a range of strain gauges due to differences in structural dynamic behaviour with respect to location. The minimum stress cycle for fatigue would be found for the strain gauge which is being used for slam identification, although reference would be made to the other strain gauges. This would be done to ensure that slam events which do not affect the fatigue life of the slam identification gauge, but have a significant fatigue effect on another location, are included.
3. The slams (as identified in step 1) with a peak value smaller than the minimum stress range for fatigue (as estimated in step 2) would then be discarded.

Therefore only those slam events which have an influence on the structural design of the vessel, through either ultimate strength or fatigue life, would be identified.

## 5.6 Conclusions

From the investigation into the influence of slamming on the fatigue life of large high-speed aluminium catamarans the following conclusions may be drawn:

- The fatigue life was found to reduce significantly with the presence of slam events. Therefore a reduction in slamming may prolong the fatigue life of a vessel markedly.
- The fatigue life reduces significantly as waveheight increases. Knowledge of the expected sea conditions that a vessel will operate in is therefore crucial for accurate fatigue life calculation.
- Fatigue life reduces significantly as slam rate increases and slam peak stress increases. Small slam events have little or no influence on fatigue life.
- Whipping behaviour has a strong influence on fatigue life. The fatigue life increases as the decay coefficient increases, and the fatigue life reduces as the frequency of slam occurrence increases.

These results indicate that slamming and whipping have a large influence on the estimated fatigue life. They give valuable guidance for designers estimating the fatigue life of large high-speed catamarans. The methods and information shown here may be used when designing new large catamaran with respect to the expected fatigue life for a given operating scenario.

The fatigue life analysis has shown that a two stage slam definition process may be appropriate in the future, where firstly a rate criterion and then a minimum stress level for fatigue damage are used.

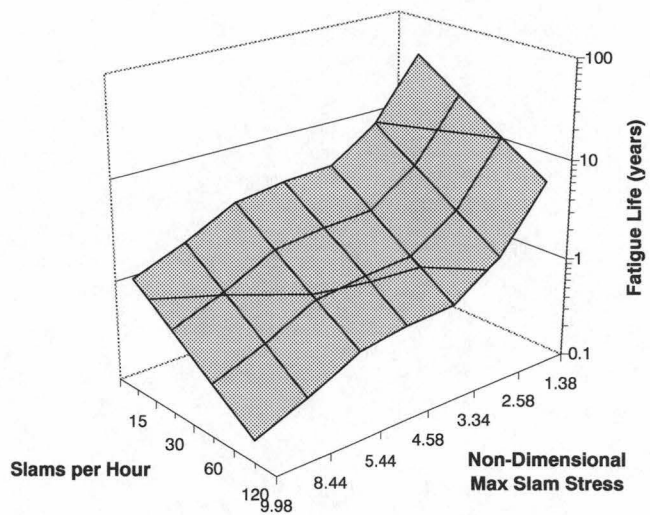


Figure 5-11: Estimated Fatigue Life for varying Frequency of Slam Occurrence and Slam Peak Stress - Hull 042

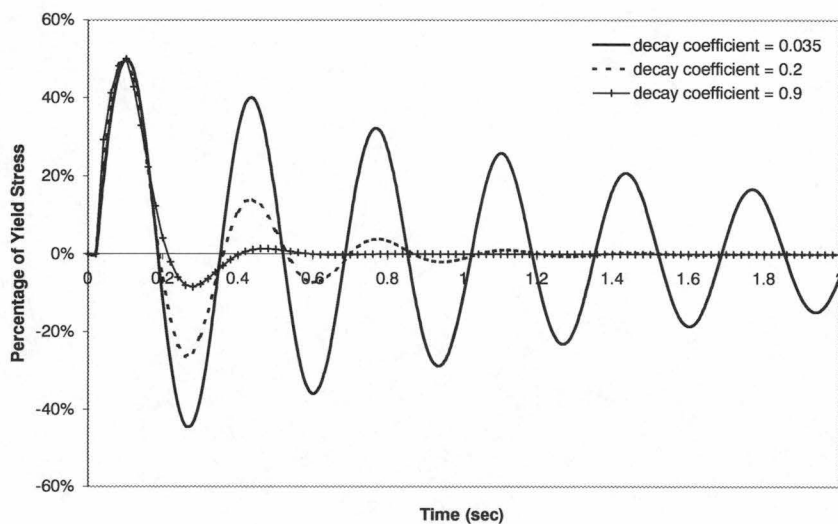


Figure 5-12: Example Simulated Slam Events

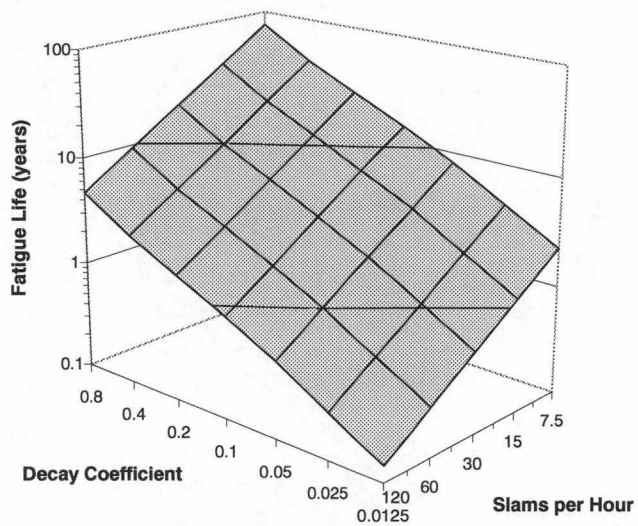


Figure 5-13: Fatigue Life for varying Slams per Hour Rate and Decay Coefficient

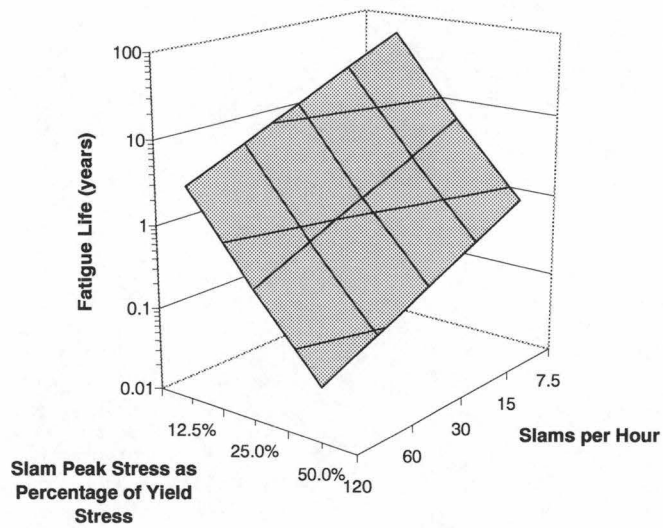


Figure 5-14: Fatigue Life for varying Slams per Hour Rate and Slam Peak Stress

# Chapter 6

## Dynamic Slam Loads

### 6.1 Introduction

Knowledge of the dynamic slamming response developed in Chapter 4 may now be used, in combination with the full-scale trials data, to develop a dynamic extreme slam design load case. This load case is based on time-varying loads and responses and is an extension of the quasi-static load case developed in Chapter 3. As illustrated by the strain gauge raw data traces a slam is a very dynamic event and whilst a quasi-static assumption may yield good correlation between derived and measured stresses, a dynamic approach to stress prediction is to be preferred. This dynamic load case more realistically simulates the dynamic structural response of the vessel to a slam and is the core component of the practical methodology for the structural design of large high-speed catamarans for slamming. The results from this analysis may be used in the structural design process. They also provide data for the validation of theoretical and experimental prediction techniques of loads on large high-speed catamarans.

Finite element dynamic analysis differs from static analysis in two basic aspects. Firstly, dynamic loads are applied as a function of time and secondly, this time-varying load application induces time-varying responses (displacements, velocities, accelerations, forces and stresses). Whilst dynamic analysis is complicated by these time-varying characteristics it also provides a more realistic solution than static analysis for cases such as slamming events which are very dynamic scenarios of loading and response. The focus of the load case development was on the magnitude and time history of the impact loading required to achieve stress results to match those of the initial impact stresses measured in the full-scale trials. The methods and results developed in Chapter 4 were used to ensure that the whipping behaviour output of the FE analysis was appropriate.

Dynamic structural finite element techniques do not appear to have been used previously for simulating slamming events for an entire vessel. Pegg et al. [153] conducted dynamic finite element analysis on a model of the starboard bow section of a research vessel, when

subjected to periodic wave loadings rather than slam impact loads. Using measured pressures as inputs to the model, calculated stresses were within 20% of those measured by high-speed strain gauges. No modelling of the added mass of the surrounding fluid was included in the analysis. A similar study was conducted by Rothe et al. [3] on the wet-deck of a large catamaran. Dynamic pressures, derived from a computational method, were applied to a model of a section of the wet-deck. Dynamic finite element analysis was used to obtain the time varying local bending stresses in the wet-deck plating for a number of vessel speeds. The peak stress levels, in various hot spot locations, were found to exceed allowable stresses as prescribed by Classification Society Germanischer Lloyd by as much as 230%. However no comparisons were made with full-scale slam impact stress data.

Finite element modelling was used by Murray et al. [154] to investigate the dynamic response of a whole vessel to ramming ice floes. A vessel ramming an ice floe produces a similar structural response to a slam impact including whipping effects, although the impact loading is somewhat slower than for a slam, with a time of approximately 0.5 seconds to reach maximum load from the initial time of impact (compared with approximately 0.2 seconds for a large slam event). Murray et al. calculated the response for twelve ramming cases, including three asymmetric rams, using loads measured in full-scale tests. The calculated bending stresses showed reasonable agreement with the measured responses. This suggests that dynamic finite element modelling may be a useful tool for simulating a slam event and the subsequent whipping behaviour of an entire vessel.

## 6.2 Dynamic Finite Element Analysis

### 6.2.1 Finite Element Dynamic Analysis Theory

In a direct transient response analysis the structural response is calculated by solving a set of coupled equations using direct numerical integration [126]. The equation of motion in matrix form is

$$[M] \{\ddot{u}(t)\} + [B] \{\dot{u}(t)\} + [K] \{u(t)\} = \{P(t)\}, \quad (6.1)$$

where

$[M]$  = mass matrix

$[B]$  = damping matrix

$[K]$  = stiffness matrix

$P(t)$  = time varying force.

The fundamental structural response (displacement,  $\{u\}$ ) is solved at discrete times with

a fixed integration time step  $\Delta t$ .

By using a central three point finite difference representation for the velocity  $\{\dot{u}(t)\}$  and acceleration  $\{\ddot{u}(t)\}$  at discrete times,

$$\{\dot{u}(t)\} = \frac{1}{2\Delta t} \{u_{n+1} - u_{n-1}\} \quad (6.2)$$

$$\{\ddot{u}(t)\} = \frac{1}{\Delta t^2} \{u_{n+1} - 2u_n + u_{n-1}\}, \quad (6.3)$$

and if the applied force is averaged over three adjacent points in time, the equation of motion may be written as

$$\begin{aligned} & \left[ \frac{M}{\Delta t^2} \right] (u_{n+1} - 2u_n + u_{n-1}) + \left[ \frac{B}{2\Delta t} \right] (u_{n+1} - u_{n-1}) + \left[ \frac{K}{3} \right] (u_{n+1} + u_n + u_{n-1}) \\ & = \frac{1}{3} (P_{n+1} + P_n + P_{n-1}). \end{aligned} \quad (6.4)$$

If terms are collected the equation of motion becomes

$$[A_1] \{u_{n+1}\} = [A_2] + [A_3] \{u_n\} + [A_4] \{u_{n-1}\} \quad (6.5)$$

where

$$\begin{aligned} [A_1] &= \left[ \frac{M}{\Delta t^2} + \frac{B}{2\Delta t} + \frac{K}{3} \right] \\ [A_2] &= \frac{1}{3} (P_{n+1} + P_n + P_{n-1}) \\ [A_3] &= \frac{2M}{\Delta t^2} - \frac{K}{3} \\ [A_4] &= \left[ -\frac{M}{\Delta t^2} + \frac{B}{2\Delta t} - \frac{K}{3} \right]. \end{aligned} \quad (6.6)$$

Matrix  $[A_1]$  is the dynamic matrix, and  $[A_2]$  is the applied force. The transient solution is found by inverting  $[A_1]$  and pre-multiplying the right hand side of Eqn. 6.5. The solution behaves like a succession of static solutions with each time step performing a forward/backward substitution on a new load vector. The  $[M]$ ,  $[B]$  and  $[K]$  matrices are assumed not to change with time and therefore remain constant throughout the analysis. Hence only a single matrix inversion is required.

Structural damping may be included by converting it to an equivalent viscous damping, as first proposed by Lord Rayleigh in 1877 [155] [156]. Although the actual mechanism of energy dissipation in real structures is closer to the so-called hysteretic damping than viscous damping, the latter is an efficient and reliable mechanism for computational purposes. The

damping matrix  $[B]$  represents the energy dissipation characteristics of the structure. The damping matrix is composed of several matrices:

$$[B] = [B^1] + \frac{G}{W} [K], \quad (6.7)$$

where

$$\begin{aligned} [B^1] &= \text{direct input matrix plus transfer functions} \\ G &= \text{overall structural damping coefficient} \\ W &= \text{frequency of interest (rad/sec) for conversion of overall} \\ &\quad \text{structural damping to equivalent viscous damping} \\ [K] &= \text{global stiffness matrix} \end{aligned}$$

The viscous damping force is a damping force which is a function of a damping coefficient,  $b$ , and the velocity,  $\dot{u}$ . It is an induced force which is represented in the equation of motion using the  $[B]$  matrix and velocity vector, see Eqn. 6.1. The structural damping force, in contrast, is assumed to be displacement-dependent damping. The structural damping force for oscillatory response is a function of a damping coefficient,  $G$ , and a complex multiple of the structural stiffness matrix, as

$$[M] \{\ddot{u}(t)\} + (1 + iG) [K] \{u(t)\} = \{P(t)\}. \quad (6.8)$$

This is equal to Eqn 6.1 for a constant amplitude oscillatory response if

$$b = \frac{Gk}{\omega}. \quad (6.9)$$

Therefore, if the structural damping  $G$  is to be modelled using an equivalent viscous damping,  $b$ , then the equality of Eqn. 6.9 holds at only one frequency. The parameter,  $W$ , as seen in Eqn. 6.7, is the circular frequency at which conversion of the structural damping to equivalent viscous damping occurs. It is typically chosen to be the dominant frequency at which the damping is active. That the conversion only occurs at a single frequency is a drawback of the method.

## 6.2.2 Finite Element Model

The full refined global FE model of Hull 050, as described in Chapter 3, was used for developing the extreme dynamic slam load case. The fluid structure interaction also requires consideration for the dynamic solution, therefore the added mass of the surrounding fluid needed to be included as in the normal mode analysis. The added mass was calculated using the steady periodic Green function panel method as outlined in Chapter 4.

The added mass was calculated for the full-scale trials condition displacement with the vessel in calm water. It was assumed that the added mass value and distribution remained constant throughout the slam event. This is a simplification since the added mass distribution will alter as the vessel immersion changes due to the vessel global motions.

## 6.3 Extreme Slam Correlation - Dynamic Analysis

As outlined in Chapter 2, an extreme slam event occurred during the measurement sea trials of Hull 050. The data from this slam, which is described in detail in the quasi-static load case development in Chapter 3, was used to develop a dynamic asymmetric slam load case. The underlying wave loading was determined by using the wave-induced load model for a wave of length 80m, height 5m and heading angle 140 degrees. The vertical acceleration of the vessel was also taken into account when calculating the buoyancy forces using the acceleration levels of 1.9g measured at the LCG and 3.0g measured at the bow during the slam event. The global load time history was estimated from the encountered wave data recorded at the time of the slam, which gave an average peak to peak encounter period of approximately 5.1 seconds. The maximum global load was taken to occur at the time instant for the maximum slam load, with the global load varying sinusoidally with a period of 5.1 seconds. The global wave load was derived using the wave-induced load model presented in Chapter 3. The global load time history used is shown in Fig. 6-1.

In addition to the underlying global load, a load was required to simulate the slam impact force on the bow of the vessel. Different slam loading time histories were investigated systematically in order to obtain the structural response which best matched the strain gauge results. The slam load time history was derived from the strain gauge results for the forward steel post which was the gauge closest to the point of slam impact. The change in slam load with time was taken to match the change in stress with time, as shown in Fig. 6-2. A time step of 0.05 seconds was used which matched the sampling rate of the strain gauge data.

The distribution, both longitudinally and transversely, of the slam load was taken as that determined through the development of the asymmetric quasi-static load case. The magnitude of the slam force was unknown. However it was systematically altered until an acceptable correlation with the maximum values of the full-scale strain gauge data was achieved. The match between the FE results and the full-scale results was attained when the average differ-

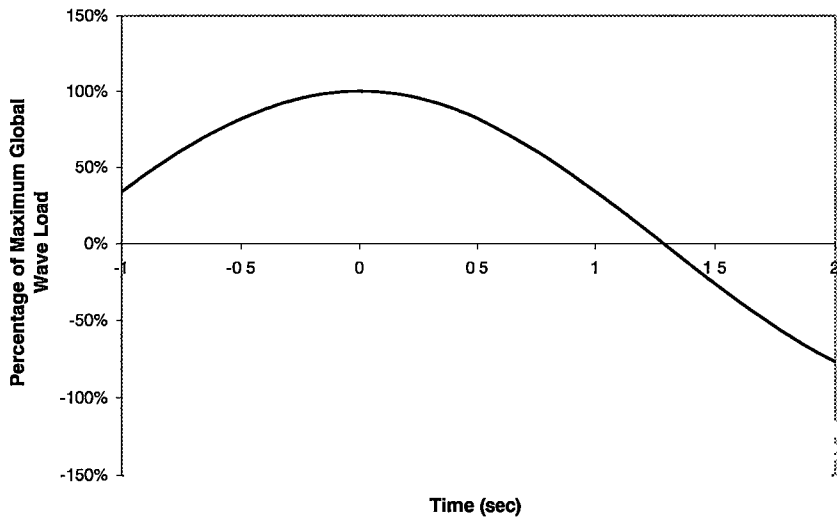


Figure 6-1: Global Wave Load Time History for Extreme Slam Event

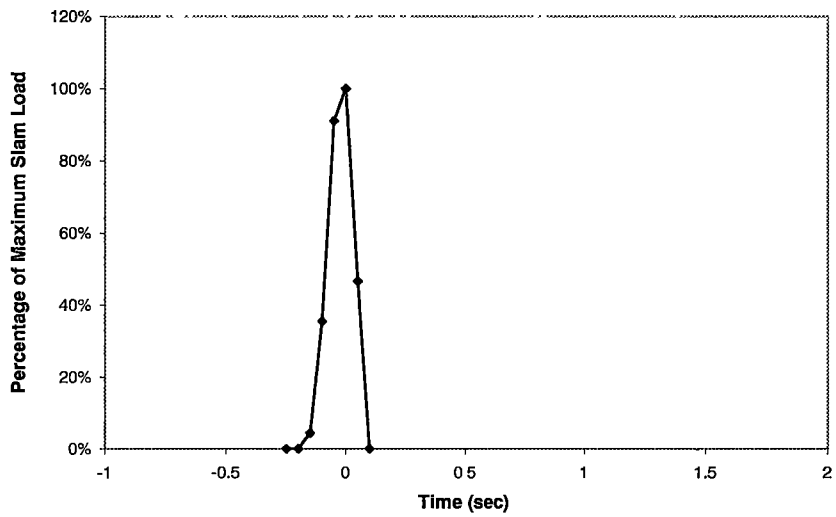


Figure 6-2: Slam Load Time History for Extreme Slam Event

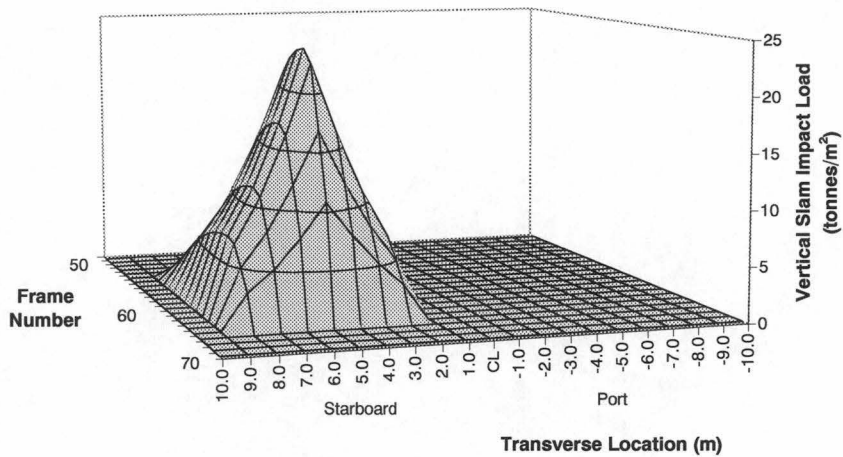


Figure 6-3: Distribution of Slam Impact Load for Extreme Slam Event - Dynamic Analysis

ence between the FE and full-scale stress results was minimised. The result of the study was that a slam load of 1025 tonnes was distributed over the starboard side of the centrebow and archway to account for the impact force. This compares with 1280 tonnes for the quasi-static analysis. The distribution of the slam impact load on the centrebow is shown in Fig. 6-3. The longitudinal distribution of the maximum buoyancy load for each hull and centrebow plus the slam impact applied forces are shown in Fig. 6-4. Note that the frames are numbered from the transom, and spaced at 1.2m.

The dynamic FE analysis was carried out using PATRAN/NASTRAN direct transient response dynamic analysis. For the analysis the FE model was subjected to one set of buoyancy forces distributed along each demihull (acting at 3 nodes for each frame per hull) and centrebow (acting at 4 nodes for each frame per side) plus a vertical inertial force equivalent to that determined from the full-scale data. The parameter,  $G$ , which has no units, is the overall structural damping coefficient used by NASTRAN. A value of 0.5 was used for  $G$  to account for the structural and hydrodynamic damping. This value was determined by performing the dynamic finite element analysis for varying levels of structural damping coefficient, until an acceptable level of correlation with the full-scale results was obtained.  $W$ , which is the frequency of interest for the conversion of overall structural damping into equivalent viscous damping, was given a value of 18.85 rad/sec to match with the first longitudinal mode of vibration identified through modal analysis.

An example of the output from the FE analysis is shown in Fig. 6-5. The plot shows the dominance of distortion in the starboard bow region due to the slamming impact force. The detailed image of Von Mises stress on the starboard side, frames 55 to 60, in Fig. 6-6, shows the concentration of stress in the region where damage was experienced by the vessel following

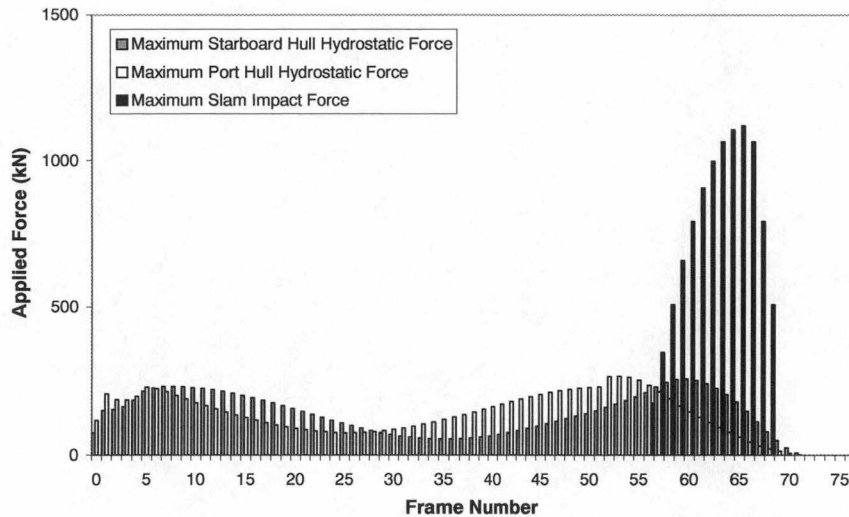


Figure 6-4: Longitudinal Distribution of Applied Force for Extreme Slam Event - Dynamic Analysis at Time of Maximum Slam Load

the extreme slam event. The units of stress used in the exaggerated plots are MPa.

Examples of the stress results for the strain gauges for the dynamic slam event FE analysis are shown in Figs. 6-7 to 6-9. These plots show that good correlation was achieved, as a function of time, for the initial slam impact peak stresses. However the subsequent whipping, with the exception of the steelposts, appears to be approximately one half a cycle out of phase. The results indicate that the slam time history used for the FE loading was realistic. Therefore for this slam event it may be concluded that the slam loading took a time of 0.2 seconds to reach a maximum value, and the slam load then expired within a further 0.1 seconds. A range of slam impact timings were investigated, however the slam timing shown gave the best comparison with the full-scale results. The level of damping used in the FE analysis gives an indication of the reduction in dynamic response of the structure during the whipping after the slam event. It should be noted that the levels of damping measured during full-scale trials after slam events varied with cycle number and strain gauge location. As noted in Chapter 2, a high level of damping was often observed for the initial whipping cycles, whilst the damping reduced as the cycles increased. Therefore the level of damping used in this dynamic FE analysis may be too high at the larger cycle numbers. The whipping periods shown in Figs. 6-7 to 6-9 are approximately 3 Hz, which correspond with the first longitudinal mode of vibration as identified previously.

Fig. 6-10 shows that good correlation was achieved for the FE dynamic analysis maximum stress results when compared with the strain gauges for the extreme slam event. The stress results were within 21.1% of the full-scale measurements except for the gauge on the port steel post. The average error for all the strain gauges was 11.1% with the major discrepancy in the

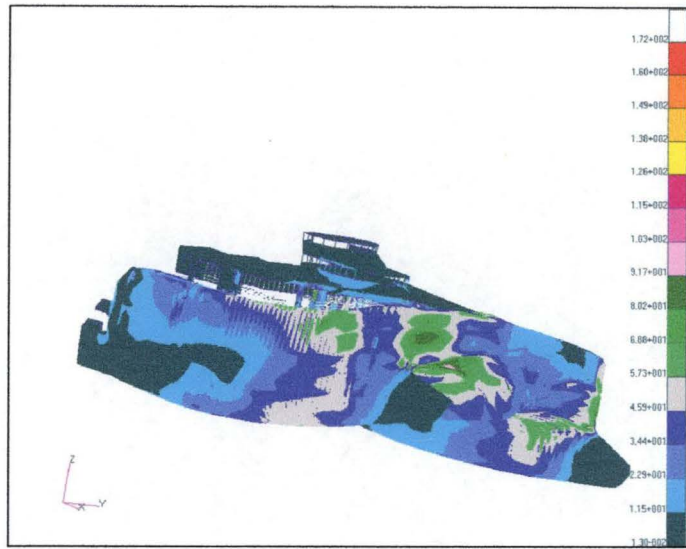


Figure 6-5: Exaggerated Deflection and Von Mises Stress Plot (units in MPa) for Dynamic Extreme Slam Load Case at Time of Maximum Slam Load

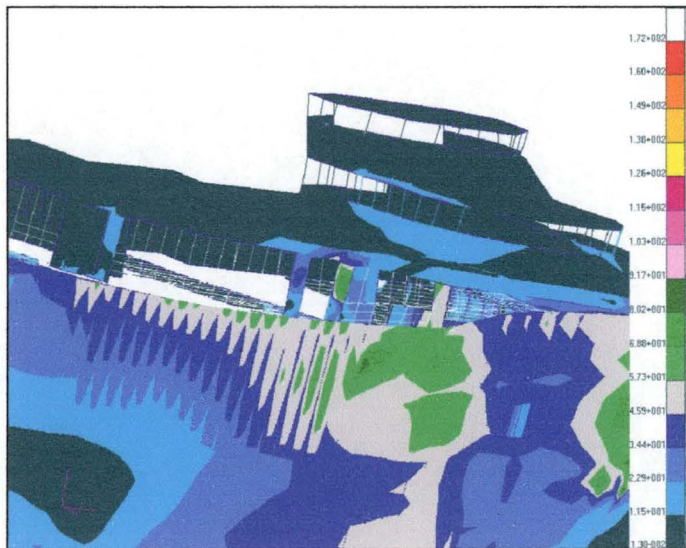


Figure 6-6: Von Mises Stress Plot (units in MPa) for Dynamic Extreme Slam Load Case - Starboard Side, Frames 55 to 60 at Time of Maximum Slam Load

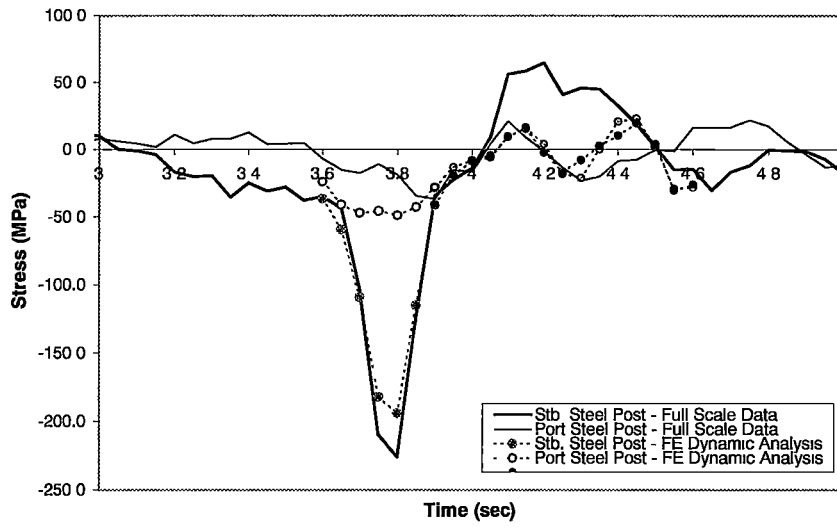


Figure 6-7: Time History of Steel Post Stress Results for Extreme Slam Event

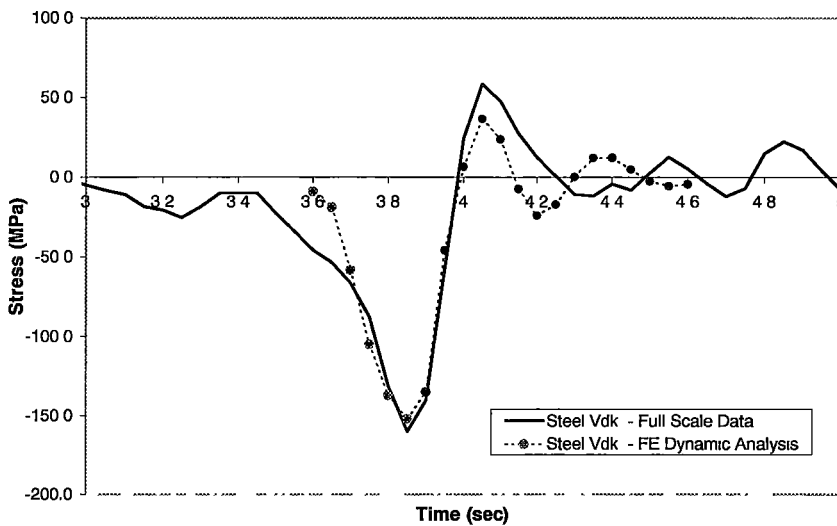


Figure 6-8: Time History of Steel Vehicle Deck Stress Results for Extreme Slam Event

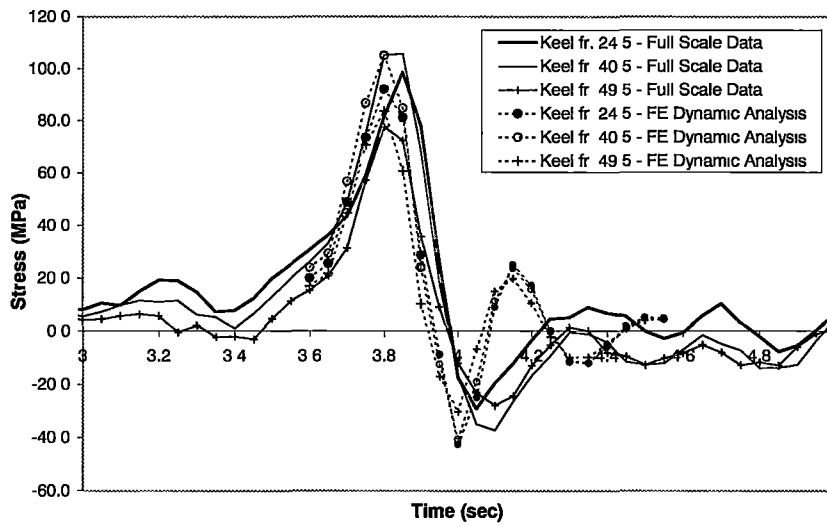


Figure 6-9: Time History of Keel Stress Results for Extreme Slam Event

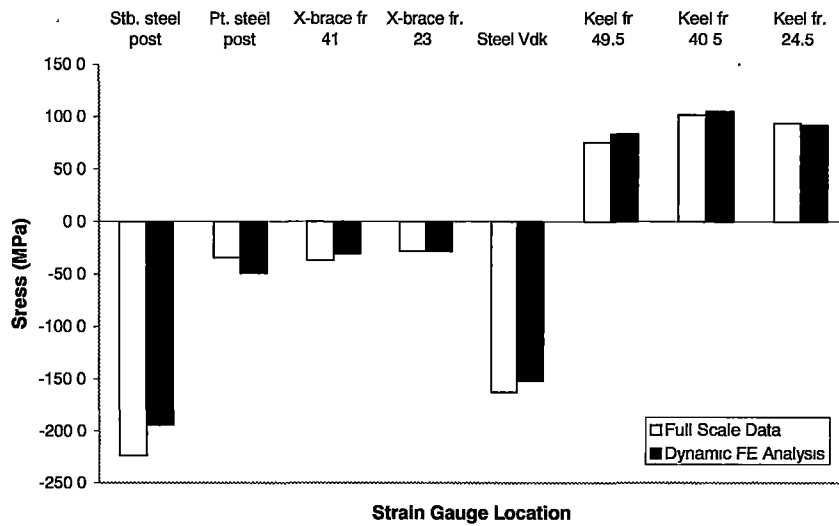


Figure 6-10: Comparison of Maximum FE Analysis and Full-Scale Data for Dynamic Extreme Slam Impact

Strain Gauge Location	Full Scale Data (MPa)	FE Analysis Axial Stress (MPa)	% Difference
Starboard Steel Post	-223.5	-194.0	15.2%
Port Steel Post	-34.2	-48.8	-30.0%
X-brace fr. 23	-36.9	-30.5	21.1%
X-brace fr. 41	-28.2	-28.1	0.4%
Steel Vehicle Deck	-162.7	-152.0	7.0%
Keel fr. 49.5	75.3	83.5	-9.8%
Keel fr. 40.5	101.9	105.0	-3.0%
Keel fr. 24.5	93.7	92.0	1.8%

Table 6.1: Comparison of Maximum FE Analysis and Full-Scale Data for Dynamic Extreme Slam Impact

results being the level of stress in the port steel post. As was found for the quasi-static analysis, it was again difficult to reduce the level of stress in this structure whilst maintaining sufficient load to retain the required stress levels at the other strain gauge locations, especially as the steel posts were very susceptible to the localised slam loading. Once again it is proposed that the discrepancy may be due to missing the peak stress value due to low sampling frequency and lack of accuracy in the heading angle and wave spreading. The stress results, including percentage differences, are also shown in Table 6.1.

The slam load used in the dynamic slam load case was 1025 tonnes which is approximately 80% of the value used in the quasi-static asymmetric load case. The reduction is probably due to the impact time history frequency being close to the natural frequency of the first longitudinal mode of vibration at 3 Hz. Using the scaling technique proposed in Chapter 2, this load case may be adapted for use with other wave piercing catamaran designs.

## 6.4 Practical Methodology for Structural Design of Large High-Speed Catamarans for Slamming

The dynamic FE analysis, incorporating the fluid-structure interaction, as outlined in this chapter, is proposed as a core component of a practical methodology for the structural design of large high-speed catamarans for slamming. The new practical methodology for the structural design of large high-speed catamarans in slamming conditions is as follows:

1. A quasi-static extreme asymmetric slam load case, which realistically simulates the loads imposed on a catamaran during an extreme slamming event, was developed for a 96m vessel. This load case may be used in finite element analysis in addition to the class rule longitudinal sagging moment as defined by Det Norske Veritas during the design process. The extreme slam load case is more conservative than the DNV sagging longitudinal bending moment load (it exceeds the maximum DNV bending moment by approximately 16%) and has a greater bias towards the bow of the vessel. The extreme slam event used

as the basis for the new load case is approximately a 1 in 240 years of service event and the bending moment due to the extreme slam event exceeded the maximum global wave loading found in the Hull 050 strain gauge records by approximately 700%.

2. The extreme asymmetric slam load case may be used in finite element analysis during the design of other large catamaran designs by using the proposed scaling technique. The data required by the wave-induced loading model is scaled assuming Froude scaling based on a scale factor  $R$  (which is derived by averaging the scaling factor of several principal parameters, i.e. overall length, waterline length, displacement, hull beam, overall beam and design draft). The slam load is scaled using the following formulation

$$F_{des} = F_{050} \left[ \left( \frac{LWL_{des}}{LWL_{050}} \right) \times \left( \frac{BOA_{des}}{BOA_{050}} \right) \times \left( \frac{TH_{050}}{TH_{des}} \right) \right]. \quad (6.10)$$

3. Dynamic FE analysis may be used to derive information on the stress time history, to ascertain whether the design meets ultimate strength requirements when subjected to an extreme slam event. Whipping frequencies may also be determined which will be important for any subsequent fatigue life estimates. In a manner similar to the quasi-static analysis, an extreme asymmetric slam load case has been developed for use with the dynamic finite element method. The method incorporates the fluid-structure interaction whereby the hydrodynamic added mass of the surrounding fluid is calculated using a steady periodic Green function panel method. The extreme asymmetric slam load case was developed for a 96m catamaran and it may be scaled for use with other designs using the technique outlined in item 2 above. The damping data determined in this study may be utilised for similar vessels.

This new methodology is currently being used by large high-speed catamaran builder, Incat Tasmania, in order to optimise the structural design of new vessels. It is to be used in the design process, in order to optimise the structural design so that the vessels remain light enough to travel at high-speed and carry large payloads, yet are strong enough to withstand severe ocean conditions. It is anticipated that use of this method will avoid the recurrence of structural damage in slamming conditions, as experienced by Hull 050 whilst operating in Cook Strait, New Zealand.

## 6.5 Conclusions

Dynamic FE analysis, incorporating the fluid-structure interaction, is proposed as a core component of a practical methodology for the structural design of large high-speed catamarans for slamming. An extreme asymmetric slam load case has been developed for a 96m catamaran which may be scaled for use with other designs using the technique set out in Chapter 2. The impact slam load was 1025 tonnes, whilst the slam timing was 0.2 seconds to reach a maximum

value, and the slam load then expired within a further 0.1 seconds. The primary outcome from such an analysis is data on whether the design meets ultimate strength requirements when subjected to an extreme slam event. The output also includes information on the stress time history and whipping frequencies which may be important for any subsequent fatigue life estimates.

Drawbacks of the method include the following:

- The dynamic FE analysis method is very computationally intensive when compared to the quasi-static approach. For a large global model, computer memory difficulties may be encountered when running a dynamic analysis for a large number of small time steps.
- Damping data is required for the dynamic FE analysis. However the data presented for Hulls 042 and 050 from the full-scale and exciter tests may be used.
- The quasi-static approach is more readily compared with the DNV rule loads and for this vessel gave a slam load and resulting stress levels which were close in value to those of the dynamic analysis.

A practical methodology for the structural design of large high-speed catamarans for slamming has been proposed, incorporating extreme slam load cases that may be scaled for use with new designs. The extreme slam load cases are more conservative than the DNV sagging longitudinal bending moment load and have a greater bias towards the bow of the vessel.

# Chapter 7

## Conclusions

This chapter summaries the main work and findings of this thesis, highlights the implications of the research and identifies possible future work in this area.

### 7.1 Summary

#### 7.1.1 Slam Occurrence and Characteristics

Full-scale hull stress, motion and wave measurements were conducted on two high-speed catamaran ferries constructed by Incat Tasmania (Hulls 042 and 050). Following the definition of a slam event for these vessels, the character and effects of identified slamming events were investigated with respect to several factors including structural loading, wave height and length, vessel speed and heading angle, relative vertical velocity and frequency of occurrence. The slamming behaviour for both vessels was found to be similar. Slam events only occurred once a certain significant wave height was reached, 0.9m for Hull 042 and 1.95m for Hull 050, the difference being mainly due to a variation in overall vessel size, wet-deck tunnel height clearance and motions behaviour as a result of ride control operability. The envelope of peak stress in a slam was found to increase with increasing wave height, however, as the wave height increases smaller slam events still occur. The distributions of slam peak stress against occurrences showed that the majority of slam events were less than the average peak stress for all events and that the distributions were similar for different wave environments. It was clear that the masters of both vessels slowed down as the significant wave height increased, although severe slams still occurred at the slower speeds. The slam peak stress tended to increase as the relative vertical velocity between the wave surface and the vessel's keel increased. The whipping responses of both vessels were similar with two dominant response frequencies at approximately 1.0 to 1.5 Hz and 2.5 to 2.8 Hz, whilst the average decay coefficient was approximately 0.09. When multiple slam events occurred within a single data record they were separated predominantly by only one wavelength with the second usually resulting in

a smaller slam peak stress. Large slam events appeared to be wet-deck slams which could change the direction of vertical bow movement.

### 7.1.2 Extreme Slam Event and Quasi-Static Slam Loads

During the full-scale measurements Hull 050 suffered an extreme slam event which led to substantial structural damage. An indication of the severity of this slam is that the bending moment experienced by the vessel during the impact exceeded the maximum global wave loading found in all the Hull 050 strain gauge records by approximately 700%. Realistic quasi-static slam load scenarios were developed using the strain gauge data from the full-scale slam events, including this extreme slam event. This was achieved by correlating the peak slam stress levels with results obtained through finite element structural modelling. The global wave loading, used as an input into the finite element model, was derived from a Froude-Krylov wave-induced load model. The extreme asymmetric slam load case, with a slam impact load of 1280 tonnes, was found to be greater than the class rule longitudinal sagging moment as defined by Det Norske Veritas with a larger maximum starboard hull bending moment (1.16 times that of DNV). The peak value was further forward than for the DNV case, ahead of amidships, due to the slam impact load on the centrebow and archway region.

A method was proposed for applying the load cases for use with other large catamaran designs, where the slam load is scaled using the following:

$$F_{des} = F_{050} \left[ \left( \frac{LWL_{des}}{LWL_{050}} \right) \times \left( \frac{BOA_{des}}{BOA_{050}} \right) \times \left( \frac{TH_{050}}{TH_{des}} \right) \right]. \quad (7.1)$$

The data required by the wave-induced loading model is scaled assuming Froude scaling based on a scale factor  $R$  (which is derived by averaging the scaling factor of several principal parameters, i.e. overall length, waterline length, displacement, hull beam, overall beam and design draft). The use of this technique was demonstrated for a new 112m wave piercer catamaran design, with a resulting slam impact load of 1660 tonnes. A comparison of the bending moment for the new slam load case, for the 112m catamaran, and the DNV sagging rule moment again showed that the starboard hull maximum bending moment for the extreme slam load case had a greater maximum value and its peak is further forward than for the DNV longitudinal sagging rule moment. The maximum bending moment was approximately 16% greater than the DNV longitudinal sagging rule moment, which was comparable to the result for Hull 050. In general therefore the increase in vessel length from 96m to 112m did not greatly alter the comparability of the extreme slam load case with the DNV longitudinal sagging rule moment. However, it does appear that for the larger vessel, the location of the maximum bending moment in the DNV case is closer to that for the extreme slam load case than for the smaller vessel. For the 12m vessel this was due to the slam load being relatively smaller (approximately 50% of the total bending moment), when compared with the underlying global

wave loading, than was the case for the smaller vessel (approximately 55% of the total bending moment).

### 7.1.3 Dynamic Slamming Response

The dynamic behaviour associated with the slamming response of large high-speed catamarans, i.e. the whipping response, was investigated. Exciter tests for the first longitudinal mode were successfully conducted on two vessels. The frequencies (3.01 Hz for Hull 045 and 2.89 Hz for Hull 050) and damping of the whipping behaviour were determined. The average decay coefficient was 0.069 for Hull 045, whilst for Hull 050 the average value was 0.035. In order to predict the mode shape and frequency of the whipping behaviour, a finite element modal analysis method was presented, where the hydrodynamic added mass of the surrounding fluid was calculated using a steady periodic Green function panel method. The effect of forward speed on sectional added mass, (expressed in terms of the local hull deflection, slope and curvature due to longitudinal hull flexure) was found to be small. The calculated whipping modes compared closely with those found through the full-scale measurements and exciter experiments. This confirmed that the method is suitable for use in determining the whipping modes and frequencies of this type of vessel. Of the two major frequencies identified in the vibratory whipping through the full-scale measurements of slam impacts, the lower frequency (approximately 1.5 Hz) corresponded to the lateral torsion mode whilst the higher frequency (approximately 2.5 - 3 Hz) was the first longitudinal mode. It was found that the calculated added mass value is essentially independent of frequency above approximately 1.6 Hz, and the effect of forward speed on added mass and hence natural frequency was found to be negligible at the speeds and frequencies considered. In order to incorporate the added mass into the finite element models a  $\cos^2\alpha$  distribution (where  $\alpha$  is the angle of the hull section surface to the horizontal) around each hull section was used since this was close to the actual added mass distribution around a section. However it was found that placement of the added mass as a lumped mass on the keel at each section gave almost identical results. An iterative approach to applying the added mass to the finite element model, where the added mass was refined as the natural frequency changed, made no discernible difference to the resulting natural frequencies. Significant changes in natural frequency were apparent due to changes in vessel mass loading magnitude and distribution.

The damping of the whipping behaviour of large high-speed catamarans was also investigated. Methods for estimating the various components of hydrodynamic damping were considered, including wavemaking damping, viscous damping and acoustic damping. These methods were used to estimate the hydrodynamic damping for the first longitudinal and lateral torsional modes of a large high-speed catamaran, Incat Hull 050. An experimental investigation was conducted into the material damping of the aluminium used in the construction of large high-speed catamarans. Other contributors to damping, such as the superstructure

rubber mounts, were also addressed. The predicted and measured components of damping were compared with the total damping for a vessel measured through exciter tests. The total predicted hydrodynamic and material damping was found to be only a small proportion of the measured total damping. The shortfall was therefore presumed to be due to additional structural damping, which is estimated to be approximately 16 times the level of the inherent material damping. This ratio is similar to that found in aeronautical and similar structural applications. This additional structural damping is likely to be composed of many items of damping which are not accounted for in a simple structural model, including: fuel and water in tanks, all fittings, soft materials and furnishings, bonded joints, fireproofing and pipe work.

#### **7.1.4 Influence of Slamming and Whipping on Fatigue Life**

The influence of slamming on the fatigue life of large high-speed aluminium catamarans was investigated. The fatigue life was found to reduce significantly with the presence of slam events, and therefore a reduction in slamming may prolong the fatigue life of a vessel markedly. Since fatigue life reduces as waveheight increases, knowledge of the expected sea conditions that a vessel will operate in is crucial for accurate fatigue life calculation. Fatigue life reduces significantly as slam peak stress increases and small slam events have little or no influence on fatigue life. Whipping behaviour was found to have a strong influence on fatigue life, with the fatigue life increasing as the decay coefficient increases.

#### **7.1.5 Dynamic Slam Loads**

A dynamic extreme slam design load case was developed using knowledge of the dynamic slamming response. This load case is based on time-varying loads and responses and is an extension of the quasi-static load case. It more realistically simulates the dynamic structural response of the vessel to a slam and is the core component of the practical methodology for the structural design of large high-speed catamarans for slamming. An extreme asymmetric dynamic slam load case was developed for a 96m catamaran, with a slam impact load of 1025 tonnes and a total slam load time duration of approximately 0.3 seconds. This load case may be scaled for use with other designs, with the primary outcome from such an analysis being information on whether the design meets ultimate strength requirements when subjected to an extreme slam event. The output also includes information on the stress time history and whipping frequencies which may be important for any subsequent fatigue life estimates.

## **7.2 Implications of Research**

This research has provided a new practical methodology for the structural design of large high-speed catamarans in slamming conditions as follows:

1. A quasi-static extreme asymmetric slam load case, which realistically simulates the loads imposed on a catamaran during an extreme slamming event, was developed for a 96m vessel. This load case may be used in finite element analysis in addition to the class rule longitudinal sagging moment as defined by Det Norske Veritas during the design process. The extreme slam load case is more conservative than the DNV sagging longitudinal bending moment load (it exceeds the maximum DNV bending moment by approximately 16%) and has a greater bias towards the bow of the vessel. However if the consequence of this is that strength is added where it is needed, and reduced where it is not, the resulting impact on total vessel weight may be minimal. The extreme slam event used as the basis for the new load case is approximately a 1 in 240 years of service event and the bending moment due to the extreme slam event exceeded the maximum global wave loading found in the Hull 050 strain gauge records by approximately 700%.
2. The extreme asymmetric slam load case may be used in finite element analysis during the design of other large catamaran designs by using the proposed scaling technique. The data required by the wave-induced loading model is scaled assuming Froude scaling based on a scale factor  $R$  (which is derived by averaging the scaling factor of several principal parameters, i.e. overall length, waterline length, displacement, hull beam, overall beam and design draft). The slam load is scaled using the formulation shown in Eqn. 7.1.
3. In order to derive information on the stress time history and whipping frequencies which may be important for any subsequent fatigue life estimates, in addition to data on whether the design meets ultimate strength requirements when subjected to an extreme slam event, dynamic FE analysis may be used. In a manner similar to the quasi-static analysis, an extreme asymmetric slam load case has been developed for use with the dynamic finite element method. The method incorporates the fluid-structure interaction whereby the hydrodynamic added mass of the surrounding fluid is calculated using a steady periodic Green function panel method. The extreme asymmetric slam load case was developed for a 96m catamaran and it may be scaled for use with other designs using the technique outlined in item 2 above.

This new methodology is currently being used by large high-speed catamaran builder, Incat Tasmania, in order to optimise the structural design of new vessels. It is to be used in the design process so that the vessels remain light enough to travel at high-speed and carry large payloads, yet are strong enough to withstand severe ocean conditions. It is anticipated that use of this method will avoid the recurrence of structural damage in slamming conditions, as experienced by Hull 050 whilst operating in Cook Strait, New Zealand.

Through the full-scale measurements, the understanding of slam events, in particular the nature and influence of slam events with respect to environmental and vessel operating con-

ditions, of large high-speed catamarans has been extended. The analysis of the data has provided information on the character and effects of these slamming events with respect to several factors including structural loading, wave height and length, vessel speed and heading angle, relative vertical velocity and frequency of occurrence. This information is valuable since it gives designers and operators data on the slamming behaviour of large high-speed catamarans. For example, the designers are now aware that a 96m design, such as Hull 050, will not slam in sea conditions with a significant wave height less than 1.95m and that reducing speed in bigger waves will not necessarily prevent the occurrence of slamming events. The data acquisition and analysis methods may be used on future vessels to obtain further information on their slamming behaviour. The slam definition employed in this study was successful in identifying slam events from the full-scale strain gauge records. By using a rate criterion a slam was defined as having occurred if a peak in the stress record occurred with the maximum rate of change of stress prior to the peak exceeding a designated value. This, along with filtering of the raw data, enabled slam events to be clearly discriminated from global wave loads. This was important since it is the slam loads that can impart severe loads and whipping response on such vessels. The extreme slam experienced by Hull 050 resulted in a 700% increase over the maximum global wave load encountered. However, as discussed in Section 7.3, the slam definition technique may be extended in the future to account for the influence of stress range on fatigue damage.

The proposed method of using finite element mode analysis, in combination with a Green function panel method for added mass determination, was shown to be suitable for estimating the whipping modes of large high-speed catamarans. This method has given the designers of such vessels a tool for predicting the whipping modes and frequencies during the design process. It has also increased the fundamental knowledge of the dynamic behaviour associated with the slamming of large high-speed catamarans. The method used for measuring the first longitudinal mode through an exciter test was proven to be successful. The experimental set up used, which involved dropping the anchor and then instantaneously restraining it whilst measuring the vertical acceleration at a range of locations, may be easily carried out in the future.

Additional understanding of the problem of damping of whipping behaviour of large high-speed catamarans resulted from the damping investigation. For example, it was shown that the hydrodynamic components were all small, as was the fundamental structural material damping. The damping was therefore concluded to originate predominantly from the structural damping due to a build up of structure, including: fuel and water in tanks, all fittings, soft materials and furnishings, bonded joints, fireproofing and pipe work. This work has added to an area of research which, to date, has been lacking in substantial practical knowledge.

It has been shown that slamming and whipping have a large influence on the estimated fatigue life of large high-speed catamarans. The methods and results provide, if combined

with information on an expected operational scenario, guidance to designers for estimating the fatigue life of large high-speed catamarans. For example, the information on the effect of sea state on estimated fatigue life may be used with expected sea conditions for a particular route of operation, to give an estimated fatigue life for various structural locations on a vessel.

### 7.3 Recommendations for Further Work

1. The slam definition used in this study was based solely on a rate criterion, as discussed in Chapter 2. A slam was defined as having occurred if a peak in the stress record occurred with the maximum rate of change of stress prior to the peak exceeding a designated value. This ensured that impact slam events, as opposed to global wave loads, were identified. An appropriate rate factor was chosen to ensure that signal noise peaks were not included in the defined slams. From the fatigue study results it was apparent that very small stress cycles have no effect on the cumulative damage due to fatigue. Obviously these small stress cycles do not have implications for the ultimate strength of the vessel's structure, problems of this nature are due to the very large slam events. Therefore it may be applicable in the future to use a two stage slam definition process. Firstly the slams would be identified using the existing method based on a rate criterion, since this would enable all the slam events to be located. Then a fatigue analysis would be conducted on typical full-scale data to obtain the contribution of the various stress ranges to the predicted damage. The minimum stress cycle which has an effect on the fatigue damage would then be defined for the strain gauge which is being used for slam identification, although reference would be made to the other strain gauges. This would be done to ensure that slam events which do not affect the fatigue life of the slam identification gauge, but have a significant fatigue effect on another location, are included. The slams with a peak value smaller than the minimum stress range for fatigue would then be discarded. Therefore only those slam events which have an influence on the structural design of the vessel, through either ultimate strength or fatigue life, would be identified.
2. There remains further work to be conducted on the issue of the damping of the whipping behaviour. A process of elimination was used to determine that it is the build up of structure which greatly increases the structural damping, since the hydrodynamic damping components were all found to be small. However work focussing on the increase in damping due to structure build up, such as fittings and furnishings, would probably provide stronger evidence towards this conclusion. For example the measurement of the damping of a built up panel in air may give an indication of the change in damping due to an increase in structural complexity.
3. It is recommended that the monitoring of these vessels remains ongoing, particularly

as their overall size continues to increase. This will provide additional data on slam loads which will strengthen the confidence of designers in design loads. Similar methods to those employed in this study may also be used to estimate the underlying global loads experienced by these vessels, when slam loads are absent. Such analysis would give valuable information on the loads large high-speed catamarans are subjected to and supply data for comparison with ship motions and load prediction programs. As an extension of a monitoring program, the development of a fatigue monitoring feedback system is proposed. Such a system would work by firstly acquiring data from an array of strain gauges. This data would be processed by an on-line rainflow counter and then the stress cycle data would be analysed to give information on the estimated fatigue life. This would provide the operator with feedback on the amount of fatigue life that has expired due to operating the vessel in the given conditions, enabling them to make informed decisions on the speed and heading angle that are allowable from a fatigue life standpoint. As part of the development of this system, it is recommended that the assessment of the amount of damage incurred by given stress levels and cycles, for typical structures used in the construction of these vessels, is investigated. This should give a better indication of the relationship of stress cycles to damage than using the existing data which was determined from small material samples.

# Bibliography

- [1] Blunden, A., editor. *Fast Ferry International*. Fast Ferry Information Ltd., 1990-2000.
- [2] High Speed Vessels Committee V.2. Structural design of high speed vessels. In *14th International Ship and Offshore Structures Congress*, Nagasaki, Japan, 2000.
- [3] Rothe, F., Sames, P.C. and Schellin, T.E. Catamaran wetdeck structural response to wave impact. In *FAST '01*, volume 3, pages 125–133, 2001.
- [4] Aertssen, G. An estimate of whipping vibration stress based on slamming data of four ships. *International Shipbuilding Progress*, Vol. 26, No.294:Pages 23–31, 1979.
- [5] Olkinuora, P., Knuuttila, E., Hakala, M.K., Rintala, S. and J. Vuorio. Structural design of an aluminium missile boat. In *FAST '91*, pages 727–764, 1991.
- [6] Iaccarino, R., Monti, S. and Sebastiani, L. Evaluation of hull loads and motion of a fast vessel based on computations and full scale experiments. In *NAV 2000*, pages 5.9.1–5.9.10, Venice, Italy, 2000.
- [7] Haugen, E.M. and Faltinsen, O. Theoretical studies of wetdeck slamming and comparisons with fullscale measurements. In *FAST '99*, pages 577–591, Seattle, USA, 1999.
- [8] Steinmann, P., Fach, K. and Menon, B. Global and slamming sea loads acting on an 86m high speed catamaran ferry. In *FAST '99*, pages 709–718, Seattle, USA, 1999.
- [9] Roberts, T.J., Watson, N.L. and Davis, M.R. Evaluation of sea loads in high speed catamarans. In *FAST '97*, pages 311–316, Sydney, Australia, 1997.
- [10] Watson, N.L., Davis, M.R. and Roberts, T.J. Shipborne measurement of sea conditions and seakeeping response of high speed ferries. In *FAST '97*, pages 713–718, Sydney, Australia, 1997.
- [11] Faltinsen, O., Hoff, J.R., Kvålvd, J. and Zhao, R. Global loads on high-speed catamarans. In *PRADS '91*, pages 1.360–1.373, 1991.
- [12] Holloway, D.S. and Davis, M.R.,. Seakeeping computations of semi-SWATHs at high froude number. *Accepted for publication for Written Discussion by RINA*, 2002.

- [13] Kring, D.C., Mantzaris, D.A., Tcheou, G.B. and P.D. Sclavounos. A time-domain sea-keeping simulation for fast ships. In *FAST '97*, pages 455–461, 1997.
- [14] Kvålsvold, J. and Faltinsen, O.M. Slamming loads on wetdecks of multihull vessels. In *International Conference on Hydroelasticity in Marine Technology*, pages 205–222. AA. Balkema, Rotterdam, 1994.
- [15] Økland, O.D., Moan, T. and Aarnes, J.V. Structural response in large twin hull vessels exposed to severe wet deck slamming. In *PRADS '98*, pages 69–78, 1998.
- [16] Fukasawa, T., Yamamoto, Y., Fujino, M. and Matora, S. Motion and longitudinal strength of a ship in head sea and the effects of non-linearities (4th report - experiments). *Journal of SNAJ*, No. 150:Pages 308–314, 1981.
- [17] Watanabe, I. and Sawada, H. Effects of elastic responses to the longitudinal bending moment in two-directional irregular waves. *Journal of SNAJ*, Vol. 158:Pages 91–102, 1985.
- [18] McTaggart, K., Datta, I., Stirling, A., Gibson, S. and I. Glen. Motions and loads of a hydroelastic frigate model in severe seas. *Trans. SNAME*, Vol. 105:Pages 427–453, 1997.
- [19] Clarke, J.D. Measurement of hull stresses in two frigates during a severe weather trial. *Trans. RINA*, Vol. 124:63–84, 1982.
- [20] R.E.D. Bishop and W.G. Price. *Hydroelasticity of Ships*. Cambridge University Press, 1979.
- [21] Belik, O., Bishop, R.E.D. and Price, W.G. Influence of bottom and flare slamming on structural responses. *Trans. RINA*, Vol. 129:Pages 261–276, 1987.
- [22] Aksu, S., Price, W.G. and Temarel, P. A comparison of two-dimensional and three-dimensional hydroelasticity theories including the effect of slamming. *Journal of Mechanical Engineering Science*, Vol. 205, No. C1:Pages 3–16, 1991.
- [23] Stavovy, A.B. and Chuang, S. Analytical determination of slamming pressures for high-speed vehicles in waves. *Journal of Ship Research*, Vol. 20, No. 4:Pages 190–198, 1976.
- [24] Faltinsen, O.M. and Zhao, R. Numerical predictions of ship motions at high forward speed. *Philosophical Transactions of the Royal Society*, Vol. 334:Pages 241–252, 1991.
- [25] Hermundstad, O. A., Aarnes, J.V. and Moan, T. Hydroelastic analysis of a flexible catamaran and comparison with experiments. In *FAST '95*, pages 487–500, 1995.
- [26] Hermundstad, O.A., Aarsnes, J.V. and Moan, T. Hydroelastic analysis of a high speed catamaran in regular and irregular waves. In *FAST '97*, pages 447–454, Sydney, Australia, 1997.

- [27] Betts, C.V., Bishop, R.E.D. and Price, W.G. A survey of internal damping. *Trans. RINA*, Vol. 119:Pages 125–142, 1977.
- [28] Clarke, J.D. Prediction of fatigue cracking in warship hulls. In *PRADS '87*, pages Pages 718–728, 1987.
- [29] Kannari, P., Klinge, P., Rintala, S., Karppinen, T., Mikkola, T.P.J. and A. Rantanen. Comparison of simulated global stresses with full-scale measurements on an aluminium fast patrol vessel. In *International Conference on Hydroelasticity in Marine Technology*, pages 477–484. Kyushu University, 1998.
- [30] Hermundstad, O.A., Wu, M. and Moan, T. Hydroelastic response analysis of a high speed monohull. In *International Conference on Hydroelasticity in Marine Technology*, pages 245–259. A.A. Balkema, Rotterdam, 1994.
- [31] Friis-Hansen, P., Jensen, J.J. and Pedersen, P.T. Wave-induced springing and whipping of high-speed vessels. In *International Conference on Hydroelasticity in Marine Technology*, pages 191–204. A.A. Balkema, Rotterdam, 1994.
- [32] Friis-Hansen, P. On combination of slamming and wave-induced responses. *Journal of Ship Research*, Vol. 38, No. 2:Pages 104–114, 1994.
- [33] Friis-Hansen, P., Jensen, J.J. and Pedersen, P.T. Long term springing and whipping stresses in high speed vessels. In *FAST '95*, pages 473–487, 1995.
- [34] Gerritsma, J. Results of recent full scale seakeeping trials. *International Shipbuilding Progress*, Vol. 27, No. 315:Pages 278–300, 1980.
- [35] Bishop, R.E.D., Clarke, J.D. and Price, W.G. Comparison of full scale and predicted responses of two frigates in a severe weather trial. *Trans. RINA*, Vol. 125:Pages 153–166, 1983.
- [36] Hope, K.J. Full scale ship motions - a review of sea trials data compared with theory. Technical Report AME 12/94, Dept of Defence, Canberra, Australia, 1994.
- [37] Maggi, A., Thomas, G. and McRae, B. Seakeeping: A comparison of numerical and towing tank predictions with full scale measurement. In *International Conference on Ship Motions and Manoeuvrability*, pages 16.1–16.13, 1998.
- [38] Strand, R. Structural analysis of boats through strain gauging. *Trans SNAME*, pages 485–489, 1970.
- [39] Tanaka, N., Sanbongi, S. and Kawaii, T. A torsional strength analysis on the container ship by means of the finite element procedure and full-scale testing. *International Shipbuilding Progress*, pages 198–214, 1971.

- [40] Vulovich, R., Hirayama, T., Toki, N. and H. Mizuno. Characteristics of hull stresses measured on a large container ship in rough seas. *Trans SNAME*, pages 397–428, 1989.
- [41] Stredulinsky, D.C., Pegg, N.G. and Gilroy, L.E. Motion, load and structural response predictions and measurements on cfav quest. *Trans. SNAME*, pages 117–123, 1999.
- [42] Sellers, F.H. Comparison of model and full-scale slamming impact pressure data. Technical Report Report MPR-351, MPR Associates, 1972.
- [43] Nagai, T. and Chuang, S. Review of structural response aspects of slamming. *Journal of Ship Research*, Vol. 21, No. 3:Pages 182–190, 1977.
- [44] Rosen, A. and Garne, K. Slamming studies on high-speed planing craft through full-scale trials and simulations. In *FAST '99*, pages 683–697, Seattle, USA, 1999.
- [45] Grossi, L. and Dogliani, M. Load and seakeeping assessment of hsc based on full scale monitoring. In *NAV 2000*, pages 4.1.1–4.1.11, Venice, Italy, 2000.
- [46] Joubert, P.N. Strength of bottom plating of yachts. *Journal of Ship Research*, Vol. 26(No. 1):Pages 45–49, 1982.
- [47] Manganelli, P. and Wilson, P. An experimental investigation of slamming on ocean racing yachts. In *15th Chesapeake Sailing Yacht Symposium*, pages 79 –87, 1999.
- [48] Jensen, A.E., Taby, J. and Høyning, B. Structural design and results from full scale structural measurements on the RNON high speed SES "KNM Skjold". In *FAST '01*, pages 143–151, 2001.
- [49] Yakimoff, P. State-of-the-art computer simulation for structural analysis of high speed catamarans. In *FAST '97*, pages 107–113, Sydney, Australia, 1997.
- [50] Roberts, T. and Yakimoff, P. Adequate global design loads for fast ferry vessels. In *14th Fast Ferry International Conference*, Copenhagen, 1998.
- [51] Thomas, G. Incat hull 042 full scale trials: Data acquisition and analysis. Technical Report SERR 01/01, School of Engineering, University of Tasmania, February 2001.
- [52] Thomas, G. Incat hull 050 full scale trials: Data acquisition and analysis. Technical Report SERR 01/00 (revision1), School of Engineering, University of Tasmania, February 2000.
- [53] Panel HS2. Notes on ship slamming. Technical Report Technical and Research Bulletin 2-30, Society of Naval Architects and Marine Engineers, 1993.
- [54] Lloyd, A.R.J.M. *Seakeeping: Ship Behaviour in Rough Weather*. Ellis Horwood, 1st edition, 2001.

- [55] Li, C.S. Estimation of system damping ratios of ship hull-girders in response to random environment. *Marine Structures*, Vol. 4:Pages 1–15, 1991.
- [56] Davis, M.R., Watson, N.L. and Holloway, D.S. Observation and prediction of the wave response of Incat Hulls 038 and 042. Technical Report SERR 05/01, School of Engineering, University of Tasmania, August 2001.
- [57] Davis, M.R. and Holloway, D.S. Passenger acceleration and MS index values for a 112m catamaran car ferry and comparisons with 86m and 96m vessels. Technical Report SERR 05/02, School of Engineering, University of Tasmania, May 2002.
- [58] Haywood, A.J., Duncan, A.J., Klaka, K.P. and J. Bennett. The role of simulation in the development of a ride control system for fast ferries. In *MCMC '94*, pages 261–270, 1994.
- [59] Morris, J.A. A three dimensional structural analysis of a large wave piercing catamaran design. In *IMAS 91 High Speed Marine Transportation*, pages 11.1–11.14, Sydney, Australia, 1991. Institute of Marine Engineers.
- [60] Hughes, O.F., McNatt, T. and Spradbrow, B.J. Structural design of large, fast marine vehicles based on first principles. In *FAST '93*, pages 489–500, 1993.
- [61] Faltinsen, O. Slamming. In *Advances in Ship and Offshore Hydrodynamics*, pages 20–31. Institut fur Schiffbau der Universität Hamburg, 1996.
- [62] Davis, M.R., Whelan, J.R. and D.S. Holloway. Drop tests of bow profile models. Technical Report SERR 01/03, School of Engineering, University of Tasmania, January 2003.
- [63] Zhu, L. and Faulkner, D. Design pressure for the wet-deck structure of twin-hull ships. In *FAST '95*, pages 257–268, 1995.
- [64] Karpipinen, T., Rantanen, A. and Hellevaara, M. Wave-induced motions and loads on fast monohulls - correlation of theoretical predictions with model and full scale experiments. In *FAST '93*, pages 177–189, 1993.
- [65] Nordenstrøm, N., Faltinsen, O. and Pedersen, B. Prediction of wave-induced motions and loads for catamarans. In *Offshore Technology Conference*, pages 1–52, Houston, USA, 1971.
- [66] Humphrey, R. and Nybø, T. Det norske veritas - direct calculation methods for high speed craft, light craft and naval surface craft. In *Pacific 2002 International Maritime Conference*, pages 10.1–10.12, 2002.
- [67] Pettersen, O. and Wiklund, K.M. Det norske veritas requirements for direct calculation of high speed and light craft. In *FAST '99*, pages 399–407, Seattle, USA, 1999.

- [68] Det Norske Veritas. *Rules for Classification of High Speed, Light Craft and Naval Surface Craft*. Det Norske Veritas, Høvik, Norway, 2002.
- [69] Lloyd's Register of Shipping. *Rules and Regulations for the Classification of Special Service Craft*. Lloyd's Register of Shipping, London, UK, 2002.
- [70] American Bureau of Shipping. *Guide for Building and Classing High Speed Craft*. American Bureau of Shipping, Houston, USA, 1997.
- [71] UNITAS. *Rules for the Construction and Classification of High Speed Craft*. Germanischer Lloyd, Bureau Veritas and Registro Italiano Navale (UNITAS), 2002.
- [72] Fan, M. and Pinchin, M. Structural design of high speed craft - a comparative study of classification requirements. In *FAST '97*, pages 27–34, 1997.
- [73] Holloway, D.S. *A High Froude Number Time Domain Strip Theory Applied to the Seakeeping of Semi-SWATHs*. PhD thesis, University of Tasmania, 1998.
- [74] Kring, D. and Sclavounos, P. A new method for analyzing the seakeeping of multi-hull ships. In *FAST '91*, pages 429–444, 1991.
- [75] Adegeest, L.J.M., Braathen, A. and Vada, T. Evaluation of methods for estimation of extreme non-linear ship responses based on numerical simulations and model tests. In *Proceedings 22nd ONR Symposium on Naval Hydrodynamics*, pages 45–57, 1998.
- [76] Weems, K., Zhang, S., Lin, W., Bennett, J. and Y. Shin. Structural dynamic loadings due to impact and whipping. In *PRADS '98*, pages 79–85, 1998.
- [77] Ito, A., Sasaki, H., Mizoguchi, S. and Miyata, H. Waveloads of a 30m ssth in sea. In *FAST '93*, pages 275–281, 1993.
- [78] Chan, H.S. Prediction of motion and wave loads of twin-hull ships. *Marine Structures*, Vol. 6:Pages 75–102, 1993.
- [79] Chan, H.S. On the calculations of ship motions and wave loads of high-speed catamarans. *International Shipbuilding Progress*, Vol. 42(No. 431):Pages 181–195, 1995.
- [80] Andrews, J.N., and Sikora, J.P. Determination of wave-induced loads on a 3,000-ton, SWATH ship. Technical report, David Taylor Model Basin, 1979.
- [81] Reilly, E.T., Shin, Y.S. and Kotte E.H. A prediction of structural load and response of a swath ship in waves. *Naval Engineers Journal*, Vol 100, No. 3:Pages 251–264, 1988.
- [82] Cheung, K.F., Seidl, L.H. and Wang, S. Analysis of swath ship structures. *Marine Technology*, Vol. 35(No. 2):Pages 85–97, 1998.

- [83] Kaplan, P. Structural loads on advanced marine vehicles, including effects of slamming. In *FAST '91*, pages 781–795, 1991.
- [84] Paulling, J.R. The analysis of complex ship structures by the finite element technique. *Journal of Ship Research*, pages 1–14, 1964.
- [85] Yamamoto, M., Sugimoto, H., Kada, K. and Higashi, K. Global strength analysis of wave piercing catamarans. In *FAST '93*, pages 1167–1177, 1993.
- [86] Latorre, R.G. and Herrington, P.D. Design of a 33-knot aluminium catamaran ferry. *Marine Technology*, Vol. 37, No. 2:Pages 88–99, 2000.
- [87] Tulk, R.J. The BC ferries' catamarans. *Trans IMarE*, Vol 111, Part 3:Pages 145–154, 2000.
- [88] Kaldjian, M.J., Woodward, J.B. and Reid, W.R. Deflections of great lakes ore carrier hull structure by finite element analysis. In *SNAME, Great Lakes and Great Rivers Section*, pages 1–21, 1982.
- [89] Herrington, P.D. and Latorre, R.G. Development of an aluminium hull panel for high-speed craft. *Marine Structures*, Vol. 11:Pages 47–71, 1998.
- [90] Pegg, N. G., Gilroy, L. E. and Kumar, R. Full scale verification of finite element modelling of a 75 tonne swath vessel. *Marine Structures*, Vol. 8:Pages 211–228, 1995.
- [91] Ziliotto, F., Ebert, J., Hakala, M., Hong, D.P., Ivanov, L.D., Pegg, N.G., Sakato, T., Senjanovic, I. and W.H. Wang. Comparison of different finite element analyses of the transverse frame of a 350000 tdw tanker. *Marine Structures*, Vol. 4:Pages 231–255, 1991.
- [92] Basu, R., Kirkhope, K. and Srinivasan, J. Assuring quality and reliability of ship structure finite element analysis. In *Ship Structure Symposium '96 - Human and Organisational Error in Marine Structures*, pages M1–M17. SSC and SNAME, 1996.
- [93] Hay, B., Bourne, J., Engle, A. and Rubel, R. Characteristics of hydrodynamic loads data for a naval combatant. In *International Conference on Hydroelasticity in Marine Technology*, pages 169–188. A.A. Balkema, Rotterdam, 1994.
- [94] Det Norske Veritas. *Tentative Rules for Construction and Classification of Light Craft*. Det Norske Veritas, Høvik, Norway, 1972.
- [95] Det Norske Veritas. *Rules for Classification of High Speed and Light Craft*. Det Norske Veritas, Høvik, Norway, 1985.
- [96] Det Norske Veritas. *Strength Analysis of Hull Structures in High Speed and Light Craft*. Det Norske Veritas, Høvik, Norway, 1996.

- [97] Davidson, G. Yard 050, 95 metre wave piercing catamaran global report. Technical Report 050-DOC-30-001 3 Volumes, Incat Tasmania Pty. Ltd., 1998.
- [98] Salvesen, N., Tuck, E.O. and Faltinsen, O. Ship motions and sea loads. *Trans. SNAME*, Vol. 78:Pages 250–279, 1970.
- [99] Lee, C.M., Jones, H.D. and Curphey, R.M. Prediction of motion and hydrodynamic loads of catamarans. *Marine Technology*, Vol. 10, No. 4:Pages 392–405, 1973.
- [100] Thomas, G., Davis, M., Whelan, J. and Roberts, T. Slamming response of large high speed catamarans. In *FAST '01*, volume Vol. 3, pages 97–107, 2001.
- [101] J.M. Lee. *MSC/Nastran Linear Static Analysis User's Guide*. MSC.Software, 1997.
- [102] Det Norske Veritas. *Classification Notes 30.1, Buckling Strength Analysis*. Det Norske Veritas, Høvik, Norway, 1995.
- [103] McCallam, J. The strength of fast cargo ships. *Trans. RINA*, Vol. 116:Pages 1–15, 1974.
- [104] Hoffman, D. Analysis of ship structural loading in a seaway. *Marine Technology*, Vol. 9, No. 2:Pages 173–195, 1972.
- [105] Kumai, T. and Tasai, F. On the wave-exciting force and response of whipping of ships. *European Shipbuilding*, No. 4:Pages 20–34, 1970.
- [106] Yamamoto, Y., Fujino, M., Fukasawa, T. and Ohtsubo, H. Slamming and whipping of ships among rough seas. In *Proceedings Euromech Colloquium*, volume 122, pages 19–33, 1979.
- [107] Ochi, M.K. and Motter, L.E. Prediction of slamming characteristics and hull responses for ship design. *Trans. SNAME*, Vol. 81:Pages 144–176, 1973.
- [108] Kawakami, M. and Tanaka, T. Stochastic prediction of whipping vibration of very high speed ship due to slamming. In *Proceedings Euromech Colloquium*, No. 122, pages 171–186, 1979.
- [109] Hirdaris, S.E., Price, W.G., and Temarel, P. Hydroelastic analysis of a bulk tanker. In *NAV 2000*, pages 5.6.1–5.6.12, Venice, Italy, 2000.
- [110] Louarn, F. and Temarel, P. An investigation of the structural dynamics of a racing yacht. In *14th Chesapeake Sailing Yacht Symposium*, pages 123–142, 1999.
- [111] Price, W.G., Temarel, P. and Keane, A.J. Hydroelastic analysis of a swath in waves. In *International Conference on Hydroelasticity in Marine Technology*, pages 231–243. A.A. Balkema, Rotterdam, 1994.

- [112] Evans, H.J. Preliminary design estimation of hull girder response to slamming. *Trans. SNAME*, Vol. 90:Pages 55–83, 1982.
- [113] Jiao, G. Probabilistic prediction of extreme stress and fatigue damage for ships in slamming conditions. *Marine Structures*, Vol. 9:Pages 759–785, 1996.
- [114] Wagner, H. Landing of seaplanes. Technical Report TH 3212, National Advisory Committee for Aeronautics, 1932.
- [115] Ramos, J. and Guedes Soares, C. Vibratory response of ship hulls to wave impact loads. *International Shipbuilding Progress*, Vol.45(No. 441):Pages 71–87, 1998.
- [116] Takahashi, T. and Kaneko, Y. Experimental study on wave loads acting on a semi-displacement type high-speed craft by means of elastic backbone model. In *High-Speed Surface Craft Conference*, pages 160–169, 1983.
- [117] Chou, S.K., Chiu, F.C. and Lee, Y.J. Nonlinear motions and whipping loads of high-speed crafts in head sea. In *Naval Hydrodynamics Symposium*, pages 157–170, 1990.
- [118] Hakala, M.K. Application of the finite element method to fluid-structure interaction in ship vibration. Technical Report 433, Technical Research Centre of Finland, Espoo, Finland, 1986.
- [119] Nestegård, A. and Mejlænder-Larsen, M. Hydrodynamic added mass of a floating vibrating structure. In *International Conference on Hydroelasticity in Marine Technology*, pages 261–272, Trondheim, Norway, 1994. A.A.Balkema, Rotterdam.
- [120] Riska, K. and Kukkanen, T. Speed dependence of the natural modes of an elastically scaled ship model. In *International Conference on Hydroelasticity in Marine Technology*, pages 157–168. A.A.Balkema, Rotterdam, 1994.
- [121] Riska, K. Ship ramming multi-year ice floes. Technical Report No. 818, Technical Research Centre of Finland, Espoo, Finland, 1988.
- [122] Oei, T.H. Finite element ship hull vibration analysis compared with full scale measurements. Technical Report No. 70-379-ST, Netherlands Ship Model Basin, 1976.
- [123] Landweber, L. and de Macagno, M.C. Added mass of two-dimensional forms oscillating in a free surface. *Journal of Ship Research*, Vol. 2(No. 4), 1967.
- [124] Kumai, T. Damping factors in the higher modes of ship vibrations. *European Shipbuilding*, Vol. 1:Pages 29–34, 1958.
- [125] Sunnersjo, S. and Janson, C. Hydrodynamic inertia and damping of ship hull vibrations. *Trans. RINA*, Vol. 130:Pages 107–117, 1988.

- [126] MSC.Software, Los Angeles, USA. *NASTRAN Basic Dynamic Analysis*, 2001.
- [127] MSC. Software, Los Angeles, USA. *NASTRAN Advanced Dynamic Analysis*, 2001.
- [128] Doctors, L.J. Application of the boundary-element method to bodies oscillating near a free surface. In *Computational Fluid Dynamics - Proc. International Symposium on Computational Fluid Dynamics ISCFD-Sydney*, pages 377–386. Elsevier Science Publishers B.V., Amsterdam, 1988.
- [129] Wehausen, J.V. and Laitone, E.V. *Surface Waves*, volume 9 of *Handbuch der Physik*. Springer-Verlag, 1960.
- [130] Holloway, D.S. and Davis, M.R. Green function solutions for the transient motion of water sections. *Journal of Ship Research*, Vol. 46(No. 2):Pages 99–120, 2002.
- [131] F. Ursell. On the heaving motion of a circular cylinder in the surface of a fluid. *Quarterly Journal of Mechanics and Applied Mathematics*, Vol. 2:Pages 218–231, 1949.
- [132] Rao, S. *Mechanical Vibrations*. Addison-Wesley, 1986.
- [133] Kundu, P. *Fluid Mechanics*. Academic Press Inc., 1990.
- [134] Beranek, L.L. and Ver, I.L. *Noise and Vibration Control Engineering: Principles and Applications*. John Wiley and Sons, 1992.
- [135] Pierce, A. D. *Acoustics: An Introduction to Its Physical Principles and Applications*. McGraw-Hill, 1981.
- [136] Kirkup, S. *The Boundary Element Method in Acoustics*. Integrated Sound Software, London, 1998.
- [137] Nashif, A.D., Jones, D.I.G. and Henderson, J.P. *Vibration Damping*. John Wiley and Sons, 1985.
- [138] Lazan, B.J. *Damping of Materials and Members in Structural Mechanics*. Pergamon Press, 1968.
- [139] Xie, C.Y., Schaller, R. and Jaquerod, C. High damping capacity after precipitation in some commercial aluminium alloys. *Materials Science and Engineering*, A252:Pages 78–84, 1998.
- [140] White, R.G. and Walker, J.G. *Noise and Vibration*. Ellis Horwood Limited, 1986.
- [141] Mead, D.J. Prediction of the structural damping of a vibrating stiffened plate. In *AGARD Conference No.277*, pages 2.1–2.15, 1979.
- [142] Ungar, E.E. The status of engineering knowledge concerning the damping of built-up structures. *Journal of Sound and Vibration*, Vol. 26 (1):Pages 141–154, 1973.

- [143] Clarkson, B.L. and Ford, R.D. The response of a typical aircraft structure to jet noise. *Journal Royal Aeronautical Society*, Vol. 66:Pages 31–40, 1962.
- [144] Grice, R.M. and Pinnington, R.J. A method for the vibration analysis of built-up structures, part i: Introduction and analytical analysis of the plate-stiffened beam. *Journal of Sound and Vibration*, Vol. 230(No. 4):Pages 825–849, 2000.
- [145] Gounaris, G.D. and Anifantis, N.K. Structural damping determination by finite element approach. *Computers and Structures*, Vol. 73:Pages 445–452, 1999.
- [146] Simmonds, I. Personal correspondence. Mackay Consolidated Industries Pty. Ltd., March, 2002.
- [147] Sharp, M.L., Nordmark, G.E. and Menzemer, C.C. *Fatigue Design of Aluminium Components and Structures*. McGraw Hill, 1996.
- [148] Fredriksen, A. Fatigue aspects of high speed craft. In *FAST '97*, pages 217–224, Sydney, Australia, 1997.
- [149] Tongue, E. Fatigue assessment of aluminium fast craft. In *Third International Forum on Aluminium Ships*, pages 1–14, Haugesund, Norway, 1998.
- [150] Collins, J. A. *Failure of Materials in Mechanical Design*. John Wiley and Sons, 2nd edition, 1993.
- [151] Sumi, Y., Yamamoto, Y. and Suzuki, M. The effect of whipping stresses on fatigue of a fast container ship in rough seas. *Naval Architecture and Ocean Engineering*, Vol. 27:Pages 145–153, 1990.
- [152] British Standards. *Structural Use of Aluminium, BS8118, 1991: Part1, Code of Practice for Design. 1991: Part 2, Specification for Materials, Workmanship and Protection*, 1991.
- [153] Pegg, N.G., Vernon, T.A., Wegner, L. and Nethercote, W.C.E. Finite element prediction of measured bow flare plate stresses under dynamic wave loading. *Trans RINA*, pages 135–143, 1988.
- [154] Murray, M.A., Evensen, K., Ghoneim, G.A. and Grinstead, J. Finite element modelling of the dynamic response of the icebreaker canmar kigoriak to ice ramming forces. In *Offshore Technology Conference*, pages 423–437, 1985.
- [155] Adhikari, S. and Woodhouse, J. Identification of damping: Part 1, viscous damping. *Journal of Sound and Vibration*, Vol. 243(No. 1):Pages 43–61, 2001.
- [156] Oliveto, G. and Greco, A. Some observations on the characterization of structural damping. *Journal of Sound and Vibration*, Vol. 256(No. 3):Pages 391–415, 2002.

The following abbreviations are used in the bibliographical details:

FAST	International Conference on Fast Sea Transportation
SNAJ	Society of Naval Architects of Japan
PRADS	Practical Design of Ships and Mobile Units
RINA	Royal Institution of Naval Architects
SNAME	Society of Naval Architects and Marine Engineers

## **Appendix A**

### **Strain Gauge Locations:**

### **Detailed Drawings**

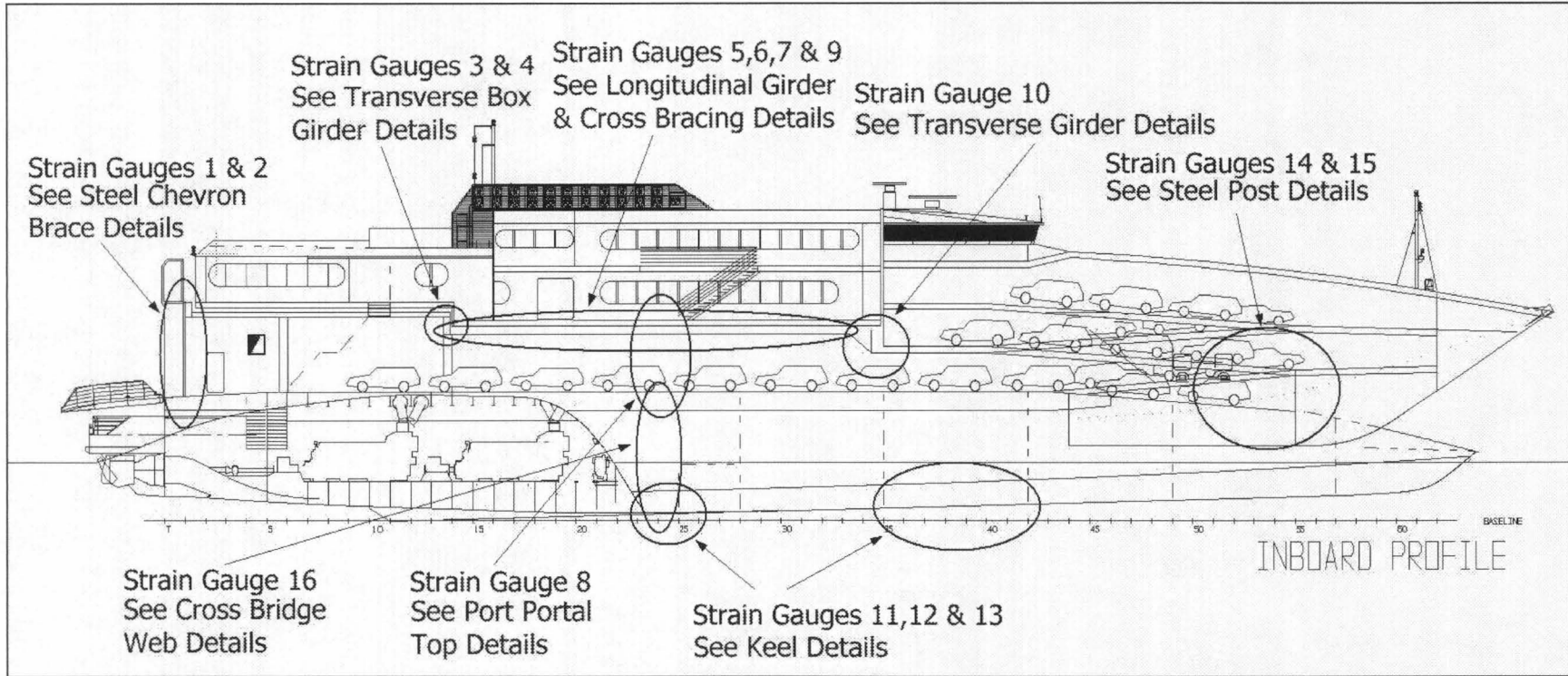
**Part I**

**Hull 042**

Strain Gauge Number	Location
1	Port steel chevron brace at frame 2 close to CL. Chevron brace is a 200mm x 9mm steel box section. See Fig. A-3.
2	Stb. steel chevron brace at frame 2 close to CL. Chevron brace is a 200mm x 9mm steel box section. See Fig. A-3.
3	Top of aft transverse box at frame 14 on CL. Transverse box is a 500mm wide and 1000mm deep with plate thicknesses: top = 25mm, bottom = 20mm, fwd = 10mm & aft = 14mm. See Figs. A-4 & A-5.
4	Bottom of aft transverse box at frame 14 on CL. Transverse box is 500mm wide and 1000mm deep with plate thicknesses: top = 25mm, bottom = 20mm, fwd = 10mm & aft = 14mm. See Figs. A-4 & A-5.
5	Top of inner cross brace at frame 14. Cross brace is a 260 x 4mm box section. See Fig. A-5.
6	Top of bat wing on x-brace at frame 17. Batwing is a 14mm plate horizontal bracket. See Fig. A-5.
7	Top of longitudinal girder, 4600mm off CL, at frame 24. Longitudinal Girder is I beam with 250 x 5mm plate web & 160 x 10mm plate riders. See Figs. A-7 & A-6.
8	Top of port portal top at frame 24 on 25mm plate deck. See Fig. A-8.
9	Top of longitudinal girder, 4600mm off CL, at frame 32. Longitudinal Girder is I beam with 370 x 10mm plate web & 250 x 16mm plate riders. See Figs. A-7 & A-6.
10	Bottom of transverse girder at frame 35 on CL. Transverse girder is an I beam with 964 x 8mm plate web & 400 x 12mm plate riders. See Figs. A-7 & A-6.
11	Stb. hull keel rider at frame 24.5. Keel is 400 x 10mm plate web and 300 x 20mm plate rider, see Figs. A-9 & A-11.
12	Stb. hull keel rider at frame 35.5. Keel is 400 x 10mm plate web and 300 x 20mm plate rider, see Figs. A-10 & A-11.
13	Stb. hull keel rider at frame 41.5. Keel is 400 x 10mm plate web and 300 x 20mm plate rider, see Figs. A-10 & A-11.
14	Port lower steel post at frame 54, aft side. Steel post is a 150mm x 5mm steel box section. See Fig. A-12.
15	Std. lower steel post at frame 54, aft side. Steel post is a 150mm x 5mm steel box section. See Fig. A-12.
16	Cross bridge 7mm plate web at frame 24 on CL, fwd side. See Fig. A-13.

Table A.1: Hull 042- Strain Gauge Guide

Figure A-1: Hull 042 - Profile View Guide to Detailed Drawings of Strain Gauge Locations  
218



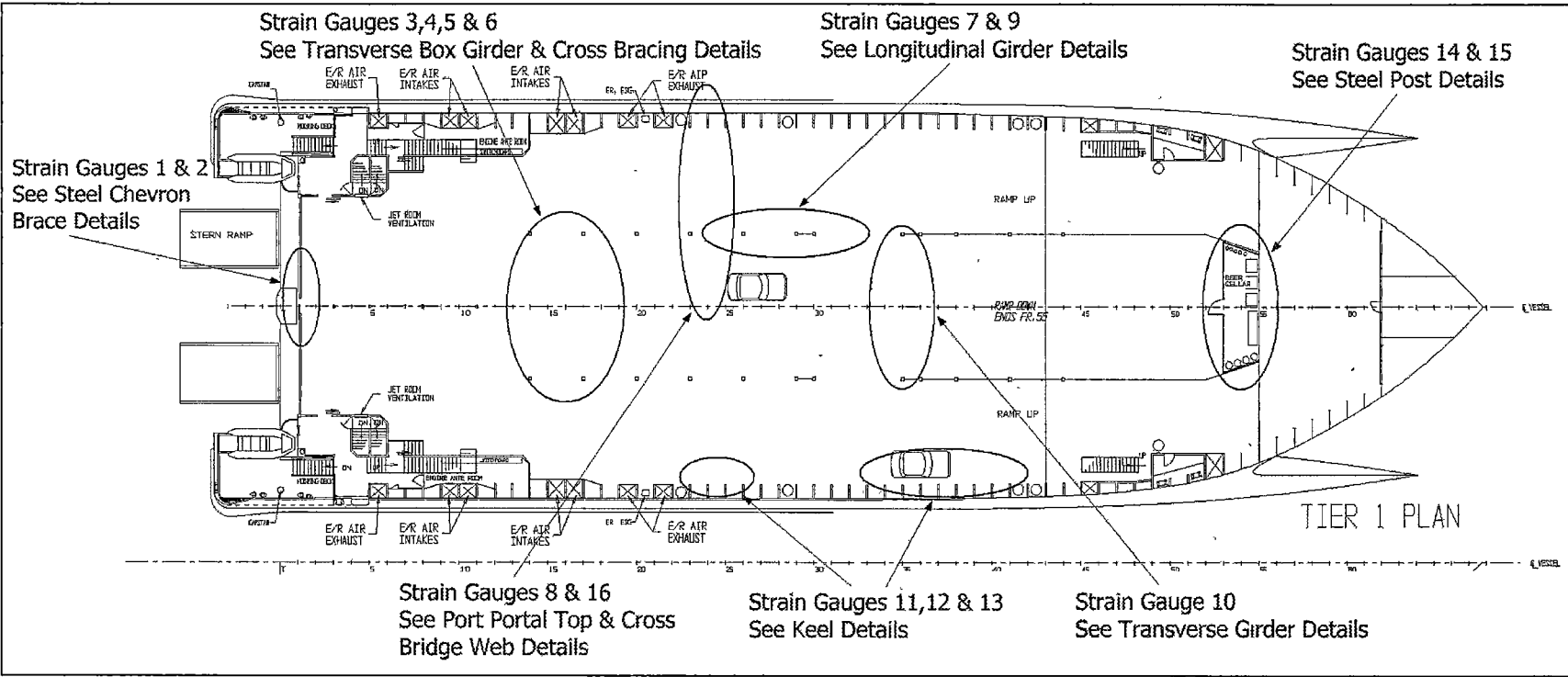


Figure A-2: Hull 042 - Plan View Guide to Detailed Drawings of Strain Gauge Locations





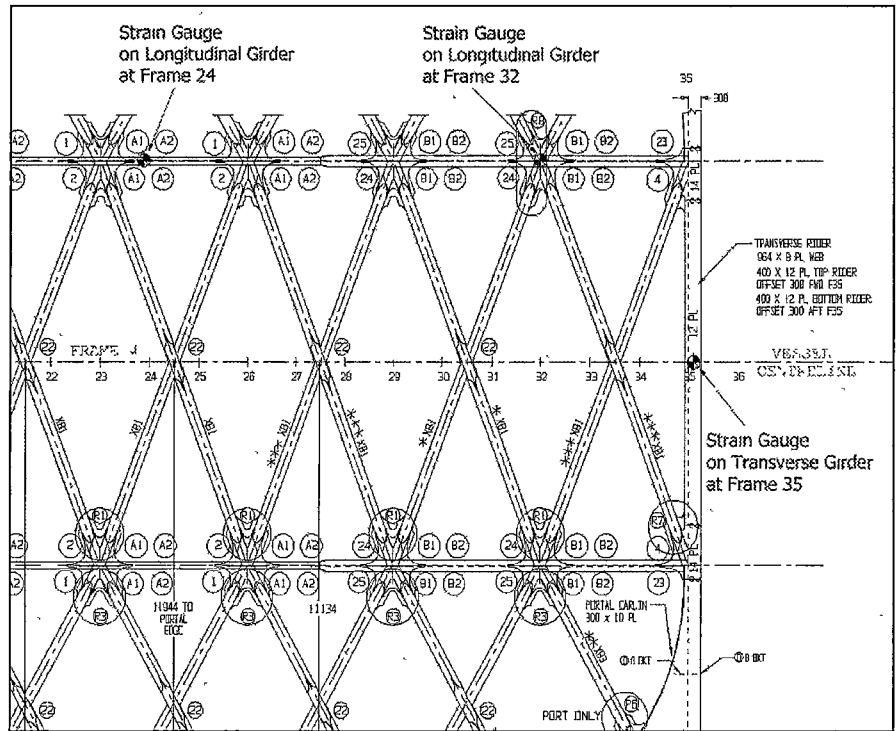


Figure A-7: Hull 042 - Plan View of Cross Bracing showing Strain Gauges 7 & 9 on Longitudinal Girder and Strain Gauge 10 on Transverse Girder

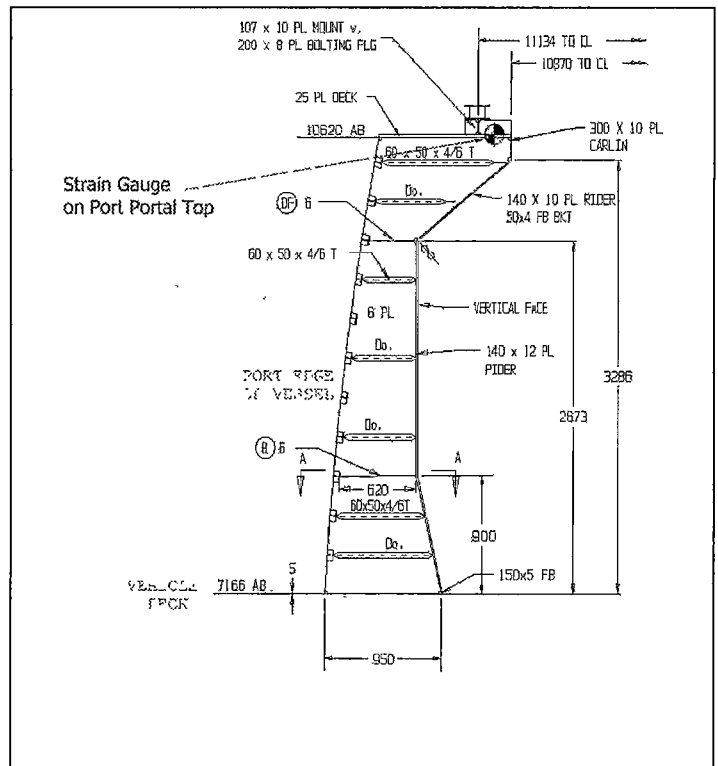


Figure A-8: Hull 042 - Frame 24 Portal Top (Port Side Looking Forward) showing Strain Gauge 8 on Port Portal Top





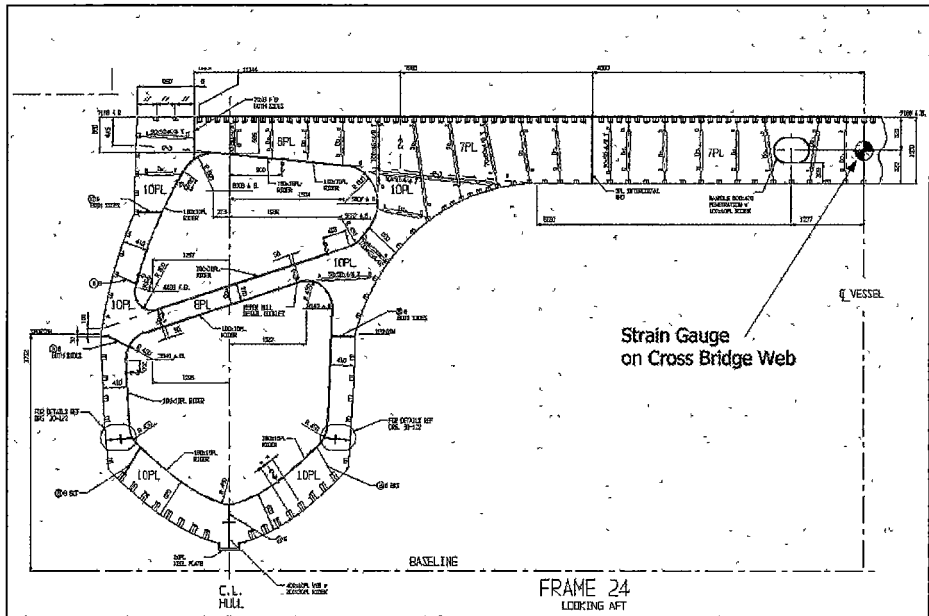


Figure A-13: Hull 042 - Hull Section 24 showing Strain Gauge 16 on Cross Bridge Web

## **Part II**

# **Hull 050**

Strain Gauge Number	System Number	Location
1	1	Top of transverse top rider at frame 69 on CL. Top rider is a 180 x 12mm plate rider. See Fig. A-16.
2	1	Top of transverse top rider at frame 67 on CL. Top rider on I-beam 274 x 6mm plate web and 160 x 12mm plate riders. See Fig. A-17.
3	1	Top of transverse top rider at frame 66 on CL. Top rider on I-beam 274 x 6mm plate web and 160 x 12mm plate riders. See Fig. A-18.
4	1	Top of transverse top rider at frame 65 on CL. Top rider on I-beam 274 x 6mm plate web and 160 x 12mm plate riders. See Fig. A-19.
5	1	Stb. fwd diagonal at frame 62. Diagonal is a 100 x 6mm steel box section. See Fig. A-20.
6	1	Stb. aft diagonal at frame 59. Diagonal is a 100 x 6mm steel box section. See Fig. A-20.
7	1	Port fwd diagonal at frame 62. Diagonal is a 100 x 6mm steel box section. See Fig. A-20.
8	1	Port aft diagonal at frame 59. Diagonal is a 100 x 6mm steel box section. See Fig. A-20.
9	2	Port lower steel post at frame 63. Steel post is a 150 x 6mm steel box section. See Fig. A-20.
10	2	Stb. lower steel post at frame 63. Steel post is a 150 x 6mm steel box section. See Fig. A-20.
11	2	Stb. portal x-brace at frame 41. Cross bracing is a 260 x 180mm x 12mm box section. See Fig. A-21.
12	2	Stb. portal x-brace at frame 23. Cross bracing is a 260 x 180mm x 12mm box section. See Fig. A-21.
13	2	Stb. steel diagonal on vehicle deck at frame 18. Steel diagonal is a 200 x 5mm box section. See Fig. A-22.
14	2	Stb. hull keel at frame 49.5. Keel is a 400 x 10mm plate web and 200 x 20mm plate rider. See Figs. A-23 & A-26.
15	2	Stb. hull keel at frame 40.5. Keel is a 400 x 10mm plate web and 200 x 20mm plate rider. See Figs. A-24 & A-26.
16	2	Stb. hull keel at frame 24.5. Keel is a 400 x 10mm plate web and 200 x 20mm plate rider. See Figs. A-25 & A-26.

Table A.2: Hull 050- Strain Gauge Guide

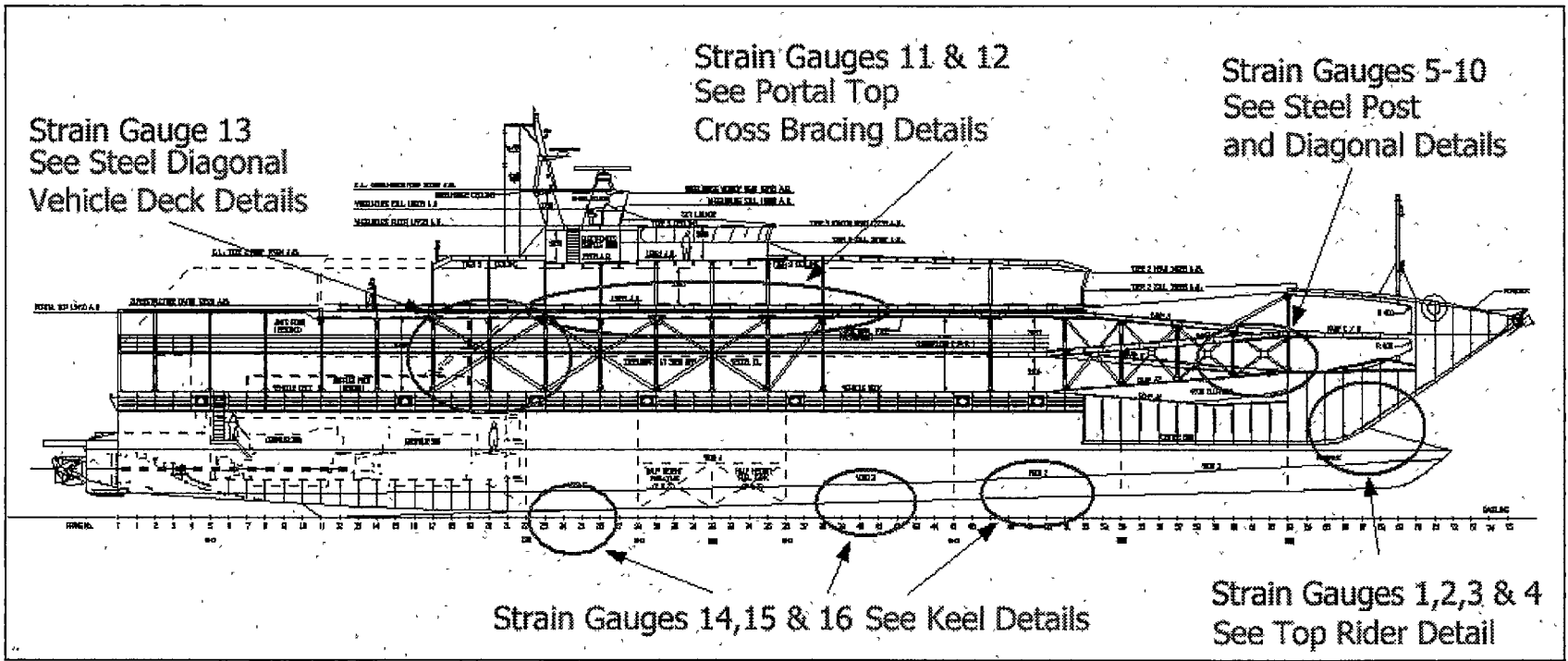


Figure A-14: Hull 050 - Profile View Guide to Detailed Drawings of Strain Gauge Locations

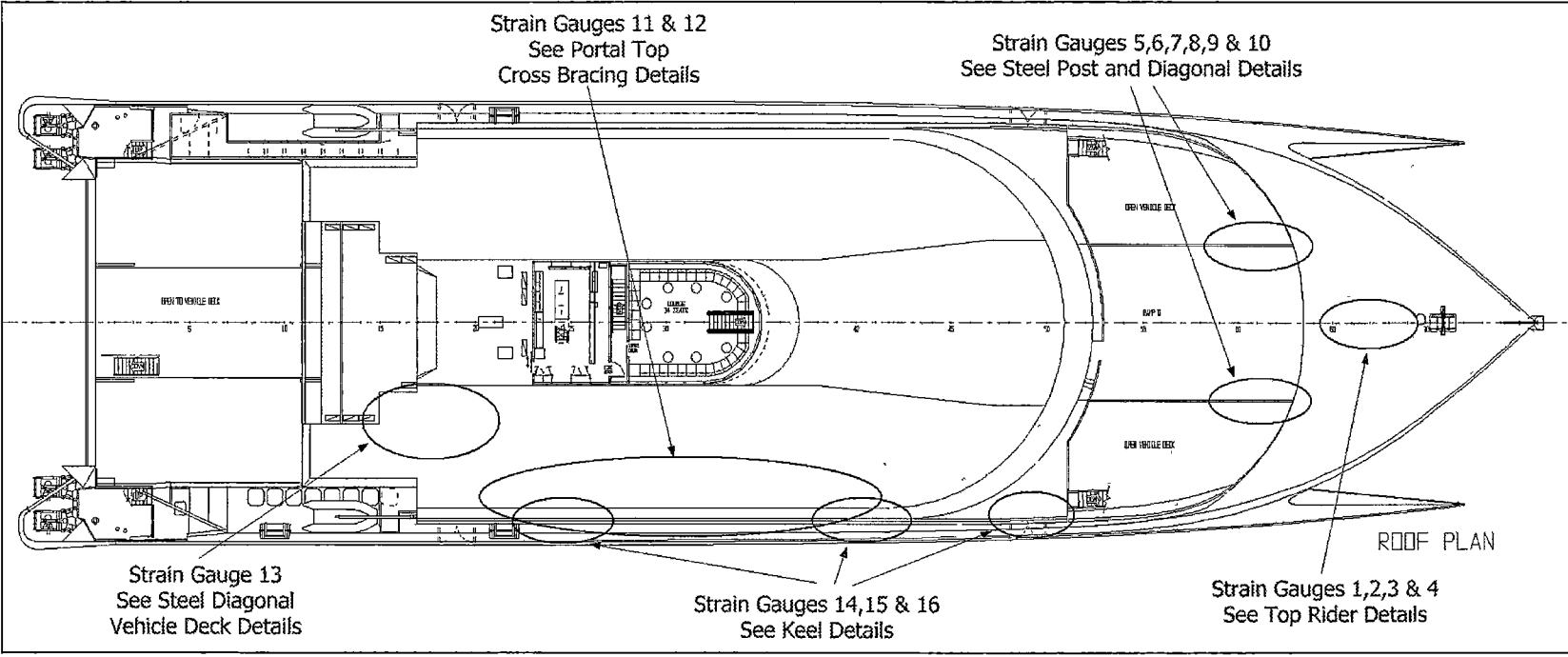


Figure A-15: Hull 050 - Plan View Guide to Detailed Drawings of Strain Gauge Locations

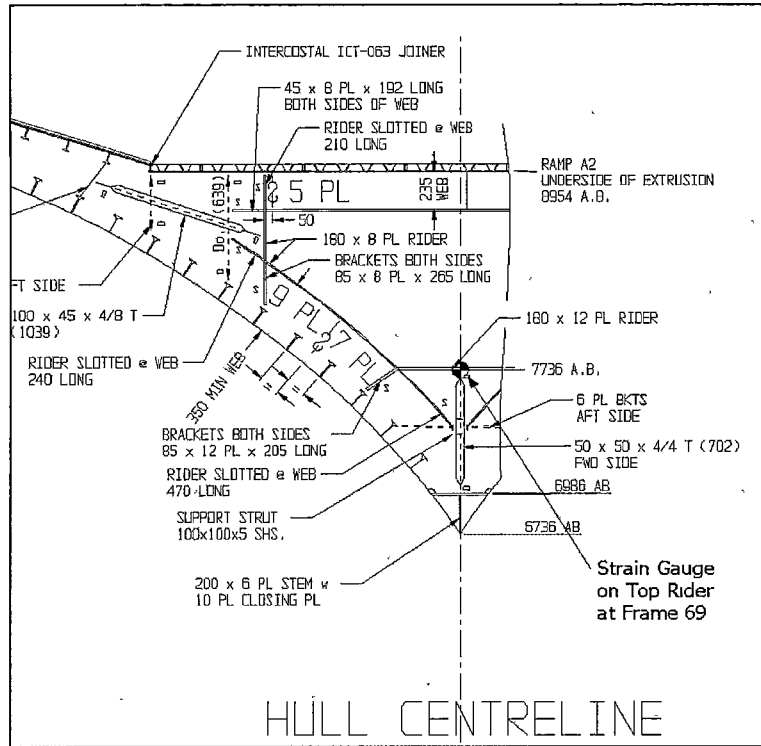


Figure A-16: Hull 050 - Centrebow Hull Frame 69 (Looking Aft) showing Strain Gauge 1 on Top Rider at Frame 69

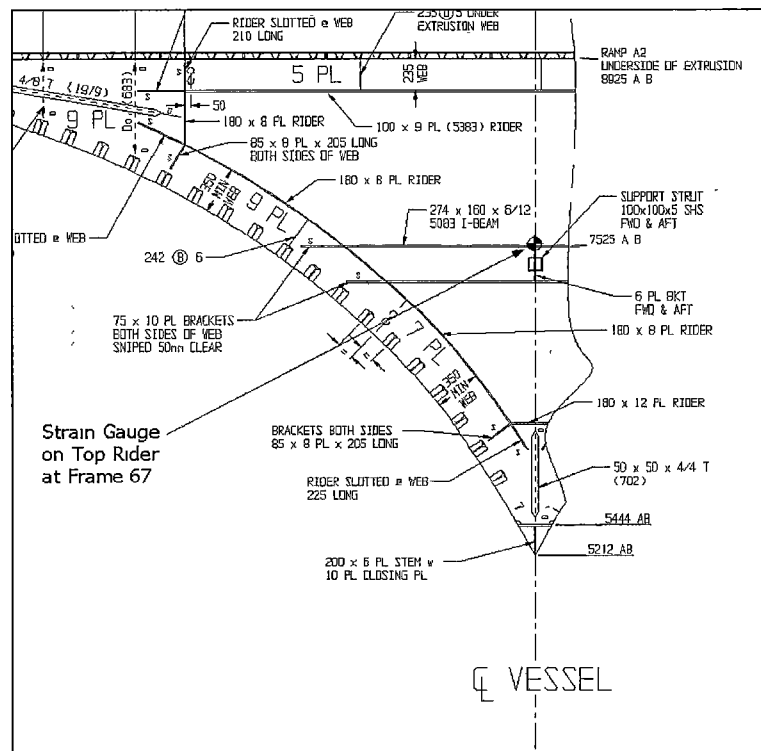


Figure A-17: Hull 050 - Centrebow Hull Frame 67 (Looking Aft) showing Strain Gauge 2 on Top Rider at Frame 67

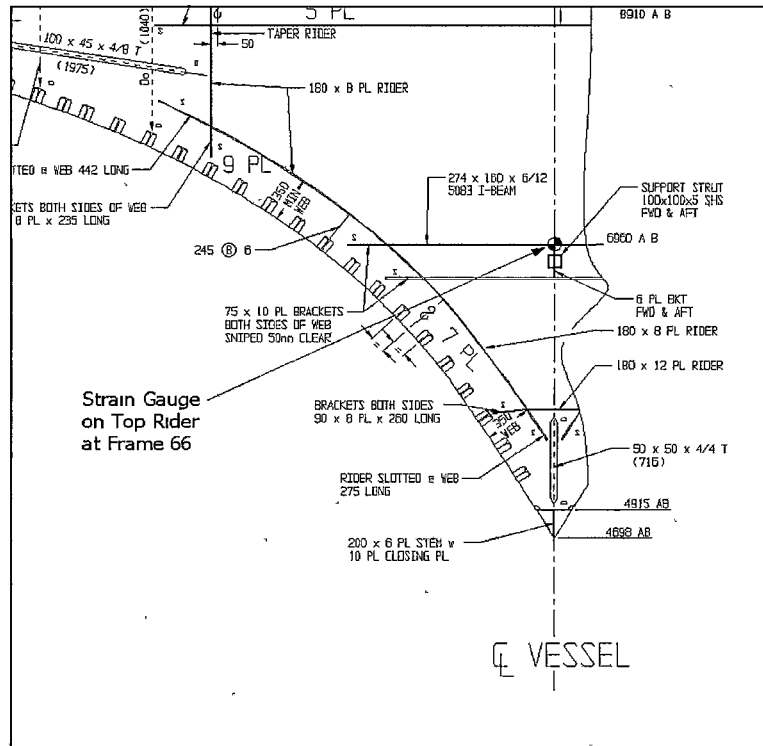


Figure A-18: Hull 050 - Centrebow Hull Frame 66 (Looking Aft) showing Strain Gauge 3 on Top Rider at Frame 66

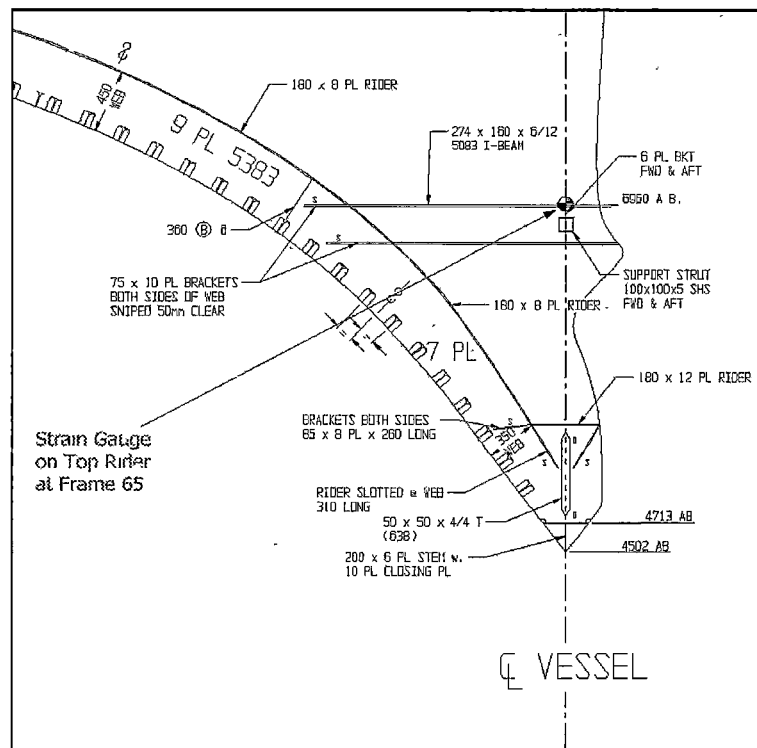


Figure A-19: Hull 050 - Centrebow Hull Frame 65 (Looking Aft) showing Strain Gauge 4 on Top Rider at Frame 65

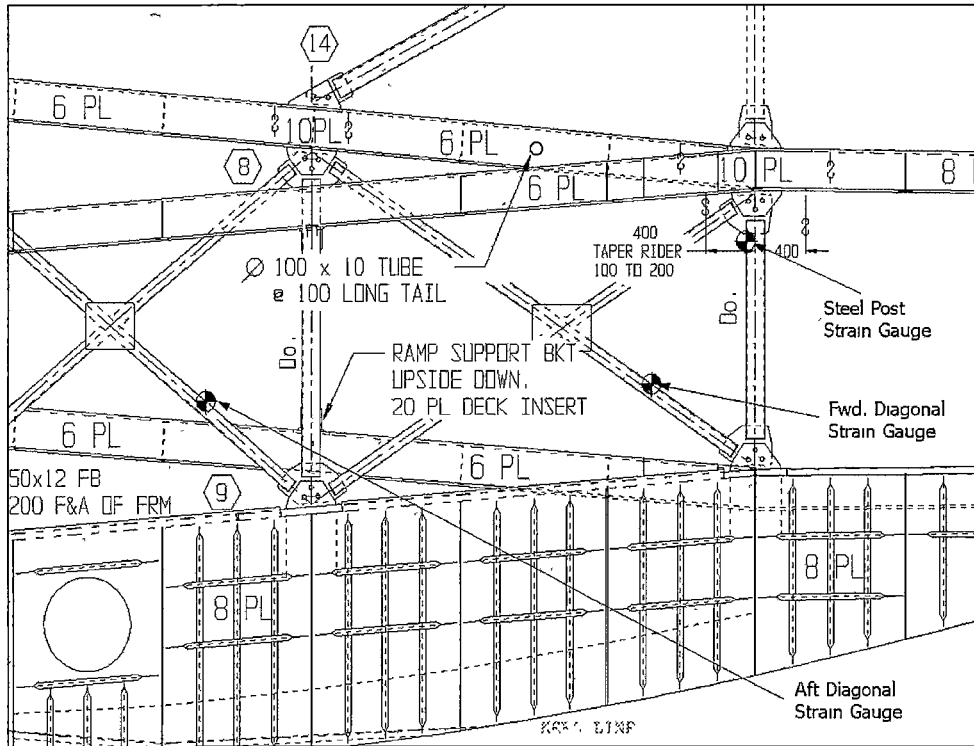


Figure A-20: Hull 050 - Fwd. Longitudinal Girder 4500mm Off Centreline (Stb. Side Looking Inboard) showing Strain Gauges 5 & 6 on Fwd. and Aft Steel Diagonals and Strain Gauge 10 on Steel Posts

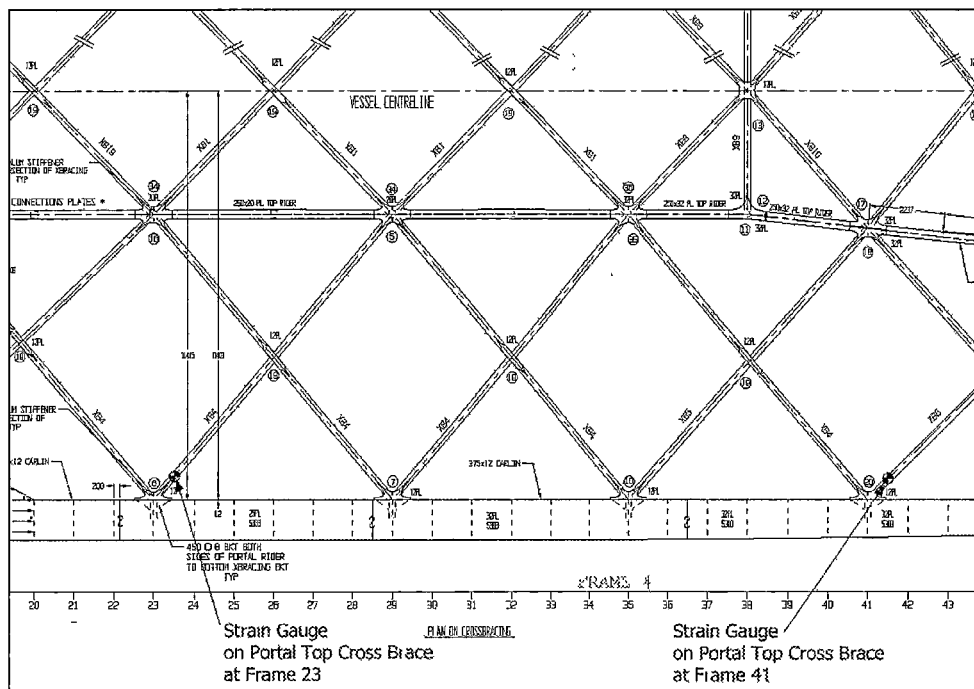


Figure A-21: Hull 050 - Plan View of Cross Bracing showing Strain Gauges 11 & 12 on Portal Top Crossing Bracing at Frames 23 and 41

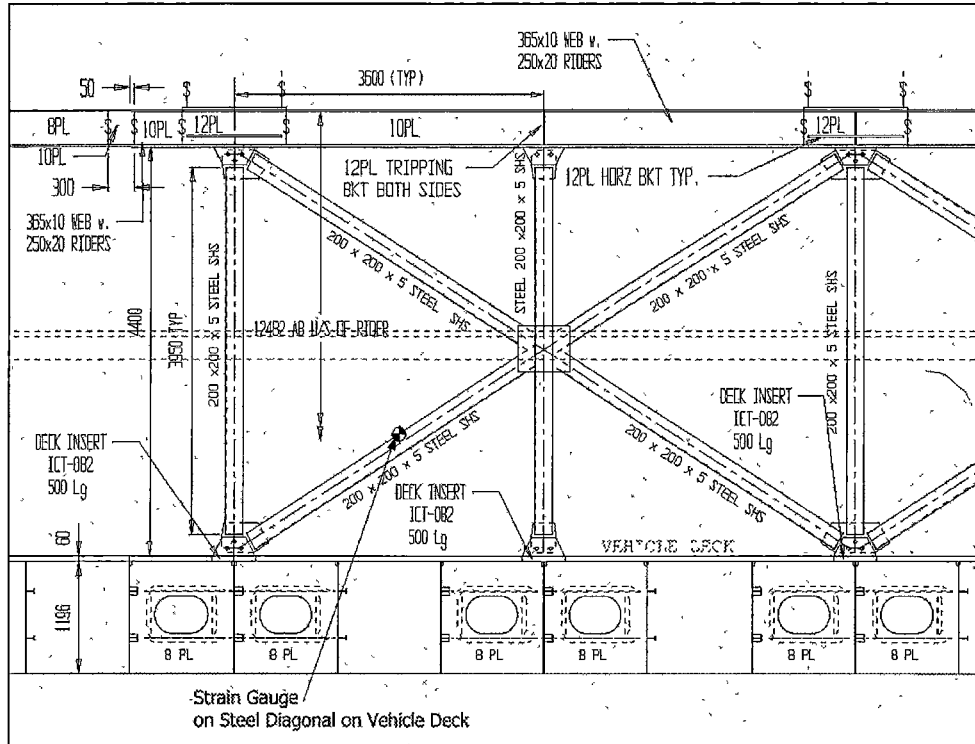


Figure A-22: Hull 050 - Section at 3450mm Off Centreline (Stb. Side Looking Inboard) showing Strain Gauge 13 on Steel Diagonal on Vehicle Deck

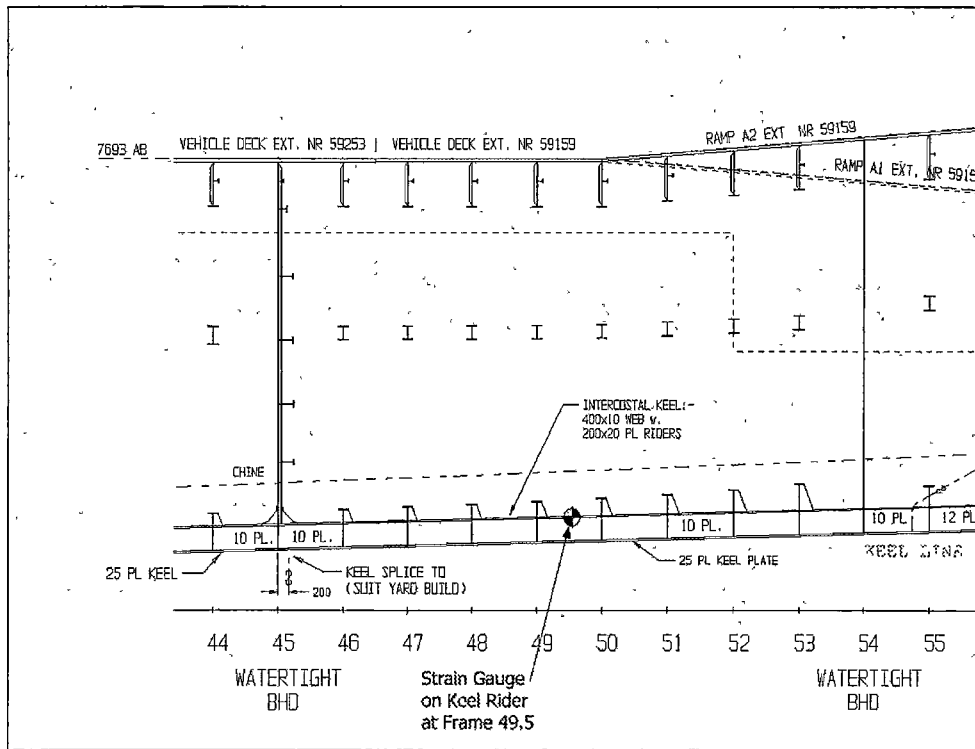


Figure A-23: Hull 050 - Hull Inboard Profile showing Strain Gauge 14 on Keel at Frame 49.5

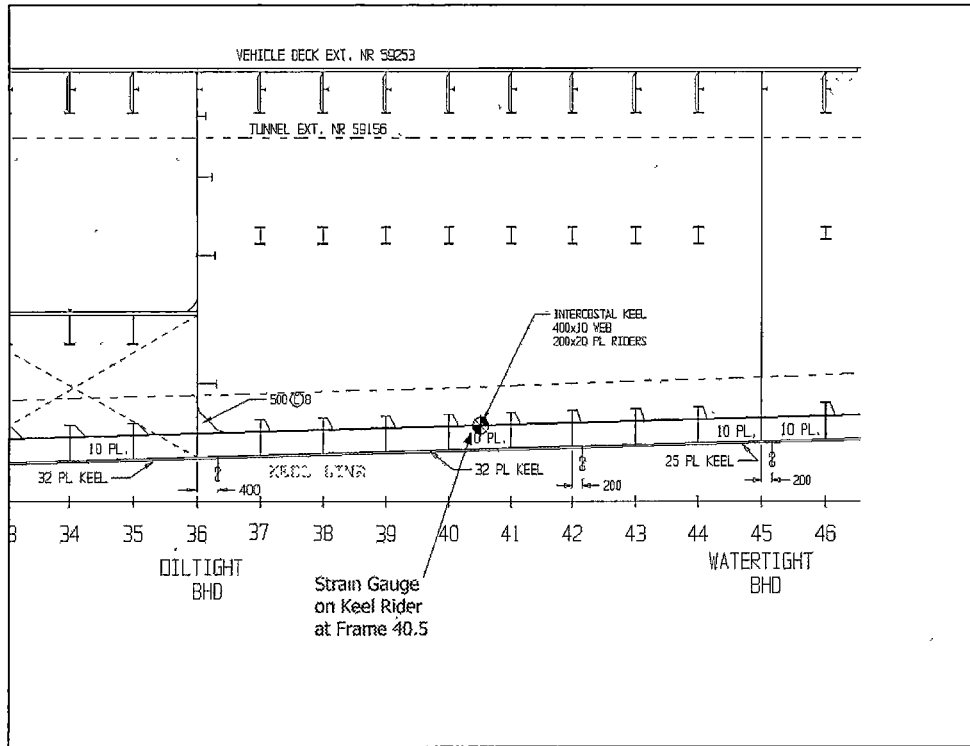


Figure A-24: Hull 050 - Hull Inboard Profile showing Strain Gauge 15 on Keel at Frame 40.5

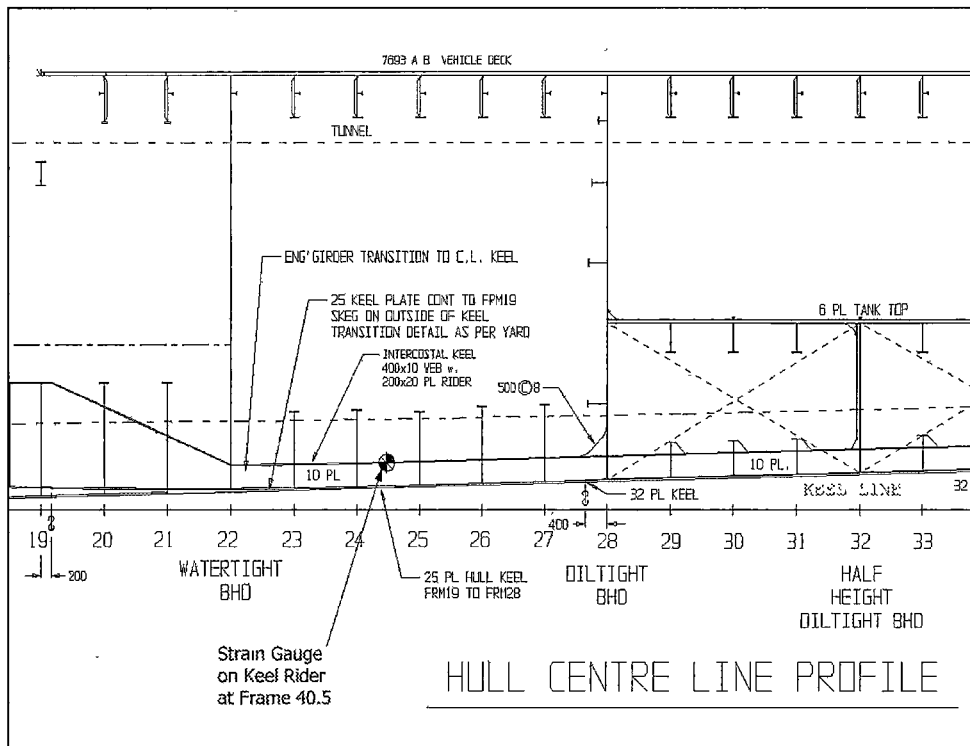


Figure A-25: Hull 050 - Hull Inboard Profile showing Strain Gauge 16 on Keel at Frame 24.5

